THE ART OF BALANCE: CANONICAL AND NON-CANONICAL MECHANISMS OF DEVELOPMENTAL NEUROGENESIS

Yiling Li

Graduate School of
Systemic Neurosciences

LMU Munich

Dissertation at the
Graduate School of Systemic Neurosciences
Ludwig-Maximilians-Universität München

<March 24, 2025>

Supervisor
Prof. Dr. Magdalena Götz

Institute of Stem Cell Research
Helmholtz Zentrum München

Department of Physiological Genomics
Ludwig-Maximilians-Universität München

First Reviewer: Prof. Dr. Magdalena Götz
Second Reviewer: Prof. Dr. Hongjun Song
External Reviewer Prof. Dr. Simon Hippenmeyer

Date of Submission: 24th March 2025
Date of Defense: 29th September 2025

Index

1 Introduction

The seat of our higher cognitive functions—the brain—originates from a simple sheet of cells known as neural stem cells (NSCs). They give rise to neurons and other essential cell types that constitute the brain during development. The process of generating neurons, or neurogenesis, has captivated scientists for decades, if not centuries. Yet, we are still scratching the surface of understanding how NSCs balance their plasticity with their commitment to differentiate into neurons.

One focal point of research lies in the role of transcription factors (TFs). These potent regulators of gene expression are pivotal in determining cell fate and have been extensively studied in the context of NSCs. While numerous TFs critical to neurogenesis have been identified, the search continues for a universal regulator—a pan-factor—that regulates neural stem cell fate and neurogenesis. Furthermore, beyond transcriptional control, emerging evidence suggests the importance of non-canonical mechanisms that remain largely unexplored but may hold the key to uncovering novel regulatory pathways in neurogenesis.

In this thesis, I will explore both canonical and non-canonical mechanisms that govern the balance between self-maintenance and differentiation of NSCs during developmental neurogenesis. Understanding these mechanisms is not only essential for decoding the complexities of brain development but also carries significant implications for developing therapies for neurodevelopmental disorders and brain injuries.

1.1 Mammalian Neurogenesis

Neurogenesis, the process to generate new neurons, is a dynamic and regulated process that ensures the proper formation and maintenance of neuronal circuits in the brain for proper brain functions. Neurogenesis occurs predominantly during embryonic development, laying the foundation for the complex architecture and functionality of the brain. It starts with a limited number of NSCs that proliferate and generate diverse neuronal subtypes, followed by the production of glial cells as neurogenesis largely diminishes at the end of embryonic development (Figure 1). However, neurogenesis continues in certain regions of the adult brain, such as the sub-ventricular zone (SVZ), derived from lateral ganglionic eminence (LGE) in the embryonic brain (Lledo et al., 2008), and the hippocampal dentate gyrus (DG), derived from embryonic dentate neuroepithelium (Urbán & Guillemot, 2014), although in both regions neurogenesis is restricted to specific neuronal subtypes.

1.1.1 Principles of Mammalian Cortical Neurogenesis

Mammalian embryonic telencephalon is subdivided into the cerebral cortex and a transitory structure called ganglionic eminence (GE), including lateral, medial, and caudal GEs. The cerebral cortex in mammals represents the advancement of brain evolution, as it is the seat of higher cognitive functions, supported by a large diversity of neuronal subtypes. A complex network regulates the cortical neurogenesis to ensure everything happens at the right time and place, which attracts exploration in understanding the underlying mechanisms.

At the onset of cortical neurogenesis, the mono-layered neuroepithelial stem cells that form neural tube wall transition from self-amplification to NSCs (Götz & Huttner, 2005) (Figure 1). Embryonic NSCs, also known as radial glial cells, are multipotent cells with the unique ability to self-renew and differentiate into neurons, and later astrocytes and oligodendrocytes. Both neuroepithelial stem cells and NSCs span the cortical columns bipolarly, with their apical plasma membrane contacting the ventricular surface, and their basal membrane anchored at the pial surface (Götz & Huttner, 2005). During early neurogenesis, NSCs largely divide symmetrically to expand the NSC pool. As development proceeds, NSCs start to divide asymmetrically, which maintains the NSC pool while giving rise to neurons. The daughter neurons are generated either directly, or indirectly via intermediate progenitor cells (IPCs), which divide symmetrically to give rise to two neurons, thereby amplifying neuronal output.

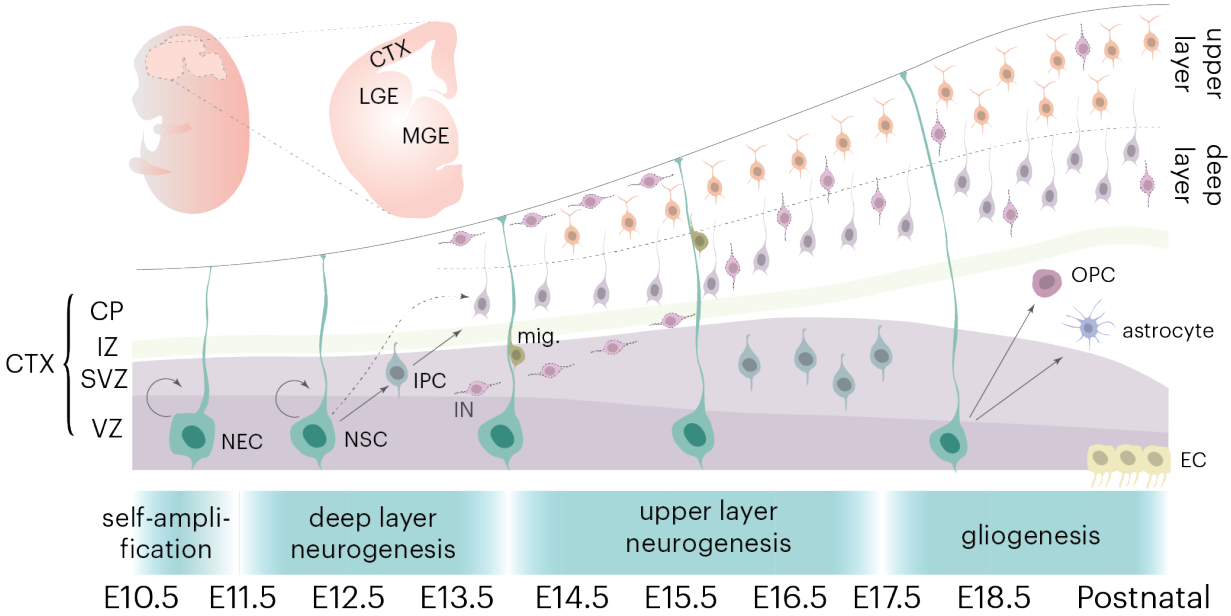

Figure 1. Mammalian neurogenesis timeline and principles
Schematic illustration of cortical neurogenesis from embryonic day 10.5 (E10.5) to immediate postnatal. A coronal section of embryonic murine brain is shown on top, composed of cortex, LGE, and MGE. CGE is on the caudal section of the brain and is not shown here. GE-derived interneurons are depicted with dashed lines. CTX: cortex; LGE: lateral ganglionic eminence; CP: cortical plate; IZ: intermediate zone; SVZ: subventricular zone; VZ: ventricular zone; NEC: neuroepithelial cell; NSC: neural stem cell; IPC: intermediate progenitor cell; IN: interneuron; mig.: migrating neuron; OPC: oligodendrocyte progenitor cell; EC: ependymal cell.

The balance between NSC maintenance and differentiation is critical for proper neurogenesis, which depends on the balance between symmetric or asymmetric cell divisions, and the balance between indirect and direct neurogenesis. A disbalance in these processes can lead to various neurodevelopmental disorders and cortical malformations (T. Sun & Hevner, 2014). For instance, an excessive proliferation of NSCs with disrupted onset of neurogenesis may lead to macrocephaly and/or autism spectrum disorder (ASD) (M. Wang et al., 2020), whereas a premature differentiation of NSCs may cause microcephaly (Jayaraman et al., 2018).

1.1.2 Spatial Temporal Order of Mammalian Neurogenesis

The mammalian neocortex is formed in an "inside-out" manner sequentially. That is, early NSCs generate deep layer neurons (E11.5-E13.5), while late NSCs give rise to upper layer neurons (E13.5-E17.5) (Figure 1). Newly born neurons migrate radially along the scaffold of NSCs to the cortical plate, with late-born upper layer neurons traversing past early-born deep layer neurons and stacking on top of them. A similar trend is observed with interneuron migration from GE. Between E12 and E15, interneuron production shifts from deep layers to upper layers, whereas this is shifted from upper layers to deep layers again from E15 to E17 (Sultan et al., 2018).

This common principle of temporal order is considered to be induced by a sequential and hierarchical cascade of TFs through feedforward and feedback mechanisms in *Drosophila* (Kohwi & Doe, 2013) (Figure 2a). Namely, NSCs progressively restrict their neurogenic competence in a fixed order, determined by TFs acting as temporal-identity factors. A similar mechanism is observed in mammalian retinal progenitors (Kohwi & Doe, 2013), but remains largely elusive in the mammals. TF Ikaros, for example, was identified as a temporal-identity factor that specifies early-born neuron fate in the retina and cortex, but without extending the neurogenic competence window (Alsiö et al., 2013; Kohwi & Doe, 2013). Sustained expression of Ikaros extends the generation of early-born deep layer neurons at the expense of later-born upper layer neurons. In the hypothalamus, the cascade is hierarchical but NSCs do not become fate restricted over time. TF retina and anterior neural fold homeobox (RAX)+ NSCs continuously generate TF Achaete-scute Complex Homolog 1 (ASCL1)+ and TF Neurogenin2 (NGN2)+ IPCs in parallel, which subsequently generate mutually exclusive neuronal subtypes (Y.-H. Zhang et al., 2021) (Figure 2b).

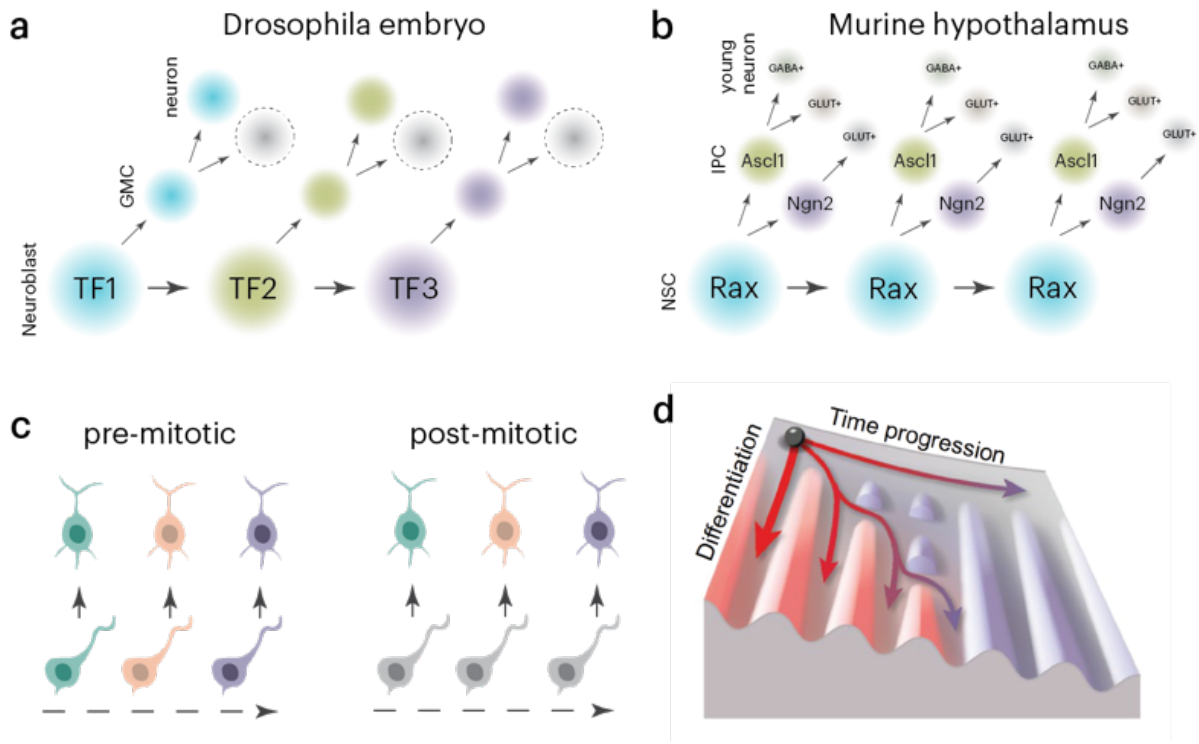

Figure 2. Temporal identify factors and models of generating neuronal diversity
a. A simplified model of TF as temporal identity factors cascade to generate neuronal diversity in Drosophila embryo. Dashed lines indicate the two daughter neurons from ganglion mother cells (GMCs) adopt distinct fates; however, the mechanism to distinguish their temporal identity is unknown.
b. TF cascade model proposed in murine hypothalamus. Rax+ NSCs generate Ascl1+ and Ngn2+ IPCs, which respectively give rise to nascent neurons. Ascl1+ IPCs bifurcate to generate both GABAergic (GABA+) and glutamatergic (GLUT+) nascent neurons, whereas Ngn2+ IPCs are fate-restricted to generate glutamatergic neurons.
c. Schematic illustration of pre-mitotic and post-mitotic models.
d. Schematic showing early-stage progenitors generate more heterogenous neuronal progeny, while late-stage progenitors are more fate-restricted to defined neuronal subtypes. Excerpt from Magrinelli et al. (2022), used with permission from Springer Nature.

In fact, the molecular mechanisms of fate specification of mammalian neurogenesis have been debated over a love time and can be grouped into two models: pre-mitotic and post-mitotic models of producing neuronal diversity (Figure 2c). That is, whether different neuronal subtypes are generated from correspondingly different stem/progenitor cells, or they arise from a homogeneous population of stem/progenitor cells and only diverge later by integrating environmental cues. The famous example supporting the pre-mitotic model is that CUX2+ progenitors are fated to become upper layer neurons regardless of birthdate and niche (Franco et al., 2012; Zimmer et al., 2004). However, accumulating data support a post-mitotic model (Mayer et al., 2018; Mi et al., 2018; Toma et al., 2014), especially with the flourishing single-cell

RNA-sequencing (scRNA-seq) data of developing brain tissue, which revealed that the lineage divergence emerges post-mitotically.

The evidence suggests that neuronal fate specification follows a mixed model. While at the large scale, early and late NSCs generate deep or upper layer neurons respectively, early NSCs generate a more heterogenous population of deep layer neurons and later NSCs generate homogeneously layer-restricted upper layer neurons, shown by isochronic transplantations (i.e., E12 NSCs into E12 cortex, E15 NSCs into E15 cortex) with fate mapping (Magrinelli et al., 2022) (Figure 2d). At the same time, birth-dating experiments coupled with scRNA-seq suggest that early NSCs (E12) are more "introverted", while late NSCs (E15) are more "extraverted", meaning NSCs become more susceptible over time to extrinsic cues in the environment and shifting their transcriptional profile similar to their neuronal progeny (Telley et al., 2019).

The nuances of this mixed model is further complemented by heterochronic transplantations (i.e., E15 NSCs into E12 cortex) with fate mapping experiments: late-stage (E15) NSCs have the capacity to generate deep-layer neurons when transplanted in E12 cortex (Oberst et al., 2019). This plasticity is driven by Wnt signaling in the niche, which is known to regulate neurogenic competence of NSCs, as canonical Wnt signaling is higher in the early stages of neurogenesis and diminishes over time (Oberst et al., 2019). Similar findings were obtained with interneuron transplantation into the cortex. E12 interneurons are typically destined for deep layers, while E15 interneurons migrate to upper layers (Sultan et al., 2018). When E15 medial ganglionic eminence (MGE) cells were transplanted into E12 cortex, they shifted their fate and settled in deep layers. Conversely, young-into-old (E12 into E15) transplantation of MGE cells into cortex shifted their destination to middle layers instead of completely upper layers (Valcanis & Tan, 2003), suggesting they are less susceptible to environmental cues than E15 cells.

Altogether, these isochronic and heterochronic transplantations of cortical stem/progenitors with fate mapping suggest that a variety of transcriptional trajectories are preserved pre-mitotically at early stages of neurogenesis, and fade over time as differentiation progresses.

1.2 Neurogenic Priming

Fate specification during mammalian neurogenesis seems to involve a combination of maintaining intrinsic molecular programs in stem/progenitors and their subsequent integration of environmental cues. A unifying concept for such a mixed model is lineage priming.

Lineage priming refers to a state in which stem cells already exhibit chromatin accessibility at cis-regulatory elements (CREs) of lineage-specific progeny genes, even though the expression of these genes remains low at the mRNA level (Meng & Nerlov, 2024). In *C. elegans*, for example, the functional left and right asymmetry arises from a two-step activation of lsy-6 miRNA locus:

the chromatin was decompacted at the precursor stage several divisions before neurons are born, only on the left but not right. A bilaterally expressed TF at later stage then activates lsy-6 only in the primed left neuron (Cochella & Hobert, 2012), offering progenitors a unique regulatory mechanism for fate commitment. At the same time, priming can be accompanied by a decrease in chromatin accessibility of alternative lineages, as shown by endoderm differentiation of human pluripotent stem cells (Madrigal et al., 2023).

Primed stem cells are therefore poised to differentiation and can upregulate lineage-specific genes in a timely manner but retain a certain degree of plasticity. While priming is well studied in hematopoietic progenitors (Meng & Nerlov, 2024), how the priming is regulated in NSCs is not yet well understood. Several studies have observed that neurogenic TFs are already expressed in NSCs. For example, human fetal NSCs express low levels of neurogenic TF mRNAs, including Ngn2 and neurogenic differentiation 1 (Neurod1) (Nowakowski et al., 2017). Similarly, minimal but detectable mRNA expressions of Eomes and Neurod4 were observed in embryonic mouse cortical NSCs (Li et al., 2020). A critical missing piece in understanding neurogenic priming is how the expression of the neuronal progeny genes in NSCs remains low. While this was partially explained at the translational level (Zahr et al., 2018), we uncovered a transcriptional mechanism regulating the neurogenic priming in NSCs in Chapter 2.

1.3 Canonical Mechanisms Regulating Neurogenesis

For the complex neurogenesis to proceed correctly both temporally and spatially, intricate transcriptional and epigenetic programs tightly control this process. A cascade of differentiation programs unfolds and transitions, such as from stem cell self-renewal to cell cycle exit and lineage commitment. TFs are key regulators that activate or repress genes. Particularly, pioneer factors, usually master regulators of cell fate changes, can bind to compact and silent chromatin, followed by recruitment of SWI/SNF chromatin remodeling complexes and rearrangement of the chromatin configuration to an open state (Barral & Zaret, 2024). This allows additional TFs and protein complex to access the open chromatin.

On the other hand, the negative regulators can induce chromatin closure or sterically block the access of other TFs. They can also recruit histone deacetylases (HDACs), such as HDAC1 and HDAC2, which participate in multiple transcriptional corepressor complexes, including corepressor for element-1-silencing transcription factor (CoREST), nucleosome-remodeling and deacetylase (NuRD), and switch-independent 3 (SIN3) (Park et al., 2022). NuRD is among the best characterized co-repressor complexes during neurogenesis. It balances the acetylation and methylation state of histone H3 lysine 27 (H3K27) by removing H3K27ac active marks

(Reynolds et al., 2012). In general, transcriptional repressors can ensure that differentiation-promoting pathways are held in check, maintaining the undifferentiated state of NSCs.

Understanding how these positive and negative regulatory machineries interact is crucial for unraveling the mechanisms underlying both brain development and potential regenerative therapies.

1.3.1 Transcription Factors Regulating NSC Maintenance

NSC maintenance relies on the expression of key TFs that promote self-renewal and repress premature differentiation. Below are examples of the best-characterized TFs for maintaining various aspects of NSCs.

SOX2

One of the most well-characterized TFs in NSC maintenance is sex determining region Y-box 2 (SOX2), a member of the SOX family TFs, which share a highly conserved DNA binding domain known as high-mobility group box domain (Sarkar & Hochedlinger, 2013). While being widely known as a pluripotency factor in embryonic stem cells (ESCs) with octamer-binding transcription factor 4 (OCT4) and NANOG (Boyer et al., 2005), SOX2 is critical in maintaining NSC identity by repressing differentiation-associated genes and promoting the expression of self-renewal-related genes. In fact, SOX2 was proposed to have dual functions in human ESCs: it interacts with OCT4, which is lost upon SOX2's interaction with paired box protein 6 (PAX6) during neural fate transition, leading to genome-wide relocalization of SOX2 (S. Zhang et al., 2019).

SOX2 occupies genomic sites involved in cell cycle exit and expression of differentiation genes in neural progenitor cells (NPCs) (Graham et al., 2003; Lodato et al., 2013). The activation of neurogenic differentiation genes requires the replacement of SOX2 by beta-catenin (Kuwabara et al., 2009). Furthermore, SOX2 was shown to bind and maintain the bivalent state (high levels of H3K27me3 and H3K4me3) of poised pro-neural genes, such as Ngn2 and Neurod1 in mouse NPCs, and limit the excessive activity of polycomb repressive complex 2 (PRC2) (Amador-Arjona et al., 2015). Together, SOX2 gives an example of a master regulator of NSC maintenance by repressing neural differentiation and ensuring the proper poised chromatin state for neurogenesis.

PAX6

PAX6 is one of the most well-known TFs that regulates various aspects of neurogenesis, including patterning, cell cycle and division regulation, and directing NSCs towards neurogenesis by inhibiting gliogenesis (Asami et al., 2011; Heins et al., 2002; Manuel et al., 2022; Osumi et al., 2008; Walcher et al., 2013). With a paired domain and a homeodomain,

PAX6 binds to specific DNA sequences in the promoter and enhancer regions of its target genes and shares many binding sites with SOX2 (Thakurela et al., 2016). PAX6 activates pro-neural genes (i.e., Ngn2) (Scardigli et al., 2003) and represses glia-specific TFs for neural lineage (Jang & Goldman, 2011). PAX6 interacts with chromatin-modifying complexes, including SWI/SNF and HDACs (Ninkovic et al., 2013), to either open or compact chromatin of neural or non-neural loci, respectively. In addition to transcriptional regulations, PAX6 also integrates signals from multiple signaling pathways (i.e., Notch and Wnt) to fine-tune the behavior and differentiation of NSCs.

FOXG1

Forkhead Box G1 (FOXG1) is a TF sharing aspects of patterning function such as PAX6 and promoting NSC proliferation such as SOX2. Different from SOX2 and PAX6, however, FOXG1 primarily acts as a repressor (Murphy et al., 1994). Highly expressed in the forebrain, FOXG1 controls the self-renewal of NSCs, the expansion of IPCs, and the timing of neurogenesis (Fasano et al., 2009; Shen et al., 2006; Siegenthaler et al., 2008). Foxg1 deficiency in mice reduces the size of the cerebral cortices due to premature differentiation, as reduced levels of Foxg1 lead to premature depletion of the progenitor pool and hence reduction of late-born neurons (Dou et al., 1999; Hanashima et al., 2004; Xuan et al., 1995). Over-expression of Foxg1 expanded the neural progenitor pool, delayed neurogenesis, and increased neuronal output (Brancaccio et al., 2010).

1.3.2 Transcription Factors Driving Neuronal Differentiation

While there are TFs supporting the maintenance of NSCs, neural differentiation is induced when specific TFs that promote the commitment of the neuronal lineage are activated. The following are the most well-known TFs for inducing the commitment of neuronal fate in progenitors. Some of them are also known as proneural genes, which encode basic-helix–loop–helix (bHLH) TFs (Huang et al., 2014). They were first identified in *Drosophila* for their ability to induce neural identity instead of epidermal in naïve ectodermal cells (Ghysen & Dambly-Chaudière, 1988).

ASCL1

The most famous proneural TF is ASCL1, known as a master regulator and a pioneer factor of the neuronal lineage, particularly for the ventral telencephalon (Fode et al., 2000). As a member of the bHLH family, it binds to E-box sequences and induces conformation changes of permissive chromatin. Genomic profiling of ASCL1 targets in embryonic brain and NSC cultures identified regulators to promote cell cycle progression and arrest, TFs important for

neurogenesis such as DLX2 and NFIB, as well as genes related to later stages of neural differentiation, including signal transduction and neurite morphogenesis (Castro et al., 2011).

During neuronal induction, there is a switch of expression mode of ASCL1 from oscillatory to sustained. Oscillatory expression of ASCL1 in neural progenitors promotes proliferation by increasing symmetric proliferative divisions, whereas elevated and sustained levels of ASCL1 biases the cells towards neuronal fate, by increasing asymmetric neurogenic cell divisions (Imayoshi et al., 2013).

For its role as a proneural factor, ASCL1 can be used to reprogram astrocytes into GABAergic neurons (Masserdotti et al., 2015), and also reprogram fibroblasts and ESCs into neurons *in vitro* (Chanda et al., 2014). Surprisingly, the induced neurons from fibroblasts are excitatory, suggesting ASCL1 is permissive but not deterministic for the inhibitory neuron lineage.

NGN2

Another pro-neural bHLH TF and pioneer factor is NGN2, which represses ASCL1 (Fode et al., 2000). Similar to ASCL1, NGN2 (and also NGN1) dimerizes with bHLH proteins (i.e., E47) to bind to E box consensus motifs to activate tissue-specific neuronal differentiation genes (Cau et al., 1997). NGN2 is directly regulated by PAX6, which binds to the E1 enhancer element of Ngn2 (Scardigli et al., 2003). Conversely, NGN2 downregulates PAX6 expression and therefore forms a negative feedback regulation (Bel-Vialar et al., 2007).

NGN2 promotes cell cycle exit by reducing the expression of cell cycle regulators including Ccnd1, Ccne1/2, Ccna2 (Lacomme et al., 2012). In the telencephalon, specifically, NGN2 is required for specifying neocortical, glutamatergic, early-born (deep layer) neurons, while inhibiting GABAergic neuronal fate (Schuurmans et al., 2004). At the same time, NGN2 is repressing the generation of astrocytes (S. Sun et al., 2019) and oligodendrocytes (Jiang et al., 2020). Therefore, it is also widely used for the generation of induced neurons from astrocytes and pluripotent stem cells *in vitro* (Hulme et al., 2021).

Nuclear Factor One (NFI) Factors

Besides the bHLH family factors (including NeuroD family not described in detail here), another TF family, known as the NFI family factors (NFIA, NFIB, NFIX), promotes differentiation of neural as well as glial lineage at the expense of stem cell self-renewal (Harris et al., 2015). They are master regulators that homo- or heterodimerize to activate expression of neuronal and glial genes. NFIA, B, X are expressed in the VZ starting from embryonic day 12 (E12) until the end of neurogenesis (Campbell et al., 2008; Plachez et al., 2008). Knockout (KO) mice of Nfia and Nfix have expanded pool of NSCs with a delayed production of IPCs and reduced expression of astrocytic marker glial fibrillary acidic protein (GFAP) (Harris et al., 2016; Heng et al., 2014; Piper et al., 2010). NFIB and NFIX were further revealed to drive the acquisition, maintenance, and

maturation of ependymal cell fate, which occurs after the end of neurogenesis (Harkins et al., 2022; Lahti et al., 2024). Nfix KO mice display hydrocephalus with abnormal morphology of ependymal cells, which also aberrantly and largely retained the expression of PAX6 (Harkins et al., 2022). Together, NFI factors are involved in promoting all sequential steps of neurogenesis and were proposed to regulate the timing of neurogenesis (Lahti et al., 2024).

1.3.3 Feedback and Cross-Regulation of TFs

As we have seen above, there are groups of TFs either promoting NSC maintenance, or promoting neuronal differentiation. The crosstalk and feedback mechanisms among these TFs (and their associated signaling pathways) are thus important to balance maintenance and differentiation of NSCs. For example, Notch signaling maintains NSCs by activating HES1/5, which represses pro-neural genes, and its downregulation allows for the activation of Neurogenins and neuronal differentiation.

As already mentioned in 1.1.2 and 1.3.2, during neuronal differentiation cascade, TFs cross-regulate each other, such as the negative feedback regulation between PAX6 and NGN2. Another classic example of TF cascade guiding neural progenitor progression, lineage commitment, and differentiation is the regulation cascade among PAX6, TBR2, and TBR1 (Elsen et al., 2018) (Figure 3a). PAX6 represses itself and activates TBR2, which represses PAX6 and activates TBR1 (Sessa et al., 2017). In other words, these three TFs form a positive feedforward cascade, with PAX6 negatively self-regulating itself and TBR2 negatively regulating PAX6 to form a negative feedback loop. This TF cascade for neural differentiation is further complemented by HES1 trajectory in parallel. Similar to PAX6, HES1 also represses itself (Takebayashi et al., 1994). While PAX6 facilitates the neurogenic cascade progression, HES1 antagonizes some of PAX6's downstream activation targets, including Tbr2 and Ngn2, to expand the NSC pool (Sansom et al., 2009). At the same time, NGN2 induces TBR2, which represses HES1 (Shimojo et al., 2024). This cross-regulation among the above TFs and their expression during neural differentiation are summarized in Figure 3a and 3b.

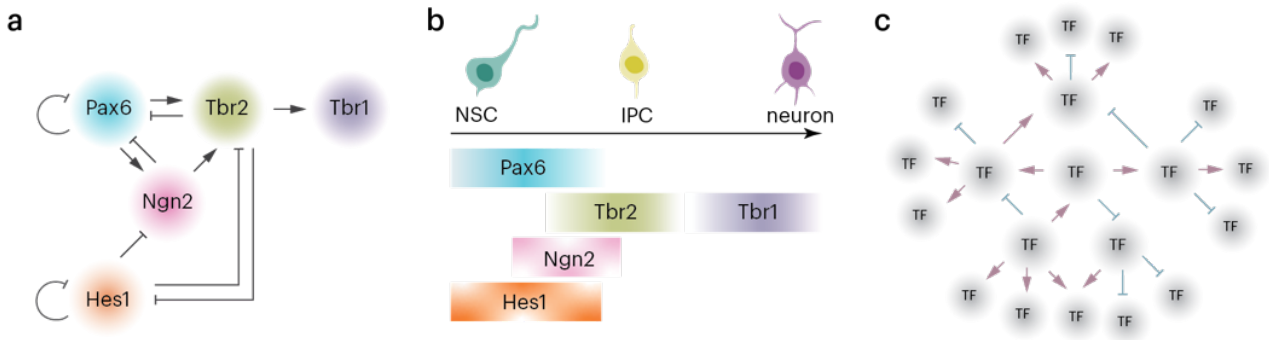

Figure 3. TF cross-regulation and gene regulatory network

a. A summary schematic showing cross-regulation among PAX6, TBR2, TBR1, NGN2, and HES1.
b. Expression profile along developmental trajectory of TFs in (a). HES1 and NGN2 oscillations represented by fluctuating gradient.
c. Schematic illustration of gene regulatory network. Positive regulation is represented by pink arrows, with negative regulation represented by blue arrow with a dash.

1.3.4 Gene Regulatory Network (GRN)

As what is shown above, TFs during mammalian neuronal differentiation form networks that cross-activate and repress each other. Tapping on one TF may lead to a change of dynamics in the whole network. Such a GRN (Figure 3c) is getting well-characterized with the advancement of single-cell multi-omics that correlate open chromatin with gene expression to identify gene regulation relationships among TFs (Bravo González-Blas et al., 2023; Fleck et al., 2023). Comparing human and mouse cortical GRNs revealed that while TF combinations for specific cell types are highly conserved, TF-binding site (TFBS) and enhancers show great turnover (Bravo González-Blas et al., 2023). This eludes to the concept that a cell type is defined by the core TF regulatory complex (Arendt et al., 2016), composed of "terminal selectors" that are mainly homeobox TF family (Hobert, 2021).

GRNs provide a significant groundwork for understanding central TFs maintaining a certain cell state or a differentiation trajectory. After establishing a GRN, one can perturb a TF *in silico* and predict downstream transcriptomic changes or differentiation trajectory changes (Bravo González-Blas et al., 2023; Fleck et al., 2023).

1.4 Non-canonical Mechanisms Regulating Neurogenesis

While TF-associated regulations and signaling pathways have been extensively investigated in neurogenesis, emerging non-canonical mechanisms are revealing new layers of regulation critical for neurogenesis. These include metabolic dynamics (Iwata et al., 2023), the mechanical and bioelectric membrane properties within cells or tissues (Petrik et al., 2018; Vitali et al., 2018), and the niche environment (i.e. stiffness) created by extracellular matrix (ECM) (Kjell et al., 2020).

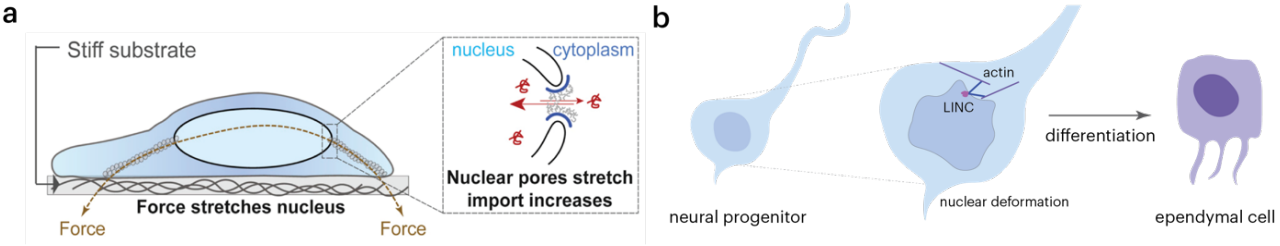

Figure 4. Mechanical coupling between cytoplasm and nucleus modulates cell fate

a. Illustration of YAP translocation via force sensing in ECM and stretching of nuclear pores. Excerpt from Elosegui-Artola et al. (2017), used with permission from Elsevier.
b. Schematic of LINC complex and actin levels regulating ependymal cell differentiation.

Among these, mechanotransduction through cytoskeletal proteins serves as a crucial link between extracellular cues and nuclear responses though its role in neurogenesis remains underexplored. Studies have shown that the mechanical coupling between the nucleus and the cytoskeleton is essential for cellular adaptation to environmental forces. For example, ECM-generated forces are transmitted to the nucleus through cytoskeletal tension, stretching the nuclear pores and facilitating the nuclear translocation of transcriptional regulator yes-associated protein (YAP), which is required for mesenchymal stem cell differentiation and endothelial cell survival (Figure 4a) (Aragona et al., 2013; Driscoll et al., 2015; Dupont et al., 2011; Elosegui-Artola et al., 2017). This cytoskeletal-nuclear coupling is important for cell fate transitions and differentiation. When the linker of nucleoskeleton and cytoskeleton (LINC) complex is disrupted or when actin is decreased globally, ependymal differentiation is impaired. Conversely, mechanical compression or increased actin polymerization accelerated ependymal differentiation (Figure 4b) (Basso et al., 2024).

Given these findings, cytoskeletal proteins are increasingly recognized not just for their structural roles, but also as dynamic regulators that mediate cellular sensing and adaptation. In fact, their roles can even extend beyond integrating extracellular signals with nuclear responses.

1.4.1 Nuclear Functions of Cytoskeletal Proteins

Traditionally considered as restricted to the cytoplasm, cytoskeletal proteins were also identified to be located inside the nucleus and involved in important functions inside the nucleus, including transcription and chromosome organization (Hofmann et al., 2004; Xie, Almuzzaini, et al., 2018).

The best characterized cytoskeletal protein with fundamental nuclear functions is actin, well-known for its involvement in intracellular trafficking at the plasma membrane and cell morphology related to cytokinesis and cell adhesion (Bettinger et al., 2004). When actin was found to be inside nucleus in the beginning, it was hypothesized that nuclear actin simply plays the role as a nucleoskeletal protein. However, nuclear actin is actively transported into the nucleus via importin/exportin (Dopie et al., 2012; Stüven et al., 2003), and was found to be a component of chromatin remodeling complexes, including the SWI/SNF family BAF complex (Nishimoto et al., 2012; Olave et al., 2002), and influences chromatin accessibility (Sen et al., 2024) and genome architecture (Mahmood et al., 2021). Loss of actin can induce genome-wide

loss of BRG1 (a catalytic subunit of the SWI/SNF complex) binding and alterations in histone modifications (Xie, Almuzzaini, et al., 2018), and also compromised neurogenesis in the context of direct neuronal reprogramming (Xie, Jankauskas, et al., 2018). Nuclear actin is also directly involved in the transcription: it interacts with RNA polymerase II and is necessary for transcription initiation (Hofmann et al., 2004), and was found to interact with proteins essential for various steps of transcription and RNA processing (Viita et al., 2019).

Besides actin, many other cytoskeletal proteins were found to be shuttling between the nucleus and cytoplasm, including tubulin (Akoumianaki et al., 2009; Schwarzerová et al., 2019), profilin (Stüven et al., 2003), and keratin (Kumeta et al., 2013). However, none of the above cytoskeletal proteins were reported to have nuclear functions important for physiological neurogenesis. In Chapter 3, we explored microtubule proteins during neurogenesis and uncovered a microtubule-associated protein—microtubule-associated protein 1B (MAP1B)—with an essential nuclear function. We discovered that the compartmental dynamics of Map1b are critical for neurogenesis progression and the pathology of periventricular heterotopia (PH).

1.4.2 Moonlighting Proteins during Neurogenesis

The discovery of nuclear actin has challenged the functional exclusivity between nuclear and cytoplasm. This paradigm shift has been reinforced by the identification of numerous proteins that exhibit two or more functions depending on their subcellular localization. They are known as a subgroup of moonlighting proteins.

Moonlighting proteins are a subclass of multifunctional proteins with two or more unrelated physiological functions within one peptide chain (Jeffery, 2017) (Figure 5). Protein isoforms resulting in alternative functions do not belong to moonlighting. Moonlighting proteins are found in various species, from bacteria to humans. The majority of them are constitutively expressed enzymes adopting unrelated functions, such as autophagy (Huberts & van der Klei, 2010). So is the case with the first discovered moonlighting protein—crystallin—a structural protein in the duck lens, and lactate dehydrogenase in the duck heart (Hendriks et al., 1988). Because of the lack of methods to systematically search moonlighting proteins, so far the databases of moonlighting proteins are based on publications discovering secondary functions of existing proteins, accumulating to 300-500 proteins depending on the curation criteria in the database (Mani et al., 2015; Ribeiro et al., 2019). One promising direction of high-throughput discovery of moonlighting proteins is to look for proteins with multiple subcellular localizations, because different localization indicates potential different functions (Figure 5).

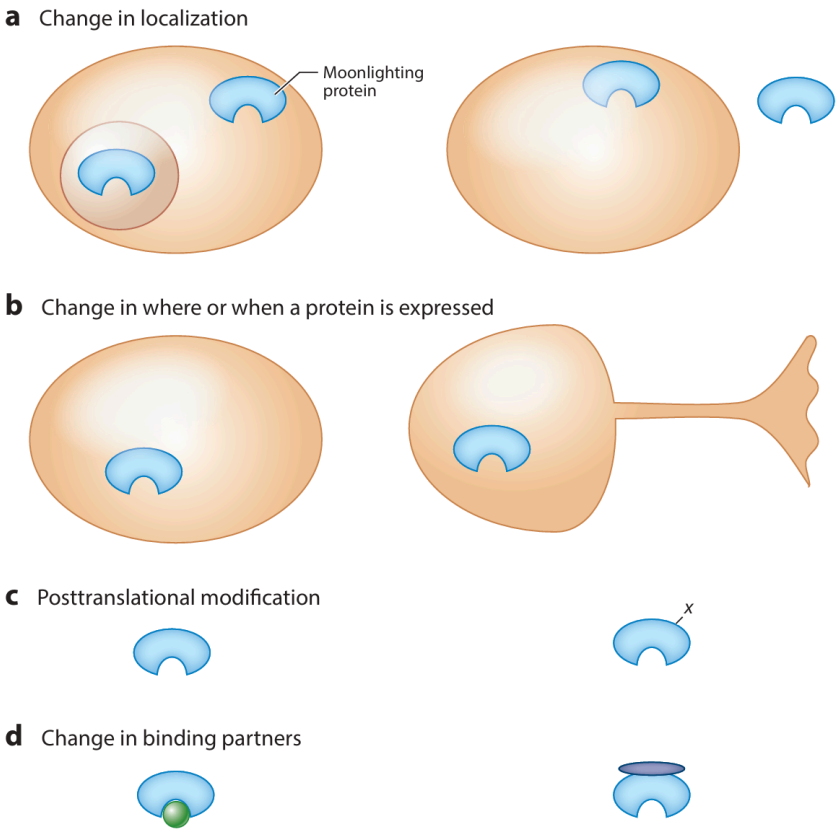

Figure 5. Principles of moonlighting.

Moonlighting function can arise from (a) change in localization; (b) change in the cell stage or cell type of expression; (c) post-translational modification such as phosphorylation; and/or (d) change in interacting partners. The moonlighting protein in oval with a pocket represents a potential enzymatic site. Excerpt from Singh & Bhalla (2020), used with permission from Annual Reviews.

In the context of neurogenesis, autism susceptibility candidate 2 (Auts2) was found to have important functions both in the cytoplasm and nucleus (Figure 6a). As its name suggests, single nucleotide polymorphisms (SNPs) of Auts2 are associated with ASD, but also with other neurological and psychiatric diseases (Hori et al., 2021). AUTS2 protein was detected initially in the nucleus of newborn neurons at E12.5, and the expression slowly equilibrates between nucleus and cytoplasm around E14.5, which persists to adolescence (Hori et al., 2014). Nuclear AUTS2 interacts with PRC1 and binds to genes associated with neuronal development, gene expression, and RNA processing (Gao et al., 2014; Oksenberg et al., 2014). Interestingly, different from PRC1's canonical role, AUTS2-PRC1 complex activates transcription, mediated by recruitment of casein kinase 2 (CK2), and histone acetyltransferase P300/CBP (Gao et al., 2014). At the same time, AUTS interacts with RNA-binding proteins such as NONO and SFPQ to regulate RNA metabolism (Castanza et al., 2021). On the other hand, cytoplasmic AUTS2 regulates cell morphogenesis, motility and migration by interacting with guanine nucleotide-

exchange factors (GEFs), which activates Rac1 signaling pathway and further remodels actin cytoskeleton, facilitating the monomer form G-actin polymerizing to F-actin (Hori et al., 2014). Both nuclear and cytoplasmic AUTS2 act in synergy to promote neural differentiation and migration.

Different from the case of AUTS2, there are multifunctional proteins with exclusively distinctive roles between the nucleus and cytoplasm. Their nucleo-cytoplamic distribution and respective enrichment, therefore, is important for their downstream regulations. One famous example is beta-catenin, which regulates cell-cell adhesions by interacting with E-cadherins at the plasma membrane and indirectly modulating actin cytoskeleton (Hülsken et al., 1994; McCrea et al., 1991), and in the nucleus acts as a central effector of Wnt signaling (Miller & Moon, 1996) and is important for various aspects of mammalian development including neurogenesis (Rosenbloom et al., 2020) (Figure 6b). Under homeostatic conditions, beta-catenin shuttles between the nucleus and the cytoplasm and distribute equally (Yokoya et al., 1999). Upon activation of Wnt signaling, beta-catenin is translocated and accumulated in the nucleus. Interestingly, this shuttling is independent of nuclear localization signal (NLS) and importin/Ran-dependent nuclear transport machineries (Fagotto et al., 1998). Studies have suggested that the localization of beta-catenin is mediated by a piggyback mechanism via interactions with its nuclear (i.e., TCF) or cytoplasmic partners (i.e., AXIN) (Cong & Varmus, 2004; Krieghoff et al., 2006). It was then revealed that the nucleo-cytoplasmic distribution of beta-catenin is regulated by nuclear export and compartmental retention (Cong & Varmus, 2004; Henderson, 2000). c-Jun N-terminal kinase 2 (JNK2)-mediated phosphorylation facilitates the nuclear localization and function of beta-catenin (X. Wu et al., 2008), while glycogen synthase kinase 3 (GSK3)-mediated phosphorylation in the cytoplasm marks beta-catenin for degradation (J. Liu et al., 2022). Thus, cytoplasmic retention of beta-catenin inhibits Wnt signaling. In this case, cytoplasmic and nuclear localization of beta-catenin functions in a seesaw effect—repressing or activating Wnt signaling.

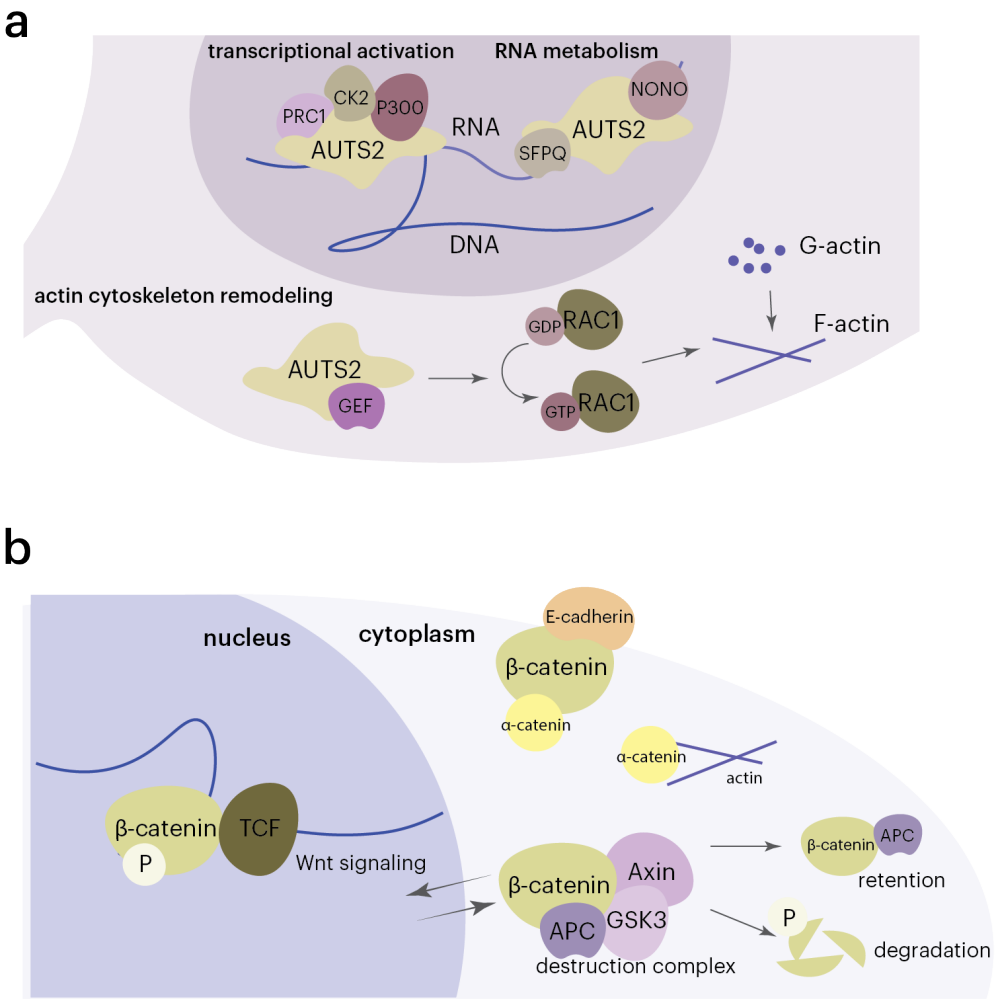

Figure 6. Moonlighting proteins and their compartmental functions

Schematics of AUTS2 (a) and beta-catenin (b) functions in the nucleus and cytoplasm.

Such a see-saw effect based on nuclear-cytoplasmic shuttling is also observed with MAP1B, promoting either maintenance of NSCs or neuronal differentiation, which will be explained in more details in Chapter 3.

1.5 Aims and Scope of This Thesis

This thesis investigates a canonical and a non-canonical mechanism that regulates developmental neurogenesis progression, highlighting the importance of maintaining equilibrium in transcriptional regulation and compartmental dynamics in NSCs. In Chapter 2, I focus on a transcription factor, TGIF2 (TGFbeta-induced factor 2). TGIF2 ensures the preservation of stemness by repressing neurogenesis programs and preventing precocious differentiation. This balance is crucial: overexpression of TGIF2 resulted in enhanced NSC maintenance, while downregulation of TGIF2 led to aberrant differentiation. Through transcriptomic, epigenetic, and functional analyses, this study elucidates TGIF2's role as a

central regulator of NSC fate and underscores the importance of fine-tuned transcriptional control during neurogenesis. By elucidating TGIF2's function, we aim to shed light on broader mechanisms that govern the balance of NSC fate decisions and neurogenesis during brain development.

In Chapter 3, we investigated a microtubule protein and found it in the nucleus: MAP1B. It is implicated in PH, in which a subset of neurons fails to migrate and remain stuck at the ventricular zone. As a protein traditionally associated with microtubule organization, MAP1B was revealed to be in the nucleus, and even regulates BRG1 binding to the genome. The level of MAP1B in the nucleus versus cytoplasm seems to be crucial for the developmental trajectory. Nuclear retention of MAP1B was found in human induced pluripotent stem cell (iPSC)-derived brain organoids carrying PH mutations and therefore suggesting that PH may originate from a NSC pathology instead of migration pathology that was previously believed.

Together, these two manuscripts underscore the critical role of balance in NSC biology. TGIF2 regulates the equilibrium between NSC maintenance and differentiation by repressing neurogenesis and neurogenic priming genes, and MAP1B as well, but by a different mechanism: MAP1B enrichment in the nucleus promotes NSC fate, while cytosolic enrichment promotes neuronal differentiation. By exploring these mechanisms, this thesis provides insights into how NSC homeostasis is achieved and maintained, as well as the consequences of its disruption for brain development and disease.

Chapter 2

TGIF2 is a major regulator of neural stem cell fate and neurogenic priming

Yiling Li (李怡灵)[1,2,3], Anthi C. Krontira[1,2], Franziska Vierl[1,2], Maria L. Richter[1,2], Weixu Wang (汪伟旭)[4,5], Juliane Merl-Pham[6], Fabian J. Theis[4,5,7], Stefanie M. Hauck[6], Magdalena Götz[1,2,8]

[1]Institute for Stem Cell Research, Helmholtz Center Munich, Biomedical Center, Planegg-Martinsried, Germany

[2]Biomedical Center Munich, Physiological Genomics, Biomedical Center, LMU Munich, Planegg-Martinsried, Germany

[3]Graduate School of Systemic Neurosciences, LMU Munich, Planegg-Martinsried, Germany

[4]Institute of Computational Biology, Computational Health Center, Helmholtz Munich, Munich, Germany

[5]TUM School of Life Sciences Weihenstephan, Technical University of Munich, Germany

[6]Research Unit Protein Science and Metabolomics and Proteomics Core, Helmholtz Center Munich, Neuherberg, Germany

[7]School of Computation, Information and Technology, Technical University of Munich, Munich, Germany.

[8]Excellence Cluster of Systems Neurology (SyNergy), Biomedical Center, LMU Munich, Planegg-Martinsried, Germany

Lead and corresponding author: Magdalena.goetz@helmholtz-munich.de

Abstract

During brain development, neural stem cells (NSCs) must balance self-renewal with differentiation and ensure lineage progression. To identify novel regulators of NSCs during neurogenesis, we isolated NSCs by FACS from the mouse cerebral cortex and ganglionic eminence at mid-neurogenesis, and at birth, when gliogenesis starts in both, but neurogenesis only continues in the latter region. RNA-seq and ATAC-seq revealed major transcriptional and chromatin changes between these stages and identified TGFB-Induced Homeobox Factor 2 (TGIF2) as a key candidate factor in neurogenic NSCs. *In vitro* and *in vivo* experiments demonstrated a potent role of TGIF2 controlling NSC fate maintenance mediated by its interaction with the SIN3A/HDAC repressor complex suppressing neuronal differentiation genes. Multiomic comparison of NSC and neuron gene expression allowed the comprehensive analysis of neurogenic priming in cortical NSCs, identifying TGIF2 as its major regulator by restraining neuronal differentiation gene activation in NSCs.

Introduction

Stem cells need to balance self-renewal versus generation of differentiated progeny during organogenesis. In the context of brain development, this balance is crucial for regulating brain size and ensuring proper neural function. During neurogenesis, neural stem cells (NSCs) are endowed with the capacity to generate neurons, while they lose this property and disappear in most brain regions, when gliogenesis starts[1]. However, in certain regions such as the murine lateral ganglionic eminence (LGE), adult neural stem cells emerge that continue to generate a subset of neurons—the olfactory bulb interneurons in mice—throughout life. This prompts two main questions: first, which factors regulate the neurogenic fate of NSCs, and second, how do NSCs generate neurons, while remaining undifferentiated themselves?

Lineage priming has been proposed in several stem cell types as a mechanism to ensure generation of the right type of progeny. In hematopoietic stem cells (HSCs) for example, the opening of regulatory elements for lymphoid genes, while keeping their expression levels low, biases HSCs toward generating the lymphoid lineage rather than other types of progeny[2]. Similarly, NSCs are primed for the generation of specific neuronal subtypes[3], but the mechanisms retaining expression of these neuronal subtype genes at basal levels remain poorly understood[4]. However, balancing NSC fate with differentiation is essential for the timing of neurogenesis and the brain size. Thus, while significant progress has been made in understanding the transcriptional regulators of neurogenesis and gliogenesis[1,5,6], our knowledge remains limited regarding the key factors governing neurogenic priming and equipping NSCs with neurogenic potential, while preventing their premature differentiation. Moreover, our knowledge about pan-neurogenic regulators is still rather limited[7]. Most known major potent regulators of neurogenesis, such as the proneural factors NEUROG1/2 and ASCL1, or PAX6, DLXs, and ISLET[8–11], are expressed and function in a region-specific manner, contributing to the generation of different neuronal subtypes. However, we still know very little about non-patterned pan-neurogenic regulators.

To identify such factors, we choose to isolate NSCs labelled for CD133/Prominin1, and neurons labelled for PSA-NCAM using fluorescence-activated cell sorting (FACS) as described before[12,13] from the cerebral cortex and the LGE. NSCs and neurons were collected at the peak of neurogenesis at embryonic day 14 (E14), and the transition to gliogenesis at E18. In the cerebral cortex, neurogenesis largely ends at E18, whereas it continues in the LGE for at least some neuronal subtypes, such as olfactory bulb interneurons, alongside the initiation of gliogenesis. This comprehensive analysis not only provides a rich resource for the first time directly comparing the two regions across developmental stages, but also led to the discovery of TGIF2 as a pan-regional key regulator of NSC fate and neurogenic priming, preventing premature neuronal differentiation and thereby maintaining the pool of NSCs during neurogenesis.

Results

Transcriptional and chromatin regulators of neurogenesis across forebrain regions and time

To uncover critical regulators of NSC fate and neurogenesis, we chose to perform bulk RNA-seq and ATAC-seq for deeper sequencing and more sensitive analysis of the NSCs populations isolated by FACS from E14 and E18 murine cerebral cortex and LGE (Figure 1A). Region of origin and developmental stage explained more than 90% of the variance, as seen with principal component analysis (PCA) for both the RNA-seq (Figure S1A) and the ATAC-seq data (Figure S2A), while technical aspects of the experimental procedures did not affect the distribution of the data (Figure S1B, S2B).

Towards a comprehensive understanding of molecular regulators of neurogenesis, we first compared the transcriptome of cortical NSCs at E14 and E18 to identify transcripts with high expression at the peak of neurogenesis (E14). We found 7,455 differentially expressed (DE) genes in the cortex (at 1% false discovery rate, FDR; Table S1, Figure S1C), representing 33,55% of all detected genes (22,215 total). In the LGE, likewise 8,517 genes (38,33% of detected genes) were differentially expressed between the peak of neurogenesis and the onset of gliogenesis (1% FDR; Table S2, Figure S1D). Also the chromatin state was extensively regulated between the two developmental stages with 7,654 differentially accessible regions (DARs) in the cortex, albeit proportionally less than observed for RNA (16.2% of total) (Table S3; Figure S2C). Notably, this chromatin remodeling was less pronounced in the LGE with 4,710 accessible regions (11% of total) regulated between E14 and E18 (Table S4, Figure S2D), which may be related to neurogenesis not ending in this region. Intriguingly, a greater number of chromatin-associated factors are down-regulated at the end of neurogenesis (1% FDR: 308 for the cortex and 314 for the LGE, with 246 in common, Table S5) than up-regulated for gliogenesis (1% FDR: 52 for the cortex and 68 for the LGE, with 33 in common, Table S6). This may be consistent with larger plasticity of the neurogenic NSCs than the gliogenic NSCs. For example, we found a switch in the ATPase of the SWI/SNF complex from *Brg1* at E14 to *Brm* at E18, consistent with other tissues, where this switch occurs in more differentiated stages[14,15].

To further explore the genes involved in the developmental stage switch we performed gene ontology (GO) term analysis and found genes with higher expression at E14 in both cortex and LGE enriched in biological pathways associated with stem cell population maintenance and differentiation, cell cycle, cell division and DNA replication (Figure S1E and S1F; Tables S7 and S8). Likewise, DARs at E14 in both cortex and LGE, compared to those at E18, were enriched with GO terms associated with nervous system development, cell differentiation and neurogenesis (Figure S2, Tables S9, and S10), further highlighting the higher degree of neurogenesis and proliferation in both regions at E14. In addition, the DE genes that were

higher at E14 were enriched for nuclear localization and molecular functions such as nucleic acid and histone binding (Figure S1E and S1F; Table S3 and S4), pointing to an active role of nuclear proteins and chromatin regulation in peak neurogenesis. Thus, we specifically scrutinized transcription factors (TFs) and chromatin regulators (ChRs), as they are pivotal in regulating developmental decisions at the molecular and cellular level[12,16,17].

We reasoned that the factors which define long-term maintenance of neurogenic stemness, thus representing essential regulators of neurogenesis, would exhibit higher expression in the E14 neurogenic cortex compared to the E18 gliogenic cortex, but would also be differentially upregulated in the E18 LGE that continues neurogenesis at larger scale compared to the cortex at the same stage. However, LGE and cerebral cortex also differ profoundly in their regional specification, as they express different patterning TFs. As we wanted to search for pan-neurogenic NSC factors, we excluded the factors that are already differentially expressed between the regions at E14 to avoid known region-specific regulators of neurogenesis. Following this rationale, we found 225 transcripts that we consider neurogenic fate regulators (Figure 1B, Table S11), 44 of which are TFs and/or ChRs (Figure 1C, Table S11). These were enriched for terms associated with regulation of developmental processes, cell differentiation and cell population proliferation (Figure 1D, Table S12), supporting our approach.

To further identify the most relevant of these TFs regulating neurogenesis, we explored which of them would have significantly more open target sites in neurogenic NSCs at E14. Following the same reasoning as for the transcriptome, we compared the differentially enriched motifs of the E14 versus E18 cortex, the E18 LGE versus E18 cortex, and focused on the ones in the commonly accessible regions between the cortex and LGE at E14. These comparisons resulted in 98 differentially enriched motifs in the neurogenic NSCs (Figure 1E, Table S13). Overlapping the 44 neurogenic fate determinants from the transcriptome analysis with the 98 neurogenic enriched motifs identified a single common key TF, whose expression and binding motifs are significantly enriched in neurogenic NSCs, namely TGFB-induced Factor Homeobox 2 (TGIF2) (Figure 1F-H). Our interest in this candidate factor was further supported by our finding that direct neuronal reprogramming of astrocytes by Neurogenin2 increases the accessibility of TGIF1 and TGIF2 binding motifs[18], implying these factors may have a pan-neurogenic role.

TGIF2 has so far mostly been studied in the context of cancer, where it is involved in regulating migration and epithelial to mesenchymal transition[19,20]. In development, TGIF2 is a key regulator of patterning and fate in the endoderm[21,22], but its role in the developing nervous system and neurogenesis remains unexplored. The other family member, TGIF1, is important in very early brain development where TGF-β[23] and Sonic Hedgehog signaling regulate gastrulation and formation of the telencephalic hemispheres[24], respectively. When TGIF1 is mutated or deleted, it can cause holoprosencephaly[24], a phenotype where the telencephalic

hemispheres are fused. Only in the adult brain, TGIF2 has been implicated in regulating behavioral aspects of autism spectrum disorder (ASD) in neurons[25], which were improved upon TGIF2 overexpression. Thus, nothing is known about the role of TGIF2 in neurogenesis, which we decided to focus on.

TGIF2 promotes NSC and later NPC fate in a cell-autonomous manner in vitro

TGIF2 is highly enriched in the ventricular zone (VZ), where neural stem and progenitor cells reside (Figure S3A). It has two protein-coding isoforms in rodents[26], with the longer isoform (TGIF2IR), which contains a retained intron, being the canonical and more highly expressed isoform[26](Figure 2A). To explore first the function of endogenous TGIF2, we started by performing knockdown experiments (TGIF2 KD) using an siRNA pool targeting all TGIF2 isoforms (Figure S3B and S3C). Cells dissociated from cerebral cortices at E12 (Figure 2B) were co-transfected with the siRNA pool and a GFP control plasmid to label proliferating cells and their progeny. At three days post-transfection (3dpt), the cells were fixed and stained for GFP, PAX6 for NSCs, TBR2 for neural progenitor cells (NPCs), and TUBB3 (tubulin beta 3 class III) for young neurons (Figure 2C and 2D). Interestingly, TGIF2 KD showed significantly reduced proportions of PAX6+ NSCs (Figure 2E) and increased proportions of TUBB3+ neurons at 3dpt (Figure 2F), suggesting a role of TGIF2 in inhibiting neuronal differentiation and favoring NSC fate.

To explore these findings further and to understand the role of the different TGIF2 isoforms, we cloned each isoform into a bicistronic expression vector driven by the CAG promoter. The vector also included GFP connected by an internal ribosome entry site (IRES) to ensure the co-expression of TGIF2 and GFP within the same cells. A monocistronic vector expressing only GFP served as the control. The constructs were transfected into dissociated cells and analyzed at 3dpt as described above (Figure 2C and 2D). Notably, we found the opposite phenotype as in the KD conditions, namely a significant increase of PAX6+ NSCs at 3dpt of both TGIF2 isoforms, with TGIF2IR showing a stronger effect (Figure 2E). Correspondingly, TUBB3+ neurons significantly decreased with the TGIF2d isoform (Figure 2F). At a later stage (7dpt), PAX6+ NSC numbers were no longer increased; however, TBR2+ NPCs significantly increased upon overexpression of TGIF2IR, with a similar but less pronounced trend for TGIF2d (Figure 2G). However, no significant difference was observed anymore for TUBB3+ neurons at 7dpt (Figure 2H), suggesting that TGIF2 overexpression promotes NSCs and delays neuronal differentiation, but does not block it. This is also consistent with TGIF2 promoting NSC maintenance initially (3dpt), followed by an enhancement of NPC fate at 7dpt.

TGIF2 overexpression in vivo increased neural stem and progenitor cells

To probe the function of TGIF2 and their different isoforms *in vivo*, the same overexpression (OE) constructs were *in utero* electroporated (IUE) into the mouse cortex at E13 (Figure 3A). Three days post-IUE, we examined NSCs by immunostaining, using PAX6 for labelling NSCs and TBR2 for labelling NPCs (Figure 3B-D). Importantly, both TGIF2 constructs resulted in a significant enrichment of PAX6+ NSCs, with no differences observed for TBR2+ cells (Figure 3E), mirroring the effect observed at 3dpt *in vitro* (Figure 2E). As in the control condition, most PAX6+ cells after TGIF2 OE were located in the ventricular zone, corresponding to bin1 when the cortical column is divided into 5 bins and no ectopic PAX6+ or TBR2+ cells were detected in the OE conditions. Immunostaining for the mitotic protein phospho-histone 3 (pH3) revealed a more than two-fold increase in pH3+/GFP+ cells under TGIF2 OE compared to the control, with the TGIF2d isoform showing the stronger, significant effect (Figure S3D, E). These data suggest that both TGIF2 isoforms promote and prolong the NSC state.

To check if the electroporated cells are stuck as NSCs or can still differentiate and migrate, the percent of GFP+ cells in each bin was determined (Figure 3F-I). We noted a trend of increased cell proportions in bins 1 and 2 upon TGIF2IR OE (Figure 3I), consistent with the significant increase in NSCs described above. The shorter isoform, TGIF2d, exhibited similar but generally milder phenotype (Figure 3I). Furthermore, overexpression of TGIF2IR resulted in a significant increase of GFP+ cells in bin 3, which contained mostly NEUROD2+ young neurons (Figure S3F-I). We also observed a concomitant reduction of GFP+ cells (by 24.7%) in the outer most bin 5, where differentiated neurons form the cortical plate (Figure 3H, I). Interestingly, the 2 isoforms differed in the size of the effect, with TGIF2d affecting proliferation stronger and TGIF2IR affecting neuronal differentiation and positioning more. However, both isoforms prolonged the NSC state leading to an increase of immature neurons in bin3 and a decrease of mature neurons in the cortical plate (bin5), highly reminiscent of the *in vitro* phenotype with reduced neuronal numbers.

TGIF2 overexpression reduces cells expressing more mature neuronal differentiation genes shown by scRNA-seq

To investigate transcriptomic changes underlying TGIF2's effect in retaining NSC state, we performed scRNA-seq on GFP+ cells isolated 36 hours post-IUE using FACS (Figure 4A). A total of 51,392 cells were obtained after quality control filtering. Dimensionality reduction via UMAP showed consistent overlap among conditions and replicates (Figure S4A). Cell clusters were identified via the Leiden algorithm (Figure S4B) and annotated based on marker gene expression (Figure 4B, Figure S4D, E). For instance, we identified NSCs, marked by *Pax6*, *Sox2*, and the radial glia marker *Fabp7* (Fatty acid binding protein 7), and NPCs, marked by expression of *Eomes* (also known as TBR2), *Neurog2*, and *Elavl2* (Figure S5E). Cell cycle

phases were inferred through cell cycle marker genes to identify cycling cell populations (Figure S4C).

Comparing TGIF2 expression levels between GFP control (representing endogenous TGIF2 levels) and TGIF2IR conditions revealed that TGIF2IR overexpression was prominent in all stem and progenitor clusters, migrating neurons and in upper layer neurons (UL neurons) (Figure S4F). Using a maturation score (Figure 4C), calculated by average expression of genes related to neuronal maturation (see Methods), we could observe that cells were in a less mature state in TGIF2 conditions, with TGIF2IR being even less mature than TGIF2d. We then conducted DE analysis across cell types, which revealed that more genes were downregulated in TGIF2IR over-expression condition compared to the control (Figure 4D), highlighting a potential repressive role of TGIF2. GO analysis on DE genes within UL_neuron (upper layer neuron) cluster showed general terms for neurogenesis, such as “neuron projection development” and “regulation of cell communication” for both GFP control and TGIF2IR conditions (Figure 4E, F), but TGIF2IR did not acquire terms for a more mature state, such as “axon” and “postsynaptic density” (Figure 4E). Altogether, these data suggest that TGIF2-overexpressing conditions result in transcriptomic downregulation across all cell types, which are in a less mature state of differentiation.

This maturation difference prompted us to conduct pseudotime trajectory analysis. RNA velocity pseudotime analysis, based on spliced and unspliced RNA ratio[27], uncovered that TGIF2IR-expressing cells remained predominantly in early differentiation stages, while GFP control cells having progressed to later stages of differentiation (Figure 4G, Figures S5A-C). This delayed differentiation across pseudotime is particularly evident in NPC 2 and post-mitotic neurons (Figure S5D-F). This is concomitant with higher expression of *Fabp7* in NSCs and lower expression of neuronal genes (*Tubb3, Bcl11b, Stmn2*) in neuronal clusters in the TGIF2IR condition (Figure 4H-J). Additionally, CellRank analysis[28,29] based on RNA velocity assigned 13 macrostates for fate prediction (Figures S5G-R). Interestingly, TGIF2IR overexpression delayed the assignment of upper layer neuron fates and maintained cells more in NPC states (Figures 4K and 4L). The overexpression of the shorter isoform TGIF2d also delayed differentiation, maintaining some cells in NPC states, although the effect was slightly less pronounced than with TGIF2IR (Figure 4M). Surprisingly, there was no upper layer neuronal fate being predicted in TGIF2d condition, but only deep layer neuronal (DL neuron) fate (Figure 4M, Figure S5O-R). Collectively, these analyses unbiasedly confirmed that TGIF2 overexpression downregulates expression of neuronal differentiation genes, and upregulates genes in NSCs, thereby maintaining cells in progenitor states, similar to our findings based on immunostainings (Figures 2J, 3D-F).

TGIF2 binds and negatively regulates neuronal differentiation genes

To better understand the molecular mechanisms by which TGIF2 TFs promote NSC fate and limit neuronal differentiation, we first aimed to identify direct binding targets, focusing on TGIF2IR, as it is the major isoform expressed and generally had stronger effects *in vivo*. Cut&Run analysis was performed after dissecting IUE regions based on GFP at 36 hours post-electroporation, the same timepoint as the scRNA-seq (Figure 5A). This analysis uncovered 10,688 peaks (Figure 5B), with TGIF2IR predominantly binding to intronic (44.57%) and intergenic regions (33.5%), indicating a preference for proximal regulatory elements over promoters (10.23%) (Figure 5C). Motif enrichment analysis identified many important TFs for neurogenesis and neuronal differentiation, such as ASCL1, NEUROD2, NEUROG2, MEIS1,2, and MYC (Figure 5D). Although TGIF2 itself was not among the top enriched motifs, motif scanning analysis using the known TGIF2 motif identified 3,176 occurrences (p-value <0.001) among the peaks (Table S14). It is worth noting that the known TGIF2 motif was derived from ChIP-seq data in mouse embryonic stem cells, which may differ from the motif in neural stem and progenitor cells.

Annotation of the nearest genes to the identified peaks revealed 5,783 target genes (Table S15). GO analysis of these targets showed significant enrichment in terms such as “neurogenesis,” "postsynapse,” “dendrite,” and "cell projection morphogenesis," all of which are crucial processes in neurogenesis, supporting cell migration and synaptic maturation (Figure 5E). In addition, we also found TGIF2 targeting many RNA-binding and splicing factors (e.g. *Stau1/2*, *Pum1/2*, *Ptbp2*, *Snrnps*) and signaling mediators, such as *Tle4*, *Tcf7l1* and *Smad4*. Further examination of peak distribution using GREAT[30] identified genes highly regulated by TGIF2IR (Figure 5F, Table S16). For instance, *Auts2* and *Nfia* were associated with around 20 peaks across their gene bodies, indicating extensive regulation by TGIF2IR (Figure 5G). These highly regulated genes are associated with “H4 histone acetyltransferase complex” (*Kansl1*, *Epc1*, *Mllt3*), “growth cone” (*Dcc*, *Auts2*, *Myh10*), and “chromatin” (*Brd4*, *Smarcc1*, *Arid1b*) (Table S17), highlighting TGIF2 as an upstream regulator of chromatin factors and neuronal differentiation genes.

In order to determine the importance of these direct targets, we performed two analyses: (1) overlaying them with genes regulated by TGIF2 in scRNA-seq and (2) using RegVelo[31] to explore the transcriptional networks influenced by TGIF2. For the first analysis, we overlapped annotated genes from TGIF2 Cut&Run peaks with the DEGs between TGIF2 and GFP conditions from scRNA-seq across all cell types (Figure 5H). In general, there were more overlaps in the downregulated genes by TGIF2, constituting more than half of the DEGs in most cell types, suggesting TGIF2’s function as a transcriptional repressor. Focusing on the NSCs, the downregulated genes were enriched in GO terms such as “neuron differentiation” and “neurogenesis” (Figure 5I), the central regulated terms of TGIF2 (Figure 5E).

To understand this regulation by TGIF2 further, we used RegVelo, which relied our bulk ATAC-seq data from E14 cortical NSCs and TGIF2IR Cut&Run data for building a *priori* Gene Regulatory Network (GRN) to perform dynamic inference on scRNA-seq GFP control dataset (Figure 5J). This GRN revealed a network of targets negatively regulated by TGIF2 and highlighted “neuron fate commitment” and “neuron differentiation” as key regulated terms. Among these RegVelo-refined and negatively regulated targets, Fezf2 and Bcl11b are two critical TFs for DL neuron fate, suggesting TGIF2 may have a repressive role on DL neurons production. Indeed, when we applied weighted simulations in RegVelo to mimic TGIF2 OE, TGIF2 weights promoted NSC and UL neuron fates, simultaneously depleting DL neuron progeny (Figure 5K). Also, the more added weights we simulated, the bigger the enrichment in NSC fate, resonating with the phenotype *in vitro* and *in vivo* (Figure 2 and Figure 3).

TGIF2 interacts with HDAC1/2 and SIN3 co-repressor complex

Seeing that TGIF2 downregulates neuronal differentiation genes and directly binds to neurogenesis associated genes, we examined if it acts as a transcriptional repressor during neurogenesis. To determine its interaction with possible repressors, we performed mass spectrometry after co-immunoprecipitation (co-IP-MS) of FLAG-tagged TGIF2IR transfected in P19 cells in two independent replicates (Figure 6A). The results (LFQ intensity ratio more than 3-fold in TGIF2IR compared to GFP; Table S18) revealed that TGIF2IR robustly interacts with components of the SIN3A co-repressor complex, including HDAC1/2[32] and RBBP4/7, as well as lamina-associated proteins such as BANF1 and TMPO (as known as LAP2), which are known to mediate gene repression through chromatin localization[33]. Additionally, we identified interactors involved in cell cycle regulation (RPA1/2/3) and metabolism (PARP1, SSBP1) (Figure 6B). These findings confirm that TGIF2 associates with repressor proteins, specifically within the SIN3A co-repressor complex, consistent with previous data[32] thereby further supporting its role as a transcriptional repressor.

TGIF2 function is dependent on its repressor domain and phosphorylation

TGIF2 has been reported to exhibit repressor activity in various cell types, particularly in cancer cells[20,26], but has also been reported to act as a co-activator[34]. To functionally manipulate repressor and activator functions of TGIF2, we first aimed to identify the repressor domain within TGIF2, utilizing sequence alignment with its paralog, TGIF1, which is better characterized[35]. This alignment revealed that the SIN3A-interacting domain (SID), interacting with the SIN3A co-repressor complex in TGIF1 and suggested to maintain pluripotency[35,36], is conserved in TGIF2, in line with our findings in co-IP-MS.

To explore the function of the SID, we replaced it either by a more potent repressor domain, KRAB, or by an activator domain, VP64 (Figure 6D). Overexpression of TGIF2IR-KRAB in E12

dissociated cortical cell cultures resulted in an even stronger phenotype than TGIF2IR, showing a significantly higher proportion of PAX6+ NSCs (32.8%), compared to TGIF2IR (17.2%) and control (8.7%) (Figure 6E-F). This was accompanied by a substantial reduction in the neuronal population in the TGIF2IR-KRAB condition (Figure 6G). Conversely, the overexpression of TGIF2IR-VP64 led to a drastic decrease in progenitors (Figure 6E-F), with over 90% of cells differentiating into neurons (Figure 6G), thus indicating that activating TGIF2-repressed targets strongly promotes neuronal differentiation. These data suggest that TGIF2 represses neuronal differentiation genes and thereby promotes NSC fate.

Protein structure prediction of TGIF2IR using AlphaFold[37] suggested MAPK phosphorylation sites potentially linking the DNA-binding homeodomain to the SID repressor domain (Figure 6C). Phosphorylation has been shown to regulate TGIF2 function in other contexts, particularly cancer cells[20]. To examine the role of phosphorylation of TGIF2IR in neurogenesis, we generated a phosphorylation-deficient TGIF2IR mutant by substituting the two MAPK threonine residues with glycine (TGIF2IR_pp) (Figure 6D). Overexpression of this phospho-resistant TGIF2 in E12 cortical cultures did not affect NSC maintenance or neuronal differentiation (Figure 6E-G), suggesting that TGIF2's function in promoting NSCs is mediated by the phosphorylated form.

Collectively, these findings demonstrate that phosphorylated TGIF2 represses neurogenesis-related genes and retains NSCs and later NPCs by interacting with SIN3A co-repressor complex (Figure 6H).

A mutation in SID overturns the effect of TGIF2 and unravels interactors essential for TGIF2 function

Given the critical role of the SID in TGIF2 function, we introduced a point mutation within SID (A210V), referred to as TGIF2IRmut (Figure S6A). Overexpression of this TGIF2IRmut in E12 cortical cell cultures lead to an increase of TUBB3+ neurons promoting differentiation (Figure S6B-D). This suggested that the mutation in the SID domain abrogates the normal repressor function of TGIF2. Indeed, the effects obtained with the TGIF2IRmut were very similar to the TGIF2 KD (Figure 2F). To explore if this is also the case *in vivo*, we employed the same IUE paradigm as described above (Figure 3A). Overexpression of TGIF2IRmut resulted in a phenotype opposite to TGIF2IRwt (Figures S6E and S6F), as more cells were found in bin5, corresponding to the cortical plate, where most mature neurons are located (Figure S6G). Indeed, morphology and immunostaining confirmed that these are neurons, especially UL neurons (Figure S6H) supporting that TGIF2IRmut OE causes faster neuronal differentiation also *in vivo*.

To get a comprehensive idea of how gene expression is changed by the TGIF2IRmut, we performed scRNA-seq and Cut&Run experiments as described above. Using Cut&Run, we

observed a surprisingly large number of targets bound by TGIF2IRwt no longer detected in TGIF2IRmut (Figures S6I-J). This included *Arid4b* (Figure S6K), a component of the SIN3A complex that interacts with the SID domain of canonical TGIF2IRwt (Figure 6B). To understand how this loss of binding affects gene regulation, we overlaid genes aberrantly upregulated in TGIF2IRmut (Table S19) with the peaks bound by TGIF2IRwt, but not the TGIF2IRmut (Figure S6L). This showed an interesting signature revealing *Gatad2* as differentially bound and regulated (Table S20). This factor is part of the NURD complex that regulates neuronal activity genes[38]. In addition, mutations of *Gatad2* cause delayed neuronal differentiation in patients, highlighting *Gatad2* as a possible key down-stream effector[39]. We further found stem cell factors, such as *Vcam1* and *Fabp7* affected in their expression (Table S20), alongside with many genes involved in translation and proliferation. Thus, lack of DNA-binding and target gene regulation leads to the loss of TGIF2 function upon the mutation in the SID domain.

Next, we aimed to explore, if also the interactome of this TGIF2IRmut would differ from the TGIF2IRwt in P19 cells (Figure S6M). Interestingly, interactome changes were less abundant than those seen in Cut&Run, revealing the loss of only 7 protein interactions for the TGIF2IRmut compared to TGIF2IRwt (Figure S6N). Amongst them we observed again ARID4B. Thus, *Arid4b* is not only a direct target of TGIF2IRwt, that is no longer bound by TGIF2IRmut, but also an interactor of TGIF2IRwt.

As both the Cut&Run and interactome pointed to a key role of ARID4B involved in TGIF2 function, we examined if ARID4B is essential for the function of TGIF2IRwt. Using the same E12 assay as described above, we transfected either an shRNA targeting the open reading frame of *Arid4b* (Figure S8O), following a GFP reporter (pCAG-GFP-shArid4b), or a non-targeting control shRNA (pCAG-GFP-shCtrl), either with the GFP control (pCAG-GFP) or with TGIF2IRwt (pCAG-TGIF2IRwt-IRES-GFP) vectors. KD of *Arid4b* abolished the effect of TGIF2IRwt overexpression in retaining PAX6+ NSCs (Figure 6I), confirming our hypothesis that ARID4B interaction is necessary for TGIF2IR's repressor function. We have thus identified a crucial interactor and down-stream target of TGIF2 involved in its key functions in neurogenesis.

TGIF2 as major regulator of primed neuronal lineage genes in NSCs

Given the function of TGIF2 in repressing neuronal differentiation genes in NSCs, we considered that TGIF2 could be involved in lineage priming by restraining the expression of neuronal genes that may be accessible already in NSCs. In other stem cell systems, lineage priming involves the opening of regulatory elements for progeny-specific genes, while restraining their expression levels[2]. However, the mechanisms underlying neurogenic priming in NSCs are still poorly understood[3,40]. To address this, we stained for PSA-NCAM to isolate neurons by FACS from the E14 cerebral cortex (Figure 7A) and performed RNA-seq to identify

differential gene expression between neurons and NSCs. Among 5835 DEGs higher in neurons than NSCs (at FDR 1%), 4984 (85.4%) displayed open chromatin accessibility in our ATAC-seq of cortical NSCs already at E14, thus fitting the definition of priming with being accessible but lower expressed than later in the lineage. Focusing on the genes whose regulatory sites experienced significantly reduced accessibility in NSCs at the end of neurogenesis (E18), we identified 433 genes, which we named as neurogenic priming genes (Figure 7B, Table S21). Notably, 225 of these genes (51.9%) were direct targets of TGIF2, as determined by our Cut&Run data (Figure 7B, Table S22). Both the neurogenic priming genes and the TGIF2-regulated subset were enriched for GO terms such as "axonogenesis" and "neuron differentiation" (Figure 7C and 7D). Our data revealed that TGIF2 binds directly to these accessible chromatin regions of priming genes in NSCs, as exemplified in Figure 7E. To assess if the enrichment of TGIF2 targets in neurogenic priming genes is significant, we generated 100,000 permutations of equal-sized, randomly selected gene sets that are not TGIF2 targets. Remarkably, no other gene set exhibited more than 77 overlapping genes with the neurogenic priming gene set (Figure 7F), underscoring the specificity and importance of TGIF2's regulatory role on neurogenic priming. Together, these findings identify TGIF2 as not only a novel and non-patterned regulator of neurogenesis, but also a major regulator of neurogenic priming in NSCs.

Discussion

Here we provide a comprehensive resource profiling RNA- and ATAC-seq data in NSCs across distinct brain regions, and timepoints—at the peak of neurogenesis and onset of gliogenesis, with one region continuing neurogenesis. This dataset not only enables the identification of novel pan-neurogenic regulators, exemplified by the hundreds of candidates listed in Table S11. Among these, we focused on TGIF2, showcasing its critical role in regulating NSC fate and neurogenic priming. Beyond TGIF2, our dataset also provides insights into chromatin and epigenetic regulatory dynamics during this fundamental switch in lineage transition from neurogenesis to gliogenesis. Notably, the differential chromatin regulators between these two stages provide a valuable entry point towards a better understanding of this transition across regions. To facilitate further exploration of this dataset, a Shiny App will be made publicly available.

Our focus on TGIF2 stemmed from its expression pattern correlating with neurogenesis across regions and its enriched motif within neurogenesis-restricted open chromatin regions identified by ATAC-seq. We showed TGIF2 as a key regulator of NSC maintenance and neuronal differentiation by knock-down and overexpression experiments. TGIF2 functions as a molecular "brake" on neurogenesis programs, actively gatekeeping NSC and later NPC states, thereby interfering with premature differentiation and fine-tuning the timing of cortical development. By integrating single-cell transcriptomics, Cut&Run, proteomics, and functional

assays of fusion and mutant proteins, we demonstrated that TGIF2 maintains NSC fate not through its canonical role in antagonizing TGFβ signaling[19], but rather by repressing neuronal differentiation genes targeted by key neurogenic regulators. This function allowed us to discover that TGIF2 is a major regulator of neurogenic priming.

Lineage priming can occur via transcriptional priming, where genes defining the later lineage are already expressed in stem or progenitor cells at low mRNA levels without protein translation[3], or via epigenetic priming, where regulatory sites of these genes are open and sometimes epigenetically "poised" or "primed" by specific marks[2]. Here we considered priming genes in NSCs as those expressed significantly higher in neurons, but already with open chromatin in NSCs at E14. Remarkably, TGIF2 bound more than half of them. As it is a pan-neurogenic factor expressed not only in LGE and cortex NSCs, but throughout CNS regions[41], we would propose TGIF2 functions as a central regulator of neurogenic priming in a wider context. Supporting the wider relevance of our data also across species, RNA-seq data from the human cortex also revealed that TGIF2 expression steeply declines at gliogenesis stages (post-conceptual week 20)[42]. Thus, TGIF2 represents a novel regulator of neurogenesis and neurogenic priming, complementing the translational repression previously described[4]. TGIF2-mediated transcriptional repression allows primed NSCs to remain poised for differentiation cues and respond in a timely manner during the dynamic changes in neurogenesis. By maintaining basal expression levels of neuronal differentiation genes, TGIF2 ensures NSCs are primed for lineage commitment without undergoing premature differentiation.

In this regard, it is also important to mention that TGIF2 itself is regulated by signaling pathways, namely MAPK/ERK signaling induced phosphorylation, as shown before in cancer cells[20,43]. Mutating the two MAP kinase phosphorylation sites in TGIF2 completely abolished its ability to promote NSC fate. Interestingly, proteomic analysis of human iPSC-derived NSCs and neurons[44] revealed that TGIF2 is phosphorylated only in NSCs, but not in neurons, while its total protein levels remain unchanged (data not shown). Indeed, the activation of MAPK/ERK is required for NSC proliferation, and has to decline for neuronal differentiation[45,46]. ERK activity is also suggested to be a gating mechanism for neural differentiation, as inhibition of ERK induced more accessible chromatin and precocious transcription of neural genes in spinal cord precursors[48]. These findings suggest that TGIF2's activity is developmentally regulated by endogenous signaling pathways, such as MAPK/ERK signaling[20,43], modulating TGIF2's interaction with the SIN3A complex.

Notably, TGIF2 binding sites determined by Cut&Run are enriched with motifs for proneural TFs, such as ASCL1 and NEUROG2, as well as NEUROD2, MEIS1 and 2, which are known to promote neurogenesis and neuronal differentiation in both developmental as well as adult contexts[47,49–52]. This suggests that TGIF2 occupies neuronal differentiation gene loci to repress targets of and/or sterically block the access of proneural TFs, thereby inhibiting premature

neural differentiation. This interplay between TGIF2 and neurogenic TFs may serve as a checkpoint to ensure the proper timing of neural differentiation during cortical development. Additionally, among the genes repressed by TGIF2, we observed significant regulation of the nuclear factor I (NFI) family of TFs, including *Nfia*, *Nfib*, and *Nfix*, which are known to function synergistically[53]. Double knockout of *Nfia* and *Nfib* has been shown to cause ventricular enlargement from progenitor proliferation and reduced neural differentiation[54], a phenotype resembling TGIF2 overexpression–increased neural stem/progenitor cells and delayed differentiation. This finding places TGIF2 upstream of NFI family members in the regulatory hierarchy, functioning as a negative regulator of neuronal differentiation promoted by these TFs.

TGIF2 also regulates various chromatin factors and histone modifiers, including *Arid1b*, *Arid4b*, and the histone methyltransferases/demethylases *Setbp1*, *Kdm1a*, and *Kdm7a*. Histone modifications, such as H3K36 methylation and H3K4 methylation in the context of bivalent marks, have been implicated in establishing epigenetically primed and "poised" transcriptional states[55]. Thus, TGIF2's regulatory influence may extend beyond direct transcriptional repression, potentially contributing to neurogenic priming through additional epigenetic mechanisms.

Interactome analysis further determined factors that cooperate with TGIF2 to mediate repression, such as SIN3A and NURD repressor complexes. Functional assays using the TGIF2-KRAB and TGIF2-VP64 fusion proteins further reinforced its role as a transcriptional repressor, as shown before[20,32]. SIN3A, in particular, regulates diverse cellular processes such as cell cycle, differentiation, and development[56,57], and has been implicated in neurological disorders such as intellectual disability , as well as cancer progression[59,60], some of the previously described roles of TGIF2[19,20]. TGIF2 appears to guide the SIN3A complex to specific DNA targets, restricting the expression of primed genes and fine-tuning the transcriptional regulation of neurogenesis and neural differentiation. Additionally, we identified ARID4B, a component of the SIN3A complex, as a critical TGIF2 interactor as *Arid4b* KD abolished TGIF2 function. In mouse embryonic stem cells, *Arid4b* KD led to downregulation of differentiation programs of mesoderm and endoderm fate[61]. This is interesting in light of *Arid4b* also being a target of TGIF2 and hence reduced in expression by TGIF2. *Arid4b* KD in E12 cortex cells shows a trend of slight increase in Pax6+ NSCs compared to the control, although mild, but in the same direction of TGIF2 overexpression. Altogether, this indicates a negative feedback loop–TGIF2 interacts with ARID4B, and this complex represses the *Arid4b* transcript–as a molecular pathway regulating neural differentiation programs. Also, *Arid4b* KD was shown to increase globally H3K27me3 repressive histone marks[61]. The repressive histone mark H3K27me3 is particularly enriched at genes involved in neuronal maturation, serving as an epigenetic barrier during cortical development to ensure a protracted neurogenesis in human[62].

This resonates with TGIF2 overexpression phenotype that cells remain longer in progenitor state and a delayed neural differentiation.

It is worth noting that TGIF2's function in the developing nervous system differs significantly from its role in other tissues. Unlike its reported interactions with SMAD proteins to regulate TGFβ target genes in other contexts, TGIF2 was not found to interact with SMAD proteins in this study. Additionally, while in many cancer cells TGIF2 promotes epithelial-mesenchymal transition (EMT), e.g. in lung adenocarcinoma (LUAD) cells[20], it maintains the epithelial-like NSCs in the developing cortex as shown here. Therefore, TGIF2's role in the nervous system exhibits significant mechanistic differences compared to cancer cells and endoderm-derived tissues, where it has been more extensively examined[22,26]. Most importantly, it was never characterized in priming and no major factors regulating neurogenic priming were previously known.

In summary, our findings establish TGIF2 as a master regulator of neurogenic priming and NSC fate across regions, using transcriptional repression to ensure the precise timing of cortical development.

Methods

RNA-seq and ATAC-seq libraries preparation

Wild type C57BL/6J embryos at E14 and E18 were used for the RNA sequencing experiments, with tissue of one litter/mother being pooled and considered one biological replicate. Brains were dissected in 1× HBSS (Gibco, cat. no. 14025) with 10 mM HEPES (Gibco, cat. no. 15630). Lateral cortex from the mediolateral to the cortex-LGE border, and LGE without overlying ventrolateral cortex, were dissected and centrifuged at 1000 rpm, 4 °C for five minutes. Dissection buffer was aspirated, and tissue was enzymatically dissociated with 1 ml of 0.05 % Trypsin/EDTA (Gibco, cat. no. 25300) for 15 minutes at 37 °C. Digestion was inhibited by adding 2 ml DMEM (Gibco, cat. no. 61965) with 10 % FBS (PAN Biotech, cat. no. P30-3302) and tissue was further mechanically dissociated with a fire-polished glass Pasteur pipette coated with DMEM + 10% FBS to obtain a single-cell suspension. The suspension was centrifuged at 1000 rpm, 4 °C for 5 minutes, the supernatant aspirated and the cells resuspended in 1× Staining Solution (1x HBSS, 1% Glucose, 1M HEPES, 1% FBS, 0.1% w/v NaN_3, 1mM EDTA and DMEM-F12). The cell suspension was stained with the pre-absorbed antibody mCD133-PE at 1:500 dilution (Anti-Mouse-CD133-PE [13A4], eBioscience/Invitrogen, cat. no. 12-1331-82). A corresponding isotype control antibody (Mouse IgM-APC, Miltenyi Biotec, cat. no. 130-093-176) was added to an isotype control sample in the same dilution. Cells were incubated at 4 °C in the dark for 25 minutes, then DAPI (1:1000 dilution of 1 mg/ml stock; Sigma-Aldrich, cat. no. D9542) was added followed by another 5 minutes of incubation. To wash the cells, the suspension was filled up to 10 ml with PBS (Gibco, cat. no. 14190) and centrifuged at 1000 rpm, 4 °C for 5 minutes. Cells were resuspended in PBS and filtered through a cell strainer (pluriStrainer Mini 40 µm, PluriSelect, cat. no. 43-10040-60) into suitable sample tubes (Falcon™ Round Bottom Polypropylene Test Tubes with Cap, Falcon, cat. no. 352063).

Cells were sorted on a FACSAria™ III Cell Sorter (BD Biosciences) with FACSDiva software (version 6.1.3, BD Biosciences). To separate the populations the first gate was set to separate small debris (low FSC) and dead or damaged cells, which were DAPI+ (high 450/40 signal). The second gate was set to remove doublets or cell aggregates by FSC-area/FSC-width. The third gate separated the stained populations by the laser lines 582/15 for PE, with the gate set so that max. 0.1 % of the parent population in the isotype control was detected as single or double positive. Sorted cells were collected in PBS and centrifuged at 1000 rpm, 4 °C for 10 minutes. The supernatant was aspirated, and cells were immediately lysed in RNA extraction buffer.

For the RNA-seq libraries, total RNA extraction was performed with the PicoPure™ RNA Isolation Kit (Applied Biosystems, cat. no. KIT0204) according to the manufacturer's protocol with on-column DNase digestion (On-Column DNase I digestion set, Sigma-Aldrich, cat. no.

DNASE70). RNA concentration and quality were evaluated on the Bioanalyzer (Model 2100, Agilent) using the RNA 6000 Pico Kit (Agilent, cat. no. 5067-1513) according to the manufacturer's protocol. Samples with an RNA Integrity number (RIN) <8.0 were excluded from library preparation. First-strand cDNA was prepared from 2 ng RNA per sample with the SmartSeq v4 Ultra Low Input RNA Kit for Sequencing (TaKaRa/Clontech, cat. no. 634897) according to the manufacturer's instructions. Number of amplification cycles for each sample was deter- mined with a side qRT-PCR reaction performed after the first 4 amplification cycles to avoid over-amplification bias. With this, the number of required total amplification cycles for each sample corresponded to the cycle number at ¼ of the maximum fluorescence signal (Rn).

The amplified cDNA was purified using AMPure XP magnetic beads (Beckmann Coulter, cat. no. QT650) and quality and quantity analyzed by Bioanalyzer (High Sensitivity DNA Kit, Agilent, cat. no. 5067-4626) and Qubit Assay (Qubit™ dsDNA HS Assay Kit and tubes, Invitrogen, cat. nos. Q32854/Q32856). Purified cDNA was fragmented by ultrasonic shearing on the Covaris AFA S220 system using corresponding tubes (microtube AFA Fiber Pre-Slit Snap-Cap 6x16mm, Covaris, cat. no. 520045), resulting in approximately 200 bp – 500 bp long fragments that were purified by ethanol precipitation. Samples were evaluated again on the Bioanalyzer (HS DNA assay) before proceeding to the library preparation with the MicroPlex Library Preparation Kit v2 (Diagenode, cat. no. C05010014) according to the manufacturer's instructions, using 10 ng of cDNA per sample. Following the library amplification, cDNA concentration was verified by Qubit assay and the libraries were purified over AMPure XP magnetic beads. Quality and quantity of these final libraries was evaluated by Bioanalyzer HS DNA assay and samples were multiplexed at 5nM each. Next generation sequencing was performed on an Illumina HiSeq 4000system with 100-bp paired-end deep sequencing.

For the ATAC-seq libraries, nuclei were isolated from 50,000 cells using a cell lysis buffer containing Tris-HCl 1M, NaCl 5M, MgCl2 1M, 10% NP40, 10% Tween-20 and 2% Digitonin. They were subsequently resuspended in transposition mixture containing the transposase enzyme, 2% digitonin and 10% Tween-20 and incubated for 30 minutes at 37^{o}C. After the incubation the samples were immediately put on ice and DNA was purified with the MinElute Reaction Cleanup kit (Qiagen, #28204). The transposed DNA was PCR amplified with the NEBNext High-Fidelity 2x PCR Master Mix (NEB, #M0541S). The number of cycles was determined with a qRT-PCR using the SensiMix SYBR No-ROX 2x Master Mix (Bioline, #QT650) as the number of cycles that corresponds to ¼ of the maximum fluorescence. The amplified libraries were purified and the quality was assessed with a High Sensitivity DNA Chip (Agilent, #5067-4626). Size selection between 100bp and 600bp was performed with AMPure beads (BeckmannCoulter, #A63881) and libraries were pooled and sequenced on an Illumina HiSeq 4000system with 100-bp paired-end deep sequencing.

RNA-seq analysis

The quality of sequencing data was analyzed with FastQC v0.11.4[63] and adapter trimming was performed with cutadapt v1.11[64]. Reads were aligned with the mouse reference genome (mm39) using STAR v2.6.0a[65]. Afterwards, reads were deduplicated and gene expression was quantified with featureCounts v1.6.4[66]. The subsequent analysis was performed in R version 4.4.1[67]. Genes with less than 10 counts across all samples were excluded. The expression data was normalized and transformed using the vst function of DESeq2 v1.44.0[68] for plotting and outliers' analysis. To identify outliers, we performed a principal component analysis (PCA). Samples with a distance of more than 2.5 standard deviations from the mean in the first principal component were excluded (no outliers were detected). Differential expression (DE) analysis was performed using DESeq2 v1.44.0[68]. DE analysis for each comparison was done separately. We tested for DE with DESeq2 using the Wald test and reported the genes with a false discovery rate (FDR) below 1% as significant. Overrepresentation analysis for GO-Biological processes, Molecular pathways and Cellular compartment was done using ClusterProfiler v4.12.6. As background we used all genes on our dataset (22,125 genes). For all analyses, we used an FDR cutoff of 1% as significant threshold. Grouped semantic representation analysis was used to plot the significantly enriched GO terms. For this we used hierarchical clustering with the "Ward.D2" clustering method and Jaccard similarities. All data were plotted using the ggplot2 v3.5.1 package.

For identification of transcription factors, we used the GO term GO:0140110. For identification of chromatin remodelers, we used the GO terms: GO:0034724, GO:0031497, GO:0031498, GO:0034401, GO:0006338, GO:0016569, GO:0090202, GO:0070828, GO:0034728, GO:0006342.

ATAC-seq analysis

FastQC was used to assess initial data quality. Reads were trimmed using *trim-galore* with parameter *--nextera* after contamination of Nextera Transposase Sequence was found in the reads. After trimming, reads were aligned to mm39 reference genome using *bwa-mem.* The *ATACseqQC* R-package tutorial was followed to assess data quality and to shift reads by 5bp as recommended[69]. For each individual sample, peaks were called using MACS3 with parameters *-f BAMPE -g mm -q 0.01*[70]. Differential openness of peaks between either time points per tissue or tissues per time point was identified using *DiffBind*with parameter *peakFormat="narrow"* when loading the samples. *Homer* was used to find motifs in the resulting differentially open peaks. *Homer* was also used for labeling the differential or consensus peaks by genes in proximity. MonaLisa was used for motif enrichment analysis on differential or consensus peaks[71]. *ShinyGO 0.80*[72] was used to assess pathway enrichment of the genes in proximity to peaks. Overlaps between peaks were identified by the

function*subsetByOverlap.* From the 44 neurogenic fate determinants of Figure 1C, five had known binding motifs: *Atf3*, *Etv6*, *Mafk*, *Mycn* and *Tgif2*.

Plasmids

TGIF2 cDNA isoforms plasmids were obtained from as a kind gift from previously described[26]. All plasmids for expression were cloned into a Gateway (Invitrogen) form of pCAG-IRES-GFP (kind gift of Paolo Malatesta) through pENTR1a vector. TGIF2 cDNA were amplified by PCR with primers containing triple FLAG sequence for inserting the FLAG tag at N-terminus of TGIF2 and cloned into the pCAG plasmid via Gibson Assembly. shRNA plasmids were designed using Invitrogen Block-iT RNA designer and ordered as oligos from Eurofins, then ligated to pENTR1a vector with a GFP reporter, which was finally cloned into a pCAG destination vector via Gateway LR clonase.

Mice

The animals were housed in the Core Facility Animal Models (CAM), Biomedical Center (BMC), Faculty of Medicine, LMU Munich. They were maintained under specified pathogen-free conditions and housed in groups of 2-3 animals in individually ventilated cage systems with a 12 h/12 h light/dark cycle. C57BL/6J mice (Charles River Laboratories; Sulzfeld, Germany) were utilized for this study, and all animals undergoing in utero electroporation were females aged between 3 and 6 months. Embryonic day 0 (E0) was designated as the day of vaginal plug detection. Mice had free access to water and standard rodent chow (Altromin, 1310M). Experimental procedures were performed in accordance with animal welfare policies and approved by the Government of Upper Bavaria (Germany).

Anesthesia

For surgical procedures, mice were anesthetized via intraperitoneal injection of a solution containing Fentanyl (0.05 mg/kg), Midazolam (5 mg/kg), and Medetomidine (0.5 mg/kg). Anesthesia was terminated with a subcutaneous injection of a solution comprising Buprenorphine (0.1 mg/kg), Atipamezole (2.5 mg/kg), and Flumazenil (0.5 mg/kg).

In Utero Electroporation

Pregnant dams at E13 were anesthetized and operated on according to established procedures[44]. Briefly, endotoxin-free plasmids at 0.5 to 0.7 µg/µl, controlled for molar ratio across conditions, were diluted in 0.9% NaCl and mixed with FastGreen FCF dye. Subsequently, 1 µl of this mixture was injected into the lateral ventricle of embryos at E13 within anesthetized C57BL/6J mice. Embryonic brains were harvested at 3 days post-electroporation and fixed using 4% paraformaldehyde (PFA) in 1× PBS for durations of 4 hours.

Analysis involved embryos obtained from at least two female mice, with quantification carried out on two to three coronal sections from three to five embryos.

Cell culture

Cerebral cortices from C57BL/6J E12 mouse embryos were dissected in ice-cold Hanks' balanced salt solution buffered with 10mM HEPES (both from Life Technologies). Cells were enzymatically dissociated with 0.05% Trypsin and mechanically triturated with a Pasteur pipette to obtain a single-cell suspension. These cells were then seeded in poly-d-lysine-coated coverslips in 24-well plates at 350,000 – 500,000 cells per well in DMEM-GlutaMAX supplemented with 10% FBS and 1% Pen/Strep and incubated at 37°C with 5% CO_2. After 24 hours, 2% B27-supplemented DMEM-GlutaMAX with 1% Pen/Strep were added at 1:1 ratio. Three days or 7 days post transfection, cells were fixed with 4% PFA for 10 min at room temperature.

For transfection experiments, cells were plated and allowed to adhere for 2-3 hours before transfection with either 0.5 to 0.7 µg of plasmids controlled for molar ratio, or 25nM siRNA Tgif2 mouse (ON-TARGETplus SMARTpool) using Lipofectamine™ 2000 following the manufacturer's guidelines (Invitrogen™). When shRNAs were co-transfected with GFP or TGIF2IR overexpression plasmids, equal molarity ratio was controlled.

Immunohistochemistry and Immunocytochemistry

Sections underwent triple washes with 1× PBS at room temperature before being incubated overnight at 4°C with primary antibody in a blocking solution, composed of 10% Normal Goat Serum and 0.5% Triton-X100 in 1× PBS. Cells were first incubated in blocking solution for 1 hour at room temperature, followed by overnight incubation with primary antibody. After triple wash with 1× PBS at room temperature, cells and sections were stained with secondary antibodies diluted in blocking solution for 1 hour at room temperature. Nuclei were visualized using 0.5µg/ml 4,6-diamidino-2-phenylindole (DAPI, Sigma-Aldrich). Finally, immunostained sections and cells were examined using a Zeiss confocal microscope. The list of antibodies utilized in the experiments is provided for reference.

scRNA-seq library prepration

36 hours after IUE, cortices were dissected in ice-cold Hanks' balanced salt solution buffered with 10 mM HEPES (both from Life Technologies) under florescent microscope to enrich for electroporated region. The cells were dissociated to arrive at single cell suspension with Neural Tissue Dissociation Kit(P) (Milteny, #130-092-628) and red blood cell removal solution (Miltenyi, #130-094-183) following manufacture's protocol. The cells were passed through a 40µm cell strainer and placed on ice for FACS to further isolate electroporate cells.

FACS sorting was performed at a FACSAria III (BD Biosciences) in FACSFlow sheath fluid (BD Biosciences), with a nozzle diameter of 100 µm. Debris and aggregated cells were gated out by forward and side scatter, respectively. Single cells were selected by FSC-W/FSC-A. Gating for GFP fluorescence was done using non-electroporated cortices.

FAC-sorted cells were multiplexed using Cell Multiplexing Oligo Labeling and loaded onto 10X Chromium chip following Single Cell 3' v3.1 (Dual Index) protocols with Feature Barcode technology for Cell Multiplexing (CG000388). The library was sequenced with one Novaseq 6000 S2 flowcell to reach 30,000 reads per cell for gene expression library and 5,000 reads per cell for multiplexing library, which was then aligned and demultiplexed using cellranger multi pipeline.

scRNA-seq analysis

The analysis followed Scanpy's[73] tutorial, starting with preprocessing of raw sequencing data to filter out low-quality cells (counts per cell = 1100-33000, minimal genes per cell = 700) with high mitochondrial content (5% cutoff), followed by log transformation normalization. Dimensionality reduction using principal component analysis (PCA) and Uniform Manifold Approximation and Projection (UMAP) was performed to visualize cell-to-cell relationships. Leiden clustering identified distinct cell populations based on gene expression profiles, and marker genes were determined to characterize each cluster's cell types. Maturation score included genes *Neurog2*, *Dcx*, *Tubb3*, *Elavl4*, *Map2*, *Stmn2*, *Rbfox3*, *Syt1*, *Nefl*, *Syn1*, *Syp*, *Camk2a*, Bsn. DE between TGIF2IRwt and GFP was analyzed using built-in "rank genes" function in Scanpy with Wilcoxon rank-sum test, and associated GO term was analyzed using Shiny GO 0.80[72]. DE between TGIF2IRmut and GFP was analyzed using pseudobulk and DESeq2 v1.44.0[68] to be comparable to the bulk Cut&Run. CellRank analysis based on RNA velocity was conducted followed CellRank's tutorial[28,29].

Cleavage under targets and release using nuclease (CUT&RUN) and library preparation

Electroporated embryos underwent the same procedure as described in scRNA-seq section until before FACS. Cut&Run was performed using CUT&RUN assay kit (Cell Signaling Technologies, 86652) according to the manufacturer's instructions. Briefly, 250,000 cells per reaction were collected and bound to Concanavalin A Magnetic beads. Cells were permeabilized and incubated with 1 µg of primary antibody against FLAG (DYKDDDDK Tag (D6W5B), rabbit, Cell Signalling) per sample overnight at 4°C. The rabbit (DA1E) mAb IgG XP® Isotype Control antibody was used as IgG control. Subsequently, cells were incubated with pAG-MNase for 1 h at 4°C. pAG-MNase was activated by adding calcium chloride and incubation at 4°C for 30 minutes. Stop buffer (Cell Signaling Technologies) was added to each

sample to stop the reaction. DNA was purified using phenol/chloroform extraction and ethanol precipitation as described in the manufacturer's protocol.

DNA sequencing libraries were generated using the SimpleChIP® ChIP-seq DNA Library Prep Kit for Illumina (Cell Signaling Technologies, 56795) and SimpleChIP® ChIP-seq Multiplex Oligos for Illumina® (Dual Index Primers, Cell Signaling Technologies, 46538) following the manufacturer's instructions specifically for CUT&RUN Assay kit protocol. Briefly, 5ng of DNA was used for all CUT&RUN and IgG control samples. DNA ends were ligated with adaptors and amplified using PCR and Dual Index primers for Illumina® (Cell Signaling Technologies, 47538). All clean-up steps were performed with 1.1× volume of SPRIselect® beads to increase the capture of smaller DNA fragments. Generated libraries were pooled and sequenced using 2 × 75 bp paired-end sequencing strategy on an Illumina® NextSeq550 sequencer.

Cut&Run analysis

Sequenced reads were aligned to the mm39 genome using Bowtie2[74]. Peak calling was performed using the MACS3 pipeline[70] with corresponding IgG control bam files, using q value 0.01, and minimal fragment length 100. An enrichment heatmap of the peaks was produced using deepTools's computeMatrix function[75] on Galaxy platform[76]. FIMO motif scanning was conducted on MEME Suite website using bed file of identified peaks[77]. The peaks were analyzed for genomic distribution with ChIPpeakAnno[78] and annotated using GREAT for single nearest gene within 250kb[30]. GO term enrichment analysis with ShinyGO 0.80 was conducted on the annotated genes[72].

Gene regulatory dynamic analysis

RegVelo is an end-to-end deep generative model designed to infer cellular dynamics through coupled splicing dynamics and gene regulation[31]. It requires users to define the prior gene regulatory network and allows the model to refine this network by improving the reconstruction of observed gene expression. Using a bulk ATAC-seq dataset, we followed CellOracle's tutorial[79]. First, we identified transcription start sites (TSS) using the get_tss_info function, which annotates each peak with its corresponding gene. Next, we scanned transcription factor (TF) binding motifs in these peak regions using the tfi.scan function with an FPR of 0.02. Subsequently, we filtered motifs using the filter_motifs_by_score function with a threshold of 10. Finally, we replaced the bulk ATAC-seq-derived TGIF2 targets with CUT&RUN-inferred target genes and incorporated this prior GRN for downstream RegVelo analysis.

We trained the RegVelo model with default parameters. To mimic overexpression effects, we manually perturbed the inferred gene regulation by multiplying TGIF2 downstream

regulation weights by a specific factor to amplify the regulatory effects of TGIF2. We used four different values [0, 50, 100, 150] and employed RegVelo to predict the depletion scores[31] for defined terminal states, including NSCs, UL neurons, and DL neurons. RegVelo-inferred GRN targets were used for downstream gene functional analysis. We curated all negatively regulated genes inferred by RegVelo and applied the clusterProfiler package to perform GO enrichment analysis.

Coimmunoprecipitation

For interactome analysis, P19 cells were seeded in 10cm dishes for transfection when the cells reached 50% confluency. After 48 hours, cells were scraped on ice and lysed in non-denaturing lysis buffer (20mM Tris-HCl, pH 8.0, 137mM NaCl, 1% Nonidet P-40, 2mM EDTA) containing cOmplete proteinase inhibitor. Lysates were incubated with DYKDDDDK Tag (D6W5B) FLAG rabbit antibody (Cell Signaling) for 1 hour, followed by addition of Protein G Dynabeads for an additional 2 hours at 4°C with rotation. Following three washes with wash buffer (10mM Tris, pH 7.4, 1mM EDTA, 150mM NaCl, 1% Nonidet P-40), the immunoprecipitated lysates were boiled in 1× Laemmli buffer and subsequently stored at –80°C until mass spectrometry analysis.

Mass spectrometry

The interactome samples were digested using a modified FASP procedure as described[80,81]. Digested peptides were measured on a QExactive HF X mass spectrometer (Thermo Scientific) online coupled to an Ultimate 300 nano-RSLC (Thermo Scientific) as described[82].Generated raw files were quantitatively analyzed in the MaxQuant software[83] (MPI Martinsried, version 2.4.9.0), applying default settings and a minimum LFQ ratio count of 1, quantification on unique peptides with matching between runs for LFQ quantification[84]. Searches for peptide identifications were performed in the integrated search engine Andromeda[85] with default settings, using the canonical SwissProt Mouse protein database including the described TGIF2 sequences. Results were filtered for contaminant hits, reverse hits and “only identified by site” hits. LFQ intensity values in the filtered proteingroups list were used for enrichment ratio calculations.

Western Blot

P19 cells transfected with various shRNA constructs were lysed with RIPA buffer and the proteins were extracted by centrifugation at 13,000 x g for 15 minutes at 4°C. 30 µg protein per sample was diluted to the desired concentration in 1× Laemmli Buffer and boiled at 95°C for 5 min. Gel electrophoresis was conducted using 12.5% polyacrylamide SDS gels, followed by transfer to nitrocellulose membranes. For immunodetection, membranes were initially

blocked with 5% nonfat dry milk in TBS-T (Tris-buffered saline/0.1% Tween20, pH 7.4) for either 1 hour at room temperature or overnight at 4°C, and then incubated overnight with primary antibodies (ARID4B, Bethyl Laboratories, 1:2000) diluted in 1% nonfat dry milk in TBS/T. The following day, the membranes were incubated with HRP-coupled secondary antibodies diluted in 1% nonfat dry milk in TBS-T. Finally, the signal was visualized using the ECL method with the ChemiDoc™ instrument from Biorad.

Statistical analysis

The statistical tests were performed using GraphPad Prism 9. If the data passed the Shapiro-Wilk normality test, and F test (two conditions) or Barlett's test (three or more conditions) for equal variance, they were subject to either unpaired t-tests when there were two conditions, or ordinary ANOVA with Tukey's multiple comparisons test when there were three or more conditions. If the data passed the normality test but not equal variance, they were subject to Welch t-test when there are two conditions, or Brown-Forsythe and Welch ANOVA tests with Dunnett's T3 multiple comparisons test when there were three or more conditions. If the data did not pass the normality test, they were subject to Mann-Whitney test when there were two conditions, or Kruskal-Wallis ANOVA with Dunn's multiple comparisons test when there were three or more conditions.

Acknowledgements

We are particularly grateful to Hyung-Seo Kang, Arie Geerlof and Michael Sattler for excellent input on the structure of TGIF2 including the mutations. Special thanks to Tatiana Simon-Ebert, Martina Buerkle, Paulina Chlebik for excellent technical support. We acknowledge the Core Facility Bioinformatics at the Biomedical Center, LMU Munich, especially Tobias Straub for consultation on Cut&Run analysis and HPC server usage, and then to Core Facility Flow Cytometry (Benjamin Tast and Roqayeh Noori) at the Biomedical Center, LMU Munich for FACS of cells for the scRNA-seq experiments. Sequencing of the bulk libraries was performed at the NGS facility, Institute of Human Genetics, Helmholtz Center Munich. Sequencing of the rest of the experiments was performed at the Next Generation Sequencing (NGS) Core Facility at the Institute of Human Genetics in Bonn. We are also very grateful to Giacomo Masserdotti and Stefan Stricker for excellent comments on the manuscript.

This study was supported by the advanced ERC Grant Neurocentro (885382 to M.G.) and the European Union's Horizon 2020 research and innovation program under grant agreement no. [3,40] (NSC Reconstruct to M. G.), as well as the German Research Foundation TRR274 (no. 408885537, M. G.), FOR2879/2 (no. 405358801, M. G.) and SyNergy (EXC2145/Project-ID 390857198, to M.G.). Parts of this work were supported by a New Frontiers in Research Fund Transformation grant to M. Götz, funded through three Canadian federal funding agencies (CIHR, NSERC, and SSHRC).

Contributions

M.G. conceived the project and together with Y.L. designed the study. Y.L. performed experiments and data analysis, including cloning, IUE experiments, E12 transfection experiments, imaging, data analyses, Cut&Run experiment and analysis, scRNA-seq experiment and analysis, IP experiment. F.V. acquired bulk RNA- and ATAC-seq data. A.K analyzed bulk RNA-seq data and M.R. analysed ATAC-seq data and priming data. W.W. performed RegVelo analysis and F.T. advised on the analysis. J.M-P. and S.H. performed proteomics of IP samples. Y.L., A.K., M.R., and M.G. wrote the manuscript, with input from all co-authors. M.G. provided all the funding.

Declaration of interests

There are no competing interests to declare.

Figure legends

Figure 1. Bulk RNA- and ATAC-seq of embryonic cortex and LGE at E14 and E18
(A) Experimental scheme of RNA-seq and ATAC-seq. E: Embryonic; PROM1+: PROMININ1
(B) UpSet plot of differentially expressed genes as indicated below the plot. DE: differentially expressed; Ctx: Cortex; LGE: Lateral Ganglionic Eminence
(C) Venn diagram of neurogenic fate determinants, transcription factors and chromatin remodelers.
(D) GO terms associated with biological processes, showing top 2 terms each from 10 clusters of semantic space, taken from genes enriched in the neurogenic fate determinants that are transcription factors and/or chromatin remodelers.
(E) UpSet plot of differentially enriched motifs at E14 versus E18 cortex, at E18 LGE versus cortex and not enriched at E14 between the regions.
(F) Venn diagram of neurogenic fate determinants identified from the transcriptome analysis and the differentially enriched motifs identified in panel E. Five of the 44 neurogenic fate determinants have known binding motifs. These are *Atf3, Etv6, Mafk, Mycn* and *Tgif2*.
(G) TGIF2 motif enrichment in the E14 cortex, E18 LGE and the consensus open regions shared between cortex and LGE at E14. Color represents enrichment against genomic background.
(H) Tgif2 expression at E14 and E18, cortex and LGE. Significance was tested with two-way ANOVA with Benjamini, Krieger and Yekutieli correction.

Figure 2. TGIF2 overexpression promotes NSC state while TGIF2 knockdown promotes differentiation

(A) Schematic drawing of TGIF2 isoforms. IR: intron retention; d: deleted; SID: SIN3a-interacting domain; MAPK: mitogen-activated protein kinase sites.

(B) Schematic drawing showing the procedure of E12 cortex cells transfection assay.

(C-D) Representative images showing transfected E12 cortex cell culture at 3 days or 7 days post transfection (dpt), respectively. Magenta arrowheads for PAX6+TBR2-/GFP+ cells, blue arrowheads for TBR2+PAX6-/GFP+ cells, yellow arrowheads for PAX6+TBR2+/GFP+ double positive cells. Scale bar: 50 μm.

(E-F) Quantifications of PAX6+/GFP+, TUBB3+/GFP+ at 3dpt, mean±SD. N = 6-10 pools of embryos. Brown-Forsythe and Welch ANOVA tests with Dunnett's T3 multiple comparisons test in (D), ordinary one-way ANOVA with Tukey's multiple comparisons test in (E). * $p<0.05$, ** $p< 0.01$, *** $p<0.001$, **** $p<0.0001$.

(G-H) Quantifications of TBR2+/GFP+, PAX6+TBR2-/GFP+, and TUBB3+/GFP+ cells at 7dpt, mean±SD. N = 5-12 pools of embryos. Ordinary two-way ANOVA with Tukey's multiple comparisons test in (G) and ordinary one-way ANOVA with Tukey's multiple comparisons test in (H). ** $p< 0.01$, *** $p<0.001$.

Figure 3. TGIF2 overexpression *in vivo* retains less differentiated cells

(A) Experimental scheme of IUE, including used plasmids. F: flag

(B-D) Sections of electroporated cortices stained with PAX6 and TBR2, of which insets are to show large magnifications with orthogonal views in (B'-D'). Scale bar: 100μm.

(E) Quantification of PAX6+/GFP+ and PAX6-TBR2+/GFP+ cells in bin1, mean±SD. N = 4-5 embryos from at least two different mothers. Different symbols indicate different mothers. Ordinary two-way ANOVA with Tukey's multiple comparisons test. ** $p<0.01$, **** $p<0.001$.

(F-H) Representative images of cortex 3 days after electroporation with each condition in GFP. Scale bar: 100μm. Dashed lines indicate the 5 equal bins.

(I) Quantification of GFP+ cell distribution at 3 days post electroporation, mean±SD. N = 4-5 embryos from at least two different mothers. Different symbols indicate different mothers. Multiple unpaired t-tests with 5% FDR. *q<0.05

Figure 4. TGIF2 overexpression slows differentiation shown by scRNA-seq

(A) Schematic drawing of experimental procedures.

(B) UMAP projection with each cluster annotated with corresponding cell type.

(C) Violin plot of maturation score per condition. Kruskal-Wallis test with Dunn's multiple comparisons test.

(D) Barplot of DE genes between TGIF2IR and GFP identified in each cell cluster.

(E-F) Top 15 terms of GO term enrichment analysis of DE genes in upper layer neurons between GFP and TGIF2IR.

(G) Cell density plot along velocity pseudotime.

(H-J) Gene expression of selected markers by velocity pseudotime and differentiation lineage.

(K-M) Fate probability maps from CellRank[28,29] analysis. RGC: radial glial cells, TAP: transit-amplifying progenitors, DL neurons: deep layer neurons, UL neurons: upper layer neurons.

Figure 5. TGIF2 binds at neural differentiation genes and regulates chromatin factors

(A) Schematic drawing of experimental procedures of Cut&Run.

(B) Enrichment heatmap of TGIF2IR peaks and its corresponding IgG control, centered at the middle of the peaks.

(C) Pie chart of genomic distribution of TGIF2IR peaks.

(D) MonaLisa motif enrichment analysis of TGIF2IR peaks.

(E) Top 20 terms from GO term enrichment analysis of annotated genes.

(F) Top 20 genes with extensive regulation by GREAT.

(G) Peak examples with bigwig profiles exported from IGV[86].

(H) UpSet plot overlapping Cut&Run targets and DEGs in scRNA-seq between TGIF2IR and GFP per cell type.

(I) Top 15 enriched GO terms in biological processes of overlaps (351 genes) between TGIF2IR Cut&Run targets and downregulated genes in NSCs of TGIF2IR compared to GFP control from scRNA-seq.

(J) GRN built by CellOracle[79], representing negatively regulated TFs by TGIF2 and associated GO terms.

(K) Weighted simulations by RegVelo[31] for TGIF2 overexpression effect on cell fate bias.

Figure 6. TGIF2 interacts with the SIN3a complex and acts as a repressor

(A) Schematic drawing of IP-MS experiment in P19 cells.

(B) STRING analysis of interactors of TGIF2IR with LFQ intensity more than 3-fold compared to GFP control.

(C) AlphaFold prediction of TGIF2 structure, with DNA-binding domain and repressor domain circled, and 2 MAPK sites indicated.

(D) Schematic structures of different TGIF2 constructs. pp: phospho-mutant, TGIF2IRmut: TGIF2IR mutant form.

(E, H) Representative pictures of E12 primary cortex cells cultures transfected with different conditions at 3dpt, co-stained with PAX6, TBR2, and TUBB3. Magenta arrowheads for

PAX6+TBR2-/GFP+ cells, yellow arrowheads for TBR2+PAX6-/GFP+ cells, white arrowheads for TUBB3+/GFP+ cells. Scale bar: 50 μm.

(F-G) Quantification of PAX6+/GFP+ and TUBB3+/GFP+ in transfected E12 culture at 3dpt with TGIF2IR_pp, TGIF2IR_KRAB and TGIF2IR_VP64 constructs, mean+SD. N = 3-9 pools of embryos. Ordinary one-way ANOVA with Tukey's multiple comparisons test. ns: not significant.

(I) Quantification of PAX6+TBR2-/GFP+ and PAX6-TBR2+/GFP+ in transfected E12 culture at 3dpt with shArid4b constructs, mean+SD. N = 3 pools of embryos. *p = 0.0341. Ordinary two-way ANOVA with Šídák's multiple comparisons test.

(J) Scheme of molecular mechanisms of TGIF2: when TGIF2 is phosphorylated, it is able to interact with SIN3A complex including ARID4B and HDAC1/2, which altogether repress neurogenesis programs, including *Arid4b* itself, to maintain NSC fate. TGIF2 KD, TGIF2IR_VP64 and TGIF2IRmut act in the opposite direction from wild type TGIF2s and TGIF2IR_KRAB.

Figure 7. TGIF2 is a master regulator of neurogenic priming

(A) Scheme for the experimental setup: E14 cortices were dissected for FACSorting of PSA-NCAM+ young neurons and performed RNA-seq, to compare with E14 cortical NSCs RNA-seq data mentioned in Figure 1.

(B) Venn diagram showing data mining logic of neurogenic priming genes. DEG: differentially expressed genes. DAR: differential accessible regions. AR: accessible regions. CNR: Cut&Run. Neu: Neurons. Ctx: Cortex. NSC: Neural Stem Cells. E: embryonic.

(C) GO term analysis of neurogenic priming genes.

(D) Examples of neurogenic priming genes regulated by TGIF2, showing ATAC-seq and TGIF2 Cut&Run (CNR) profiles, together with each gene's RNA expression by violin plot in E14 cortical NSCs and neurons.

(E) Permutation test with 100,000 trials to identify the possibility of various number of random gene sets to overlap with the neurogenic priming genes.

References

1. Miller, F.D., and Gauthier, A.S. (2007). Timing Is Everything: Making Neurons versus Glia in the Developing Cortex. Neuron *54*, 357–369. https://doi.org/10.1016/j.neuron.2007.04.019.
2. Meng, Y., and Nerlov, C. (2024). Epigenetic regulation of hematopoietic stem cell fate. Trends Cell Biol. *0*. https://doi.org/10.1016/j.tcb.2024.08.005.
3. Li, Z., Tyler, W.A., Zeldich, E., Baró, G.S., Okamoto, M., Gao, T., Li, M., Sestan, N., and Haydar, T.F. (2020). Transcriptional priming as a conserved mechanism of lineage diversification in the developing mouse and human neocortex. Sci. Adv. https://doi.org/10.1126/sciadv.abd2068.
4. Zahr, S.K., Yang, G., Kazan, H., Borrett, M.J., Yuzwa, S.A., Voronova, A., Kaplan, D.R., and Miller, F.D. (2018). A Translational Repression Complex in Developing Mammalian Neural Stem Cells that Regulates Neuronal Specification. Neuron *97*, 520-537.e6. https://doi.org/10.1016/j.neuron.2017.12.045.
5. Liang, X.G., Hoang, K., Meyerink, B.L., Kc, P., Paraiso, K., Wang, L., Jones, I.R., Zhang, Y., Katzman, S., Finn, T.S., et al. (2024). A conserved molecular logic for neurogenesis to gliogenesis switch in the cerebral cortex. Proc. Natl. Acad. Sci. *121*, e2321711121. https://doi.org/10.1073/pnas.2321711121.
6. Kang, P., Lee, H.K., Glasgow, S.M., Finley, M., Donti, T., Gaber, Z.B., Graham, B.H., Foster, A.E., Novitch, B.G., Gronostajski, R.M., et al. (2012). Sox9 and NFIA Coordinate a Transcriptional Regulatory Cascade during the Initiation of Gliogenesis. Neuron *74*, 79–94. https://doi.org/10.1016/j.neuron.2012.01.024.
7. Hobert, O. (2021). Homeobox genes and the specification of neuronal identity. Nat. Rev. Neurosci. *22*, 627–636. https://doi.org/10.1038/s41583-021-00497-x.
8. Bertrand, N., Castro, D.S., and Guillemot, F. (2002). Proneural genes and the specification of neural cell types. Nat. Rev. Neurosci. *3*, 517–530. https://doi.org/10.1038/nrn874.
9. Stoykova, A., Treichel, D., Hallonet, M., and Gruss, P. (2000). Pax6 Modulates the Dorsoventral Patterning of the Mammalian Telencephalon. J. Neurosci. *20*, 8042–8050. https://doi.org/10.1523/JNEUROSCI.20-21-08042.2000.
10. Anderson, S.A., Qiu, M., Bulfone, A., Eisenstat, D.D., Meneses, J., Pedersen, R., and Rubenstein, J.L.R. (1997). Mutations of the Homeobox Genes Dlx-1 and Dlx-2 Disrupt the Striatal Subventricular Zone and Differentiation of Late Born Striatal Neurons. Neuron *19*, 27–37. https://doi.org/10.1016/S0896-6273(00)80345-1.
11. Sun, Y., Dykes, I.M., Liang, X., Eng, S.R., Evans, S.M., and Turner, E.E. (2008). A central role for Islet1 in sensory neuron development linking sensory and spinal gene regulatory programs. Nat. Neurosci. *11*, 1283–1293. https://doi.org/10.1038/nn.2209.
12. Pinto, L. (2008). Molecular mechanisms regulating neurogenesis in the developing mouse cerebral cortex.
13. Beckervordersandforth, R., Tripathi, P., Ninkovic, J., Bayam, E., Lepier, A., Stempfhuber, B., Kirchhoff, F., Hirrlinger, J., Haslinger, A., Lie, D.C., et al. (2010). In vivo fate mapping and expression analysis reveals molecular hallmarks of prospectively isolated adult neural stem cells. Cell Stem Cell *7*, 744–758. https://doi.org/10.1016/j.stem.2010.11.017.
14. Kadam, S., and Emerson, B.M. (2003). Transcriptional specificity of human SWI/SNF BRG1 and BRM chromatin remodeling complexes. Mol. Cell *11*, 377–389. https://doi.org/10.1016/s1097-2765(03)00034-0.

15. Flowers, S., Nagl, N.G., Beck, G.R., and Moran, E. (2009). Antagonistic Roles for BRM and BRG1 SWI/SNF Complexes in Differentiation*♦. J. Biol. Chem. *284*, 10067–10075. https://doi.org/10.1074/jbc.M808782200.
16. Silbereis, J.C., Pochareddy, S., Zhu, Y., Li, M., and Sestan, N. (2016). The Cellular and Molecular Landscapes of the Developing Human Central Nervous System. Neuron *89*, 248–268. https://doi.org/10.1016/j.neuron.2015.12.008.
17. Yao, B., Christian, K.M., He, C., Jin, P., Ming, G.-L., and Song, H. (2016). Epigenetic mechanisms in neurogenesis. Nat. Rev. Neurosci. *17*, 537–549. https://doi.org/10.1038/nrn.2016.70.
18. Pereira, A., Diwakar, J., Masserdotti, G., Beşkardeş, S., Simon, T., So, Y., Martín-Loarte, L., Bergemann, F., Vasan, L., Schauer, T., et al. (2024). Direct neuronal reprogramming of mouse astrocytes is associated with multiscale epigenome remodeling and requires Yy1. Nat. Neurosci. *27*, 1260–1273. https://doi.org/10.1038/s41593-024-01677-5.
19. Vinchure, O.S., Sharma, V., Tabasum, S., Ghosh, S., Singh, R.P., Sarkar, C., and Kulshreshtha, R. (2019). Polycomb complex mediated epigenetic reprogramming alters TGF-β signaling via a novel EZH2/miR-490/TGIF2 axis thereby inducing migration and EMT potential in glioblastomas. Int. J. Cancer *145*, 1254–1269. https://doi.org/10.1002/ijc.32360.
20. Du, R., Wang, C., Liu, J., Wang, K., Dai, L., and Shen, W. (2023). Phosphorylation of TGIF2 represents a therapeutic target that drives EMT and metastasis of lung adenocarcinoma. BMC Cancer *23*, 52. https://doi.org/10.1186/s12885-023-10535-9.
21. Cerdá-Esteban, N., Naumann, H., Ruzittu, S., Mah, N., Pongrac, I.M., Cozzitorto, C., Hommel, A., Andrade-Navarro, M.A., Bonifacio, E., and Spagnoli, F.M. (2017). Stepwise reprogramming of liver cells to a pancreas progenitor state by the transcriptional regulator Tgif2. Nat. Commun. *8*, 14127. https://doi.org/10.1038/ncomms14127.
22. Spagnoli, F.M., and Brivanlou, A.H. (2008). The Gata5 target, TGIF2, defines the pancreatic region by modulating BMP signals within the endoderm. Dev. Camb. Engl. *135*, 451–461. https://doi.org/10.1242/dev.008458.
23. Powers, S.E., Taniguchi, K., Yen, W., Melhuish, T.A., Shen, J., Walsh, C.A., Sutherland, A.E., and Wotton, D. (2010). Tgif1 and Tgif2 regulate Nodal signaling and are required for gastrulation. Dev. Camb. Engl. *137*, 249–259. https://doi.org/10.1242/dev.040782.
24. Taniguchi, K., Anderson, A.E., Sutherland, A.E., and Wotton, D. (2012). Loss of Tgif function causes holoprosencephaly by disrupting the SHH signaling pathway. PLoS Genet. *8*, e1002524. https://doi.org/10.1371/journal.pgen.1002524.
25. Lei, J., Deng, Y., and Ma, S. (2022). Downregulation of TGIF2 is possibly correlated with neuronal apoptosis and autism-like symptoms in mice. Brain Behav. *12*, e2610. https://doi.org/10.1002/brb3.2610.
26. Melhuish, T.A., and Wotton, D. (2006). The Tgif2 gene contains a retained intron within the coding sequence. BMC Mol. Biol. *7*, 2. https://doi.org/10.1186/1471-2199-7-2.
27. Bergen, V., Lange, M., Peidli, S., Wolf, F.A., and Theis, F.J. (2020). Generalizing RNA velocity to transient cell states through dynamical modeling. Nat. Biotechnol. *38*, 1408–1414. https://doi.org/10.1038/s41587-020-0591-3.

28. Lange, M., Bergen, V., Klein, M., Setty, M., Reuter, B., Bakhti, M., Lickert, H., Ansari, M., Schniering, J., Schiller, H.B., et al. (2022). CellRank for directed single-cell fate mapping. Nat. Methods *19*, 159–170. https://doi.org/10.1038/s41592-021-01346-6.
29. Weiler, P., Lange, M., Klein, M., Pe'er, D., and Theis, F. (2024). CellRank 2: unified fate mapping in multiview single-cell data. Nat. Methods *21*, 1196–1205. https://doi.org/10.1038/s41592-024-02303-9.
30. McLean, C.Y., Bristor, D., Hiller, M., Clarke, S.L., Schaar, B.T., Lowe, C.B., Wenger, A.M., and Bejerano, G. (2010). GREAT improves functional interpretation of cis-regulatory regions. Nat. Biotechnol. *28*, 495–501. https://doi.org/10.1038/nbt.1630.
31. Wang, W., Hu, Z., Weiler, P., Mayes, S., Lange, M., Wang, J., Xue, Z., Sauka-Spengler, T., and Theis, F.J. (2024). RegVelo: gene-regulatory-informed dynamics of single cells. Preprint at bioRxiv, https://doi.org/10.1101/2024.12.11.627935 https://doi.org/10.1101/2024.12.11.627935.
32. Melhuish, T.A., Gallo, C.M., and Wotton, D. (2001). TGIF2 Interacts with Histone Deacetylase 1 and Represses Transcription *. J. Biol. Chem. *276*, 32109–32114. https://doi.org/10.1074/jbc.M103377200.
33. Lucas, T., Hafer, T.L., Zhang, H.G., Molotkova, N., and Kohwi, M. (2021). Discrete cis-acting element regulates developmentally timed gene-lamina relocation and neural progenitor competence in vivo. Dev. Cell *56*, 2649-2663.e6. https://doi.org/10.1016/j.devcel.2021.08.020.
34. Kim, E.-J., Kim, J.Y., Kim, S.-O., Hong, N., Choi, S.-H., Park, M.G., Jang, J., Ham, S.W., Seo, S., Lee, S.Y., et al. (2022). The oncogenic JAG1 intracellular domain is a transcriptional cofactor that acts in concert with DDX17/SMAD3/TGIF2. Cell Rep. *41*, 111626. https://doi.org/10.1016/j.celrep.2022.111626.
35. He, X., Nie, Y., Zhou, H., Hu, R., Li, Y., He, T., Zhu, J., Yang, Y., and Liu, M. (2021). Structural Insight into the Binding of TGIF1 to SIN3A PAH2 Domain through a C-Terminal Amphipathic Helix. Int. J. Mol. Sci. *22*. https://doi.org/10.3390/ijms222312631.
36. Saunders, A., Huang, X., Fidalgo, M., Reimer, M.H.J., Faiola, F., Ding, J., Sánchez-Priego, C., Guallar, D., Sáenz, C., Li, D., et al. (2017). The SIN3A/HDAC Corepressor Complex Functionally Cooperates with NANOG to Promote Pluripotency. Cell Rep. *18*, 1713–1726. https://doi.org/10.1016/j.celrep.2017.01.055.
37. Varadi, M., Bertoni, D., Magana, P., Paramval, U., Pidruchna, I., Radhakrishnan, M., Tsenkov, M., Nair, S., Mirdita, M., Yeo, J., et al. (2024). AlphaFold Protein Structure Database in 2024: providing structure coverage for over 214 million protein sequences. Nucleic Acids Res. *52*, D368–D375. https://doi.org/10.1093/nar/gkad1011.
38. Massey, S., Ang, C.-S., Davidson, N.M., Quigley, A., Rollo, B., Harris, A.R., Kapsa, R.M.I., Christodoulou, J., and Van Bergen, N.J. (2024). Novel CDKL5 targets identified in human iPSC-derived neurons. Cell. Mol. Life Sci. *81*, 347. https://doi.org/10.1007/s00018-024-05389-8.
39. Werren, E.A., Guxholli, A., Jones, N., Wagner, M., Hannibal, I., Granadillo, J.L., Tyndall, A.V., Moccia, A., Kuehl, R., Levandoski, K.M., et al. (2023). *De novo* variants in *GATAD2A* in individuals with a neurodevelopmental disorder: GATAD2A-related neurodevelopmental disorder. Hum. Genet. Genomics Adv. *4*, 100198. https://doi.org/10.1016/j.xhgg.2023.100198.
40. Cai, Y., Wu, P., Ozen, M., Yu, Y., Wang, J., Ittmann, M., and Liu, M. (2006). Gene expression profiling and analysis of signaling pathways involved in priming and

differentiation of human neural stem cells. Neuroscience *138*, 133–148. https://doi.org/10.1016/j.neuroscience.2005.11.041.
41. ISH Data :: Allen Brain Atlas: Developing Mouse Brain https://developingmouse.brain-map.org/.
42. Nowakowski, T.J., Bhaduri, A., Pollen, A.A., Alvarado, B., Mostajo-Radji, M.A., Di Lullo, E., Haeussler, M., Sandoval-Espinosa, C., Liu, S.J., Velmeshev, D., et al. (2017). Spatiotemporal gene expression trajectories reveal developmental hierarchies of the human cortex. Science *358*, 1318–1323. https://doi.org/10.1126/science.aap8809.
43. Du, R., Shen, W., Liu, Y., Gao, W., Zhou, W., Li, J., Zhao, S., Chen, C., Chen, Y., Liu, Y., et al. (2019). TGIF2 promotes the progression of lung adenocarcinoma by bridging EGFR/RAS/ERK signaling to cancer cell stemness. Signal Transduct. Target. Ther. *4*, 1–12. https://doi.org/10.1038/s41392-019-0098-x.
44. O'Neill, A.C., Uzbas, F., Antognolli, G., Merino, F., Draganova, K., Jäck, A., Zhang, S., Pedini, G., Schessner, J.P., Cramer, K., et al. (2022). Spatial centrosome proteome of human neural cells uncovers disease-relevant heterogeneity. Science *376*, eabf9088. https://doi.org/10.1126/science.abf9088.
45. Wang, B., Gao, Y., Xiao, Z., Chen, B., Han, J., Zhang, J., Wang, X., and Dai, J. (2009). Erk1/2 promotes proliferation and inhibits neuronal differentiation of neural stem cells. Neurosci. Lett. *461*, 252–257. https://doi.org/10.1016/j.neulet.2009.06.020.
46. Ma, D.K., Ponnusamy, K., Song, M.-R., Ming, G., and Song, H. (2009). Molecular genetic analysis of FGFR1 signalling reveals distinct roles of MAPK and PLCγ1 activation for self-renewal of adult neural stem cells. Mol. Brain *2*, 16. https://doi.org/10.1186/1756-6606-2-16.
47. Semprich, C.I., Davidson, L., Torres, A.A., Patel, H., Briscoe, J., Metzis, V., and Storey, K.G. (2022). ERK1/2 signalling dynamics promote neural differentiation by regulating chromatin accessibility and the polycomb repressive complex. PLOS Biol. *20*, e3000221. https://doi.org/10.1371/journal.pbio.3000221.
48. Olson, J.M., Asakura, A., Snider, L., Hawkes, R., Strand, A., Stoeck, J., Hallahan, A., Pritchard, J., and Tapscott, S.J. (2001). NeuroD2 Is Necessary for Development and Survival of Central Nervous System Neurons. Dev. Biol. *234*, 174–187. https://doi.org/10.1006/dbio.2001.0245.
49. Tutukova, S., Tarabykin, V., and Hernandez-Miranda, L.R. (2021). The Role of Neurod Genes in Brain Development, Function, and Disease. Front. Mol. Neurosci. *14*. https://doi.org/10.3389/fnmol.2021.662774.
50. Dvoretskova, E., Ho, M.C., Kittke, V., Neuhaus, F., Vitali, I., Lam, D.D., Delgado, I., Feng, C., Torres, M., Winkelmann, J., et al. (2024). Spatial enhancer activation influences inhibitory neuron identity during mouse embryonic development. Nat. Neurosci. *27*, 862–872. https://doi.org/10.1038/s41593-024-01611-9.
51. Schulte, D., and Geerts, D. (2019). MEIS transcription factors in development and disease. Development *146*, dev174706. https://doi.org/10.1242/dev.174706.
52. Kolb, J., Anders-Maurer, M., Müller, T., Hau, A.-C., Grebbin, B.M., Kallenborn-Gerhardt, W., Behrends, C., and Schulte, D. (2018). Arginine Methylation Regulates MEIS2 Nuclear Localization to Promote Neuronal Differentiation of Adult SVZ Progenitors. Stem Cell Rep. *10*, 1184. https://doi.org/10.1016/j.stemcr.2018.03.010.
53. Fraser, J., Essebier, A., Brown, A.S., Davila, R.A., Harkins, D., Zalucki, O., Shapiro, L.P., Penzes, P., Wainwright, B.J., Scott, M.P., et al. (2020). Common Regulatory

Targets of NFIA, NFIX and NFIB during Postnatal Cerebellar Development. Cerebellum Lond. Engl. *19*, 89–101. https://doi.org/10.1007/s12311-019-01089-3.
54. Bunt, J., Osinski, J.M., Lim, J.W., Vidovic, D., Ye, Y., Zalucki, O., O'Connor, T.R., Harris, L., Gronostajski, R.M., Richards, L.J., et al. (2017). Combined allelic dosage of Nfia and Nfib regulates cortical development. Brain Neurosci. Adv. *1*, 2398212817739433. https://doi.org/10.1177/2398212817739433.
55. Wang, H., and Helin, K. (2024). Roles of H3K4 methylation in biology and disease. Trends Cell Biol., S0962-8924(24)00115-6. https://doi.org/10.1016/j.tcb.2024.06.001.
56. Pile, L.A., Spellman, P.T., Katzenberger, R.J., and Wassarman, D.A. (2003). The SIN3 deacetylase complex represses genes encoding mitochondrial proteins: implications for the regulation of energy metabolism. J. Biol. Chem. *278*, 37840–37848. https://doi.org/10.1074/jbc.M305996200.
57. Adams, G.E., Chandru, A., and Cowley, S.M. (2018). Co-repressor, co-activator and general transcription factor: the many faces of the Sin3 histone deacetylase (HDAC) complex. Biochem. J. *475*, 3921–3932. https://doi.org/10.1042/BCJ20170314.
58. Balasubramanian, M., Dingemans, A.J.M., Albaba, S., Richardson, R., Yates, T.M., Cox, H., Douzgou, S., Armstrong, R., Sansbury, F.H., Burke, K.B., et al. (2021). Comprehensive study of 28 individuals with SIN3A-related disorder underscoring the associated mild cognitive and distinctive facial phenotype. Eur. J. Hum. Genet. EJHG *29*, 625–636. https://doi.org/10.1038/s41431-020-00769-7.
59. Farias, E.F., Petrie, K., Leibovitch, B., Murtagh, J., Chornet, M.B., Schenk, T., Zelent, A., and Waxman, S. (2010). Interference with Sin3 function induces epigenetic reprogramming and differentiation in breast cancer cells. Proc. Natl. Acad. Sci. U. S. A. *107*, 11811–11816. https://doi.org/10.1073/pnas.1006737107.
60. Lewis, M.J., Liu, J., Libby, E.F., Lee, M., Crawford, N.P.S., and Hurst, D.R. (2016). SIN3A and SIN3B differentially regulate breast cancer metastasis. Oncotarget *7*, 78713–78725. https://doi.org/10.18632/oncotarget.12805.
61. Terzi Cizmecioglu, N., Huang, J., Keskin, E.G., Wang, X., Esen, I., Chen, F., and Orkin, S.H. (2020). ARID4B is critical for mouse embryonic stem cell differentiation towards mesoderm and endoderm, linking epigenetics to pluripotency exit. J. Biol. Chem. *295*, 17738–17751. https://doi.org/10.1074/jbc.RA120.015534.
62. Ciceri, G., Baggiolini, A., Cho, H.S., Kshirsagar, M., Benito-Kwiecinski, S., Walsh, R.M., Aromolaran, K.A., Gonzalez-Hernandez, A.J., Munguba, H., Koo, S.Y., et al. (2024). An epigenetic barrier sets the timing of human neuronal maturation. Nature *626*, 881–890. https://doi.org/10.1038/s41586-023-06984-8.
63. Andrews, S. FASTQC. A quality control tool for high throughput sequence data | BibSonomy. https://www.bibsonomy.org/bibtex/1f230a919c34360709aa298734d63dca3.
64. Martin, M. (2011). Cutadapt removes adapter sequences from high-throughput sequencing reads. EMBnet.journal *17*, 10–12. https://doi.org/10.14806/ej.17.1.200.
65. Dobin, A., Davis, C.A., Schlesinger, F., Drenkow, J., Zaleski, C., Jha, S., Batut, P., Chaisson, M., and Gingeras, T.R. (2013). STAR: ultrafast universal RNA-seq aligner. Bioinforma. Oxf. Engl. *29*, 15–21. https://doi.org/10.1093/bioinformatics/bts635.
66. Liao, Y., Smyth, G.K., and Shi, W. (2014). featureCounts: an efficient general purpose program for assigning sequence reads to genomic features. Bioinformatics *30*, 923–930. https://doi.org/10.1093/bioinformatics/btt656.
67. R Core Team (2017). R: A Language and Environment for Statistical Computing.

68. Love, M.I., Huber, W., and Anders, S. (2014). Moderated estimation of fold change and dispersion for RNA-seq data with DESeq2. Genome Biol. *15*, 550. https://doi.org/10.1186/s13059-014-0550-8.
69. Yan, F., Powell, D.R., Curtis, D.J., and Wong, N.C. (2020). From reads to insight: a hitchhiker's guide to ATAC-seq data analysis. Genome Biol. *21*, 22. https://doi.org/10.1186/s13059-020-1929-3.
70. Zhang, Y., Liu, T., Meyer, C.A., Eeckhoute, J., Johnson, D.S., Bernstein, B.E., Nusbaum, C., Myers, R.M., Brown, M., Li, W., et al. (2008). Model-based Analysis of ChIP-Seq (MACS). Genome Biol. *9*, R137. https://doi.org/10.1186/gb-2008-9-9-r137.
71. Machlab, D., Burger, L., Soneson, C., Rijli, F.M., Schübeler, D., and Stadler, M.B. (2022). monaLisa: an R/Bioconductor package for identifying regulatory motifs. Bioinformatics *38*, 2624–2625. https://doi.org/10.1093/bioinformatics/btac102.
72. Ge, S.X., Jung, D., and Yao, R. (2020). ShinyGO: a graphical gene-set enrichment tool for animals and plants. Bioinforma. Oxf. Engl. *36*, 2628–2629. https://doi.org/10.1093/bioinformatics/btz931.
73. Wolf, F.A., Angerer, P., and Theis, F.J. (2018). SCANPY: large-scale single-cell gene expression data analysis. Genome Biol. *19*, 15. https://doi.org/10.1186/s13059-017-1382-0.
74. Langmead, B., and Salzberg, S.L. (2012). Fast gapped-read alignment with Bowtie 2. Nat. Methods *9*, 357–359. https://doi.org/10.1038/nmeth.1923.
75. Ramírez, F., Ryan, D.P., Grüning, B., Bhardwaj, V., Kilpert, F., Richter, A.S., Heyne, S., Dündar, F., and Manke, T. (2016). deepTools2: a next generation web server for deep-sequencing data analysis. Nucleic Acids Res. *44*, W160–W165. https://doi.org/10.1093/nar/gkw257.
76. The Galaxy Community (2024). The Galaxy platform for accessible, reproducible, and collaborative data analyses: 2024 update. Nucleic Acids Res. *52*, W83–W94. https://doi.org/10.1093/nar/gkae410.
77. Grant, C.E., Bailey, T.L., and Noble, W.S. (2011). FIMO: scanning for occurrences of a given motif. Bioinformatics *27*, 1017–1018. https://doi.org/10.1093/bioinformatics/btr064.
78. Zhu, L.J., Gazin, C., Lawson, N.D., Pagès, H., Lin, S.M., Lapointe, D.S., and Green, M.R. (2010). ChIPpeakAnno: a Bioconductor package to annotate ChIP-seq and ChIP-chip data. BMC Bioinformatics *11*, 237. https://doi.org/10.1186/1471-2105-11-237.
79. Kamimoto, K., Stringa, B., Hoffmann, C.M., Jindal, K., Solnica-Krezel, L., and Morris, S.A. (2023). Dissecting cell identity via network inference and in silico gene perturbation. Nature *614*, 742–751. https://doi.org/10.1038/s41586-022-05688-9.
80. Grosche, A., Hauser, A., Lepper, M.F., Mayo, R., von Toerne, C., Merl-Pham, J., and Hauck, S.M. (2016). The Proteome of Native Adult Müller Glial Cells From Murine Retina. Mol. Cell. Proteomics MCP *15*, 462–480. https://doi.org/10.1074/mcp.M115.052183.
81. Wiśniewski, J.R., Zougman, A., Nagaraj, N., and Mann, M. (2009). Universal sample preparation method for proteome analysis. Nat. Methods *6*, 359–362. https://doi.org/10.1038/nmeth.1322.
82. Molitor, L., Klostermann, M., Bacher, S., Merl-Pham, J., Spranger, N., Burczyk, S., Ketteler, C., Rusha, E., Tews, D., Pertek, A., et al. (2023). Depletion of the RNA-binding protein PURA triggers changes in posttranscriptional gene regulation and loss

of P-bodies. Nucleic Acids Res. *51*, 1297–1316. https://doi.org/10.1093/nar/gkac1237.

83. Cox, J., and Mann, M. (2008). MaxQuant enables high peptide identification rates, individualized p.p.b.-range mass accuracies and proteome-wide protein quantification. Nat. Biotechnol. *26*, 1367–1372. https://doi.org/10.1038/nbt.1511.
84. Cox, J., Hein, M.Y., Luber, C.A., Paron, I., Nagaraj, N., and Mann, M. (2014). Accurate proteome-wide label-free quantification by delayed normalization and maximal peptide ratio extraction, termed MaxLFQ. Mol. Cell. Proteomics MCP *13*, 2513–2526. https://doi.org/10.1074/mcp.M113.031591.
85. Cox, J., Neuhauser, N., Michalski, A., Scheltema, R.A., Olsen, J.V., and Mann, M. (2011). Andromeda: A Peptide Search Engine Integrated into the MaxQuant Environment. J. Proteome Res. *10*, 1794–1805. https://doi.org/10.1021/pr101065j.
86. Robinson, J.T., Thorvaldsdóttir, H., Winckler, W., Guttman, M., Lander, E.S., Getz, G., and Mesirov, J.P. (2011). Integrative Genomics Viewer. Nat. Biotechnol. *29*, 24–26. https://doi.org/10.1038/nbt.1754.

Figure 1

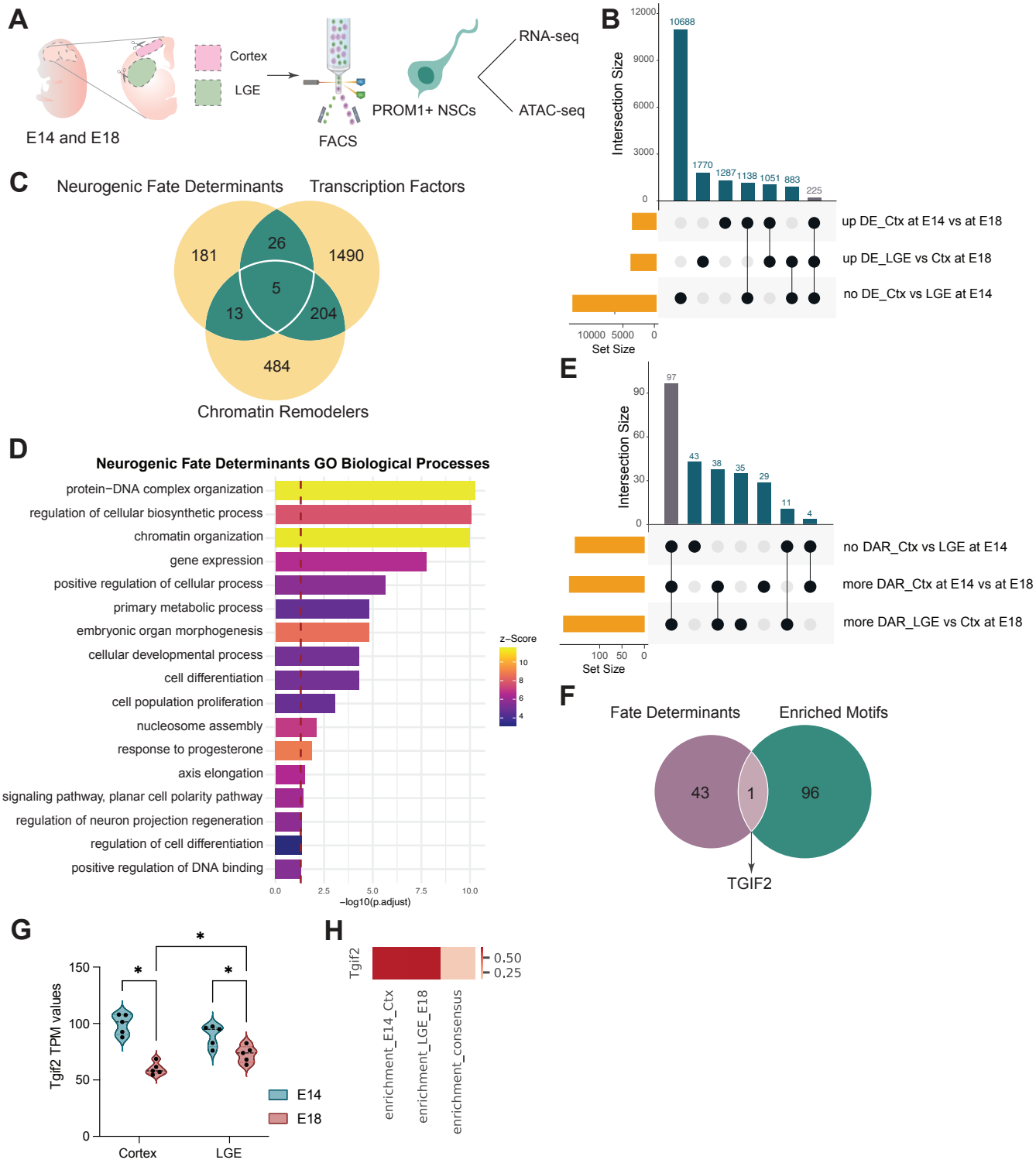
A
Cortex
LGE
E14 and E18
FACS
PROM1+ NSCs
RNA-seq
ATAC-seq
B
Intersection Size
10688
1770
1287
1138
1051
883
225
up DE_Ctx at E14 vs at E18
up DE_LGE vs Ctx at E18
no DE_Ctx vs LGE at E14
Set Size
C
Neurogenic Fate Determinants
Transcription Factors
181
26
1490
5
13
204
484
Chromatin Remodelers
D
Neurogenic Fate Determinants GO Biological Processes
protein−DNA complex organization
regulation of cellular biosynthetic process
chromatin organization
gene expression
positive regulation of cellular process
primary metabolic process
embryonic organ morphogenesis
cellular developmental process
cell differentiation
cell population proliferation
nucleosome assembly
response to progesterone
axis elongation
Wnt signaling pathway, planar cell polarity pathway
regulation of neuron projection regeneration
regulation of cell differentiation
positive regulation of DNA binding
z−Score
−log10(p.adjust)
E
Intersection Size
97
43
38
35
29
11
4
no DAR_Ctx vs LGE at E14
more DAR_Ctx at E14 vs at E18
more DAR_LGE vs Ctx at E18
Set Size
F
Fate Determinants
Enriched Motifs
43
1
96
TGIF2
G
Tgif2 TPM values
E14
E18
Cortex
LGE
H
Tgif2
0.50
0.25
enrichment_E14_Ctx
enrichment_LGE_E18
enrichment_consensus

Figure 2

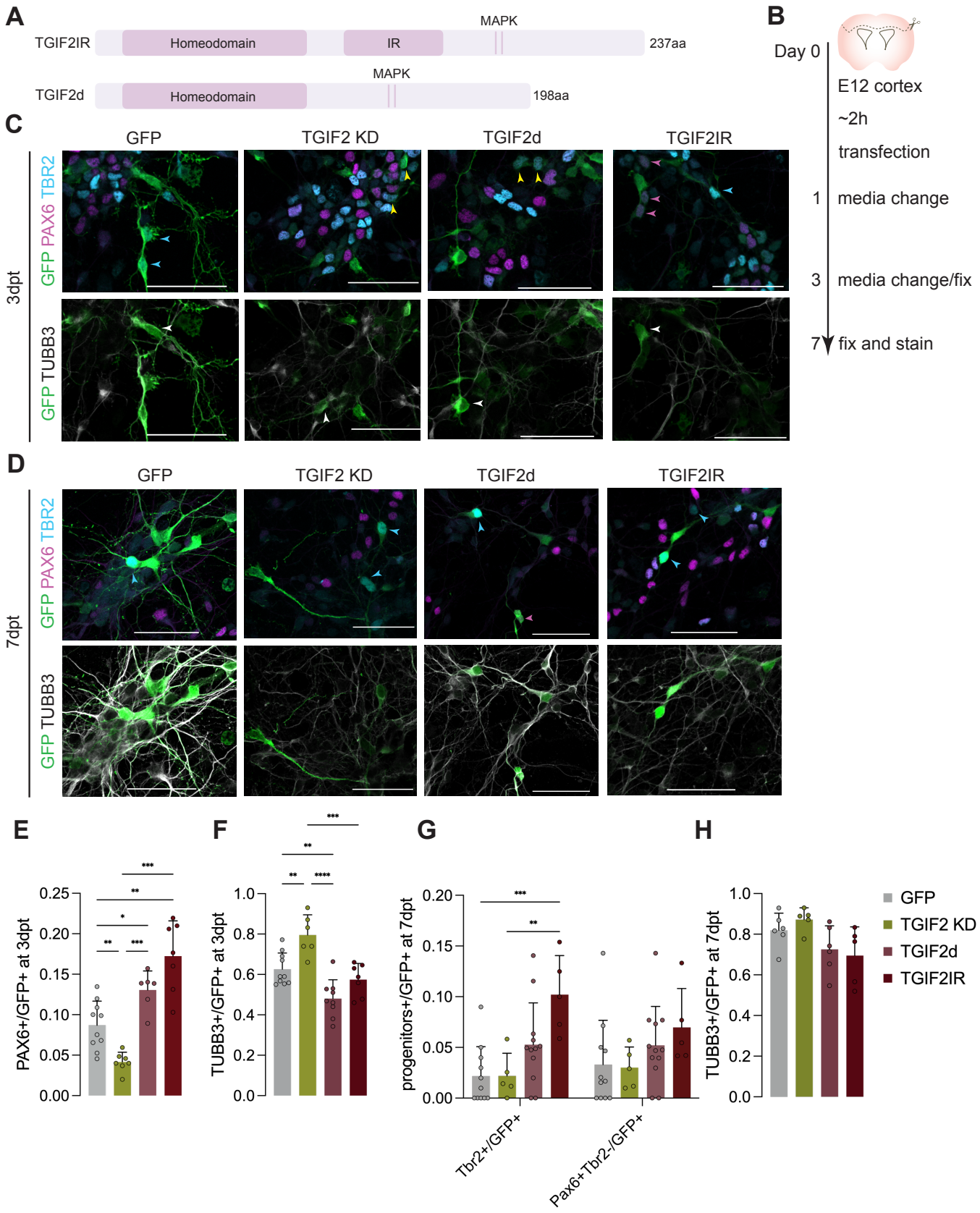
A
MAPK
TGIF2IR
Homeodomain
IR
237aa
MAPK
TGIF2d
Homeodomain
198aa
B
Day 0
E12 cortex
~2h
transfection
1
media change
3
media change/fix
7
fix and stain
C
GFP
TGIF2 KD
TGIF2d
TGIF2IR
3dpt
GFP PAX6 TBR2
GFP TUBB3
D
GFP
TGIF2 KD
TGIF2d
TGIF2IR
7dpt
GFP PAX6 TBR2
GFP TUBB3
E
PAX6+/GFP+ at 3dpt
F
TUBB3+/GFP+ at 3dpt
G
progenitors+/GFP+ at 7dpt
Tbr2+/GFP+
Pax6+Tbr2-/GFP+
H
TUBB3+/GFP+ at 7dpt
GFP
TGIF2 KD
TGIF2d
TGIF2IR

Figure 3

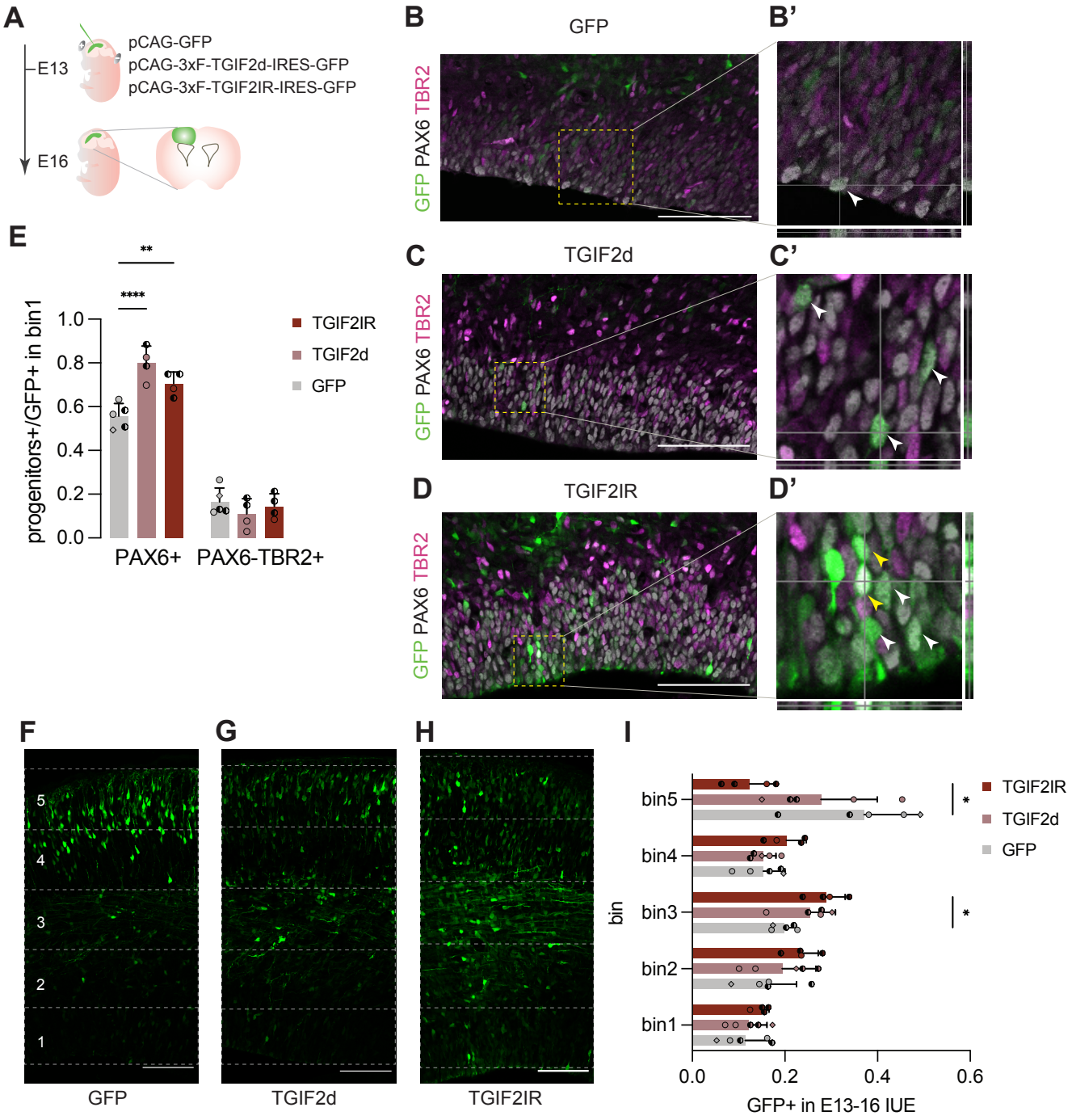
A
E13
E16
pCAG-GFP
pCAG-3xF-TGIF2d-IRES-GFP
pCAG-3xF-TGIF2IR-IRES-GFP
B
GFP
B'
GFP PAX6 TBR2
C
TGIF2d
C'
D
TGIF2IR
D'
E
**
****
progenitors+/GFP+ in bin1
1.0
0.8
0.6
0.4
0.2
0.0
TGIF2IR
TGIF2d
GFP
PAX6+
PAX6-TBR2+
F
G
H
5
4
3
2
1
GFP
TGIF2d
TGIF2IR
I
bin5
bin4
bin3
bin2
bin1
bin
*
*
TGIF2IR
TGIF2d
GFP
0.0
0.2
0.4
0.6
GFP+ in E13-16 IUE

Figure 4

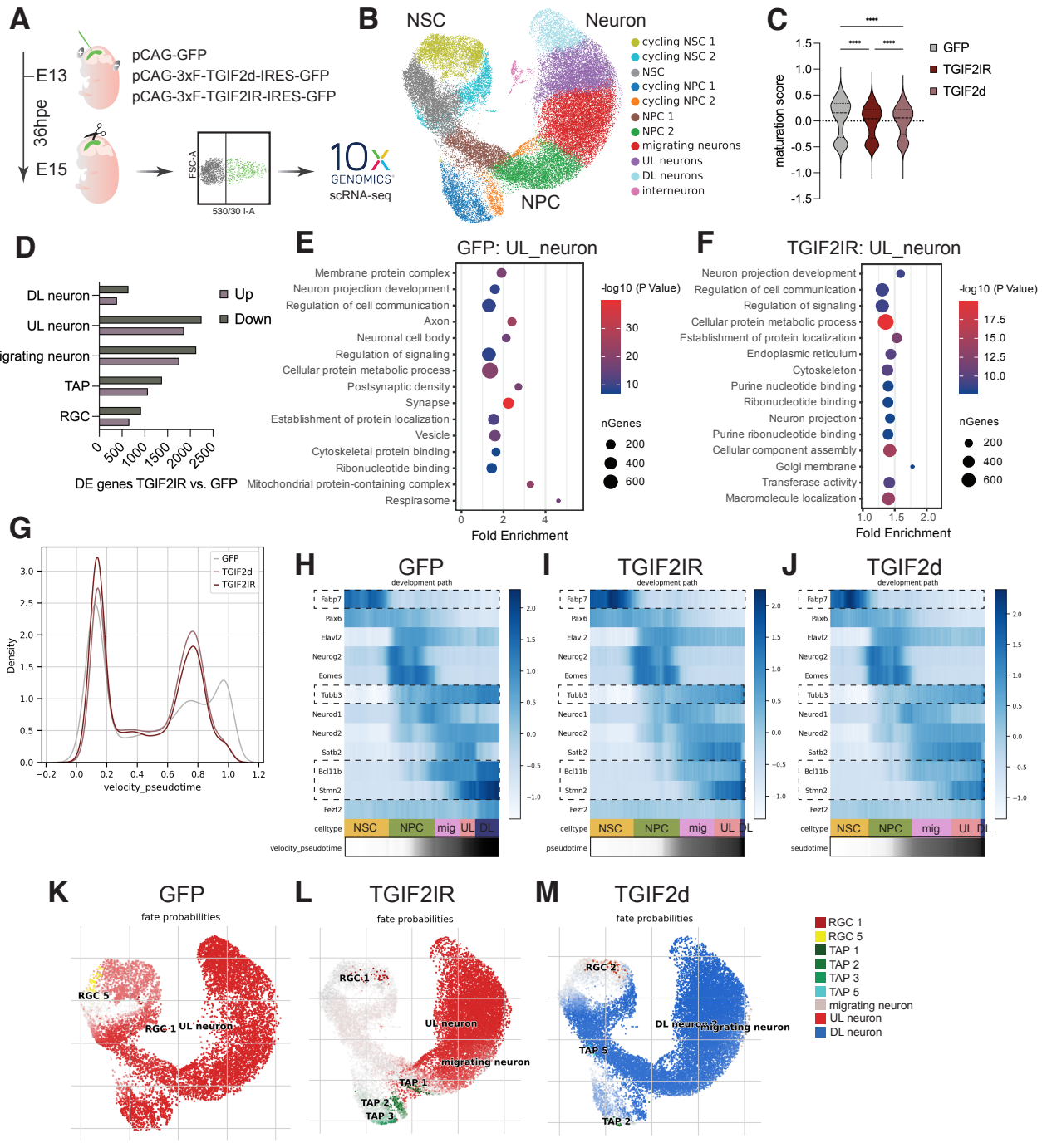
A
E13
36hpe
E15
pCAG-GFP
pCAG-3xF-TGIF2d-IRES-GFP
pCAG-3xF-TGIF2IR-IRES-GFP
FSC-A
530/30 I-A
10x GENOMICS
scRNA-seq
B
NSC
Neuron
NPC
cycling NSC 1
cycling NSC 2
NSC
cycling NPC 1
cycling NPC 2
NPC 1
NPC 2
migrating neurons
UL neurons
DL neurons
interneuron
C
maturation score
GFP
TGIF2IR
TGIF2d
D
DL neuron
UL neuron
migrating neuron
TAP
RGC
Up
Down
DE genes TGIF2IR vs. GFP
E
GFP: UL_neuron
Membrane protein complex
Neuron projection development
Regulation of cell communication
Axon
Neuronal cell body
Regulation of signaling
Cellular protein metabolic process
Postsynaptic density
Synapse
Establishment of protein localization
Vesicle
Cytoskeletal protein binding
Ribonucleotide binding
Mitochondrial protein-containing complex
Respirasome
-log10 (P Value)
nGenes
Fold Enrichment
F
TGIF2IR: UL_neuron
Neuron projection development
Regulation of cell communication
Regulation of signaling
Cellular protein metabolic process
Establishment of protein localization
Endoplasmic reticulum
Cytoskeleton
Purine nucleotide binding
Ribonucleotide binding
Neuron projection
Purine ribonucleotide binding
Cellular component assembly
Golgi membrane
Transferase activity
Macromolecule localization
-log10 (P Value)
nGenes
Fold Enrichment
G
GFP
TGIF2d
TGIF2IR
Density
velocity_pseudotime
H
GFP
development path
I
TGIF2IR
development path
J
TGIF2d
development path
Fabp7
Pax6
Elavl2
Neurog2
Eomes
Tubb3
Neurod1
Neurod2
Satb2
Bcl11b
Stmn2
Fezf2
celltype
NSC
NPC
mig
UL
DL
velocity_pseudotime
pseudotime
seudotime
K
GFP
fate probabilities
RGC 5
RGC 1
UL neuron
L
TGIF2IR
fate probabilities
RGC 1
UL neuron
migrating neuron
TAP 1
TAP 2
TAP 3
M
TGIF2d
fate probabilities
RGC 2
DL neuron
migrating neuron
TAP 5
TAP 2
RGC 1
RGC 5
TAP 1
TAP 2
TAP 3
TAP 5
migrating neuron
UL neuron
DL neuron

Figure 5

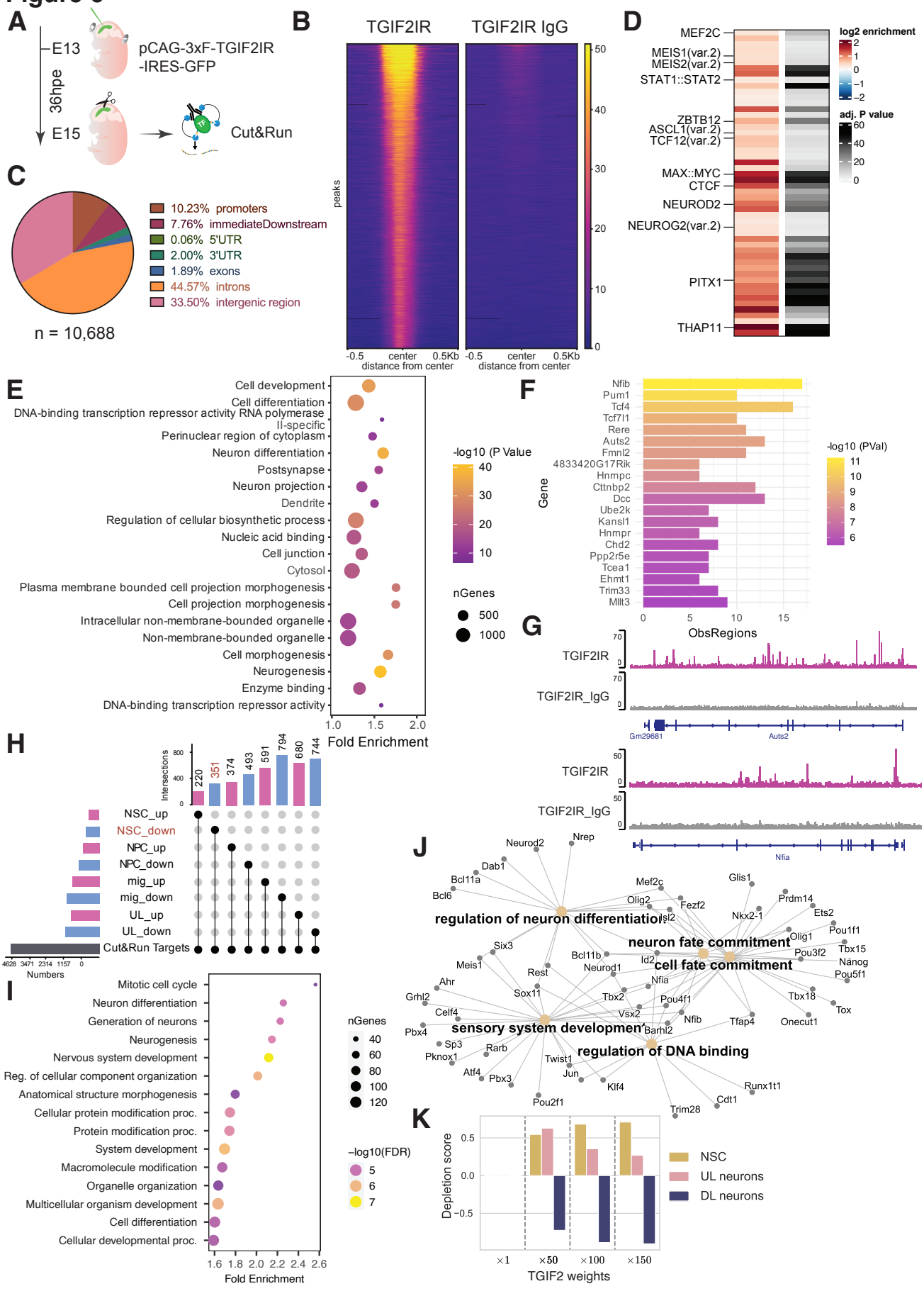
A
E13
36hpe
E15
pCAG-3xF-TGIF2IR
-IRES-GFP
Cut&Run
B
TGIF2IR
TGIF2IR IgG
peaks
-0.5
center
0.5Kb
distance from center
C
10.23% promoters
7.76% immediateDownstream
0.06% 5'UTR
2.00% 3'UTR
1.89% exons
44.57% introns
33.50% intergenic region
n = 10,688
D
MEF2C
MEIS1(var.2)
MEIS2(var.2)
STAT1::STAT2
ZBTB12
ASCL1(var.2)
TCF12(var.2)
MAX::MYC
CTCF
NEUROD2
NEUROG2(var.2)
PITX1
THAP11
log2 enrichment
adj. P value
E
Cell development
Cell differentiation
DNA-binding transcription repressor activity RNA polymerase II-specific
Perinuclear region of cytoplasm
Neuron differentiation
Postsynapse
Neuron projection
Dendrite
Regulation of cellular biosynthetic process
Nucleic acid binding
Cell junction
Cytosol
Plasma membrane bounded cell projection morphogenesis
Cell projection morphogenesis
Intracellular non-membrane-bounded organelle
Non-membrane-bounded organelle
Cell morphogenesis
Neurogenesis
Enzyme binding
DNA-binding transcription repressor activity
Fold Enrichment
-log10 (P Value
nGenes
F
Nfib
Pum1
Tcf4
Tcf7l1
Rere
Auts2
Fmnl2
4833420G17Rik
Hnmpc
Cttnbp2
Dcc
Ube2k
Kansl1
Hnmpr
Chd2
Ppp2r5e
Tcea1
Ehmt1
Trim33
Mllt3
Gene
-log10 (PVal)
G
ObsRegions
TGIF2IR
TGIF2IR_IgG
Gm29681
Auts2
Nfia
H
Intersections
220
351
374
493
591
794
680
744
NSC_up
NSC_down
NPC_up
NPC_down
mig_up
mig_down
UL_up
UL_down
Cut&Run Targets
Numbers
I
Mitotic cell cycle
Neuron differentiation
Generation of neurons
Neurogenesis
Nervous system development
Reg. of cellular component organization
Anatomical structure morphogenesis
Cellular protein modification proc.
Protein modification proc.
System development
Macromolecule modification
Organelle organization
Multicellular organism development
Cell differentiation
Cellular developmental proc.
Fold Enrichment
nGenes
−log10(FDR)
J
regulation of neuron differentiation
neuron fate commitment
cell fate commitment
sensory system development
regulation of DNA binding
Neurod2
Nrep
Dab1
Bcl11a
Bcl6
Mef2c
Olig2
Fezf2
Isl2
Glis1
Prdm14
Nkx2-1
Ets2
Pou1f1
Olig1
Pou3f2
Tbx15
Nanog
Pou5f1
Six3
Meis1
Bcl11b
Id2
Neurod1
Rest
Nfia
Ahr
Sox11
Tbx2
Pou4f1
Tbx18
Tox
Grhl2
Celf4
Vsx2
Nfib
Tfap4
Onecut1
Pbx4
Sp3
Pknox1
Rarb
Barhl2
Twist1
Atf4
Pbx3
Jun
Klf4
Pou2f1
Runx1t1
Cdt1
Trim28
K
Depletion score
NSC
UL neurons
DL neurons
×1
×50
×100
×150
TGIF2 weights

Figure 6

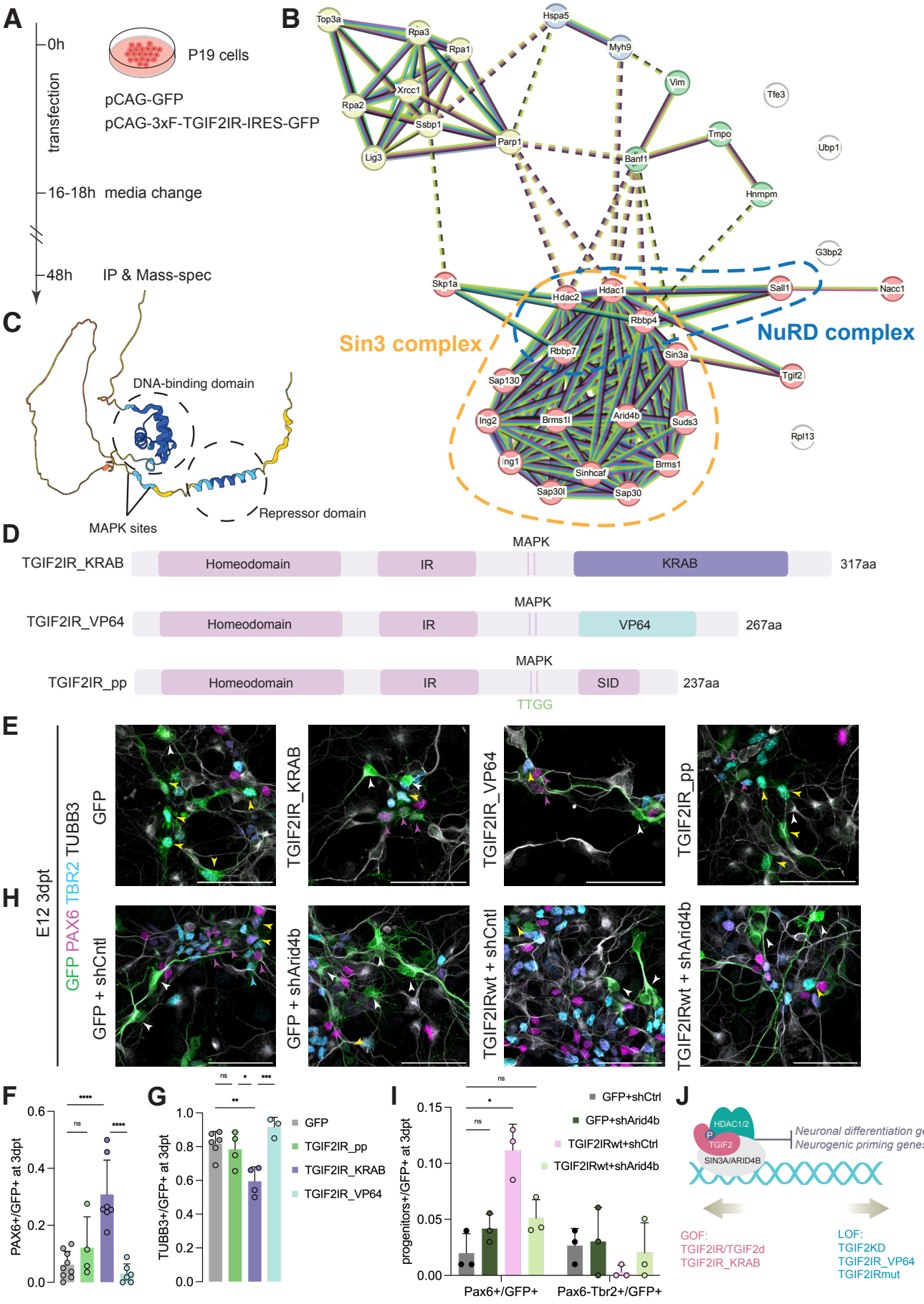
A
0h
transfection
P19 cells
pCAG-GFP
pCAG-3xF-TGIF2IR-IRES-GFP
16-18h media change
48h IP & Mass-spec
B
Top3a
Rpa3
Rpa1
Xrcc1
Rpa2
Ssbp1
Lig3
Parp1
Hspa5
Myh9
Vim
Tfe3
Tmpo
Ubp1
Banf1
Hnrnpm
G3bp2
Skp1a
Hdac2
Hdac1
Sall1
Nacc1
Rbbp4
Rbbp7
Sin3a
Tgif2
Sap130
Ing2
Brms1l
Arid4b
Suds3
Rpl13
Ing1
Sinhcaf
Brms1
Sap30l
Sap30
Sin3 complex
NuRD complex
C
DNA-binding domain
MAPK sites
Repressor domain
D
MAPK
TGIF2IR_KRAB
Homeodomain
IR
KRAB
317aa
TGIF2IR_VP64
VP64
267aa
TGIF2IR_pp
SID
237aa
TTGG
E
E12 3dpt
GFP PAX6 TBR2 TUBB3
GFP
TGIF2IR_KRAB
TGIF2IR_VP64
TGIF2IR_pp
H
GFP + shCntl
GFP + shArid4b
TGIF2IRwt + shCntl
TGIF2IRwt + shArid4b
F
PAX6+/GFP+ at 3dpt
ns
****
G
TUBB3+/GFP+ at 3dpt
GFP
TGIF2IR_pp
TGIF2IR_KRAB
TGIF2IR_VP64
I
progenitors+/GFP+ at 3dpt
GFP+shCtrl
GFP+shArid4b
TGIF2IRwt+shCtrl
TGIF2IRwt+shArid4b
Pax6+/GFP+
Pax6-Tbr2+/GFP+
J
HDAC1/2
P
TGIF2
SIN3A/ARID4B
Neuronal differentiation genes
Neurogenic priming genes
GOF:
TGIF2IR/TGIF2d
TGIF2IR_KRAB
LOF:
TGIF2KD
TGIF2IR_VP64
TGIF2IRmut

Figure 7

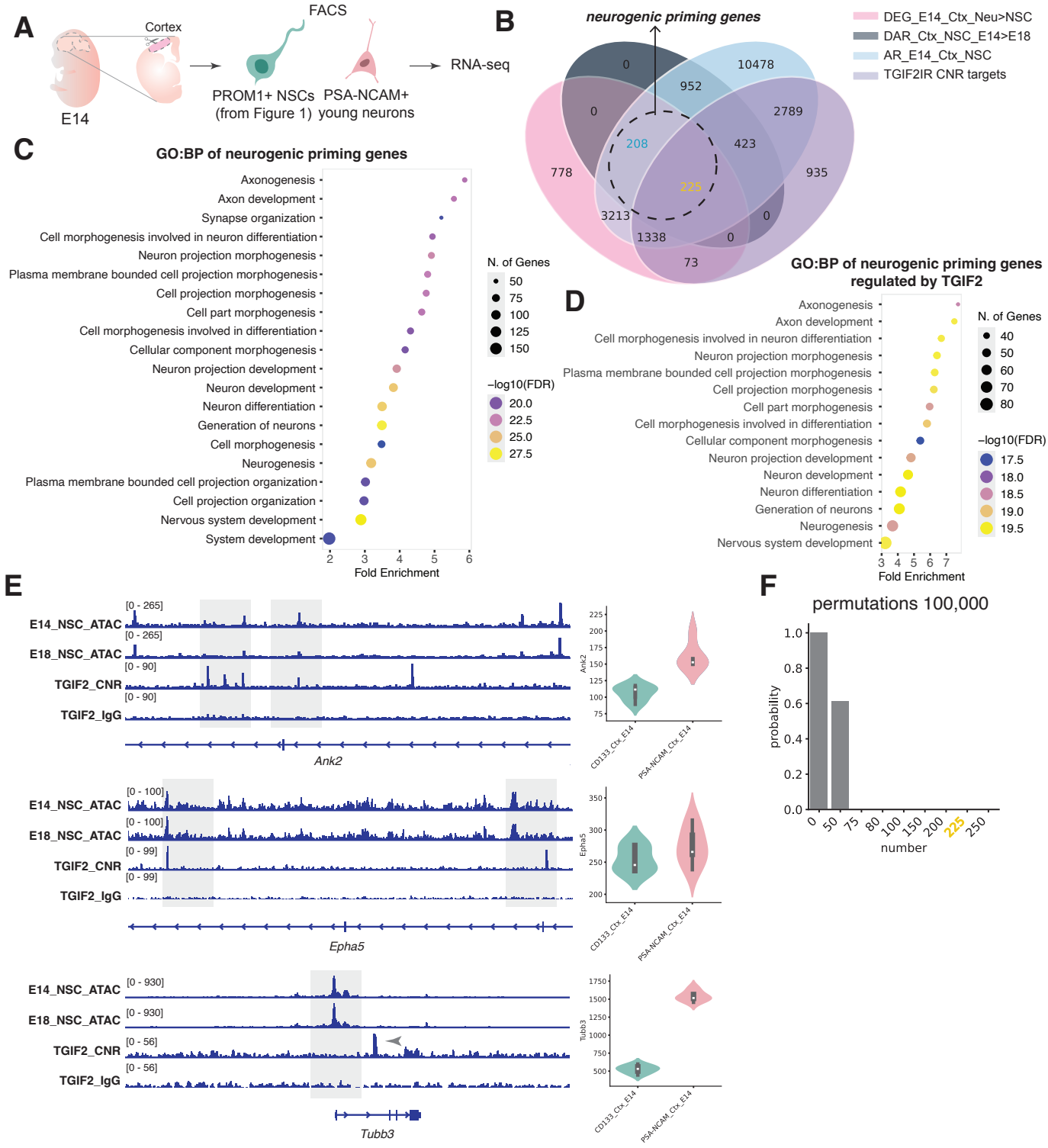
A
Cortex
E14
FACS
PROM1+ NSCs
(from Figure 1)
PSA-NCAM+
young neurons
RNA-seq
B
neurogenic priming genes
DEG_E14_Ctx_Neu>NSC
DAR_Ctx_NSC_E14>E18
AR_E14_Ctx_NSC
TGIF2IR CNR targets
0
10478
952
0
2789
208
423
778
935
225
3213
0
1338
0
73
C
GO:BP of neurogenic priming genes
Axonogenesis
Axon development
Synapse organization
Cell morphogenesis involved in neuron differentiation
Neuron projection morphogenesis
Plasma membrane bounded cell projection morphogenesis
Cell projection morphogenesis
Cell part morphogenesis
Cell morphogenesis involved in differentiation
Cellular component morphogenesis
Neuron projection development
Neuron development
Neuron differentiation
Generation of neurons
Cell morphogenesis
Neurogenesis
Plasma membrane bounded cell projection organization
Cell projection organization
Nervous system development
System development
2 3 4 5 6
Fold Enrichment
N. of Genes
50
75
100
125
150
–log10(FDR)
20.0
22.5
25.0
27.5
D
GO:BP of neurogenic priming genes regulated by TGIF2
Axonogenesis
Axon development
Cell morphogenesis involved in neuron differentiation
Neuron projection morphogenesis
Plasma membrane bounded cell projection morphogenesis
Cell projection morphogenesis
Cell part morphogenesis
Cell morphogenesis involved in differentiation
Cellular component morphogenesis
Neuron projection development
Neuron development
Neuron differentiation
Generation of neurons
Neurogenesis
Nervous system development
3 4 5 6 7
Fold Enrichment
N. of Genes
40
50
60
70
80
–log10(FDR)
17.5
18.0
18.5
19.0
19.5
E
E14_NSC_ATAC
E18_NSC_ATAC
TGIF2_CNR
TGIF2_IgG
[0 - 265]
[0 - 90]
[0 - 100]
[0 - 99]
[0 - 930]
[0 - 56]
Ank2
Epha5
Tubb3
CD133_Ctx_E14
PSA-NCAM_Ctx_E14
F
permutations 100,000
probability
number
0 50 75 80 100 150 200 225 250

Figure S1. RNA-seq analysis of Radial Glial cells isolated from cerebral cortex and LGE at E14 and E18.

(A) Principal component analysis of the RNA-seq data with region marked with different shapes and stage marked with different colours. Ctx: Cortex; LGE: Lateral Ganglionic Eminence; E: Embryonic

(B) Heatmap of samples clustered according to different parameters of the dataset.

(C) Heatmap of the top 25 differentially up- or down- regulated genes in the cortex at E14 versus E18. FC: fold change; AveExpr: average expression

(D) Heatmap of the top 25 differentially up- or down- regulated genes in the LGE at E14 versus E18. FC: fold change; AveExpr: average expression

(F) GO terms associated with biological processes, showing top 2 terms each from 10 clusters of semantic space analysis, taken from genes upregulated at E14 versus E18 cortex.

(G) GO terms associated with biological processes, showing top 2 terms each from 10 clusters of semantic space analysis, taken from genes upregulated at E14 versus E18 LGE.

Figure S2. ATAC-seq analysis of Radial Glial cells isolated from cerebral cortex and LGE at E14 and E18.

(A) Principal component analysis of the ATAC-seq data with region marked with different shapes and stage marked with different colours. Ctx: Cortex; LGE: Lateral Ganglionic Eminence; E: Embryonic

(B) Heatmap of the ATAC-seq samples clustered based on chromatin openness and annotated based on different parameters of the dataset.

(C) Volcano plot of significantly differentially open peaks in E14 versus E18 in Cortex (FDR < 0.05). Top 10 differential peaks are labeled by the nearest gene in their proximity. Ctx: Cortex; LGE: Lateral Ganglionic Eminence; E: Embryonic

(D) Volcano plot of significantly differentially open peaks in E14 versusE18 in LGE (FDR < 0.05). Top 10 differential peaks are labeled by nearest gene in their proximity. Ctx: Cortex; LGE: Lateral Ganglionic Eminence; E: Embryonic

(E) Venn diagram depicting overlap of differentially open peaks in E14 versus E18 Cortex, differentially open peaks in LGE versus Cortex E18, and the non-differential (consensus) peaks between Cortex and LGE in E14. Left: overlap of the peaks, middle: overlap of the genes in proximity to peaks, right: overlap of the motifs associated to open peaks.

(F) Venn diagram depicting overlap of genes in proximity to differentially open peaks in E14 versus E18 Cortex, differentially open peaks in LGE versus Cortex E18, and the non-differential (consensus) peaks between Cortex and LGE in E14.

(G) Venn diagram depicting overlap of motifs enriched in differentially open peaks in E14 versus E18 Cortex, differentially open peaks in LGE versus Cortex E18, and the non-differential (consensus) peaks between Cortex and LGE in E14.

(H) Barplot showing gene ontology terms enriched in genes in proximity to differentially open peaks between E14 and E18 in Cortex.

(I) Barplot showing gene ontology terms enriched in genes in proximity to differentially open peaks between LGE and Cortex in E18.

(J) Barplot showing gene ontology terms enriched in genes in proximity to non-differentially open (consensus) peaks between Cortex and LGE in E14. Terms that are shared between all 3 comparisons are highlighted in blue.

Figure S3. TGIF2 expression during development and immunostaining analysis after overexpression *in vivo*.

(A) ISH data of mouse TGIF2 across different developmental timepoints, excerpts from Allen Brain Atlas[41].

(B-C) Violin plots showing quantification of knockdown efficiency titration with siRNA pool in final concentrations, together with TGIF2IR overexpression, measured by mean intensity in the channel of TGIF2 Abcam antibody (B) and the channel of FLAG antibody (C). N=8-21 cells measured with DAPI mask. Kruskal-Wallis ANOVA with Dunn's multiple comparisons test.

(D) Representative images and their insets of *in utero* electroporated cortices from different conditions (GFP+) immunostained with pH3 and PAX6. Arrowheads indicate pH3+/GFP+ cells.

(E) Quantification of pH3+/GFP+ cells in bin 1, mean±SD. N=4 embryos from at least 2 mothers. Ordinary one-way ANOVA with Dunnett's multiple comparison's test.

(F-H) Representative images showing cortices 3 days post electroporation with different conditions in GFP, co-stained with NEUROD2. Dashed lines indicate the 5 equal bins. Scale bar: 100μm

(I) Quantification of NEUROD2+/GFP+ cells in bin 3, mean±SD. N=3-4 embryos from at least 2 mothers. Ordinary one-way ANOVA with Dunnett's multiple comparison's test. Only significant result is shown.

Figure S4. Leiden clustering and marker gene expression in the scRNA-seq data

(A) UMAP projection of cells grouped by pool, mouse, and condition.

(B) Leiden clustering with UMAP projection.

(C) Scatter plot of cell cycle phase from cell cycle marker gene expression.

(D-E) UMAP scatterplot and dot plot of marker gene expression across cell clusters.

(E) Tgif2 expression levels across different cell types and conditions.

Figure S5. Velocity pseudotime and CellRank procedures

(A-C) UMAP of velocity pseudotime across 3 conditions.

(D-F) Violin plots of velocity pseudotime across cell types in different conditions.

(G, K, O) UMAP representation of RNA velocity[27].

(H, L, P) Macrostates predicted by CellRank. RGC: radial glial cells, or NSCS; TAP: transit amplifying progenitors, or NPCs.

(I, M, Q) Terminal states predicted by CellRank[28,29].

(J, N, R) Violin plots of initial score (Fabp7, Pax6, Sox2 expression) of macrostates predicted by CellRank[28,29].

Figure S6. Mutation in SID of TGIF2 abrogates its function, some interactions and binding to target sites

(A) Schematic drawing of TGIF2IRmut construct.

(B) Representative images showing E12 primary cortex cells cultures transfected with GFP, same as in Figure 6E, and TGIF2IRmut, co-stained with PAX6, TBR2, and TUBB3. Scale bar: 50μm.

(C-D) Quantification of PAX6+/GFP+ and TUBB3+/GFP+ in transfected E12 cortex cell culture at 3dpt with different conditions as indicated in the legends, mean±SD. N= 7-11 pools of embryos. Mann-Whitney test.

(E-F) Representative images showing cortices 3 days post IUE with GFP (E) and TGIF2IRmut (F). Dashed lines indicate the 5 equal bins. Scale bar: 100μm.

(G) Quantification of GFP+ distribution in each bin, mean±SD. N=4 embryos from at least 2 mothers. Ordinary two-way ANOVA with Sidak's multiple comparisons test, with a single pooled variance.

(H) Quantification of SATB2+/GFP+ in each bin from embryos *in utero* electroporated with GFP or TGIF2IRmut. Ordinary two-way ANOVA with Sidak's multiple comparisons test, with a single pooled variance.

(I) Enrichment heatmap of TGIF2IRwt and TGIF2IRmut, centered on the middle of the peaks.

(J) Venn diagram showing the overlapped *peaks* between TGIF2IRwt and TGIF2IRmut from Cut&Run analysis.

(K) Peak examples with bigwig profile of TGIF2IRwt and TGIF2IRmut, with their corresponding IgG control at the gene locus of *Arid4b*. Dashed lines circle the peaks.

(L) Venn diagram showing the overlapped *genes* between TGIF2IRwt and TGIF2IRmut from Cut&Run analysis, as well as genes upregulated in TGIF2IRmut compared to GFP control from its scRNA-seq DE analysis (log2fc>0, pval <0.05).

(M) STRING analysis of interactors of TGIF2IRmut with LFQ intensity more than 3-fold compared to GFP control.

(N) Venn diagram comparing the interactors of TGIF2IRwt and TGIF2IRmut with LFQ intensity more than 3-fold compared to GFP control. The interactors lost in TGIF2IRmut are listed. ARID4B, which belongs to SIN3A complex, is marked in red.

(O) Western blot of P19 cells transfected with candidate shRNAs for Arid4b KD, including a mock transfection control. Blotted bands show canonical ARID4B protein. shRNA#2 (against open reading frame of *Arid4b*) with the most efficient KD was used for further experiments.

Figure S1

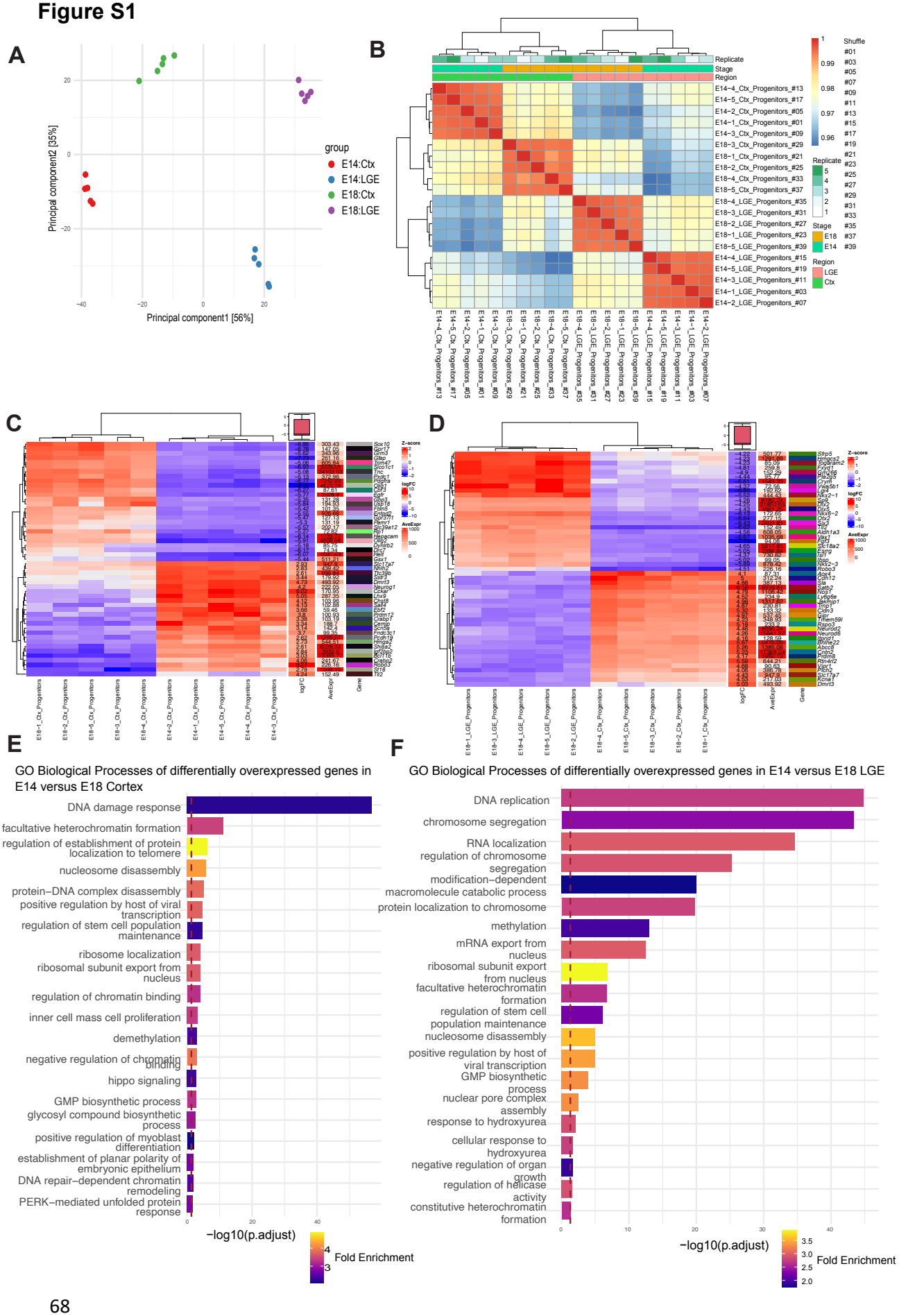
A
Principal component2 [35%]
Principal component1 [56%]
group
E14:Ctx
E14:LGE
E18:Ctx
E18:LGE
B
Replicate
Stage
Region
Shuffle
C
D
Z-score
logFC
AveExpr
Gene
E
GO Biological Processes of differentially overexpressed genes in E14 versus E18 Cortex
DNA damage response
facultative heterochromatin formation
regulation of establishment of protein localization to telomere
nucleosome disassembly
protein–DNA complex disassembly
positive regulation by host of viral transcription
regulation of stem cell population maintenance
ribosome localization
ribosomal subunit export from nucleus
regulation of chromatin binding
inner cell mass cell proliferation
demethylation
negative regulation of chromatin binding
hippo signaling
GMP biosynthetic process
glycosyl compound biosynthetic process
positive regulation of myoblast differentiation
establishment of planar polarity of embryonic epithelium
DNA repair–dependent chromatin remodeling
PERK–mediated unfolded protein response
−log10(p.adjust)
Fold Enrichment
F
GO Biological Processes of differentially overexpressed genes in E14 versus E18 LGE
DNA replication
chromosome segregation
RNA localization
regulation of chromosome segregation
modification–dependent macromolecule catabolic process
protein localization to chromosome
methylation
mRNA export from nucleus
ribosomal subunit export from nucleus
facultative heterochromatin formation
regulation of stem cell population maintenance
nucleosome disassembly
positive regulation by host of viral transcription
GMP biosynthetic process
nuclear pore complex assembly
response to hydroxyurea
cellular response to hydroxyurea
negative regulation of organ growth
regulation of helicase activity
constitutive heterochromatin formation
−log10(p.adjust)
Fold Enrichment

Figure S2

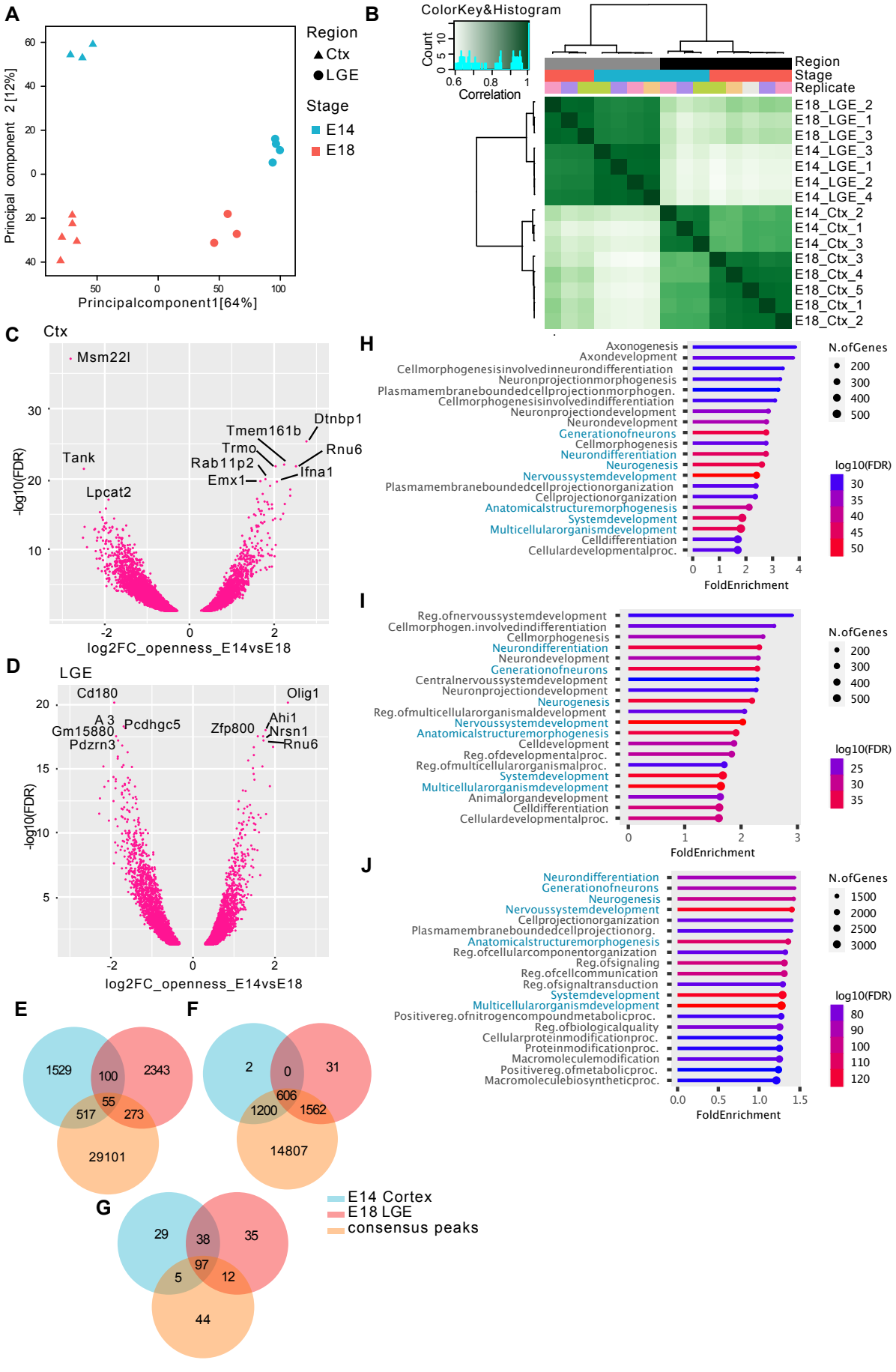
A
Region
Ctx
LGE
Stage
E14
E18
Principal component 2 [12%]
Principalcomponent1[64%]
B
ColorKey&Histogram
Count
Correlation
Region
Stage
Replicate
E18_LGE_2
E18_LGE_1
E18_LGE_3
E14_LGE_3
E14_LGE_1
E14_LGE_2
E14_LGE_4
E14_Ctx_2
E14_Ctx_1
E14_Ctx_3
E18_Ctx_3
E18_Ctx_4
E18_Ctx_5
E18_Ctx_1
E18_Ctx_2
C
Ctx
Msm22l
Dtnbp1
Tmem161b
Trmo
Rnu6
Tank
Rab11p2
Ifna1
Emx1
Lpcat2
-log10(FDR)
log2FC_openness_E14vsE18
D
LGE
Cd180
Olig1
A 3
Gm15880
Pcdhgc5
Zfp800
Ahi1
Nrsn1
Pdzrn3
Rnu6
-log10(FDR)
log2FC_openness_E14vsE18
E
1529
100
2343
55
517
273
29101
F
2
0
31
606
1200
1562
14807
G
29
38
35
97
5
12
44
E14 Cortex
E18 LGE
consensus peaks
H
Axonogenesis
Axondevelopment
Cellmorphogenesisinvolvedinneurondifferentiation
Neuronprojectionmorphogenesis
Plasmamembraneboundedcellprojectionmorphogen.
Cellmorphogenesisinvolvedindifferentiation
Neuronprojectiondevelopment
Neurondevelopment
Generationofneurons
Cellmorphogenesis
Neurondifferentiation
Neurogenesis
Nervoussystemdevelopment
Plasmamembraneboundedcellprojectionorganization
Cellprojectionorganization
Anatomicalstructuremorphogenesis
Systemdevelopment
Multicellularorganismdevelopment
Celldifferentiation
Cellulardevelopmentalproc.
FoldEnrichment
N.ofGenes
200
300
400
500
log10(FDR)
30
35
40
45
50
I
Reg.ofnervoussystemdevelopment
Cellmorphogen.involvedindifferentiation
Cellmorphogenesis
Neurondifferentiation
Neurondevelopment
Generationofneurons
Centralnervoussystemdevelopment
Neuronprojectiondevelopment
Neurogenesis
Reg.ofmulticellularorganismaldevelopment
Nervoussystemdevelopment
Anatomicalstructuremorphogenesis
Celldevelopment
Reg.ofdevelopmentalproc.
Reg.ofmulticellularorganismalproc.
Systemdevelopment
Multicellularorganismdevelopment
Animalorgandevelopment
Celldifferentiation
Cellulardevelopmentalproc.
FoldEnrichment
N.ofGenes
200
300
400
500
log10(FDR)
25
30
35
J
Neurondifferentiation
Generationofneurons
Neurogenesis
Nervoussystemdevelopment
Cellprojectionorganization
Plasmamembraneboundedcellprojectionorg.
Anatomicalstructuremorphogenesis
Reg.ofcellularcomponentorganization
Reg.ofsignaling
Reg.ofcellcommunication
Reg.ofsignaltransduction
Systemdevelopment
Multicellularorganismdevelopment
Positivereg.ofnitrogencompoundmetabolicproc.
Reg.ofbiologicalquality
Cellularproteinmodificationproc.
Proteinmodificationproc.
Macromoleculemodification
Positivereg.ofmetabolicproc.
Macromoleculebiosyntheticproc.
FoldEnrichment
N.ofGenes
1500
2000
2500
3000
log10(FDR)
80
90
100
110
120

Figure S3

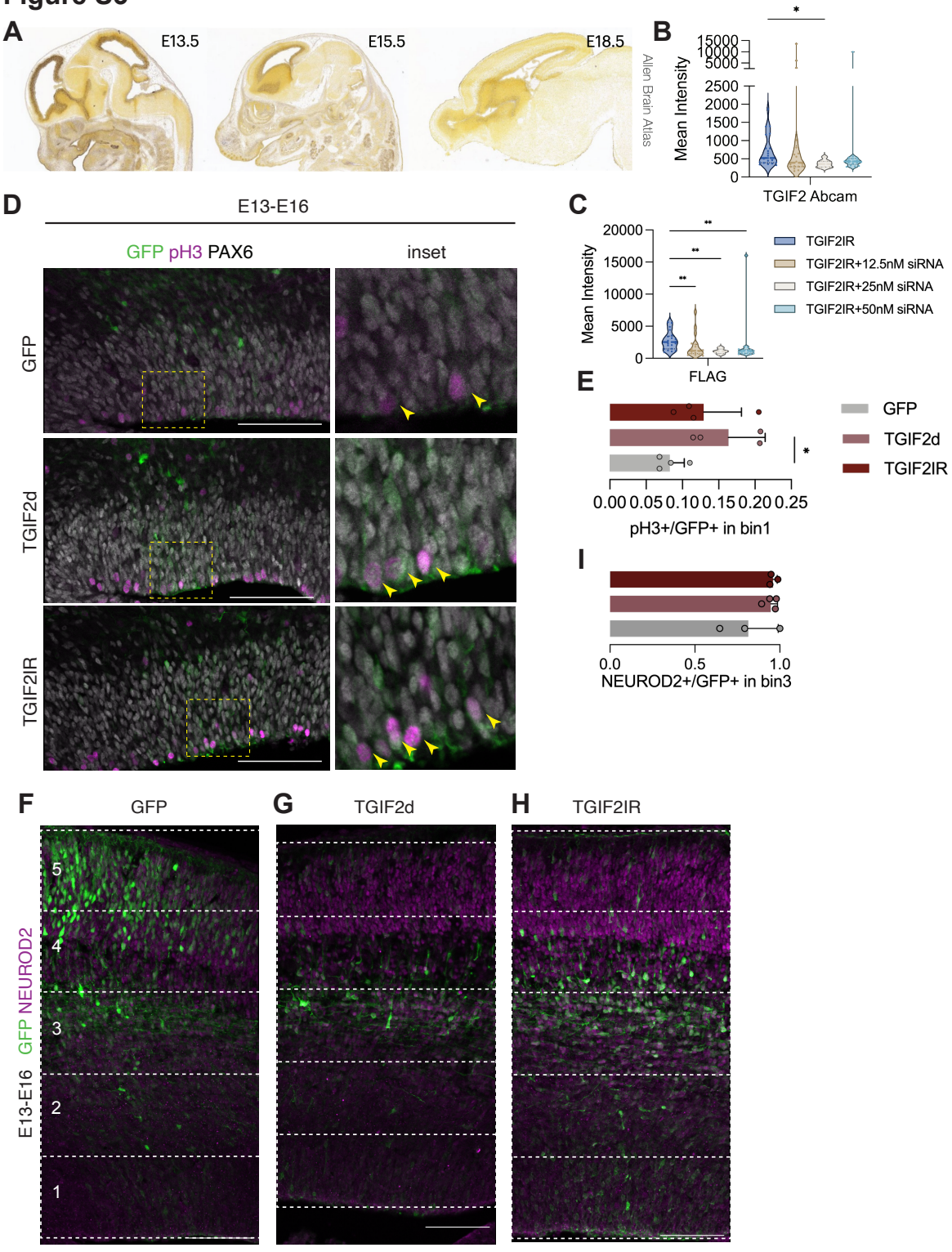
A
E13.5
E15.5
E18.5
Allen Brain Atlas
B
Mean Intensity
TGIF2 Abcam
C
Mean Intensity
FLAG
TGIF2IR
TGIF2IR+12.5nM siRNA
TGIF2IR+25nM siRNA
TGIF2IR+50nM siRNA
D
E13-E16
GFP pH3 PAX6
inset
GFP
TGIF2d
TGIF2IR
E
pH3+/GFP+ in bin1
GFP
TGIF2d
TGIF2IR
I
NEUROD2+/GFP+ in bin3
F
GFP
G
TGIF2d
H
TGIF2IR
E13-E16 GFP NEUROD2
5
4
3
2
1

Figure S4

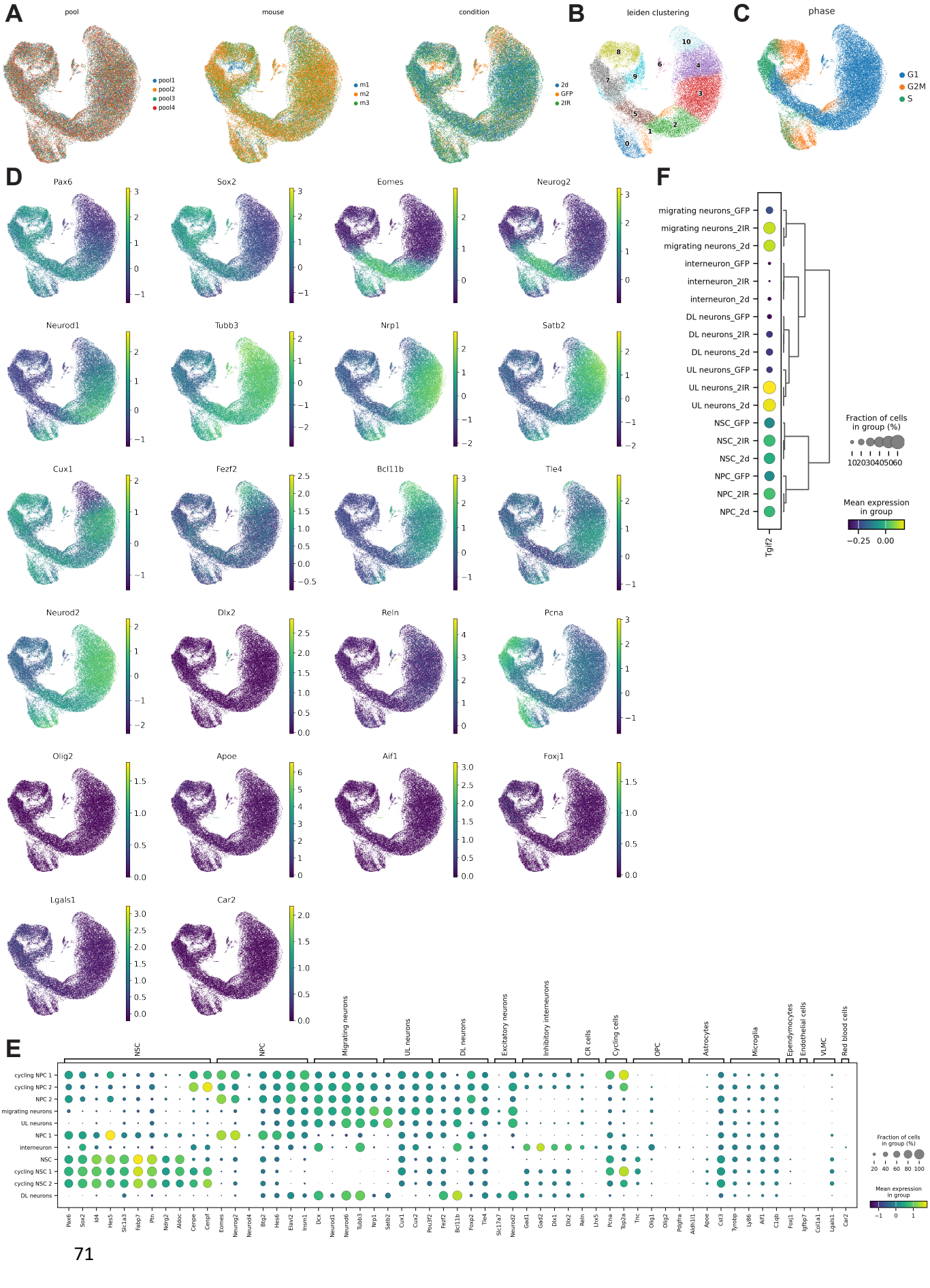
A
pool
pool1
pool2
pool3
pool4
mouse
m1
m2
m3
condition
2d
GFP
2IR
B
leiden clustering
C
phase
G1
G2M
S
D
Pax6
Sox2
Eomes
Neurog2
Neurod1
Tubb3
Nrp1
Satb2
Cux1
Fezf2
Bcl11b
Tle4
Neurod2
Dlx2
Reln
Pcna
Olig2
Apoe
Aif1
Foxj1
Lgals1
Car2
F
migrating neurons_GFP
migrating neurons_2IR
migrating neurons_2d
interneuron_GFP
interneuron_2IR
interneuron_2d
DL neurons_GFP
DL neurons_2IR
DL neurons_2d
UL neurons_GFP
UL neurons_2IR
UL neurons_2d
NSC_GFP
NSC_2IR
NSC_2d
NPC_GFP
NPC_2IR
NPC_2d
Tgif2
Fraction of cells in group (%)
Mean expression in group
E
NSC
NPC
Migrating neurons
UL neurons
DL neurons
Excitatory neurons
Inhibitory interneurons
CR cells
Cycling cells
OPC
Astrocytes
Microglia
Ependymocytes
Endothelial cells
VLMC
Red blood cells
cycling NPC 1
cycling NPC 2
NPC 2
migrating neurons
UL neurons
NPC 1
interneuron
NSC
cycling NSC 1
cycling NSC 2
DL neurons
Fraction of cells in group (%)
Mean expression in group

Figure S5

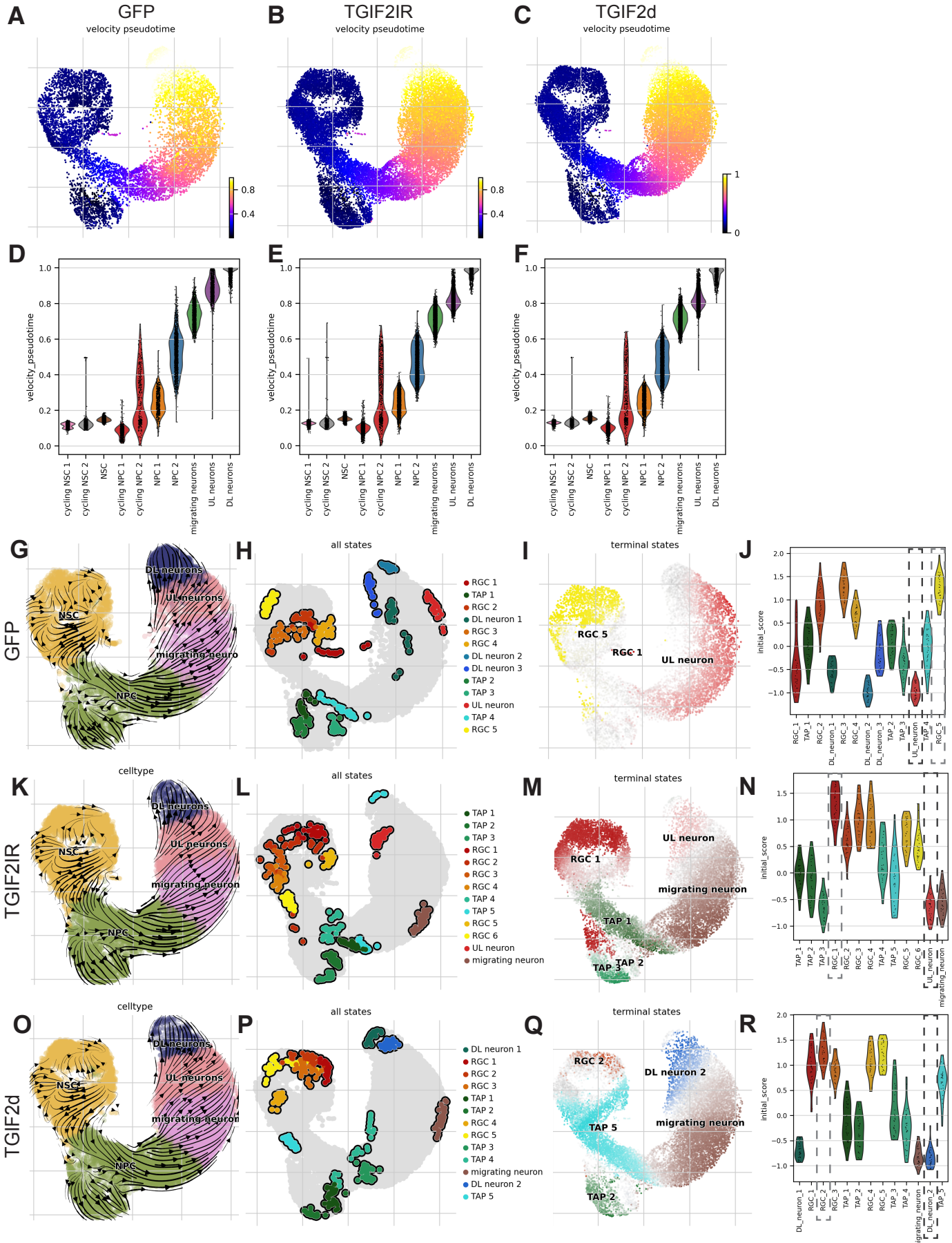
A
GFP
velocity pseudotime
B
TGIF2IR
velocity pseudotime
C
TGIF2d
velocity pseudotime
D
E
F
velocity_pseudotime
cycling NSC 1
cycling NSC 2
NSC
cycling NPC 1
cycling NPC 2
NPC 1
NPC 2
migrating neurons
UL neurons
DL neurons
G
GFP
DL neurons
UL neurons
NSC
migrating neuro
NPC
H
all states
RGC 1
TAP 1
RGC 2
DL neuron 1
RGC 3
RGC 4
DL neuron 2
DL neuron 3
TAP 2
TAP 3
UL neuron
TAP 4
RGC 5
I
terminal states
RGC 5
RGC 1
UL neuron
J
initial_score
K
TGIF2IR
celltype
DL neurons
UL neurons
NSC
migrating neuron
NPC
L
all states
TAP 1
TAP 2
TAP 3
RGC 1
RGC 2
RGC 3
RGC 4
TAP 4
TAP 5
RGC 5
RGC 6
UL neuron
migrating neuron
M
terminal states
UL neuron
RGC 1
migrating neuron
TAP 1
TAP 2
TAP 3
N
initial_score
O
TGIF2d
celltype
DL neurons
UL neurons
NSC
migrating neuron
NPC
P
all states
DL neuron 1
RGC 1
RGC 2
RGC 3
TAP 1
TAP 2
RGC 4
RGC 5
TAP 3
TAP 4
migrating neuron
DL neuron 2
TAP 5
Q
terminal states
RGC 2
DL neuron 2
TAP 5
migrating neuron
TAP 2
R
initial_score

Figure S6

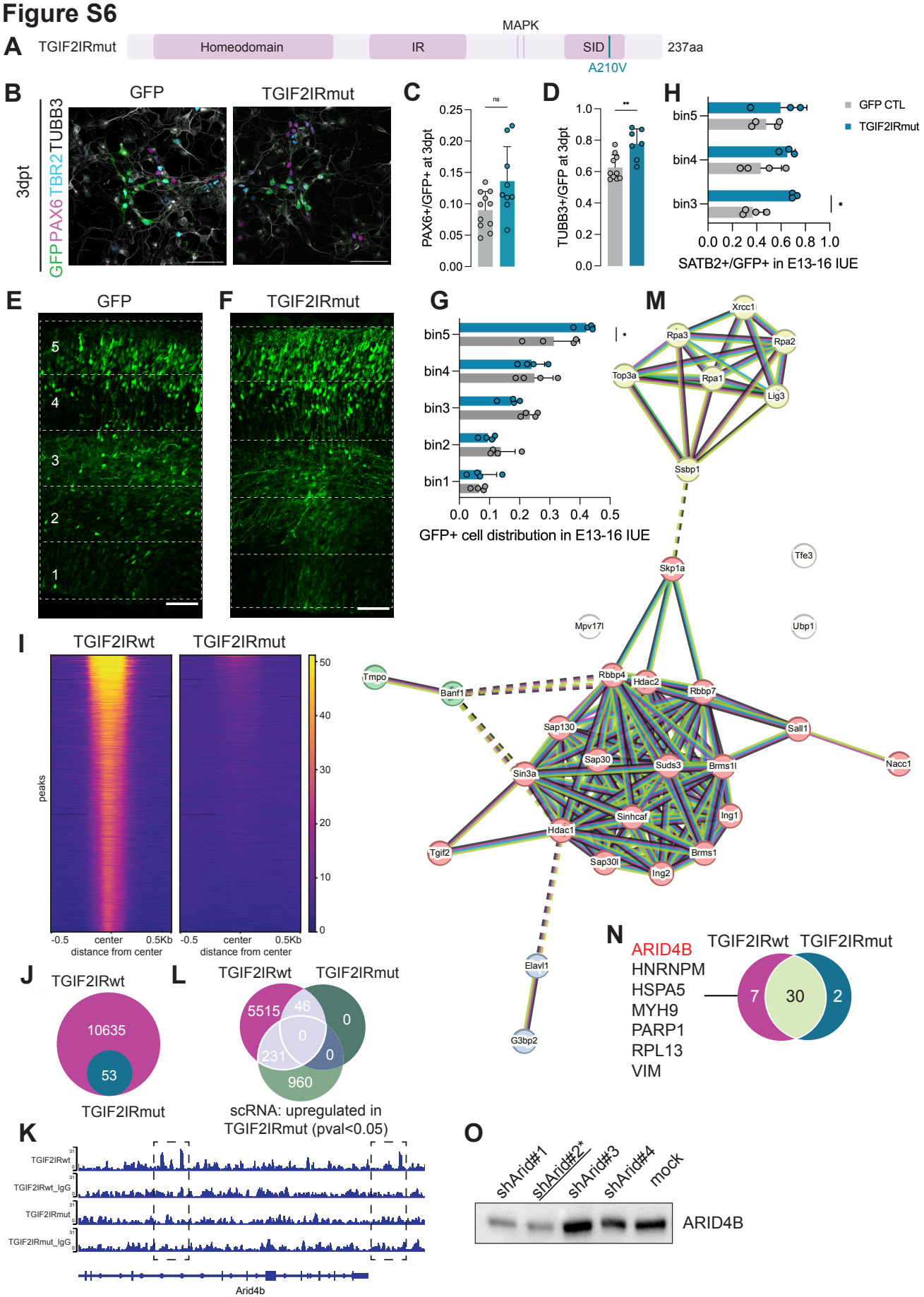
A
TGIF2IRmut
MAPK
Homeodomain
IR
SID
237aa
A210V
B
GFP
TGIF2IRmut
3dpt
GFP PAX6 TBR2 TUBB3
C
PAX6+/GFP+ at 3dpt
ns
D
TUBB3+/GFP at 3dpt
**
H
GFP CTL
TGIF2IRmut
bin5
bin4
bin3
SATB2+/GFP+ in E13-16 IUE
E
GFP
F
TGIF2IRmut
5
4
3
2
1
G
bin5
bin4
bin3
bin2
bin1
GFP+ cell distribution in E13-16 IUE
M
Xrcc1
Rpa3
Rpa2
Top3a
Rpa1
Lig3
Ssbp1
Tfe3
Skp1a
Mpv17l
Ubp1
Tmpo
Banf1
Rbbp4
Hdac2
Rbbp7
Sap130
Sall1
Nacc1
Sap30
Sin3a
Suds3
Brms1l
Sinhcaf
Ing1
Hdac1
Tgif2
Brms1
Sap30l
Ing2
Elavl1
G3bp2
I
TGIF2IRwt
TGIF2IRmut
peaks
-0.5
center
0.5Kb
distance from center
N
ARID4B
HNRNPM
HSPA5
MYH9
PARP1
RPL13
VIM
TGIF2IRwt
TGIF2IRmut
7
30
2
J
TGIF2IRwt
10635
53
TGIF2IRmut
L
TGIF2IRwt
TGIF2IRmut
5515
46
0
0
231
0
960
scRNA: upregulated in
TGIF2IRmut (pval<0.05)
K
TGIF2IRwt
TGIF2IRwt_IgG
TGIF2IRmut
TGIF2IRmut_IgG
Arid4b
O
shArid#1
shArid#2*
shArid#3
shArid#4
mock
ARID4B

Chapter 3

Nuclear function of the microtubule-associated protein MAP1B in neural stem cells drives periventricular heterotopia

Authors

Florencia Merino[1,2,3], Lucas Miranda[4], **Yiling Li**[1,2,3], Deepak Kumar Sundaramoorthy[1,2], Juliane Merl-Pham[5], Veronica Pravata[1], Martina Bürkle[1,2], Bob A. Hersbach[1,2,3], Javier Ferri Beneito[1,2], Florian Giesert[6], Louis-Jan Pilaz[7,8], Stefanie M. Hauck[5], Silvia Cappello[1,9,10] and Magdalena Götz[1,2,10*]

Affiliations:

[1]Division of Physiological Genomics, Biomedical Center, Ludwig-Maximilians-Universität, Planegg-Martinsried, Germany.

[2]Institute of Stem Cell Research, Helmholtz Center Munich, Planegg-Martinsried, Germany.

[3]Graduate school of Systemic Neuroscience, Ludwig-Maximilians-Universität, Planegg-Martinsried, Germany.

[4]Machine Learning and Systems Biology department, Max Planck Institute of Biochemistry, Planegg-Martinsried, Germany.

[5]Metabolomics and Proteomics Core, Helmholtz Center Munich, Munich, Germany.

[6]Institute of Developmental Genetics, Helmholtz Center Munich, Munich, Germany.

[7]Pediatrics and Rare Diseases Group, Sanford Research, Sioux Falls, South Dakota, USA.

[8]Sanford School of Medicine, University of South Dakota, Sioux Falls, South Dakota, USA.

[9]Max Planck Institute of Psychiatry, Munich, Germany.

[10]SYNERGY, Excellence Cluster of Systems Neurology, Ludwig-Maximilians-Universität, Planegg-Martinsried, Germany.

***Lead contact and Correspondence:** magdalena.goetz@helmholtz-munich.de

Abstract

Periventricular heterotopia (PH) is a cortical malformation characterized by misplaced cells at the ventricle considered a migration disorder, supported by mutations in neuron-enriched cytoskeletal genes such as *MAP1B*. However, recent research has also implicated neural stem cells (NSCs). As the role of MAP1B in PH as well as in NSCs is unknown, we explored its role using knock-down (KD) conditions. These indeed recapitulate a PH phenotype with ectopic cells in the periventricular regions that is dependent on a role in NSCs. We found that MAP1B localizes and functions in the nucleus in NSCs, where it interacts with the SWI/SNF chromatin remodeling complex, maintaining NSC fate.

Strikingly, patient iPSC-derived cerebral organoids show enrichment of the mutant MAP1B protein in the nucleus along with a PH phenotype. This work not only reveals the essential contribution of MAP1B function in NSCs to PH, but also uncovers its role in the nucleus regulating neurogenesis.

Introduction

Neuronal heterotopias comprise about 30% of malformations of cortical development (MDC)[1,2]. These disorders are characterized by ectopic positioning of grey matter in the brain typically associated with epilepsy and have classically been considered as neuronal migration disorders[3], supported by the identification of mutations in neuronal-enriched cytoskeletal genes[4]. However, functional studies of candidate genes associated with this MDC group does not support a unifying biological process or pathway affected[5–10]. In this context, recent evidence has also identified defects in neural stem cells[10,11]. For example, centrosome-associated proteins in NSCs, but not neurons, were found to significantly overlap with genes associated with periventricular heterotopia, a disorder that belongs to this MDC group[8]. These included unexpected new candidates, such as the splicing factor pre-mRNA processing factor 6 (PRPF6), whose mutation recapitulated a PH-like phenotype in the developing mouse cortex[8].

These considerations prompted us to explore the function of MAP1B, as it is the earliest expressed microtubule (MT) associated protein (MAP) already present in NSCs[15–17]. Moreover, nothing is yet known about the role of any MAP in stem or progenitor cells, which prompted us to explore its role by a knock-down approach. Moreover, it is one of the proteins with most frequent mutations implicated in PH risk[12]. In this regard, it is also of particular interest that MAP1B interacts with both MTs and actin filaments[13], suggesting a potential role as a connector between these cytoskeletal components. This is of particular interest given the mutations in actin cytoskeleton associated proteins in PH[14]. This may also play a role in neuronal migration, as MAP1B appears in NSCs, but then further increases in young neurons[15–17]. While previous studies have explored its role in axonogenesis and synaptogenesis[18–21], the role of *Map1b* in neural stem cells and PH etiology remains elusive.

Results

Map1b-KD models heterotopia in the murine cortex *in vivo*

To explore MAP1B function, we used short hairpin RNAs (shRNAs) against MAP1B, resulting in 50% protein reduction (Figure S1C-I). We generated two shRNAs (named shMap1b, targeting the 3' untranslated region of the gene, and shMap1b#2, targeting its open reading frame) cloned into plasmids that co-express a green fluorescent protein (GFP) under a constitutive promoter (pCAG) (Figure S1C). A scrambled shRNA, predicted not to bind to any transcript in the transcriptome, served as a control.

Notably, the *MAP1B* missense variants that have been associated with cases of Periventricular heterotopia[22–25] (Figure S1A) all introduce a premature stop and are predicted loss-of-function (Figure S1B). Therefore, our KD approach may also model the heterozygous loss-of-function mutations. To explore the function of MAP1B in cortex

development in vivo and probe for possible ectopias seen in PH, we used *in utero* electroporation (IUE) of both *Map1b* shRNAs at embryonic day (E) 13, followed by brain collection five days later for GFP immunostaining (Figure 1A). Upon *Map1b*-KD, we found a significant increase in cells in the periventricular region of the cortex (Bin 1, consisting of the ventricular zone and part of the subventricular zone) and corresponding decrease in the lower part of the cortical plate (Bin 3 and 4 for shMap1b and shMap1b#2, respectively) (Figure 1B-C). Analysis at postnatal day 10 (P10) showed that this is a persistent phenotype, as still more cells were retained in the lower part of the cortex (Figure 1D-F). Thus, *Map1b*-KD resulted in a persistent accumulation of cells in the periventricular region of the cortex, consistent with previous models of periventricular heterotopia[5,10].

Map1b-KD reveals migration to be particularly affected in a subpopulation

One possible cause of ectopic cell location is defects in migration, which have been observed in PH models[26] and upon *Map1b* manipulation[27,28]. To measure the speed and complexity of the movement (tortuosity), organotypic slices were collected 2 days after IUE and GFP+ cells were imaged for approximately 24 hours every 15 minutes between the intermediate zone and the cortical plate (Figure 1G), as done before[29]. This analysis revealed that *Map1b*-KD migrating neurons display a lower speed and an increased tortuosity index (migrated path/straight path) compared to controls (Figure 1H-J, Figure S2A).

In PH, not all neurons are affected equally, but rather only a small subpopulation of cells is retained in the periventricular region of the cortex. To probe the presence of a particularly affected subpopulation in *Map1b*-KD conditions, we performed a clustering analysis of the migrating cells using Gaussian Mixture Models. Tuning the number of components to minimize the Bayesian Information Criterion (BIC) criteria yielded an optimal three cluster solution (Figure 1K, Figure S2B). Treatment distribution analysis across these clusters showed a cluster (Cluster 3) as significantly enriched and almost exclusively formed by *Map1b*-KD cells (Figure 1L, Figure S2C), while treatment proportions were comparable for the other clusters. Cluster 3 cells migrate with particularly low speed and high tortuosity (Figure 1K). Importantly, these effects cannot be attributed to shRNA transfection levels as measured by GFP intensity (Figure S2D). Excluding cluster 3 cells from the dataset highlights the decrease in tortuosity upon *Map1b*-KD is specifically driven by the presence of this cluster (Figure S2E-F). Thus, *Map1b*-KD leads to the generation of a distinct population of neurons with particularly affected migration.

scRNAseq reveals the presence of a small aberrant neuronal subpopulation upon *Map1b*-KD

To probe if a particularly affected neuronal population may be detectable by altered gene expression possibly linked to differentiation effects, or is solely due to cytoskeletal alterations, we explored the transcriptional profile of *Map1b*-KD cells. For this, we conducted scRNAseq of the IUE cells (Figure 2A) using three litters as independent biological replicates (Figure 2B). After quality control and filtering (see Methods), a total number of 16411 cells was obtained (Figure S3A). For each litter, we validated the downregulation of *Map1b* (Figure 2B; Litter 1: logFoldChange (logFC) = -1.03, p-value_adj = $2.86e^{-148}$; Litter 2: logFC = -0.87, p-value_adj = $1.82e^{-99}$; Litter 3: logFC = -0.76, p-value_adj = $1.36e^{-53}$). Importantly, overall expression of other MAPs was not affected by the treatment (Figure S3B). Leiden clustering analysis identified all cell types expected in the cortex at this developmental stage[30] (Figure 2C, Figure S3C-E). Yet, one cluster of

neurons could not be mapped to any known neuronal subtype (cluster 'Neurons_unknown') (Figure 2D-G, S3F). Intriguingly, this cluster predominantly consisted of cells from *Map1b*-KD treatment (Figure 2D) and may represent the abnormally migrating cells observed in our imaging analysis.

To explore which genes are most affected in expression in the 'Neurons_unknown' cluster, we performed differential gene expression (DGE) analysis of this cluster against the rest of the cortical neurons coming from *Map1b*-KD (Figure 2E, Table S1). This identified 657 down- and 260 up-regulated genes in 'Neurons_unknown'. Consistent with a possible phenotype in migration, we found genes involved in cell-cell adhesion and neuronal migration (Figure 2F-G, Table S1). Of particular interest was the downregulation of *Dab1*, the intracellular mediator of Reelin signaling which controls neuronal positioning, as well as *Nrp1*, SEMA3A's receptor that regulates the radial orientation of migrating neurons[31,32]. Interestingly, other downregulated genes included *Eml1* and *Fat4*, two genes previously linked to neuronal heterotopias[5,33]. Importantly, *Map1b* was not among the differentially expressed genes (DEG), indicating that the presence of this population cannot be attributed to particularly high KD efficiency. Additionally, genes involved in key processes for neuronal development such as axonogenesis, cation channel activity, neuron projection extension and synapse organization were differentially regulated in this cluster (Figure 2F, Table S1), suggesting possibly broader deficits in differentiation beyond migration. This prompted us to explore whether changes could already be detected at the NSC/progenitor level.

Map1b-KD affects NSC differentiation

To investigate whether *Map1b*-KD affects NSCs, we performed DGE analysis on the three clusters of stem/progenitor cells identified in both treatments. We found that the most affected cluster was RGC2; composed of NSCs that already expressed neuronal and intermediate progenitor markers and therefore represent differentiating NSCs. In this cluster, we found 67 down- and 52 up-regulated genes after *Map1b*-KD (Figure 2H, Table S1). Downregulated genes included important inducers of neuronal differentiation (such as *Myt1l* and *Nfix*), while upregulated genes were associated with stemness and proliferation (such as *Sox2* and *Hmgb2*). Overall, the GO terms for biological processes for these genes comprised mitosis progression and neurogenesis, among others (Figure 2I, Table S1). Together, these data suggest that *Map1b*-KD impairs NSC differentiation, which may result in the generation of the aberrant "Neurons_unknown" population.

To further explore this notion, we used RNA velocity[34] and CellRank[35], which can predict the differentiation trajectory based on detected spliced and unspliced RNA rates. Consistent with the DGE analysis, the differentiation pseudo-time inferred from RNA velocity indicated a slower differentiation process in the *Map1b*-KD condition (Figure 2J-K), with RGC1 identified as a terminal state only upon *Map1b*-KD (Figure 2L-M), further supporting a role of *Map1b* in delayed or blocked NSC differentiation. These trajectory analyses also allowed us to explore how these stem and progenitor clusters may relate to the origin of the altered neuronal population. We hypothesized that these cells could originate either from neurons that undergo transcriptional state changes due to migratory defects or could derive from the affected stem/progenitor cells. RNA velocity[34] and CellRank[35] analyses revealed that 'Neurons_unknown' likely originated directly from stem/progenitor cells (Figure 2N, Figure S3G), and act as a terminal state in the altered differentiation trajectory (Figure 2M).

To examine if these transcriptional changes affect NSC numbers, we performed immunostaining for PAX6 to label NSCs and TBR2 to label intermediate progenitors after IUE of either of the *Map1b* shRNAs. Quantification revealed that *Map1b* KD leads to a significantly higher proportion of PAX6+ NSCs compared to the control (Figure 3A-C). Both, self-renewing (PAX6+/TBR2-) and differentiating (PAX6+/TBR2+) NSCs were increased, while intermediate progenitor proportions (PAX6-/TBR2+) were not affected (Figure 3C). These findings, together with our gene expression analysis, suggest a surprising role of *Map1b* in regulating NSCs differentiation *in vivo*.

Map1b-KD sparing NSCs shows no PH and aberrant neuron phenotype

To determine if the above described phenotypes result from *Map1b* function in NSCs or neurons, we performed *Map1b*-KD using shRNAs under the *Dcx* promoter (p*Dcx*) by IUE (Figure 3D), thereby reducing expression levels only in committed progenitors and neurons, bypassing the effects of *Map1b* in NSCs. Notably, the distribution of GFP+ cells was not different between p*Dcx*-driven *Map1b*-KD and its control (Figure 3E).

To examine possible transcriptional changes, we performed scRNAseq of the p*Dcx*-driven *in utero* electroporated cells using two litters as independent biological replicates (Figure 3F). After processing and filtering the data, we obtained a total of 19030 cells for this second dataset (Figure S4A). For each litter, we validated *Map1b* KD (Figure 3F; Litter 1: logFC = -0.48, p-value_adj = $7.04e^{-122}$; Litter 2: logFC = -0.40, p-value_adj = $2.33e^{-86}$). Leiden clustering (resolution 0.9) identified 22 clusters (Figure S4A), with no clusters enriched or depleted of *Map1b*-KD cells (Figure S4B), resulting in overlapping UMAP projections across treatments (Figure 3G). Consistent with the use of the *Dcx* promoter, the dataset was largely restricted to migrating and differentiated neurons with few neural stem and progenitor cells (Figure 3H, Figure S4C-D). To determine whether we could identify any cells with the 'Neurons_unknown' molecular profile we observed previously, we used a Z-score based on the gene expression signature of these cells. However, no group of cells with a high 'Neurons_unknown' signature score was detected after p*Dcx*-specific *Map1b*-KD (Figure 3I, Figure S4E-F). Moreover, and to make sure that the pCAG and p*Dcx* datasets were comparable, correspondence between their independently annotated cell types was obtained using FR-Match[36]. This software statistically tests whether the expression profile of each cluster across datasets comes from the same multivariate distribution, as defined by a set of minimal markers that can optimally discriminate cell types. All corresponding cell types were found to correctly match across datasets. However, Neurons_unknown cluster was left unmatched (Figure 3J). In summary, our results show that the newly identified neuronal subpopulation is only detectable when *Map1b* is downregulated in NSCs, suggesting that these cells are a product of altered differentiation.

Cell-autonomous role of MAP1B in neural stem cells

The changes observed in NSCs *in vivo* may be niche- or migration-dependent. To exclude any of these factors, we cultured dissociated E12 mouse cortices, which consist mostly of NSCs[30]. To explore cell-autonomous functions, we used a low efficiency transfection protocol on the first day in culture with either shControl or shMap1b. After three days, cells were stained for SOX2, labeling NSCs, and TBR2 for progenitors (Figure 4A). Quantification of the proportion of GFP+ SOX2+ or TBR2+ cells in the cultures revealed that *Map1b*-KD leads to a significantly higher proportion of Sox2+ NSCs *in vitro* (Figure 4B), reproducing the effects observed *in vivo* (Figure 3A-C). To determine if this outcome is due to selective cell death rather than cell fate changes, we performed live imaging of the E12 cortical cell

cultures every 15-30 minutes between 2 and 3 days in vitro (DIV) (Figure S5A). Notably, cell survival was not different between the conditions (Figure S5B), suggesting that KD of *Map1b* indeed promotes NSC fate independent of cell migration and the niche structure present *in vivo*.

Nuclear localization and function of MAP1B in neural stem cells

To better understand the function of MAP1B, we examined its protein localization in NSCs. Besides the expected colocalization with alpha-tubulin in the cytoplasm (but not at the spindle in dividing cells (Figure S5C)), we also detected MAP1B immunostaining inside the nuclei of NSCs (Figure 4C). This nuclear localization of MAP1B was confirmed by nuclear and cytoplasmic fractionation of mouse E12 cortex lysates (Figure 4D). To determine the specificity of this signal, we used the *Map1b*-KD constructs (Figure 4E) and found a significant reduction of the MAP1B-immunostaining signal in both the cytosol and the nucleus (Figure 4F), further corroborating the specificity of the staining. Interestingly, however, we noted a more efficient decrease in the cytoplasm than the nucleus (Figure 4G). This may be due to differential turnover dynamics of the protein in these respective compartments and/or different transport dynamics upon *Map1b*-KD.

Given the surprising localization of MAP1B in NSC nuclei, we aimed to explore which of the two compartments is most crucial in mediating the MAP1B's function in NSCs. For this purpose, we generated tools to drive MAP1B into the nucleus using nuclear localization signals (NLS) or enrich it in the cytoplasm using a nuclear export signal (NES) (Figure 4H, Figure S5D). Plasmids encoding these constructs were co-transfected with *Map1b* shRNA targeting its untranslated region (and therefore only downregulating the endogenous RNA) in E12 primary cortical cell cultures. Notably, combining shMap1b with NES-Map1b completely reversed the increase in NSCs caused by *Map1b*-KD, while the combination with NLS-Map1b exacerbated *Map1b*-KD effects (Figure 4I-J). These data thus demonstrate a differential effect of MAP1B in the cytoplasm versus the nucleus with the former reducing NSCs and the later increasing NSC numbers. Taken together with the increased nuclear/cytosol ratio in the *Map1b*-KD condition (Figure 4G), the balance of MAP1B distribution between cytoplasm and nucleus seems to play a key role in mediating NSC maintenance versus differentiation.

Before further exploring the mechanisms of MAP1B cytoplasmic versus nuclear function, we aimed to verify the novel role of MAP1B in the nucleus *in vivo*. To do so, shControl (containing GFP) + RFP or shMap1b (containing GFP) + NLS-Map1b (containing RFP) were *in utero* electroporated at E13 and brains collected 3 days later for immunostaining (Figure 4K). Distribution analysis of double shMap1b-*GFP*+/NLS-Map1b-RFP+ cells revealed an accumulation in the periventricular region (Bins 1 and 2), with a decreased proportion of cells reaching the upper part of the cortex (Figure 4M). NLS-Map1b combined with shMap1b also resulted in increased proportions of NSCs *in vivo* (Figure 4N) and further aggravated the phenotype with even more NSCs (compare Figure 3C to 4N); thereby replicating the *in vitro* findings *in vivo*. Staining for the young neuron marker NEUROD2 (Figure 4K-L) revealed the accumulation of neurons below the cortical plate, with a reduction in the proportion of neurons reaching the cortical plate in the NLS-Map1b condition (Figure 4O). Thus, nuclear enrichment of MAP1B increased NSCs *in vivo* and resulted in the generation of ectopic neurons.

Nuclear MAP1B interactors in NSCs include importins and the SWI/SNF chromatin remodeling complex

To understand how MAP1B may exert its function in the nucleus, we aimed to identify its interactors in the nuclei of NSCs by immunoprecipitation (IP) of endogenous MAP1B followed by mass spectrometry after subcellular fractionation in three independent replicates (Figure 5A). To obtain pure NSCs in high quantity, we chose human induced pluripotent stem cells(iPSCs)-derived cortical NSCs[8] after verifying the presence of MAP1B in their nuclei (Figure 5B). Co-IP revealed 289 MAP1B interactors in cytosol-enriched samples and 505 MAP1B interactors in nuclear-enriched samples (log_2 fold change>3 and q-value<0.05; Figure 5C, Table S2). Cytosolic interactors include cytoskeletal proteins such as TUBA1B, DNAH3, KIF23, KIF14, CAPZA2, MYL12A and MYL4, as well as cell adhesion proteins such as EPHA2, CDH2, SEMA4C, NCAM1 and EFNB1 (Table S2), reflecting the most significant GO terms related to cytoskeleton (Table S2).

GO analysis of the interactors in the nuclear fraction revealed an over-representation of proteins associated with nuclear speckles and chromatin-related processes including chromatin modifiers and remodelers such as the SWI/SFI superfamily-type complex, also known as BAF complex (Fig. 5D, Table S2). Additionally, we identified 'Nucleocytoplasmic transport' as significantly enriched among MAP1B interactors (Figure 5D, Table S2). Using methanol fixation, we validated the interaction of MAP1B with the nuclear speckle marker SRRM2 by observing notable co-localization in both iPSC-derived NSCs and E12 mouse cortex (Figure 5E-F). As shuttling from the cytoplasm into the nucleus is crucial for MAP1B's function, we next focused on the importins interacting with MAP1B, confirming the interaction with the Importin subunit alpha-1, KPNA2 (Figure 5G, Figure S5E), which is enriched in NSCs[37].

Next, we focused on MAP1B's association with the SWI/SFI complex, given its key role in regulating neurogenesis[38]. Indeed, the interaction between MAP1B and various components of this complex was validated via co-IP followed by Western Blot in both iPSC-derived NSCs and E12 mouse cortical nuclei (Figure 5G-H, Figure S5E). This included BRG1, the core ATPase component of the BAF complex, which could further be corroborated by reverse co-IP (Figure 5G).

MAP1B's nuclear effects on neuronal differentiation could be mediated by modulating the function of the SWI/SNF complex[39]. To investigate MAP1B's effects on SWI/SNF complex function, we performed BRG1 Cut&Run in iPSC-derived NSCs infected with either of the above described shRNAs. This analysis uncovered 5164 peaks for BRG1-binding in control conditions (Figure 5I), including peaks in known targets such as *SOX2*, *SOX11* and *CCND1* (Figure 5J-L). Surprisingly, Brg1-binding was much reduced upon *Map1b*-KD (Figure 5I-L). This shows that MAP1B has a critical impact on the SWI/SNF complex binding to its targets, which could be due to MAP1B's interaction with nuclear actin or potentially influencing the stability of the complex.

Microtubule-binding regulates nuclear translocation of MAP1B

As MAP1B localizes both in the cytoplasm and the nucleus, an important determinant for its novel function in the nucleus is the physiological regulation of its shuttling between these compartments. To get some insights into this, we examined the MAP1B peptides identified by mass spectrometry comparing their coverage and relative abundance in the different subcellular compartments. While peptides from both nuclear and cytosolic

MAP1B mapped to the full-length protein (Figure 6A, Table S2), phosphopeptide mapping showed a profound difference between the compartments with nuclear MAP1B being hyperphosphorylated compared to its cytosolic form (Figure 6A-B, Table S2). Kinase prediction based on MAP1B phospho-peptides indicated a significant enrichment for c-Jun N-terminal kinase 1 (JNK1) and PTEN-induced kinase 1 (PINK1) (Figure S5F, Table S2), which have already been shown to phosphorylate MAP1B[40,41], further supporting our analysis.

Interestingly, hyperphosphorylation of MT-associated proteins has been shown to weaken their microtubule-binding capacity[42], suggesting that MT-interaction may retain MAP1B in the cytoplasm, while MAP1B phosphorylation weakening these interactions could facilitate its translocation into the nucleus. This prompted us to explore if the MT-binding domain (MBD) of MAP1B was important for its nuclear shuttling. Towards this aim, FLAG-tagged truncated forms of the protein were generated and transfected into E12 primary cortical cell cultures (Figure 6C). Three days post-transfection, we assessed their distribution by FLAG-immunostaining. Indeed, the MBD fragment displayed a clear nuclear enrichment, while the other constructs were mostly located in the cytoplasm (Figure 6D). To further explore the hypothesis that MT interactions may regulate MAP1B's shuttling into the nucleus, E12 primary cortical cell cultures were treated with the MT polymerization inhibitor Nocodazole for 4 hours and the proportion of MAP1B in the nucleus versus soma was quantified (Figure 6E-F). Nocodazole treatment resulted in a significant increase of MAP1B in the nuclei, suggesting that MT binding competes with its nuclear translocation (Figure 6G). Taken together, these data suggest a dynamic translocation of MAP1B into the nucleus regulated by MT-interaction and phosphorylation thereby regulating its function in NSC fate determination.

PH-associated *MAP1B* mutations result in nuclear-enriched truncated proteins and PH phenotype in organoids

Next, we were interested to understand how the above findings relate to the mutations found in PH patients, as these have been suggested to result in loss of protein. Probing one such patient mutation (c.2133delG; p. E712Kfs*10) in the mouse developing cortex using Breasi-CRISPR[43], we observed the generation of a truncated protein, which was more enriched in the nucleus as compared to its WT counterpart (Fig. S6A-D), along with an accumulation of cells below the cortical plate (Fig. S6B vs. Fig. S6D).

To directly evaluate the impact of *MAP1B* mutations found in PH patients and the significance of its nuclear-cytosol shuttling in the human context, we generated iPSC lines carrying two specific *MAP1B* mutations. We chose to study the mutations c.3316C>T; p. R1106* and c.2133delG; p. E712Kfs*10 (Figure 7A), as these were identified in more than one patient presenting PH[12,44]. *MAP1B* c.3316C>T; p. R1106* mutation was identified in a patient with bilateral anterior predominant PH, deep perisylvian/insular polymicrogyria, and a thin, dysmorphic corpus callosum, along with collapsing episodes suggestive of seizures[12]. This *MAP1B* mutation was inherited from the patient's mother, who exhibits similar MRI findings and symptoms. *MAP1B* c.2133delG; p. E712Kfs*10 mutation was identified in 8 members of a family, 5 of whom presented PH and intellectual disability[44]. Other associated brain structure abnormalities included smaller corpus callosum and overall reduced white matter volume.

We engineered human iPSCs by introducing either mutation using CRISPR/Cas9, which provided us with isogenic controls to specifically study the effects of the introduced mutations. The presence of *MAP1B* mutations was confirmed through Sanger sequencing (Figure 7B). Using the iPSC line carrying *MAP1B* c.3316C>T; p. R1106* mutation as a proof of principle, we generated cerebral organoids to assess whether this mutant line would recapitulate the neuronal ectopia phenotype (Figure 7C). Indeed, in three independent batches, we observed the predominance of ectopic neurons (MAP2+ cells) in the PAX6+ ventricular zone of the organoid's cortical-like structure in the mutant line (Figure 7E-F). This result underscores that the mutant human cerebral organoids can effectively model the neuronal ectopia phenotype, thereby making them suitable for elucidating the impact of MAP1B nuclear-cytosol shuttling in this context.

Towards this aim, we assessed the effect of *MAP1B* mutations on its total, cytosolic, and nuclear abundance. To achieve this, we generated cerebral organoids and performed subcellular fractionation followed by Western blot analysis. As expected, both mutations resulted in a decrease in the amount of full-length MAP1B protein (Figure 7D). However, surprisingly, we identified a new MAP1B band in each mutant organoid, representing novel MAP1B isoforms that match to the presence of truncated proteins (Figure 7D). Notably, both MAP1B mutant-derived isoforms were enriched in the nuclear fraction as compared to the cytosolic one. Thus, human patient cells corroborate the mouse model findings that enrichment of nuclear MAP1B is involved PH pathogenesis.

Discussion

Here we identified a novel role of MAP1B in NSCs shuttling between the cytoplasm and nucleus with higher nuclear levels favoring NSC fate. This allowed us to gain further insights into the etiology of PH as an NSC fate pathology rather than a migration disorder.

PH as a NSC differentiation disease

In human patients with PH, not all neurons are equally impacted, but rather a relatively small subset ends up in the periventricular regions, while others reach the cortical plate normally. A big question is, why this is the case. Here we propose that this is linked to alterations in NSC differentiation (mostly RGC2) leading to the generation of a mis-specified small subpopulation of neurons. Using both live-imaging and scRNAseq of *in utero* electroporated cortical cells, we identified a particularly affected subpopulation of NSCs and neurons manifesting upon *Map1b*-KD. In live imaging we found a subpopulation of KD cells migrating particularly slow and with increased tortuosity. Similarly, in scRNAseq data we detected a small cluster of neurons with no equivalence in controls, or ever reported in the literature. Notably, scRNAseq analysis of human cerebral organoids from FAT4 and DCHS1 mutant cells, that exhibit a PH phenotype, had also identified an altered neuronal state[26], with some similarities to the signature of ours. FAT4- and DCHS1-mutant organoid neurons also exhibit a transcriptomic profile marked by dysfunctions in biological processes including axon guidance and neuronal migration. Particularly, they show an enrichment of the netrin receptor deleted in colorectal cancer (*DCC*), which is elevated in our 'Neurons_unknown' cluster as well. DCC regulates the migration of cortical neurons through reelin-independent DAB1's phosphorylation, in particular controlling multipolar

migration and multipolar-to-bipolar transition[45]. Notably, these processes take place below the cortical plate, giving a possible explanation why their dysfunction results in the accumulation of cells in the periventricular region of the brain[45]. Furthermore, *MAP1B* is among the downregulated genes in the FAT4-mutant altered neuronal subpopulation, and our 'Neurons_unknown' cluster showed reduced expression levels of *Fat4*. These results point to a common pathological process affected by alterations in these very different PH genes. Lastly, our study demonstrates that the emergence of altered neuronal subpopulations in the context of PH is not exclusive to humans, but indeed a general hallmark that also occurs in mice.

Fundamentally, scRNAseq analysis pointed to slower NSCs differentiation upon *Map1b*-KD, as confirmed by an increase in NSCs by immunostaining, showing for the first time that *Map1b* regulates NSC differentiation *in vivo*. While MAP1B's presence in NSCs has been noted for decades[17], its specific role in these cells had remained elusive. Notably, DGE analysis in differentiating radial glia (RGC2) suggests that the impairment of NSC differentiation due to *Map1b*-KD results from both the suppression of genes promoting neuronal differentiation, such as *Myt1l*, and increased expression of genes associated with stemness, such as *Sox2* and *Hmgb2*. Furthermore, RNA velocity analysis underscores a slower pace of differentiation, implying that *Map1b* levels affect the speed of NSC differentiation.

This important result raised the question whether the mis-migrating neuronal subpopulation identified may arise as a consequence of the NSC differentiation or from migration defects. Downregulating *Map1b* under a *Dcx* promoter enabled us to bypass the effects of this gene in NSCs, revealing the altered neuronal population emerges exclusively after *Map1b*-KD including NSCs. Aligned with our previous data demonstrating that the PH-associated PRPF6 mutant causes cell ectopia only when it occurs in NSCs, but not when occurring only in young neurons[8], these data further corroborate the concept of PH as a NSC pathology rather than a migration disorder. Importantly, however, our work now shows that these changes at the level of NSCs can result in the generation of a uniquely abnormal neuronal state.

Map1b-KD favors NSC fate and differentiation is slowed down as shown *in vivo* and *in vitro*. How this results in such a specifically altered neuronal population is a fascinating question. In this context it is of interest to consider previous evidence for a causal relationship between alterations in cell cycle length and NSC differentiation with altered progeny cell fate[46,47]. In these studies, the most affected NSCs show a higher probability of producing altered progeny. In our data, slower differentiation seems to affect mostly RGC2 and they seem to generate the aberrant neuronal population. CellRank analysis shows that differentiating radial glial cells (RGC2) possess the highest signature driver score for the altered neuronal population, therefore significantly expressing key genes accountable for the differentiation and development of these specific neurons. In this context, it is important to consider that differentiating radial glia cells are also the ones undergoing delamination, a process associated with PH etiology[48], highlighting further their disease relevance. Most importantly, however, we could unravel the role of the cytoskeletal protein MAP1B in NSCs with an unprecedented function in the nucleus. This has also been shown *in vivo* by driving MAP1B into the nucleus using IUE resulting likewise in accumulation of cells in the periventricular region. Moreover, we have shown that patient iPSC-derived

organoids also accumulate MAP1B protein in the nucleus, demonstrating a clear relevance of this novel function of MAP1B for PH.

Cell autonomous function of Map1b in NSCs involves cytoplasmic-nuclear shuttling

Our *in vitro* analysis uncovered that *Map1b* affects NSC fate independently of cellular displacement processes and the niche structure present *in vivo*. This ruled out classic mechanisms governed by MTs, such as regulation of the angle of cell division, or possible defects in the interkinetic nuclear migration of radial glia cells[49]. Most importantly, we could identify opposing roles of MAP1B acting pro-differentiative, when it is in the cytoplasm (as shown by the rescue of the *Map1b*-KD phenotype using NES-*Map1b*), while favoring NSC fate, when it is enriched in the nucleus (as shown by the pronounced increase in NSCs using NLS-*Map1b*). Moreover, endogenous MAP1B is detectable in the nucleus of human and murine NSCs, and its nuclear translocation is favored, when MTs are depolymerized or it is phosphorylated and hence also binds less to MTs. This presents an unprecedented mechanism for a cytoskeletal protein, while transcription factors, such as the myocardin-related transcription factors (MRTFs) that regulate the serum-response factor (SRF), have been shown to shuttle to the nucleus[50]. Indeed, SRF activity may be involved in the cytoplasmic prodifferentiative role of MAP1B, as MAP1B has been shown to inhibit RhoA activation[18], which positively regulates the transcriptional complex megakaryoblastic leukemia/serum response factor (MKL/SRF) that normally promotes NSCs[51]. Thus, more MAP1B in the cytoplasm would promote differentiation as shown with the NES-*Map1b* construct. Conversely, nuclear MAP1B promotes NSC fate, likely by its interaction with the SWI/SNF complex. We have shown that BRG1 binding to many of its targets is reduced in the *Map1b*-KD conditions, and our *Map1b*-KD phenotype is reminiscent of the cortex-specific conditional knock-out (cKO) for BRG1 showing a higher ratio of NSCs as well as neuronal heterotopia[39]. These data thus suggest that the BRG1-containing BAF complex is a mediator of MAP1B function in the nucleus. The localization and function of MAP1B in the nucleus may also provide an entry point to tackle the long-standing riddle of the roles of tubulin and actin in the nucleus. Besides tubulin, MAP1B also binds to actin that plays pivotal roles in transcription regulation and chromatin organization[52–60]. Interestingly, β-actin, which we also identified as a direct interactor of MAP1B in the nucleus, plays a role in fibroblast to neuron conversion, i.e. β-actin promotes neurogenic function[61]. Thus, the function of MAP1B in the nucleus may help to unravel the specific functional roles of the cytoskeletal elements in the nucleus.

Importantly, the nuclear function of MAP1B is highly relevant to disease. Modelling two of the PH-associated patients' mutations in *MAP1B* in human organoids demonstrated the nuclear enrichment of the truncated protein along with the enrichment of neurons in the periventricular region. The presence of E712Kfs*10 truncated protein could further be validated by introducing the corresponding mutation in the developing cortex using Breasi-CRISPR[43] (Figure S6A-C). Adding a flag to visualize the localization of the truncated protein further confirmed our results, indicating the nuclear enrichment of the truncated mutant proteins. This data thus corroborates that the relative enrichment of MAP1B in the disease condition as well as in the KD condition are causative for the PH phenotype originating in NSCs. In this regard it is particularly interesting that Filamin A, the other most frequently mutated protein in PH[12,14], also interacts with MAP1B in the nucleus. These results prompt

the hypothesis that also the Filamin A mutations may cause NSC phenotypes by their nuclear function resulting in PH, similar to the mechanism shown here for MAP1B. Overall, we have not only shown an entirely novel function of MAP1B with the nuclear-cytosolic shuttling in NSCs, but also the direct implication of its nuclear function in PH etiology. This work further opens uncharted territory of cytoskeletal interactors in regulating transcription and fate in the nucleus.

Acknowledgements

We thank Ines Muehlhahn and Paulina Chlebik for excellent technical help and Tatiana Simon and Judith Fischer for their excellent assistance with single cell sequencing experiments. We are also very grateful to the excellent characterization of the iPSC lines by the Helmholtz Core Facility by Ejona Rusha and acknowledge the Sequencing Core facility of the Helmholtz Center Munich, the Laboratory for Functional Genome Analysis (LAFUGA) of Gene Center Munich and the Flow Cytometry and Imaging Facility of the Biomedical Center of Munich for providing equipment, services, and expertise. We are particularly grateful to Laurent Nguyen, Antonela Bonafina and Julie Stoufflet for generously sharing their expertise and teaching us the live imaging used in this study. We also thank Christoph Gruber for sharing the nuclear export/localization signal sequences.

Funding: This work was supported by the European Research Council (advanced grant NeuroCentro, 885382 to M.G.) and the German Excellence Cluster SyNergy (EXC2145/Project-ID 390857198, to M.G.). L.M. is supported by the European Union's Horizon 2020 research and innovation programme under the Marie Skłodowska-Curie Ph.D grant agreement No. 813533.

Author contributions

M.G. and F.M. conceived and designed the project. F.M. performed and analyzed *in vivo, in vitro* and *ex vivo* experiments, unless otherwise stated. L.M. performed the clustering analysis of migrating neurons. F.M. and J.F.B. analyzed cell identity changes upon *Map1b* KD *in vitro.* F.M. performed scRNAseq experiments, which were analyzed by F.M. and L.M. B.H. performed the alignment of the scRNAseq data. J.M-P. performed and analyzed MS data (together with F.M. and L.M.), supervised by S.M.H. Y.L. and F.M. performed Cut&Run experiments, which were analyzed by Y.L. F.G. generated the mutant iPSC lines, M.B. performed iPSCs-derived NSCs differentiations and D.K.S. and V.P performed cerebral organoids differentiations, supervised by F.M., M.G. and S.C. D.K.S. performed immunostaining analysis in cerebral organoids. L-J.P. performed Breasi-CRISPR experiments. F.M. and M.G. wrote the manuscript and all authors contributed with suggestions and corrections.

Declaration of interest: The authors declare no competing interests.

Figure Legends

Figure 1. *Map1b* KD produces long-lasting PH in the mouse cortex

A and G, Experimental design of experiments shown in B-F and H-L, respectively. Coronal sections of E18 (B) and P10 (D) mouse cerebral cortices electroporated at E13 with shControl, shMap1b or shMap1b#2. Distribution of GFP+ cells are quantified in C, E and F. Different symbols represent different litters analyzed. Two-way ANOVA followed by Dunnett's (C) or Šídák's (F) multiple comparisons test. H, Representative images of bipolar migrating neurons, quantified in I and J and analyzed using two-tailed Mann-Whitney test. K, Normalized tortuosity and speed for all cells analyzed via live imaging. Colors correspond to the three clusters obtained using Gaussian Mixture Models. L, Treatment distribution across all three clusters; Fisher exact test. Mean & SEM; Scale bar 50 µm (B and D) and 10 µm (G). *: p-value<0.05, **: p-value<0.01, ***: p-value<0.001, ****: p-value<0.0001. CP: cortical plate; IZ: intermediate zone; SVZ and VZ: (sub) ventricular zone; WM: white matter.

Figure 2. *Map1b* KD scRNAseq reveals the presence of a divergent neuronal population.

A, Experimental design for studying transcriptomic changes upon *Map1b*-KD in the developing cortex. B, Violin plots depicting the mean expression of *Map1b* per treatment for each litter used. C, Louvain clustering superimposed on a UMAP embedding from both shControl and shMap1b cells. D, UMAP embedding from shControl (left) and shMap1b (right) cells. E, Volcano plot of differentially expressed genes (DEGs) between 'Neurons_unknown' cluster and all other neurons in the *Map1b*-KD condition. H, Volcano plots of DEGs between shControl and shMap1b of the RGC2 cluster. Yellow and Violet colored dots represent up- and down-regulated genes in the *Map1b*-KD condition, for H, or in the 'Neurons_unknown' cluster for E. Their main gene ontology terms for biological processes are shown in F, and I, respectively. G, Dot plot representing expression of selected DEG across neuronal populations within *Map1b*-KD treatment. J, RNA velocity analysis from shControl (left) and shMap1b (right) projected in the 2D expression UMAP for each treatment, calculated using scVelo[34]. K, Pseudotime histogram for shControl and shMap1b. Distributions were smoothed using a Gaussian kernel density estimation. Initial and terminal differentiation states for control (L) or *Map1b*-KD (M) cells, as predicted by CellRank[35]. N, Violin plots depicting the lineage driver Z-score signature for Neurons_unknown as a terminal differentiation state per cell type (excluding Neurons_unknown). RGCs: Radial Glia Cells; IPs: Intermediate Progenitors; IC: Intracortical; PT: Pyramidal Tract; CT: Corticothalamic; OPCs: Oligodendrocyte Progenitor Cells.

Figure 3. *Map1b* KD increases NSCs and *Map1b* KD in neurons only has no phenotype.

A, Coronal sections of E18 mouse cerebral cortices electroporated at E13 with shControl or shMap1b#2, stained as indicated and quantified in C. Zoom-in images from the ventricular zone are shown in B. Mean & SEM. Two-way ANOVA followed by Šídák's multiple comparisons test (shMap1b#2) or Two-tailed Mann-Whitney test (shMap1b). D, Coronal sections of E16 mouse cerebral cortices electroporated at E13 with p*Dcx*-driven shControl and shMap1b, stained as indicated and quantified in E. Two-way ANOVA followed by Šídák's multiple comparisons test; ns: not significant. F, Violin plots depicting the mean expression

of *Map1b* per treatment for each litter used for transcriptomic analysis of IUE cells upon p*Dcx*-driven *Map1b*-KD. G, UMAP embedding from p*Dcx*_shControl (left) and p*Dcx*_shMap1b (right) cells. H, Louvain clustering from both p*Dcx*_shControl and p*Dcx*_shMap1b cells. I, Additive Z-scored gene expression profile of neurons unknown across both pCAG and p*Dcx* datasets. J, Statistical cluster matching across pCAG and p*Dcx* datasets, obtained using FRMatch. Different symbols represent different litters analyzed (B and E). Scale bar 50 µm (A, B and D). *: p-value<0.05, ****: p-value<0.0001. CP: cortical plate; IZ: intermediate zone; SVZ and VZ: (sub) ventricular zone; RGC: Radial Glia Cells; Prog: Progenitors; IPs: Intermediate Progenitors; IC: Intracortical; PT: Pyramidal Tract; CT: Corticothalamic. White, white and yellow, and yellow arrows indicate GFP+PAX6+TBR2; GFP+PAX6+TBR2+ and GFP+PAX6-TBR2+ cells, respectively.

Figure 4. MAP1B nuclear localization promotes neural stem cell fate

A, Representative images of E12 primary cortical cells transfected with shControl or shMap1b at 1 *day in vitro* (DIV) and stained as indicated at DIV3. The proportion of double or triple positive cells are quantified in B. Two-way ANOVA followed by Šídák's multiple comparisons test. C, Orthogonal view of neural stem cells (PAX6+) from E12 cortical cultures depicting the presence of MAP1B inside the nucleus, indicated by arrows. D, Western Blot from E12 mouse cortex after subcellular fractionation, stained as indicated. E, Representative images of MAP1B intensity in shControl and shMap1b conditions in E12 cortical cultures transfected at DIV1 and stained as indicated at DIV3. F, Normalized MAP1B intensity in the soma and nucleus of from PAX6+ cells transfected with either shControl or shMap1b. Two-way ANOVA followed by Šídák's multiple comparisons test. G, Ratio of MAP1B intensity in the nucleus relative to the soma for NSCs transfected either with shControl or shMap1b. Two-tailed Mann-Whitney test. H, Schematic representation of the DNA constructs of MAP1B domains. I, Representative images of E12 primary cortical cultures transfected at DIV1 and stained at DIV3 as indicated. J, Percentage of PAX6+RFP+GFP+/ RFP+GFP+ cells, relative to shControl+RFP. Paired one-way ANOVA + Geisser-Greenhouse correction followed by Dunnett's multiple comparisons testing. K, Coronal sections of E16 mouse cerebral cortices electroporated at E13 with shControl+RFP or shMap1b+NLS-Map1b, stained as indicated and quantified in M and O. Zoom-in images from GFP+RFP+NEUROD2+ cells are shown in L. N, Percentage of PAX6+RFP+GFP+/ RFP+GFP+ cells from the electroporated cortices. Mean & SEM. Two-way ANOVA followed by Šídák's multiple comparisons test (L and O) or two-tailed Mann-Whitney test (N). Different symbols represent different litters analyzed (F, G and M-O). Scale bar: 20 µm (A, E, I and L), 5 µm (C), and 50 µm (K). Mean & SEM; *: p-value<0.05, **: p-value<0.01, ***: p-value<0.001, ****: p-value<0.0001. DIV: days in vitro; IPSCs: induced pluripotent stem cells. (A) White, white and yellow, and yellow arrows indicate GFP+SOX2+TBR2-, GFP+SOX2+TBR2+ and GFP+TBR2+ cells, respectively; White arrows indicate GFP+PAX6+ (E), GFP+RFP+PAX6+ (I) or GFP+RFP+NEUROD2+ (L) cells.

Figure 5. MAP1B interacts with SWI/SNF complex and affects its binding in the nucleus of neural stem cells.

A, Experimental design to determine the MAP1B interactome in NSCs. B, Western Blot from human IPSCs-derived NSCs after subcellular fractionation, stained as indicated. C, Volcano

plots depicting MAP1B interactome in cytosolic enriched (left) or nuclear enriched (right) fractions from human iPSCs-derived NSCs. D, Gene ontology terms of significantly enriched nuclear MAP1B interactors. Immunostainings depicting MAP1B co-localization with the nuclear speckle marker SRRM2 in human IPSCs-derived NSCs (E) and the ventricular zone of E12 mouse cortex (F). Western blot upon co-IP of MAP1B or BRG1 from nuclear enriched fractions derived from human iPSCs-derived NSCs (G) or E12 mouse cortex (H) and stained as indicated. I, Enrichment heatmap of BRG1 peaks in Cut&Run analysis from human iPSCs-derived NSCs infected with shControl (left) or shMap1b (right), centered at the middle of the peaks. Peak examples with bigwig profiles for *SOX2*, *SOX11* and *CCND1* are shown in J, K and L, respectively. CNR: Cut&Run. Scale bar: 5 µm (E and F).

Figure 6. MAP1B's microtubule binding domain regulates nuclear translocation.

A, Schematic representation of MAP1B protein structure, highlighting the actin binding domain (ABD) and the microtubule binding domain (MBD). Heatmaps depict the mapping of MAP1B peptides and phosphopeptides across the primary structure of the protein in cytosolic and nuclear enriched fractions. The x-axis corresponds to the amino acid position of MAP1B, and the color intensity represents the relative abundance of peptides, normalized per sample. B, Heatmap depicting the relative abundance of MAP1B phosphopeptides in its co-IP from cytosolic and nuclear enriched samples, normalized per sample and to the maximum abundance per phosphopeptide. Each row represents a different MAP1B phosphopeptide. C, Schematic representation of MAP1B truncation and deletion constructs used to assess localization in NSCs shown in D, Representative images of E12 cortical cultures transfected at DIV1 with the DNA constructs illustrated in C and stained as indicated at DIV3. E, Representative images of E12 cortical cultures treated with Dimethyl sulfoxide (DMSO) or Nocodazole (NZO) for 4 hours and stained as indicated at DIV1. Zoom-in images depicting MAP1B localization in NSCs are shown in F. The dashed line indicates the border of the nucleus. G, Ratio of MAP1B intensity in the nucleus relative to the soma for PAX6+ cells treated with DMSO or NZO. Different symbols represent different biological replicates. Mean & SEM; One-tailed Mann-Whitney test; *: p-value<0.05. Scale bar: 10 µm (D), 20 µm (E) and 2 µm (F).

Figure 7. MAP1B proteins with patient mutations are enriched in the nucleus and cause a PH-phenotype in organoids

A, Schematic representation of MAP1B protein structure indicating the two mutations identified in PH patients which were introduced in HMGU1 iPSC line by CRISPR/Cas9, as confirmed by Sanger sequencing profile (B), and further used for the generation of cerebral organoids as shown in the experimental scheme in C. D, Western blot upon subcellular fraction of Day40 organoids from control (WT) and PH-mutant lines, stained as indicated. E, Representative images of cortical-like structures in Day40 organoids from control (WT) or c.3316C>T MAP1B mutant depicting the enrichment of ectopic neurons (MAP2+ cells) in PAX6+ ventricular zones in the mutant, quantified in F (n=batch). Two-way matched ANOVA followed by Fisher's least significant difference test; *: p-value<0.05. Scale bar: 50 µm (left) and 20 µm (right).

References

1. Severino, M. *et al.* Definitions and classification of malformations of cortical development: Practical guidelines. *Brain* vol. 143 2874–2894 Preprint at https://doi.org/10.1093/brain/awaa174 (2020).

2. Broix, L. *et al.* Mutations in the HECT domain of NEDD4L lead to AKT / mTOR pathway deregulation and cause periventricular nodular heterotopia. **48**, 1349–1358 (2017).

3. Vriend, I. & Oegema, R. Genetic causes underlying grey matter heterotopia. *Eur J Paediatr Neurol* **35**, 82–92 (2021).

4. Francis, F. & Cappello, S. Neuronal migration and disorders – an update. *Curr Opin Neurobiol* **66**, 57–68 (2021).

5. Cappello, S. *et al.* Mutations in genes encoding the cadherin receptor-ligand pair DCHS1 and FAT4 disrupt cerebral cortical development. *Nat Genet* **45**, 1300–1310 (2013).

6. Collins, S. C. *et al.* The neuroanatomy of Eml1 knockout mice, a model of subcortical heterotopia. *J Anat* **235**, 637–650 (2019).

7. O'Neill, A. C. *et al.* Mob2 insufficiency disrupts neuronal migration in the developing cortex. *Front Cell Neurosci* **12**, (2018).

8. O'Neill, A. C. *et al.* Spatial centrosome proteome of human neural cells uncovers disease-relevant heterogeneity. *Science (1979)* **376**, (2022).

9. Carabalona, A. *et al.* A glial origin for periventricular nodular heterotopia caused by impaired expression of Filamin-A. *Hum Mol Genet* **21**, 1004–1017 (2012).

10. Broix, L. *et al.* Mutations in the HECT domain of NEDD4L lead to AKT-mTOR pathway deregulation and cause periventricular nodular heterotopia. *Nat Genet* **48**, 1349–1358 (2016).

11. Uzquiano, A. *et al.* Mutations in the Heterotopia Gene Eml1/EML1 Severely Disrupt the Formation of Primary Cilia. *Cell Rep* **28**, 1596-1611.e10 (2019).

12. Heinzen, E. L. *et al.* De novo and inherited private variants in MAP1B in periventricular nodular heterotopia. *PLoS Genet* **14**, (2018).

13. Cueille, N. *et al.* Characterization of MAP1B heavy chain interaction with actin. *Brain Res Bull* **71**, 610–618 (2007).

14. Parrini, E. *et al.* Periventricular heterotopia: Phenotypic heterogeneity and correlation with Filamin a mutations. *Brain* **129**, 1892–1906 (2006).

15. Riederer, B., Cohen, R. & Matuslt, A. *MAP5: A Novel Brain Microtubule-Associated Protein under Strong Developmental Regulation*. *Journal of Neurocytology* vol. 15 (1986).

16. Villarroel-Campos, D. & Gonzalez-Billault, C. The MAP1B case: An old MAP that is new again. *Dev Neurobiol* **74**, 953–971 (2014).

17. Cheng, A., Krueger, B. K. & Bambrick, L. L. MAP5 expression in proliferating neuroblasts. *Developmental Brain Research* **113**, 107–113 (1999).

18. Montenegro-Venegas, C. *et al.* MAP1B Regulates Axonal Development by Modulating Rho-GTPase Rac1 Activity. *Mol Biol Cell* **21**, 3518–3528 (2010).

19. Meixner, A. *et al. MAP1B Is Required for Axon Guidance and Is Involved in the Development of the Central and Peripheral Nervous System*. *The Journal of Cell Biology* vol. 151 http://www.jcb.org/cgi/content/full/151/6/1169 (2000).

20. Tortosa, E. *et al.* Microtubule-associated protein 1B (MAP1B) is required for dendritic spine development and synaptic maturation. *Journal of Biological Chemistry* **286**, 40638–40648 (2011).

21. Gonzalez-Billault, C. *et al.* Microtubule-Associated Protein 1B Function during Normal Development, Regeneration, and Pathological Conditions in the Nervous System. *Journal of Neurobiology* vol. 58 48–59 Preprint at https://doi.org/10.1002/neu.10283 (2004).

22. Arya, R., Spaeth, C. & Zhang, W. Epilepsy phenotypes associated with MAP1B-related brain malformations. *Epileptic Disorders* **23**, (2021).

23. Julca, D. M., Diaz, J., Berger, S. & Leon, E. MAP1B related syndrome: Case presentation and review of literature. *Am J Med Genet A* **179**, 1703–1708 (2019).

24. Heinzen, E. L. *et al.* De novo and inherited private variants in MAP1B in periventricular nodular heterotopia. *PLoS Genet* **14**, (2018).

25. Walters, G. B. *et al.* MAP1B mutations cause intellectual disability and extensive white matter deficit. *Nat Commun* **9**, (2018).

26. Klaus, J. *et al.* Altered neuronal migratory trajectories in human cerebral organoids derived from individuals with neuronal heterotopia. *Nat Med* **25**, 561–568 (2019).

27. Kawauchi, T., Chihama, K., Nishimura, Y. V., Nabeshima, Y. I. & Hoshino, M. MAP1B phosphorylation is differentially regulated by Cdk5/p35, Cdk5/p25, and JNK. *Biochem Biophys Res Commun* **331**, 50–55 (2005).

28. González-Billault, C. *et al.* A role of MAP1B in reelin-dependent neuronal migration. *Cerebral Cortex* **15**, 1134–1145 (2005).

29. Camargo Ortega, G. *et al.* The centrosome protein AKNA regulates neurogenesis via microtubule organization. *Nature* **567**, 113–117 (2019).

30. Di Bella, D. J. *et al.* Molecular logic of cellular diversification in the mouse cerebral cortex. *Nature* **595**, 554–559 (2021).

31. Rice, D. S. & Curran, T. Role of the Reelin signaling pathway in central nervous system development. (2001).

32. Chen, G. *et al.* Semaphorin-3A guides radial migration of cortical neurons during development. *Nat Neurosci* **11**, 36–44 (2008).

33. Kielar, M. *et al.* Mutations in Eml1 lead to ectopic progenitors and neuronal heterotopia in mouse and human. *Nat Neurosci* **17**, 923–933 (2014).

34. Bergen, V., Lange, M., Peidli, S., Wolf, F. A. & Theis, F. J. Generalizing RNA velocity to transient cell states through dynamical modeling. *Nat Biotechnol* **38**, 1408–1414 (2020).

35. Lange, M. *et al.* CellRank for directed single-cell fate mapping. *Nat Methods* **19**, 159–170 (2022).

36. Zhang, Y., Aevermann, B., Gala, R. & Scheuermann, R. H. Cell type matching in single-cell RNA-sequencing data using FR-Match. *Sci Rep* **12**, (2022).

37. Klingler, E., Francis, F., Jabaudon, D. & Cappello, S. Mapping the molecular and cellular complexity of cortical malformations. *Science* vol. 371 Preprint at https://doi.org/10.1126/science.aba4517 (2021).

38. Son, E. Y. & Crabtree, G. R. The role of BAF (mSWI/SNF) complexes in mammalian neural development. *Am J Med Genet C Semin Med Genet* **166**, 333–349 (2014).

39. Jin, Y. *et al.* Loss of BAF (mSWI/SNF) chromatin-remodeling ATPase Brg1 causes multiple malformations of cortical development in mice. *Hum Mol Genet* **31**, 3504–3520 (2022).

40. Auburger, G. *et al.* Ser thr-phospho proteome of brain from aged PINK1-KO+A53T-SNCA mice reveals pT1928-MAP1B and pS3781-ANK2 deficits, as hub between autophagy and synapse changes. *Int J Mol Sci* **20**, (2019).

41. Chang, L., Jones, Y., Ellisman, M. H., Goldstein, L. S. B. & Karin, M. JNK1 Is Required for Maintenance of Neuronal Microtubules and Controls Phosphorylation of Microtubule-Associated Proteins. *Dev Cell* **4**, 521–533 (2003).

42. Gong, C.-X. & Iqbal, K. Hyperphosphorylation of Microtubule-Associated Protein Tau: A Promising Therapeutic Target for Alzheimer Disease. *Curr Med Chem* (2008).

43. Meyerink, B. L. *et al.* Breasi-CRISPR: an efficient genome editing method to interrogate protein localization and protein-protein interactions in the embryonic mouse cortex Protein-tagging in corticogenesis. doi:10.1101/2022.02.02.478837.

44. Walters, G. B. *et al.* MAP1B mutations cause intellectual disability and extensive white matter deficit. *Nat Commun* **9**, (2018).

45. Zhang, J. H. *et al.* DCC-Mediated Dab1 Phosphorylation Participates in the Multipolar-to-Bipolar Transition of Migrating Neurons. *Cell Rep* **22**, 3598–3611 (2018).

46. Mitchell-Dick, A. *et al.* Acute Lengthening of Progenitor Mitosis Influences Progeny Fate during Cortical Development in vivo. *Dev Neurosci* (2020) doi:10.1159/000507113.

47. Pilaz, L. J. *et al.* Prolonged Mitosis of Neural Progenitors Alters Cell Fate in the Developing Brain. *Neuron* **89**, 83–99 (2016).

48. Camargo Ortega, G. & Götz, M. Centrosome heterogeneity in stem cells regulates cell diversity. *Trends in Cell Biology* vol. 32 707–719 Preprint at https://doi.org/10.1016/j.tcb.2022.03.004 (2022).

49. Wimmer, R. & Baffet, A. D. The microtubule cytoskeleton of radial glial progenitor cells. *Current Opinion in Neurobiology* vol. 80 Preprint at https://doi.org/10.1016/j.conb.2023.102709 (2023).

50. Wang, D.-Z. *et al.* Potentiation of serum response factor activity by a family of myocardin-related transcription factors. *Proc Natl Acad Sci U S A* **99**, 14855–14860 (2002).

51. Cossard, A., Stam, K., Smets, A. & Jossin, Y. MKL/SRF and Bcl6 mutual transcriptional repression safeguards the fate and positioning of neocortical progenitor cells mediated by RhoA. *Science Advances* (2023).

52. Hofmann, W. A. *et al.* Actin is part of pre-initiation complexes and is necessary for transcription by RNA polymerase II. *Nat Cell Biol* **6**, 1094–1101 (2004).

53. Xie, X., Jankauskas, R., Mazari, A. M. A., Drou, N. & Percipalle, P. β-actin regulates a heterochromatin landscape essential for optimal induction of neuronal programs during direct reprograming. *PLoS Genet* **14**, (2018).

54. Percipalle, P. *et al.* An actin-ribonucleoprotein interaction is involved in transcription by RNA polymerase II. *Proc Natl Acad Sci U S A* **100**, 6475–6480 (2003).

55. Dundr, M. *et al.* Actin-dependent intranuclear repositioning of an active gene locus in vivo. *Journal of Cell Biology* **179**, 1095–1103 (2007).

56. Akoumianaki, T., Kardassis, D., Polioudaki, H., Georgattos, S. D. & Theodoropoulos, P. A. Nucleocytoplasmic shuttling of soluble tubulin in mammalian cells. *J Cell Sci* **122**, 1111–1118 (2009).

57. Schwarzerová, K. *et al.* Tubulin is actively exported from the nucleus through the Exportin1/CRM1 pathway. *Sci Rep* **9**, (2019).

58. Ruksha, K. *et al.* Over-expression of βII-tubulin and especially its localization in cell nuclei correlates with poorer outcomes in colorectal cancer. *Cells* **8**, (2019).

59. Li, Q. & Sarna, S. K. Nuclear Myosin II Regulates the Assembly of Preinitiation Complex for ICAM-1 Gene Transcription. *Gastroenterology* **137**, (2009).

60. Obrdlik, A. & Percipalle, P. The F-actin severing protein cofilin-1 is required for RNA polymerase II transcription elongation. *Nucleus* **2**, 72–79 (2011).

61. Xie, X., Jankauskas, R., Mazari, A. M. A., Drou, N. & Percipalle, P. β-actin regulates a heterochromatin landscape essential for optimal induction of neuronal programs during direct reprograming. *PLoS Genet* **14**, (2018).

62. Rentzsch, P., Witten, D., Cooper, G. M., Shendure, J. & Kircher, M. CADD: Predicting the deleteriousness of variants throughout the human genome. *Nucleic Acids Res* **47**, D886–D894 (2019).

63. Kunze, C. *et al.* Synthetic AAV/CRISPR vectors for blocking HIV-1 expression in persistently infected astrocytes. *Glia* **66**, 413–427 (2018).

64. Borchin, B., Chen, J. & Barberi, T. Derivation and FACS-mediated purification of PAX3+/PAX7+ skeletal muscle precursors from human pluripotent stem cells. *Stem Cell Reports* **1**, 620–631 (2013).

65. D'Amour, K. A. *et al.* Efficient differentiation of human embryonic stem cells to definitive endoderm. *Nat Biotechnol* **23**, 1534–1541 (2005).

66. Shi, Y., Kirwan, P. & Livesey, F. J. Directed differentiation of human pluripotent stem cells to cerebral cortex neurons and neural networks. *Nat Protoc* **7**, 1836–1846 (2012).

67. Lancaster, M. A. & Knoblich, J. A. Generation of cerebral organoids from human pluripotent stem cells. *Nat Protoc* **9**, 2329–2340 (2014).

68. Giandomenico, S. L., Sutcliffe, M. & Lancaster, M. A. Generation and long-term culture of advanced cerebral organoids for studying later stages of neural development. *Nat Protoc* **16**, 579–602 (2021).

69. Noble, M., Lewis, S. A. & Cowan, N. J. *The Microtubule Binding Domain of Microtubule-Associated Protein MAPIB Contains a Repeated Sequence Motif Unrelated to That of MAP2 and Tau*.

70. Esgleas, M. *et al.* Trnp1 organizes diverse nuclear membrane-less compartments in neural stem cells. *EMBO J* **39**, (2020).

71. Wiśniewski, J. R., Zougman, A., Nagaraj, N. & Mann, M. Universal sample preparation method for proteome analysis. *Nat Methods* **6**, 359–362 (2009).

72. Grosche, A. *et al.* The proteome of native adult Müller glial cells from Murine retina. *Molecular and Cellular Proteomics* **15**, 462–480 (2016).

73. Molitor, L. *et al.* Depletion of the RNA-binding protein PURA triggers changes in posttranscriptional gene regulation and loss of P-bodies. *Nucleic Acids Res* **51**, 1297–1316 (2023).

74. Käll, L., Canterbury, J. D., Weston, J., Noble, W. S. & MacCoss, M. J. Semi-supervised learning for peptide identification from shotgun proteomics datasets. *Nat Methods* **4**, 923–925 (2007).

75. Tyanova, S. & Cox, J. Perseus: A bioinformatics platform for integrative analysis of proteomics data in cancer research. in *Methods in Molecular Biology* vol. 1711 133–148 (Humana Press Inc., 2018).

76. Lepiemme, F., Silva, C. G. & Nguyen, L. Time lapse recording of cortical interneuron migration in mouse organotypic brain slices and explants. *STAR Protoc* **2**, 100467 (2021).

77. Heumos, L. *et al.* Best practices for single-cell analysis across modalities. *Nat Rev Genet* **24**, 550–572 (2023).

78. Wolock, S. L., Lopez, R. & Klein, A. M. Scrublet: Computational Identification of Cell Doublets in Single-Cell Transcriptomic Data. *Cell Syst* **8**, 281-291.e9 (2019).

79. Zhang, Y. *et al.* Model-based analysis of ChIP-Seq (MACS). *Genome Biol* **9**, (2008).

80. Ramírez, F. *et al.* deepTools2: a next generation web server for deep-sequencing data analysis. *Nucleic Acids Res* **44**, W160–W165 (2016).

81. Abueg, L. A. L. *et al.* The Galaxy platform for accessible, reproducible, and collaborative data analyses: 2024 update. *Nucleic Acids Res* **52**, W83–W94 (2024).

82. McLean, C. Y. *et al.* GREAT improves functional interpretation of cis-regulatory regions. *Nat Biotechnol* **28**, 495–501 (2010).

Figure 1

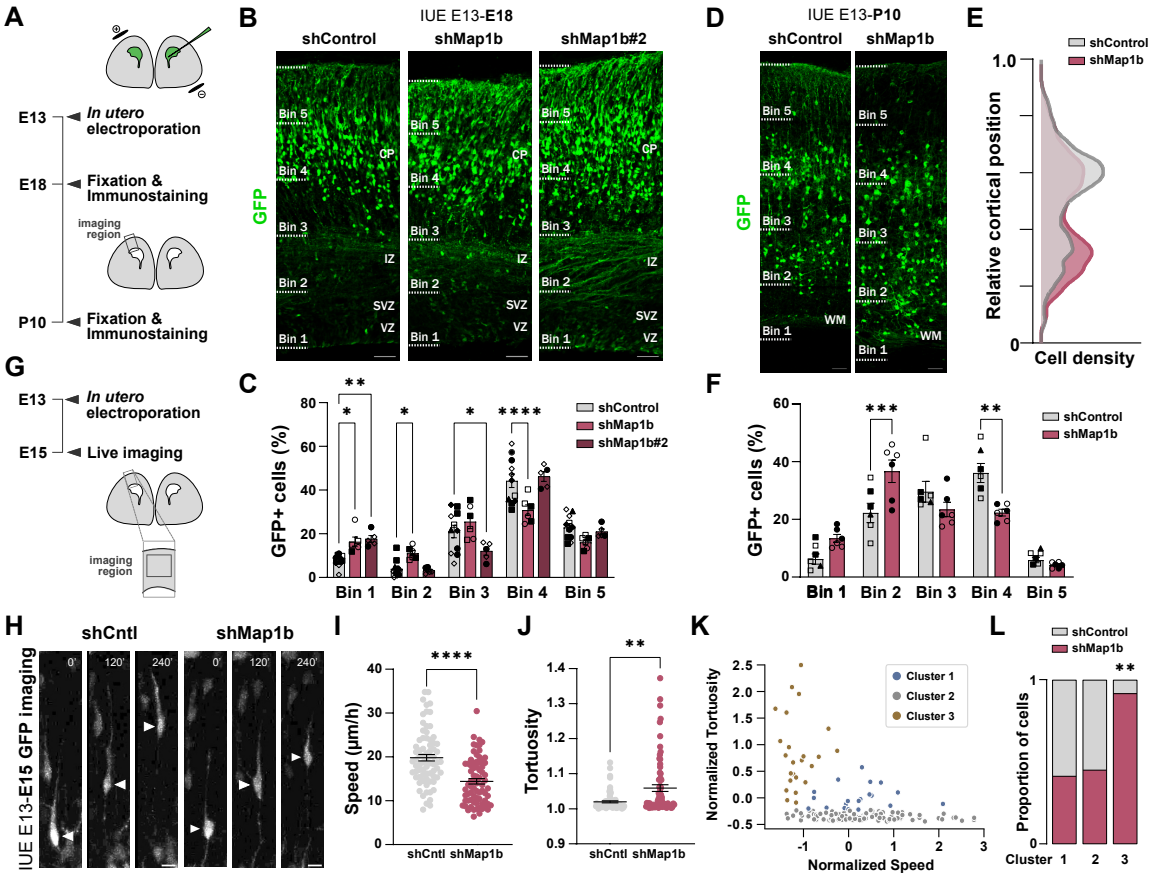
A
E13
In utero electroporation
E18
Fixation & Immunostaining
imaging region
P10
Fixation & Immunostaining
G
E13
In utero electroporation
E15
Live imaging
imaging region
B
IUE E13-E18
shControl
shMap1b
shMap1b#2
GFP
Bin 5
Bin 4
Bin 3
Bin 2
Bin 1
CP
IZ
SVZ
VZ
C
GFP+ cells (%)
shControl
shMap1b
shMap1b#2
Bin 1
Bin 2
Bin 3
Bin 4
Bin 5
D
IUE E13-P10
shControl
shMap1b
WM
E
Relative cortical position
Cell density
F
GFP+ cells (%)
H
shCntl
shMap1b
IUE E13-E15 GFP imaging
0'
120'
240'
I
Speed (µm/h)
shCntl shMap1b
J
Tortuosity
K
Normalized Tortuosity
Normalized Speed
Cluster 1
Cluster 2
Cluster 3
L
Proportion of cells
Cluster 1 2 3

Figure 2

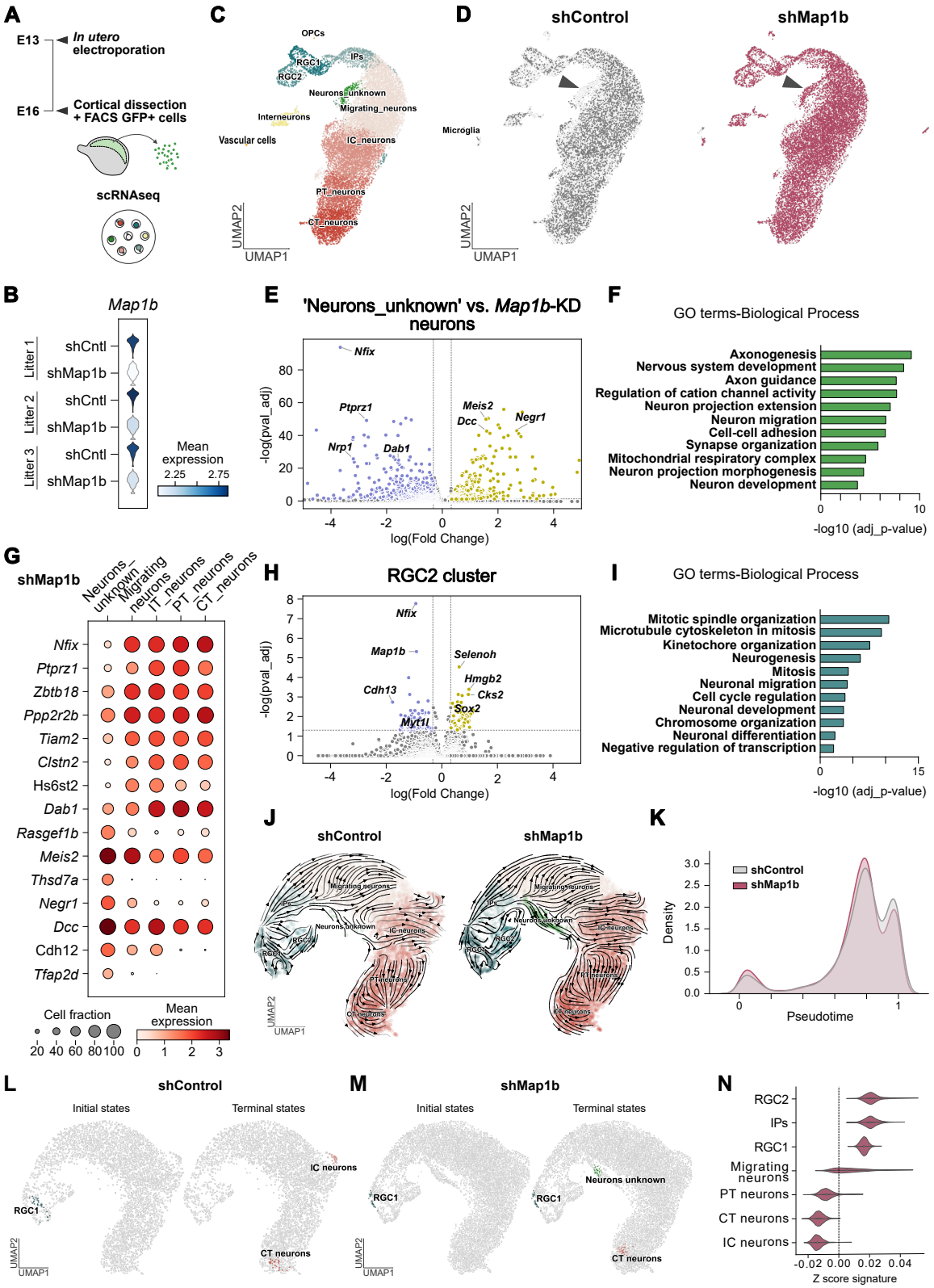
A
E13
In utero electroporation
E16
Cortical dissection + FACS GFP+ cells
scRNAseq
C
OPCs
RGC1
IPs
RGC2
Neurons_unknown
Migrating_neurons
Interneurons
Vascular cells
IC_neurons
PT_neurons
CT_neurons
UMAP2
UMAP1
D
shControl
shMap1b
Microglia
UMAP2
UMAP1
B
Map1b
Litter 1
shCntl
shMap1b
Litter 2
shCntl
shMap1b
Litter 3
shCntl
shMap1b
Mean expression
2.25
2.75
E
'Neurons_unknown' vs. Map1b-KD neurons
Nfix
Ptprz1
Nrp1
Dab1
Meis2
Dcc
Negr1
-log(pval_adj)
log(Fold Change)
F
GO terms-Biological Process
Axonogenesis
Nervous system development
Axon guidance
Regulation of cation channel activity
Neuron projection extension
Neuron migration
Cell-cell adhesion
Synapse organization
Mitochondrial respiratory complex
Neuron projection morphogenesis
Neuron development
-log10 (adj_p-value)
G
shMap1b
Neurons_unknown
Migrating neurons
IT_neurons
PT_neurons
CT_neurons
Nfix
Ptprz1
Zbtb18
Ppp2r2b
Tiam2
Clstn2
Hs6st2
Dab1
Rasgef1b
Meis2
Thsd7a
Negr1
Dcc
Cdh12
Tfap2d
Cell fraction
Mean expression
H
RGC2 cluster
Nfix
Map1b
Cdh13
Myt1l
Selenoh
Hmgb2
Cks2
Sox2
-log(pval_adj)
log(Fold Change)
I
GO terms-Biological Process
Mitotic spindle organization
Microtubule cytoskeleton in mitosis
Kinetochore organization
Neurogenesis
Mitosis
Neuronal migration
Cell cycle regulation
Neuronal development
Chromosome organization
Neuronal differentiation
Negative regulation of transcription
-log10 (adj_p-value)
J
shControl
shMap1b
Migrating neurons
IPs
Neurons unknown
IC neurons
RGC2
RGC1
PT neurons
CT neurons
UMAP2
UMAP1
K
shControl
shMap1b
Density
Pseudotime
L
shControl
Initial states
Terminal states
RGC1
IC neurons
CT neurons
UMAP2
UMAP1
M
shMap1b
Initial states
Terminal states
RGC1
RGC1
Neurons unknown
CT neurons
UMAP2
UMAP1
N
RGC2
IPs
RGC1
Migrating neurons
PT neurons
CT neurons
IC neurons
Z score signature

Figure 3

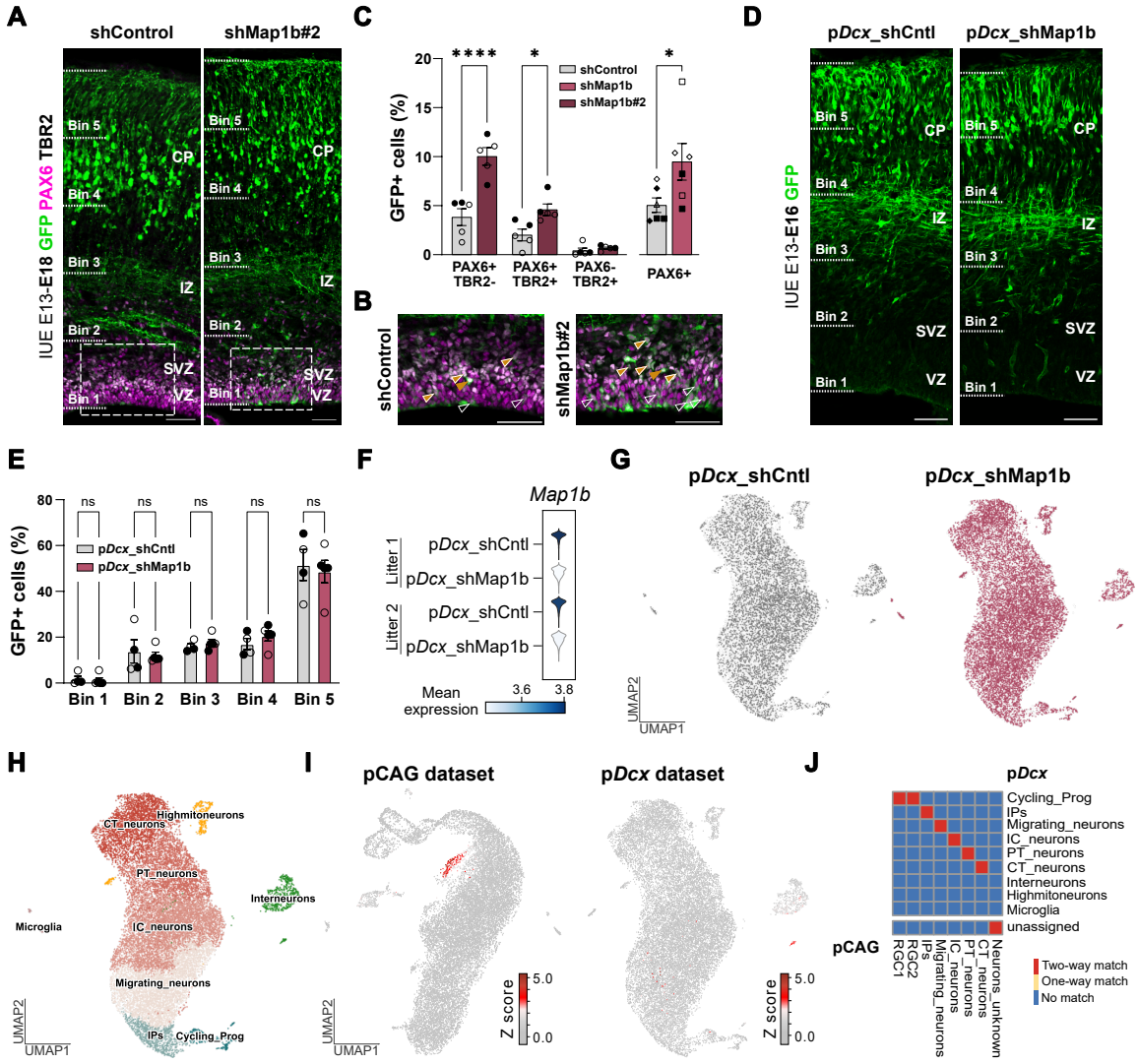
A
shControl
shMap1b#2
IUE E13-E18 GFP PAX6 TBR2
Bin 5
Bin 4
Bin 3
Bin 2
Bin 1
CP
IZ
SVZ
VZ
C
GFP+ cells (%)
shControl
shMap1b
shMap1b#2
PAX6+ TBR2-
PAX6+ TBR2+
PAX6- TBR2+
PAX6+
B
shControl
shMap1b#2
D
pDcx_shCntl
pDcx_shMap1b
IUE E13-E16 GFP
E
GFP+ cells (%)
ns
pDcx_shCntl
pDcx_shMap1b
Bin 1
Bin 2
Bin 3
Bin 4
Bin 5
F
Map1b
Litter 1
Litter 2
pDcx_shCntl
pDcx_shMap1b
Mean expression
3.6
3.8
G
pDcx_shCntl
pDcx_shMap1b
UMAP2
UMAP1
H
Highmitoneurons
CT_neurons
PT_neurons
Interneurons
Microglia
IC_neurons
Migrating_neurons
IPs
Cycling_Prog
UMAP2
UMAP1
I
pCAG dataset
pDcx dataset
Z score
5.0
0.0
UMAP2
UMAP1
J
pDcx
Cycling_Prog
IPs
Migrating_neurons
IC_neurons
PT_neurons
CT_neurons
Interneurons
Highmitoneurons
Microglia
unassigned
pCAG
RGC1
RGC2
IPs
Migrating_neurons
IC_neurons
PT_neurons
CT_neurons
Neurons_unknown
Two-way match
One-way match
No match

Figure 4

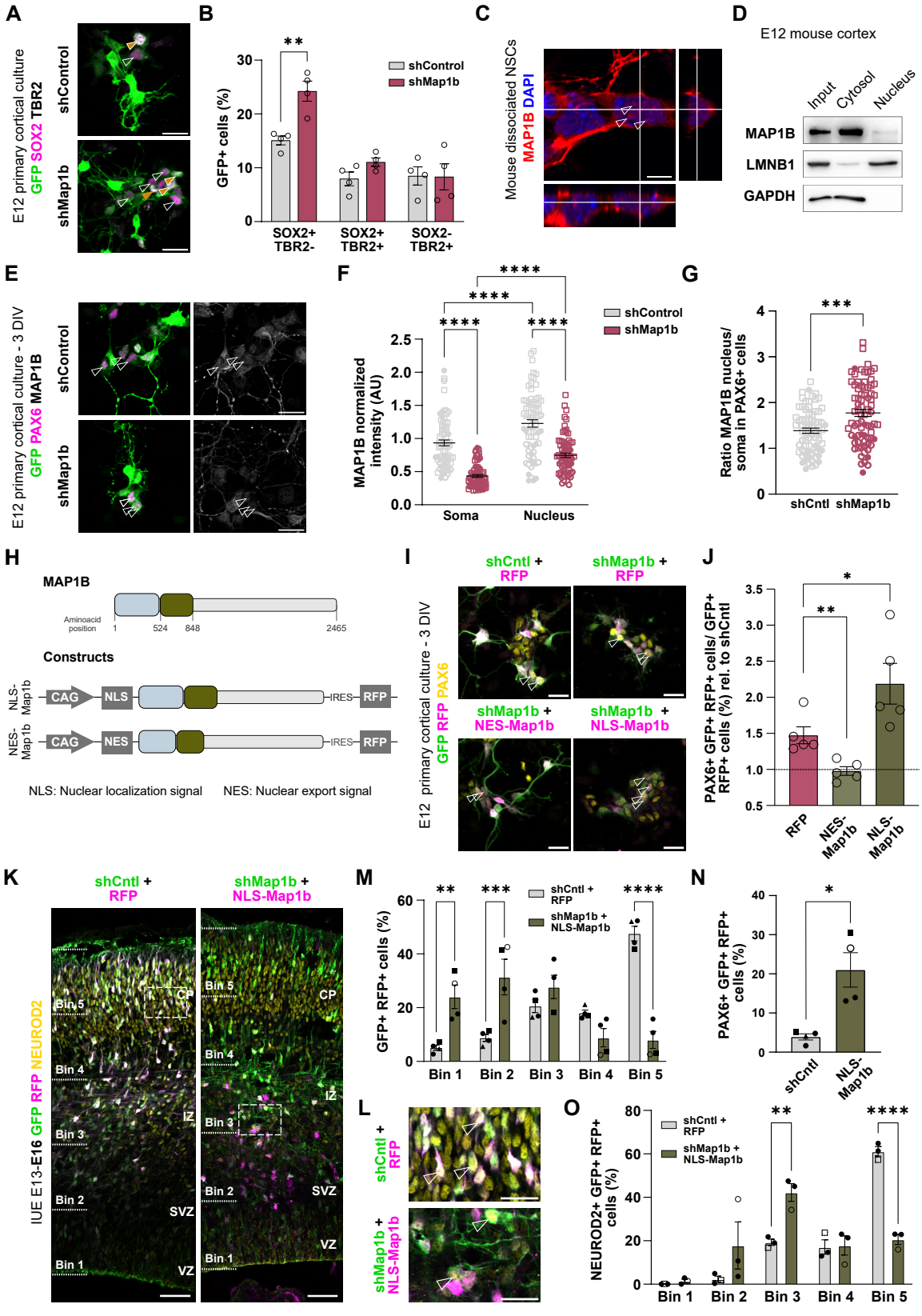
A
E12 primary cortical culture
GFP SOX2 TBR2
shControl
shMap1b
B
GFP+ cells (%)
shControl
shMap1b
SOX2+ TBR2-
SOX2+ TBR2+
SOX2- TBR2+
C
Mouse dissociated NSCs
MAP1B DAPI
D
E12 mouse cortex
Input
Cytosol
Nucleus
MAP1B
LMNB1
GAPDH
E
E12 primary cortical culture - 3 DIV
GFP PAX6 MAP1B
shControl
shMap1b
F
MAP1B normalized intensity (AU)
Soma
Nucleus
G
Ratio MAP1B nucleus/ soma in PAX6+ cells
shCntl
shMap1b
H
MAP1B
Aminoacid position
Constructs
NLS-Map1b
NES-Map1b
CAG
NLS
NES
IRES
RFP
NLS: Nuclear localization signal
NES: Nuclear export signal
I
shCntl + RFP
shMap1b + RFP
shMap1b + NES-Map1b
shMap1b + NLS-Map1b
E12 primary cortical culture - 3 DIV
GFP RFP PAX6
J
PAX6+ GFP+ RFP+ cells/ GFP+ RFP+ cells (%) rel. to shCntl
RFP
NES-Map1b
NLS-Map1b
K
shCntl + RFP
shMap1b + NLS-Map1b
IUE E13-E16 GFP RFP NEUROD2
Bin 5
Bin 4
Bin 3
Bin 2
Bin 1
CP
IZ
SVZ
VZ
L
shCntl + RFP
shMap1b + NLS-Map1b
M
GFP+ RFP+ cells (%)
shCntl + RFP
shMap1b + NLS-Map1b
Bin 1
Bin 2
Bin 3
Bin 4
Bin 5
N
PAX6+ GFP+ RFP+ cells (%)
shCntl
NLS-Map1b
O
NEUROD2+ GFP+ RFP+ cells (%)
shCntl + RFP
shMap1b + NLS-Map1b

Figure 5

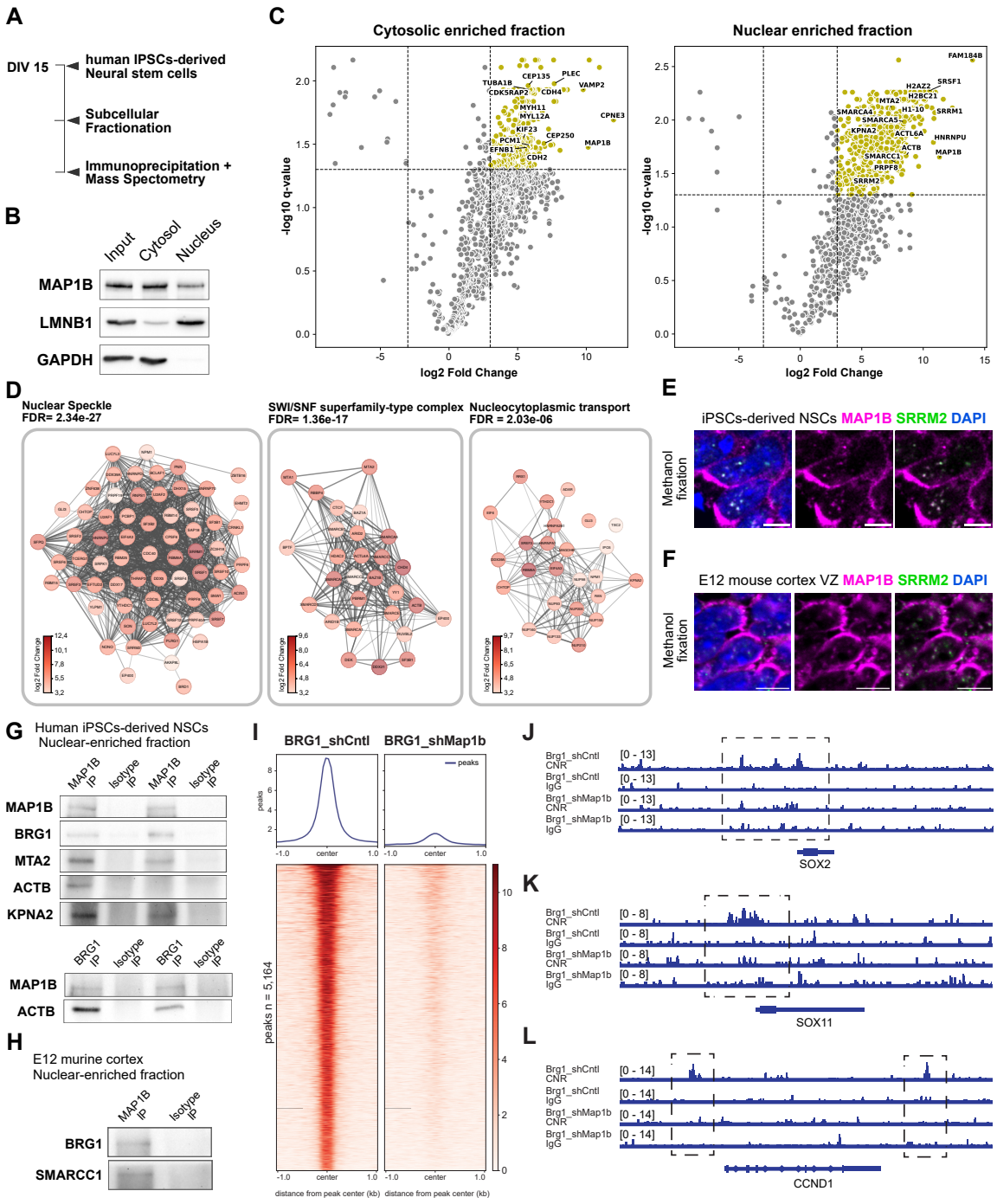
A
DIV 15
human IPSCs-derived Neural stem cells
Subcellular Fractionation
Immunoprecipitation + Mass Spectometry
B
Input
Cytosol
Nucleus
MAP1B
LMNB1
GAPDH
C
Cytosolic enriched fraction
Nuclear enriched fraction
-log10 q-value
log2 Fold Change
CEP135
PLEC
TUBA1B
VAMP2
CDK5RAP2
CDH4
MYH11
CPNE3
MYL12A
KIF23
CEP250
PCM1
MAP1B
EFNB1
CDH2
FAM184B
SRSF1
H2AZ2
H2BC21
MTA2
SMARCA4
SMARCA5
H1-10
SRRM1
KPNA2
ACTL6A
HNRNPU
ACTB
SMARCC1
MAP1B
PRPF8
SRRM2
D
Nuclear Speckle
FDR= 2.34e-27
SWI/SNF superfamily-type complex
FDR= 1.36e-17
Nucleocytoplasmic transport
FDR = 2.03e-06
log2 Fold Change
E
iPSCs-derived NSCs MAP1B SRRM2 DAPI
Methanol fixation
F
E12 mouse cortex VZ MAP1B SRRM2 DAPI
Methanol fixation
G
Human iPSCs-derived NSCs
Nuclear-enriched fraction
MAP1B IP
Isotype IP
MAP1B
BRG1
MTA2
ACTB
KPNA2
BRG1 IP
Isotype IP
MAP1B
ACTB
H
E12 murine cortex
Nuclear-enriched fraction
MAP1B IP
Isotype IP
BRG1
SMARCC1
I
BRG1_shCntl
BRG1_shMap1b
peaks
peaks n = 5,164
center
distance from peak center (kb)
J
Brg1_shCntl CNR
Brg1_shCntl IgG
Brg1_shMap1b CNR
Brg1_shMap1b IgG
[0 - 13]
SOX2
K
[0 - 8]
SOX11
L
[0 - 14]
CCND1

Figure 6

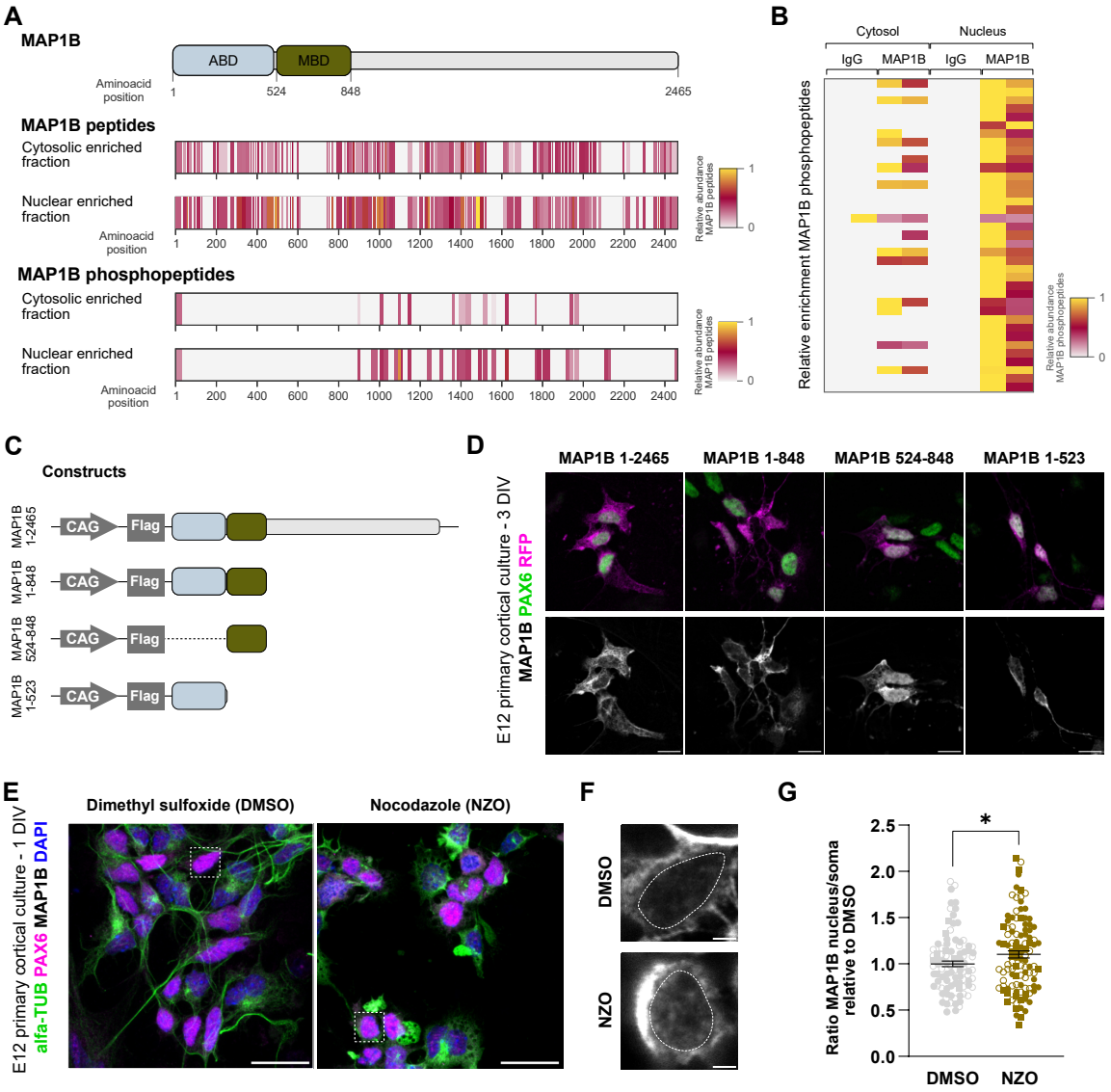
A
MAP1B
ABD
MBD
Aminoacid position
1
524
848
2465
MAP1B peptides
Cytosolic enriched fraction
Nuclear enriched fraction
Aminoacid position
1 200 400 600 800 1000 1200 1400 1600 1800 2000 2200 2400
Relative abundance MAP1B peptides
1
0
MAP1B phosphopeptides
Cytosolic enriched fraction
Nuclear enriched fraction
Aminoacid position
1 200 400 600 800 1000 1200 1400 1600 1800 2000 2200 2400
Relative abundance MAP1B peptides
1
0
B
Cytosol
Nucleus
IgG
MAP1B
IgG
MAP1B
Relative enrichment MAP1B phosphopeptides
Relative abundance MAP1B phosphopeptides
1
0
C
Constructs
MAP1B 1-2465
MAP1B 1-848
MAP1B 524-848
MAP1B 1-523
CAG
Flag
D
MAP1B 1-2465
MAP1B 1-848
MAP1B 524-848
MAP1B 1-523
E12 primary cortical culture - 3 DIV
MAP1B PAX6 RFP
E
Dimethyl sulfoxide (DMSO)
Nocodazole (NZO)
E12 primary cortical culture - 1 DIV
alfa-TUB PAX6 MAP1B DAPI
F
DMSO
NZO
G
Ratio MAP1B nucleus/soma relative to DMSO
2.5
2.0
1.5
1.0
0.5
0.0
*
DMSO
NZO

Figure 7

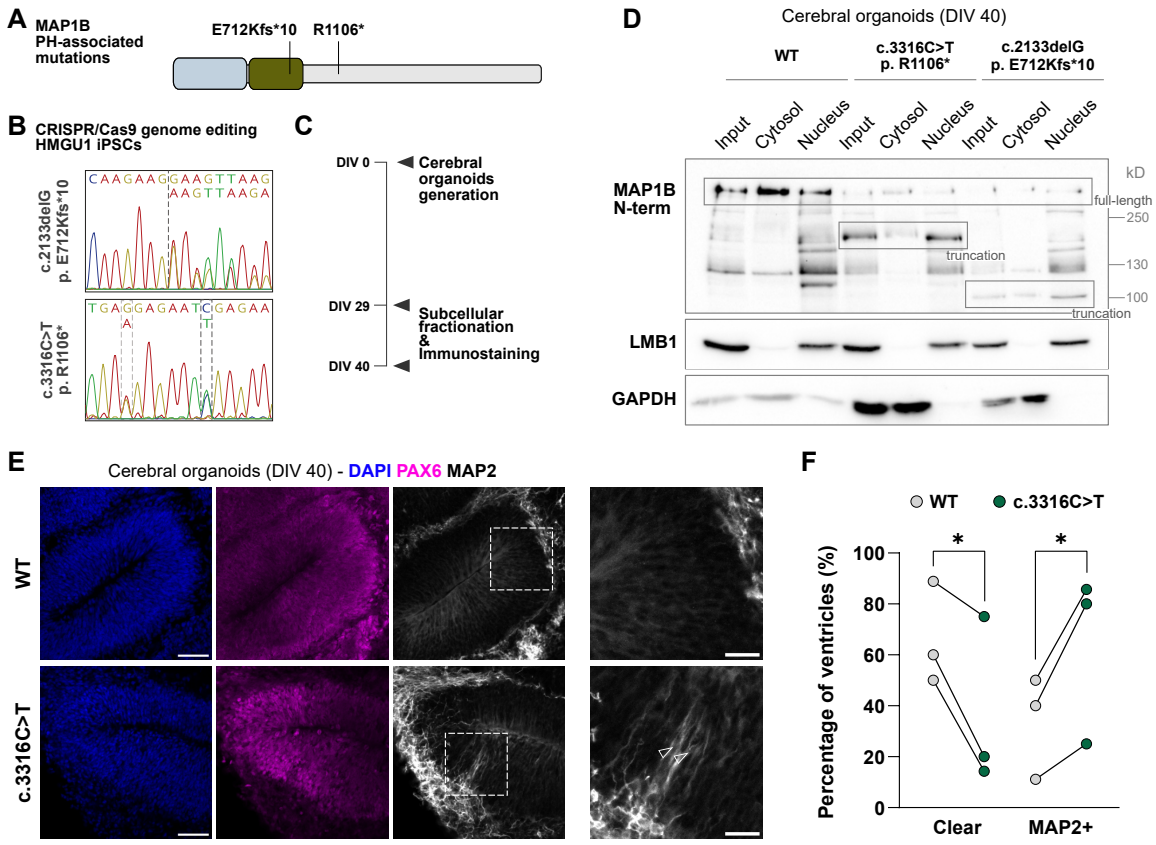
A
MAP1B
PH-associated
mutations
E712Kfs*10
R1106*
B
CRISPR/Cas9 genome editing
HMGU1 iPSCs
c.2133delG
p. E712Kfs*10
c.3316C>T
p. R1106*
C
DIV 0
Cerebral
organoids
generation
DIV 29
Subcellular
fractionation
&
Immunostaining
DIV 40
D
Cerebral organoids (DIV 40)
WT
c.3316C>T
p. R1106*
c.2133delG
p. E712Kfs*10
Input
Cytosol
Nucleus
MAP1B
N-term
kD
full-length
250
truncation
130
100
truncation
LMB1
GAPDH
E
Cerebral organoids (DIV 40) - DAPI PAX6 MAP2
WT
c.3316C>T
F
WT
c.3316C>T
Percentage of ventricles (%)
100
80
60
40
20
0
*
*
Clear
MAP2+

Figure S1. Validation of *Map1b*-KD plasmids (related to Figure 1)

A, Mis-sense mutations in *MAP1B* gene identified in patients with Periventricular Heterotopia[22–25]. B, Combined Annotation-Dependent Depletion (CADD) score[62] on *MAP1B* variants. C, Schematic representation of the *Map1b* KD construct and its control used in the study. D, G, Schematic drawings of experimental design for the validation of *Map1b* KD by western blot in N2A cells (D) or by immunostaining in primary cortical cells isolated at embryonic day 14 (G). Western blot representative images (E) and quantification of MAP1B mean intensity (F) relative to GAPDH from N2A cells transfected with shControl, shMap1b or shMap1#2. Representative images (H) and quantification of MAP1B mean intensity (I) in primary cortical cells via immunostaining. Different symbols represent different biological replicates. ABD: Actin binding domain; MBD: Microtubule binding domain; HC: Heavy chain; LC: Light chain; GFP: Green fluorescent protein. Scale bar: 10 µm. Mean & SEM; Kruskal-Wallis + Dunn's multiple comparison; ****: p-value<0.0001.

Figure S2. Identification of a subpopulation with particularly altered migration patterns upon *Map1b*-KD (related to Figure 1)

A, Histogram showing the proportion of cells for each treatment per speed interval analyzed. B, Bayesian Information Criterion (BIC) versus number of clusters for a set of Gaussian Mixture Models grouping cell trajectories based on log-transformed (normalized) speed and tortuosity values. The model with three components (highlighted with a vertical dashed red line), which minimizes the model selection criterion, was used for further processing. C, Log-transformed (normalized) speed and tortuosity for all tracked cells, colored by treatment. D, GFP fluorescence intensity for all cells analyzed per cluster. Kruskal-Wallis test followed by Dunn's multiple comparison testing. Quantification on speed and tortuosity for cells belonging to clusters 1 and 2 for each treatment shown in E and F, respectively. N=cell; different symbols represent different imaging sessions. Two-tailed Mann-Whitney test. Mean & SEM; ***: p-value<0.001.

Figure S3. Characterization of dataset from *Map1B*-KD in all cells (driven by CAG) (related to Figure 2)

A, Quality control and raw Leiden clustering results from the pCAG dataset. B, Violin plots per cell type depicting the expression of microtubule associated proteins for each treatment. C, Expression distribution over the 2D UMAP projections for cell type marker genes on the pCAG dataset. D, Dot plot showing reference cell type marker gene expression and fraction of cells in group for each annotated cell type in the pCAG dataset. Expression distribution over the 2D UMAP projections for extra-cortical markers (E) or markers of the 'Neurons_unknown' cluster (F). G, Lineage driver Z-score signature for Neurons_unknown as a terminal differentiation state over the 2D UMAP projection.

Figure S4. Characterization of dataset from *Map1B*-KD in neurons only (driven by *pDcx*) (related to Figure 3)

A, Quality control and raw Leiden clustering results from the p*Dcx* dataset. B, Cell proportion per treatment and cluster on the p*Dcx* dataset. C, Expression distribution over the 2D UMAP projections for cell type marker genes. D, Dot plot showing reference cell type marker gene expression and fraction of cells in group for each annotated cell type in the p*Dcx* dataset. Neurons_unknown signature expression score for each cell type in pCAG (E) and p*Dcx* (F) datasets. RGC: Radial Glia Cells; Prog: Progenitors; IPs: Intermediate Progenitors; IC: Intracortical; PT: Pyramidal Tract; CT: Corticothalamic.

Figure S5. MAP1B's role in NSCs (related to Figure 4, 5 and 6)

A, B, Representative images from E12 cortical cultures transfected as indicated at DIV1 and imaged between DIV 2-3 to assess differential cell survival, quantified in C. Wilcoxon test. Yellow and white arrows indicate cell division and cell death, respectively. D, Representative image from E12 cortical cultures stained as indicated depicting the absence of MAP1B in mitotic spindles. E, Representative images from E12 cortical cultures stained as indicated, depicting the distribution of MAP1B expressed with either an NLS or NES sequence, both labeled with a FLAG tag. F, Western blot images from iPSCs-derived NSCs samples upon subcellular fractionation used for validations of MAP1B nuclear interactors, stained as indicated. Note that the panels for MAP1B, LMNB1 and GAPDH for the differentiation #1 are duplicates from the images present in Figure 5B. G, Kinase prediction enrichment based on MAP1B phospho-peptides identified in NSCs. Scale bar: 20 µm (A) and 5 µm (C and D)

Figure S6. MAP1B E712Kfs*10 subcellular localization within the mouse developing cortex labelled by Breasi-CRISPR (related to Figure 7)

A, Experimental design for studying MAP1B E712Kfs*10 within the mouse developing cortex. Representative images depicting the distribution of electroporated cells (B and D) and the subcellular localization (C and E) from MYC-tagged MAP1B and MYC-tagged MAP1B E712Kfs*10, respectively. Note: Brains were fixed with 4% PFA, which lowers the detection of MAP1B in the nucleus.

Movie S1. Slice imaging of a shControl-electroporated cortex (related to Figure 1)

Movie S2. Slice imaging of a shMap1b-electroporated cortex (related to Figure 1)

Movie S3. Live imaging of E12 cortical culture transfected with shControl (related to Figure S5)

Movie S4. Live imaging of E12 cortical culture transfected with shMap1b (related to Figure S5)

Table S1. DEGs and Gene Ontology analysis identified in Map1b-KD scRNAseq (related to Figure 2)

Table S2. MAP1B interactors and peptides in cytosolic enriched and nuclear enriched fractions from iPSCs-dervied neural stem cells (related to Figure 5)

Figure S1

A

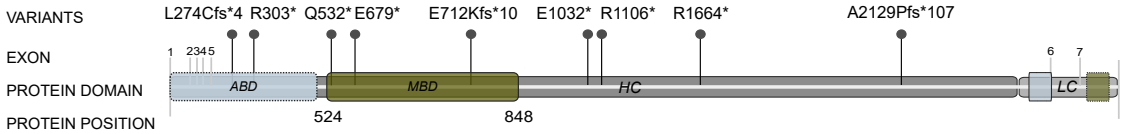

B

Chr	Position	Reference	Alternative	Protein	CADD	ClinVar
5	71490000	C	T	L274fs	**27.7**	Likely pathogenic
5	71490089	C	T	R303*	**34**	Pathogenic
5	71490776	C	T	Q532*	**34**	Pathogenic
5	71491217	G	T	E679*	**37**	Pathogenic
5	71491315	G	T	E712K	**22.1**	Pathogenic
5	71492276	G	T	E1032*	**37**	Pathogenic
5	71492498	C	T	R1106*	**36**	Uncertain
5	71494550	C	T	R1664*	**37**	Pathogenic
5	71495567	G	T	A2129P	**24.4**	-

C

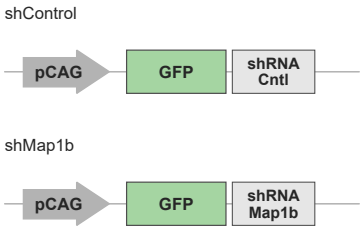

D

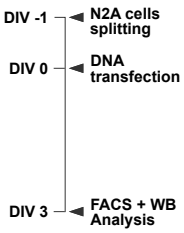

E

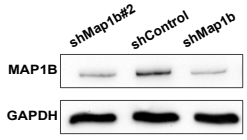

F

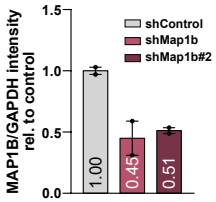

G

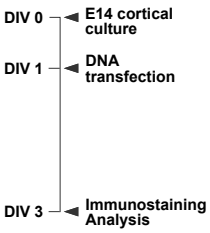

H

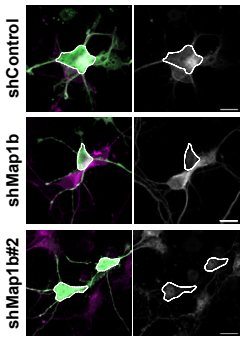

I

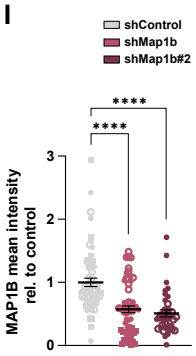

Figure S2

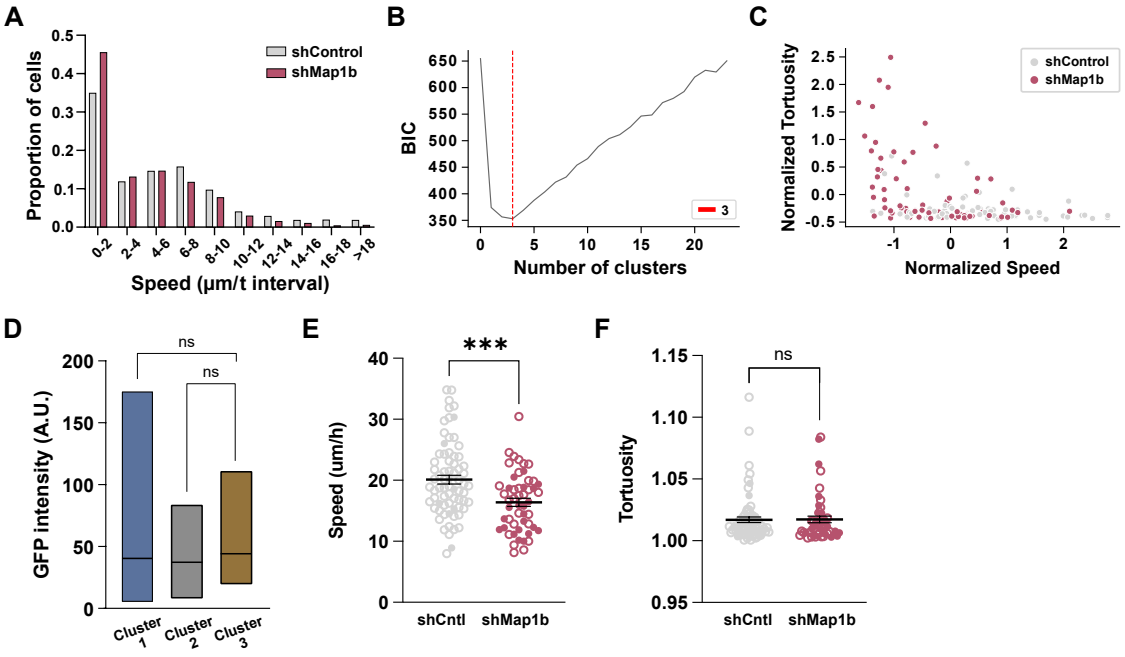
A
Proportion of cells
shControl
shMap1b
Speed (µm/t interval)
B
BIC
Number of clusters
C
Normalized Tortuosity
Normalized Speed
D
GFP intensity (A.U.)
ns
Cluster 1
Cluster 2
Cluster 3
E
Speed (um/h)
***
shCntl
shMap1b
F
Tortuosity
ns

Figure S3


A
Doublet's score
Number of counts
Number of genes
Mitochondrial fraction
Replicate's distribution
Leiden clustering
Replicate 1
Replicate 2
r=0.6
B
Map1b
Map2
Mapt
Map1a
Map1s
Dcx
shControl
shMap1b
RGC1
RGC2
IP
Migrating Neurons
IC Neurons
PT Neurons
CT Neurons
Normalized expression
C
Sox2
Pax6
Eomes
Neurog2
Dcx
Tubb3
Sema3c
Unc5d
Cux1
Satb2
Fezf2
Bcl11b
Foxp2
Tbr1
Gad1
Cd33
Olig1
Kdr
D
RGC1
RGC2
IPs
Migrating neurons
IC neurons
PT neurons
CT neurons
Neurons unknown
Interneurons
Microglia
Vascular cells
OPCs
Fraction of cells in group (%)
Mean expression in group
E
Isl1
Nkx2-1
Dlx6
Ascl1
Reln
F
Thsd7a
Tfap2d
Epha6
Gm28756
Ebf1
G
Lineage driver Score

Figure S4

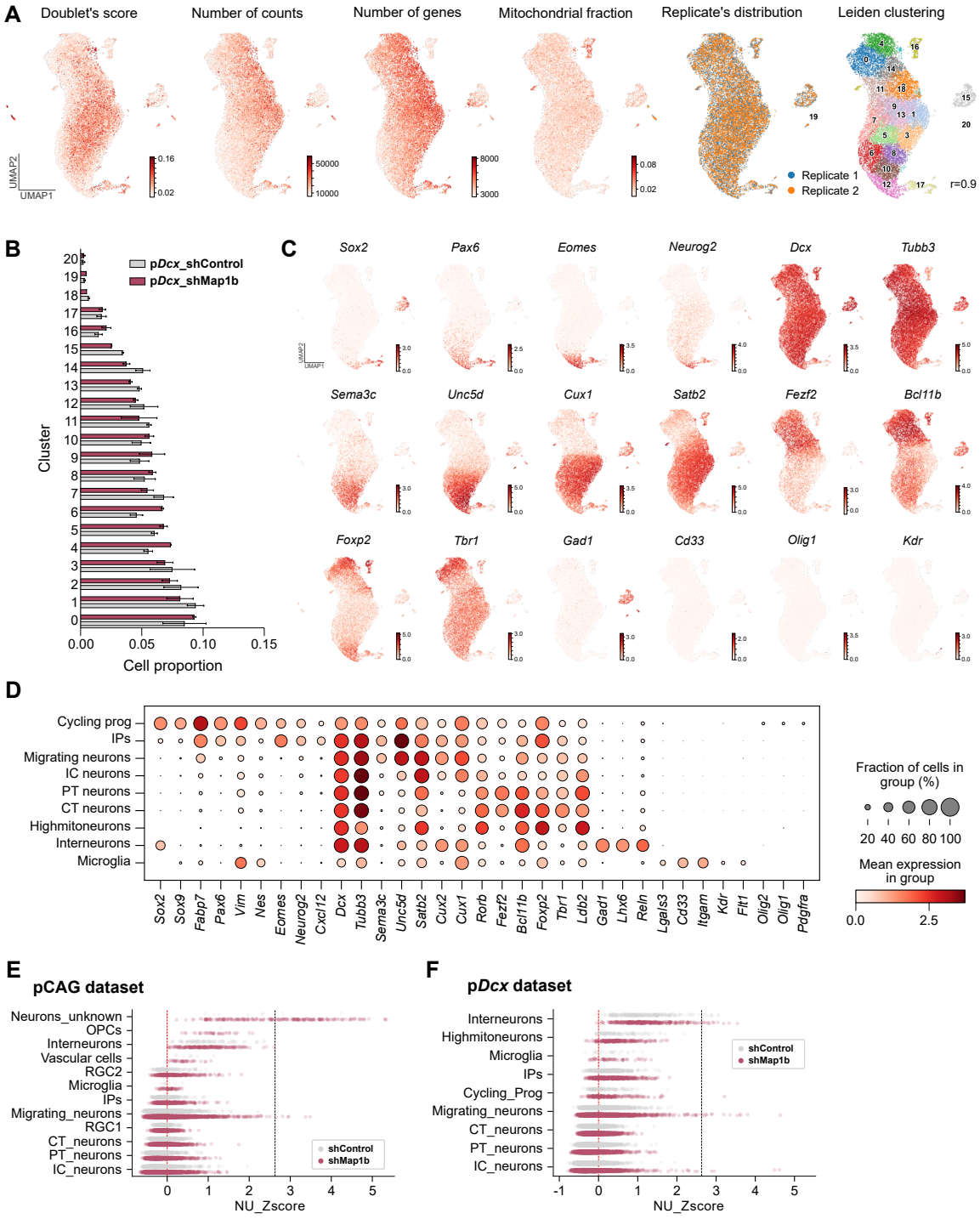
A
Doublet's score
Number of counts
Number of genes
Mitochondrial fraction
Replicate's distribution
Leiden clustering
UMAP1
UMAP2
Replicate 1
Replicate 2
r=0.9
B
pDcx_shControl
pDcx_shMap1b
Cluster
Cell proportion
C
Sox2
Pax6
Eomes
Neurog2
Dcx
Tubb3
Sema3c
Unc5d
Cux1
Satb2
Fezf2
Bcl11b
Foxp2
Tbr1
Gad1
Cd33
Olig1
Kdr
D
Cycling prog
IPs
Migrating neurons
IC neurons
PT neurons
CT neurons
Highmitoneurons
Interneurons
Microglia
Sox2 Sox9 Fabp7 Pax6 Vim Nes Eomes Neurog2 Cxcl12 Dcx Tubb3 Sema3c Unc5d Satb2 Cux2 Cux1 Rorb Fezf2 Bcl11b Foxp2 Tbr1 Ldb2 Gad1 Lhx6 Reln Lgals3 Cd33 Itgam Kdr Flt1 Olig2 Olig1 Pdgfra
Fraction of cells in group (%)
20 40 60 80 100
Mean expression in group
0.0 2.5
E
pCAG dataset
Neurons_unknown
OPCs
Interneurons
Vascular cells
RGC2
Microglia
IPs
Migrating_neurons
RGC1
CT_neurons
PT_neurons
IC_neurons
shControl
shMap1b
NU_Zscore
F
pDcx dataset
Interneurons
Highmitoneurons
Microglia
IPs
Cycling_Prog
Migrating_neurons
CT_neurons
PT_neurons
IC_neurons
shControl
shMap1b
NU_Zscore

Figure S5

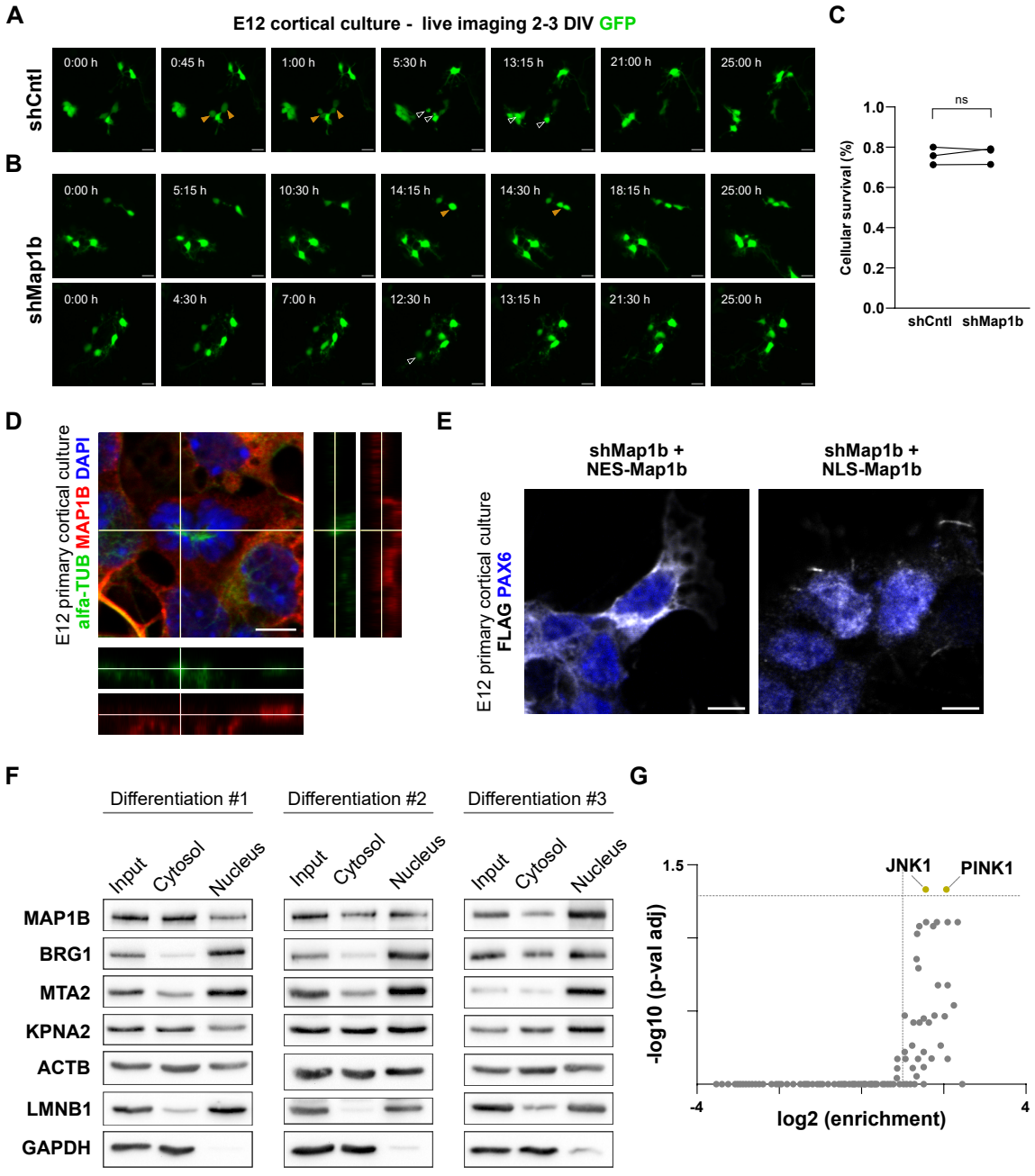
A
E12 cortical culture - live imaging 2-3 DIV GFP
shCntl
0:00 h
0:45 h
1:00 h
5:30 h
13:15 h
21:00 h
25:00 h
B
shMap1b
0:00 h
5:15 h
10:30 h
14:15 h
14:30 h
18:15 h
25:00 h
0:00 h
4:30 h
7:00 h
12:30 h
13:15 h
21:30 h
25:00 h
C
ns
Cellular survival (%)
1.0
0.8
0.6
0.4
0.2
0.0
shCntl
shMap1b
D
E12 primary cortical culture
alfa-TUB MAP1B DAPI
E
shMap1b +
NES-Map1b
shMap1b +
NLS-Map1b
E12 primary cortical culture
FLAG PAX6
F
Differentiation #1
Differentiation #2
Differentiation #3
Input
Cytosol
Nucleus
MAP1B
BRG1
MTA2
KPNA2
ACTB
LMNB1
GAPDH
G
JNK1
PINK1
1.5
-log10 (p-val adj)
-4
4
log2 (enrichment)

Figure S6

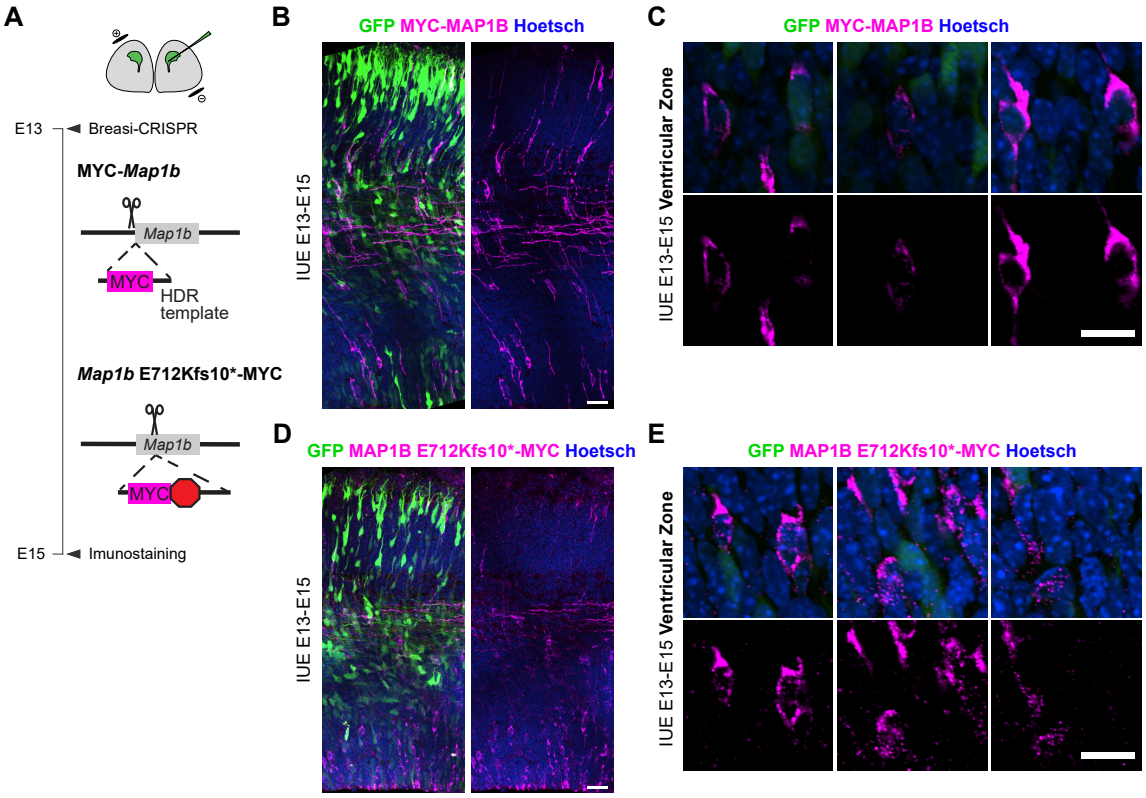
A
E13
Breasi-CRISPR
MYC-Map1b
Map1b
MYC
HDR
template
Map1b E712Kfs10*-MYC
Map1b
MYC
E15
Imunostaining
B
GFP MYC-MAP1B Hoetsch
IUE E13-E15
C
GFP MYC-MAP1B Hoetsch
IUE E13-E15 Ventricular Zone
D
GFP MAP1B E712Kfs10*-MYC Hoetsch
IUE E13-E15
E
GFP MAP1B E712Kfs10*-MYC Hoetsch
IUE E13-E15 Ventricular Zone

4 Discussion

This thesis highlights both canonical and non-canonical regulatory mechanisms that govern proper neurogenesis, emphasizing the transcriptional control in Chapter 2, and the compartmental distribution of a moonlighting protein in Chapter 3. Our findings suggest that NSCs have evolved diverse strategies to balance self-renewal and differentiation, ensuring the precise timing and progression of neurogenesis.

4.1 TGIF2 Regulates NSC Maintenance and Neurogenic Priming

Our findings from Chapter 2 establish TGIF2 as a key transcriptional repressor that safeguards NSC identity and modulates neurogenic priming by repressing neuronal differentiation genes. We further elucidate the molecular mechanisms underlying TGIF2's repressor function, which is dependent on its capability to phosphorylate and the interaction with the SIN3A repressor complex, particularly one of the components—chromatin remodeler ARID4B.

4.1.1 Control of Neurogenic Tempo and Competence by TGIF2

TGIF2 overexpression *in vitro* and *in vivo* increases NSCs, while delaying neural differentiation, without restraining the neurogenesis progression. Particularly, in E12 transfection assay that has a later timepoint, 7 days post transfection, TGIF2 overexpression increases TBR2+ IPCs, while the increase was in Pax6+ NSCs at 3 days post transfection. The neurogenesis window seems rather protracted, allowing progenitors more time to proliferate and expand. This suggests that TGIF2's repression on neuronal differentiation genes acts as barrier: the higher its expression and guarding these genes, the more difficult it is for proneural TFs to access and activate them, thereby slowing down the neurogenic tempo.

The lengthening of the neurogenic period is one of the major hallmarks behind human neocortex expansion, and this temporal extension increases upper layer neurons, predicted by mathematical modeling (Stepien et al., 2020). Consistently, TGIF2 was shown to favor upper layer neuron fate in CellRank and RegVelo simulation. To directly assess if TGIF2 overexpression prolongs neurogenesis and leads to more total neuronal output, we will analyze the electroporated cortex at postnatal day 10 (P10), when the upper layers have differentiated.

Beyond controlling the neurogenic tempo, can TGIF2 also influence the neurogenic competence, either extending its window or reactivating it? In our TGIF2 Cut&Run and GRN, we showed that TGIF2 has extensive occupancy and negative regulation on NFI factors: Nfia, Nfib, Nfix. It was found that Nfia/b/x triple KO (TKO) restores the neurogenic competence in both

hypothalamic tanycytes and Müller glia (Hoang et al., 2020; Yoo et al., 2021). In other words, NFI factors may be actively repressing the neurogenic competence in tanycytes and Müller glia. Specifically, NFI TKO in hypothalamic tanycytes—radial glial cells lining the third ventricle—induces proliferation and subsequent neurogenesis in both postnatal and adult mice (Yoo et al., 2021), when homeostatic neurogenesis is vastly diminishing or absent. Therefore, we can postulate that TGIF2 overexpression may exert the same effect via its repression on NFI factors and restore neurogenic competence in adult mice. Also, endogenous Tgif2 expression correlates nicely with the neurogenesis window, starting around E11, peaking at E14, and then decreasing at E18; in adult mice, Tgif2 is still expressing around neurogenic niches, although at rather lower levels (*ISH Data :: Allen Brain Atlas: Developing Mouse Brain*, n.d.).

To test whether TGIF2 can reactivate the neurogenic competence in adult progenitors, we can overexpress wildtype TGIF2 or TGIF2-VP64 (observed with opposite effect of wildtype) in adult murine subependymal zone (SEZ), where adult NSCs reside, and analyze the subsequent proliferation and neurogenesis.

4.1.2 TGIF2 Isoform Selectivity in Neuronal Output

In CellRank's terminal fate prediction with both TGIF2 isoform overexpression conditions and RegVelo's simulation on TGIF2IR, TGIF2 isoforms exhibit differential selectivity on neuronal subtypes. TGIF2IR favors upper layer neuronal fate, while TGIF2d favors deep layer neuronal fate. In fact, this selectivity aligns with the temporal expression dynamics of Tgif2 isoforms during development. From E10 to E12, when deep layer neurons are produced, Tgif2d is expressed at a higher level than Tgif2IR (Cardoso-Moreira et al., 2019) (Figure 7a). However, exactly when the neurogenic program shifts from deep layer neuron to upper layer neuron at E13, Tgif2IR expression surpasses that of Tgif2d, suggesting a regulatory role in this transition. These findings indicate that TGIF2 isoforms may contribute to the temporal control of neuronal fate by modulating distinct transcriptional programs at different developmental stages.

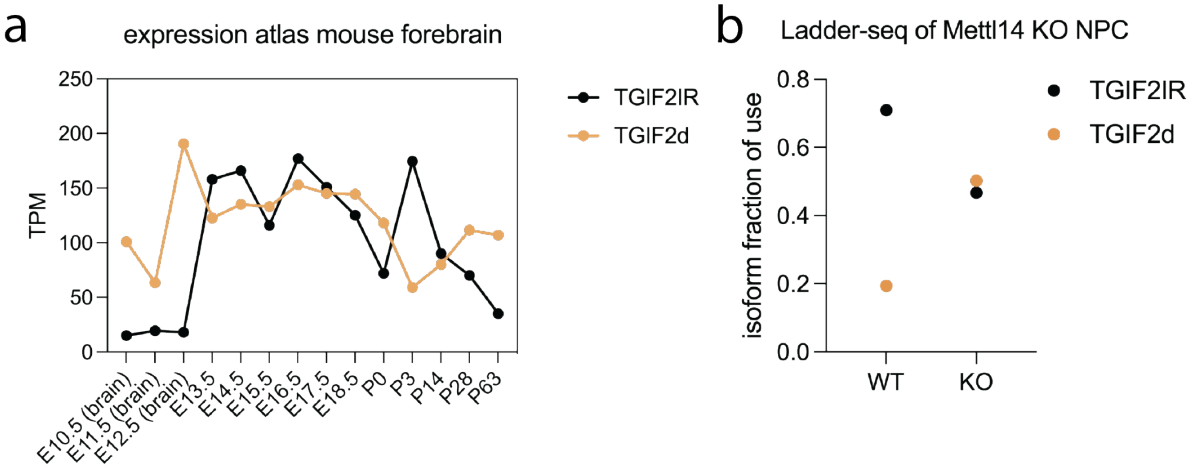

Figure 7. TGIF2 isoform expression profile during mouse forebrain development and Mettl14 KO murine cortical NPCs

RNA levels of TGIF2 isoforms plotted for different timepoints during mouse forebrain development from (Cardoso-Moreira et al., 2019) in (a) and Mettl14 KO NPCs from (Ringeling et al., 2022) in (b). WT: wildtype. KO: Mettl14 KO.

A similar isoform switch was observed in methyltransferase-like protein 14 (Mettl14) KO NPCs derived from E14 mouse cortex (Ringeling et al., 2022) (Figure 7b). In wildtype E14 cortical NPCs, Tgif2IR is more highly expressed than Tgif2d, but in the absence of Mettl14—which depletes N6-methyladenosine (m6A) modifications—Tgif2d levels surpass those of Tgif2IR. m6A RNA methylation is the most abundant and reversible modification on mRNAs that regulates the abundance and alternative splicing of target mRNAs (N. Liu et al., 2015). It plays a crucial role not only in NSC proliferation and maintenance, but also in regulating "priming", or "pre-patterning", as an epi-transcriptomic mechanism, preventing premature protein expression of later-stage lineage factors in NSCs (Yoon et al., 2017). Notably, Tgif2 isoforms are among the m6A tagged transcripts (Ringeling et al., 2022), suggesting that their differential expression may be epi-transcriptomically regulated.

In NSC-specific Mettl14 KO mice, there is a significant reduction in SATB2+ and CUX1+ late-born upper layer neurons at E17.5 and P0, while TBR1+ deep-layer neurons remain affected (Y. Wang et al., 2018). This remarkably resembles what we observed with TGIF2 overexpression using in utero electroporation from E13 to E16 (Figure 8). Specifically, TGIF2d overexpression shows a reduction in SATB2+ upper layer neurons compared to TGIF2IR (Figure 8d), while TGIF2IR overexpression results in a trend of diminution in CTIP2+ deep layer neurons (Figure 8i). Overexpression of either TGIF2 isoforms did not affect TBR1+ deep layer neurons (Figure 8e). While these relative changes are not statistically significant compared to GFP control at this early timepoint, compared to E17.5 and P0 checked in (Y. Wang et al., 2018), they suggest a potential shift in neuronal subtype specification. To better assess these effects, we can examine neuronal output at a later developmental stage (P10), when layer formation is largely complete.

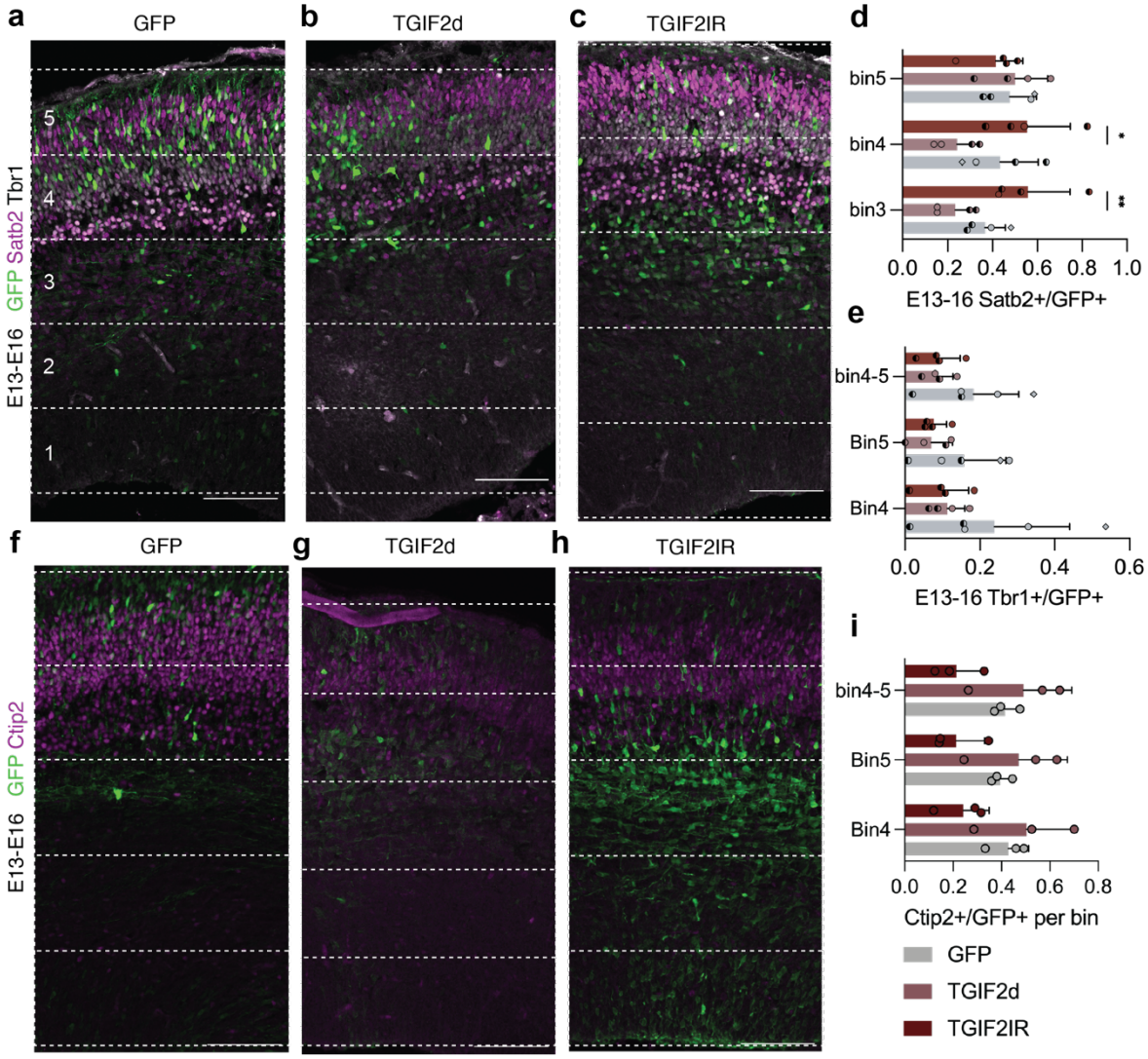

Figure 8. Neuronal progeny differences upon overexpression of the TGIF2 isoforms
(a-c) Representative images showing cortices 3 days post IUE with different conditions, co-stained for GFP, TBR1 and SATB2. Dashed lines indicate the 5 equal bins. Scale bar: 100µm.
(d-e) Quantification of TBR1+/GFP+ cells and SATB2+/GFP+ cells from images as represented above, mean±SD. N=4-5 embryos from at least 2 mothers. Ordinary two-way ANOVA with Tukey's multiple comparisons test.
(f-h) Representative images showing cortices 3 days post IUE with different conditions, co-stained for GFP and CTIP2. Dashed lines indicate the 5 equal bins. Scale bar: 100µm.
(i) Quantification of CTIP2+/GFP+ cells from images as represented above, mean±SD. N=3 embryos from at least 2 mothers. Ordinary two-way ANOVA with Tukey's multiple comparisons test.

The correlation between TGIF2 isoform selectivity in neuronal subtypes and their relative expression dynamics during early- and late-stage neurogenesis raises an intriguing question: could isoform-specific regulation serve as a mechanism for neuronal fate determination? To address this, scRNA-seq with splice variant resolution across developmental stages would be particularly informative. Full-length SMART-seq scRNA-seq, as previously applied to the adult

mouse primary motor cortex, has demonstrated isoform-level cell type specificity (Booeshaghi et al., 2021). Leveraging this approach alongside tailored trajectory analysis may uncover novel regulatory layers governing neurogenesis and neuronal subtype specification.

4.1.3 Lineage Priming Capability of TGIF2

While TGIF2 primarily binds and represses neurogenesis genes, it also targets key TFs of late temporal identify factors, such Sox9 and NFI family factors, which are also known for their gliogenic inducing ability (Blackshaw & Cayouette, 2025). This suggests that TGIF2's role may extend beyond neurogenic repression, potentially influencing lineage priming by modulating both neurogenic and gliogenic programs.

Interestingly, when analyzing our scRNA-seq dataset of TGIF2 overexpression, we found that only half of the TGIF2-bound neurogenic priming genes were significantly downregulated. The remaining genes did not appear as DE genes, meaning that either their expression levels remained unchanged or were below detection thresholds. To gain further insight, we examined the TF motifs enriched in the upstream regions of transcription start sites of these non-DE genes. The most highly enriched motif belonged to LHX2 (data not shown).

Notably, LHX2 shares a similar phenotype as TGIF2. Deletion of Lhx2 reduces progenitor proliferation and induces precocious neuronal differentiation, with an accelerated onset of generating each cortical layer (Chou & O'Leary, 2013). This effect is, at least in part, mediated by LHX2 activating Hes1 and Pax6, both of which play critical roles in maintaining neural progenitor identity and delaying differentiation. Given these parallels, it is likely that LHX2 functions as a co-regulator of neurogenic priming alongside TGIF2, helping to coordinate the timing of differentiation and the balance between proliferation and fate commitment.

4.1.4 TGIF2 Potential in Regeneration

In regeneration-competent species such as zebrafish, genes enriched in late-stage progenitors and resting glia (i.e., Sox8/9, Nfia/b/x) are rapidly downregulated, while inflammatory and proneural genes are upregulated in parallel, allowing activated glia to transition into a neurogenic state (Blackshaw & Cayouette, 2025). In contrast, in mammals, activated glia primarily trigger an inflammatory response, followed by upregulation of genes associated with late-stage progenitors and resting glia. The neurogenic latency in reactive astrocytes is rather mild *in vivo*, inhibited by Notch signaling (Magnusson et al., 2014; Zamboni et al., 2020). Murine reactive astrocytes cultured under neutrosphere conditions *in vitro* exhibit NSC markers and can be instructed into multipotency to generate neurons (Götz et al., 2015). This suggests that mammalian regeneration competence may be repressed by Notching

signaling *in vivo*, as well as the pre-emptive activation of late-stage progenitor genes (i.e., NFI factors).

A potential strategy to enhance regeneration capacity in mammals could involve delaying the onset of these genes (Sox8/9, Nfia/b/x). In this context, TGIF2 overexpression may be particularly beneficial. Investigating whether transient TGIF2 overexpression following acute brain injury in mice enhances regenerative potential would be an intriguing avenue for future research. Additionally, TGIF2 has been found to play a neuroprotective role, including reducing apoptosis (Lei et al., 2022), which could further support brain repair following injury.

4.2 MAP1B as a Moonlighting Protein Modulating Neurogenesis

We have demonstrated that MAP1B, a cytoskeletal protein, has a moonlighting function in the nucleus. While its cytoplasmic enrichment promotes neuronal differentiation, the nuclear enrichment promotes NSC maintenance, revealing a compartment-dependent role in regulating neurogenesis.

4.2.1 MAP1B's Moonlighting Function in the Nucleus

Cut&Run analysis of organoids carrying PH patient knock-in (KI) mutations revealed that nuclear enrichment of MAP1B enhances global BRG1 binding (data from recent experiment, not shown). Given BRG1's primary role in transcriptional activation (Ren et al., 2024), particularly at stemness- and proliferation-associated genes such as Sox2 and Ccnd1 as we observed, this suggests that MAP1B promotes NSC fate by modulating BRG1 occupancy. Conversely, Map1b knockdown (KD) in human iPSC-derived NSCs resulted in a global reduction of BRG1 binding, further confirming MAP1B's role in regulating BRG1 activity. This effect is reminiscent of what is observed in actin KO cells—loss of chromatin association by BRG1 (Xie, Almuzzaini, et al., 2018). While both gain- and loss-of-function alterations in BRG1 binding lead to neuronal heterotopia, it is MAP1B's relative compartmental expression that modulates these dynamics within individual cells to ultimately influence fate decisions.

Beyond chromatin regulation, we found that MAP1B also interacts with nuclear ribonucleoproteins, including splicing factors. Immunostainings revealed that nuclear MAP1B co-localizes with nuclear speckles, membrane-less organelles (MLOs) that serve as hubs for gene expression, RNA processing, and storage. The assembly of nuclear speckles is facilitated by liquid–liquid phase separation (LLPS), which relies on intrinsically disordered regions (IDRs) in nuclear speckle proteins (Ilik et al., 2020; Kim et al., 2019). Notably, a significant portion of MAP1B's structure consists of IDRs, including its microtubule-binding and assembly domains—

regions essential for its cytoplasmic function but potentially repurposed for novel nuclear roles, such as interactions with nuclear speckle components.

Disruptions in nuclear speckle proteins, termed “nuclear speckleopathies,” are linked to neurodevelopmental disorders, including developmental delay and intellectual disability (Regan-Fendt & Izumi, 2024). Loss of nuclear speckle integrity in human iPSC-derived neurons leads to exon skipping and intron retention, resulting in neuronal toxicity (R. Wu et al., 2024). Additionally, nuclear-speckle-associated intron retention plays a role in cell cycle progression, thereby may influence NSC proliferation. A relevant example is TMF1-regulated nuclear protein 1 (TRNP1), previously identified in our lab as a key regulator of NSC self-renewal and brain folding (Stahl et al., 2013), whose pro-proliferative function depends on its LLPS capacity and interaction with MLOs, including nuclear speckles (Esgleas et al., 2020). It remains to be explored how MAP1B extends its nuclear functions in regulating nuclear speckles and RNA metabolism.

4.2.2 Evolution of Moonlighting Proteins

The mechanisms prompting proteins to adopt moonlighting functions remain largely elusive. One hypothesis is the chance interaction model (Copley, 2014), which suggests that proteins may acquire secondary functions through a serendipitous interaction with another protein or DNA, leading to an adaptive advantage for the cell or organism that is selected for over evolutionary time. Relocations of proteins to new environments, such as from plasma membrane to the nucleus, particularly, can expose them to novel interaction partners, facilitating the emergence of new functions. This model also explains why moonlighting proteins are often constitutively expressed proteins, as they are more likely to encounter diverse intracellular environments.

In the case of MAP1B, it is well-established that it interacts with actin (Cueille et al., 2007), a cytoskeletal protein that is actively transported into the nucleus via importins (Dopie et al., 2012; Stüven et al., 2003) as mentioned in the introduction. Given this, we hypothesize that MAP1B’s interaction with actin may facilitate its engagement with the importin/Ran system. Indeed, we observed that MAP1B interacts with importin alpha subunit 1 (as known as KPNA2), RAN, and nuclear pore complex subunits, supporting the idea that nuclear transport mechanisms contribute to its moonlighting function. Additionally, within the nucleus, MAP1B associates with the SWI/SNF BAF complex—a chromatin remodeling complex that actin belongs to (Nishimoto et al., 2012; Olave et al., 2002). This suggests that actin may play a crucial role in mediating MAP1B’s nuclear localization and function.

A complementary theory inspired by moonlighting enzymes and chaperones is that—while the active site pocket is often buried within the protein structure, there is a significant portion of surface area exposed and available for interactions with other molecules (Jeffery, 2017). In some cases, a functional interaction domain can be as small as nine amino acids, as demonstrated by *Streptococcus* enolase (Ehinger et al., 2004). For MAP1B, an evolutionary adaptation may have introduced an NLS—a short amino acid motif—that enabled its translocation to the nucleus mediated by importin/RAN system. Given its interaction with actin, it is plausible that MAP1B acquired an NLS through evolutionary pressures, subsequently leading to new nuclear interactions and functions.

While these theories remain largely hypothetical and challenging to test, they highlight how moonlighting proteins can provide a selective advantage. In the case of NSCs, a protein capable of modulating developmental dynamics based on localization—without requiring new transcription and translation—could offer a rapid and energy-efficient response to environmental cues. As the first microtubule-associated protein (MAP) expressed in the embryonic brain (Bloom et al., 1985), MAP1B is well-positioned to play such a role. Moreover, we have demonstrated that phosphorylation serves as a regulatory mechanism for MAP1B's localization—hyperphosphorylation reduces its microtubule binding and facilitates its nuclear translocation. This dynamic regulation enables NSCs to rapidly adjust to differentiation signals in an energy-efficient manner, further emphasizing the functional adaptability of MAP1B as a moonlighting protein.

4.2.3 Compartmental Distribution of Moonlighting Proteins Regulates NSC Fate

While MAP1B is the first cytoskeletal protein we identified to regulate NSC fate dependent on its localization, it is not the only moonlighting protein that influences cell fate decisions. The RNA-binding protein CUG-BP Elav-like family 2 (CELF2) is known to regulate alternative splicing and alternative polyadenylation (APA) inside nucleus of T cells (Chatrikhi et al., 2019; Gazzara et al., 2017). In NSCs, however, CELF2 resides in the cytoplasm, where it represses mRNAs mediating neuronal differentiation (MacPherson et al, 2021), also supporting a translational mechanism to regulate priming via repression. Once it is translocated to the nucleus, the repressed transcripts are released for translation, allowing NSCs to differentiate.

Mutations in Celf2 are implicated in cortical malformations. Patient-derived CELF2 variants abnormally accumulate in the cytoplasm, losing their ability to translocate to the nucleus, thereby stalling NSCs from differentiating. This bidirectional transport mechanism of moonlighting proteins enables NSCs to rapidly respond to differentiation cues, illustrating how spatially regulated moonlighting proteins fine-tune neurogenesis.

4.2.4 Moonlighting Proteins' Involvement in Human Diseases

Given that both MAP1B and CELF2 are moonlighting proteins involved in cortical malformations, it is not surprising that 78% of known moonlighting proteins are implicated in human diseases, compared to only 17.8% in human proteins overall (Franco-Serrano et al., 2018). This highlights the significant enrichment of moonlighting proteins in human diseases, their functional complexity and their potential role in multifaceted disease mechanisms.

Because moonlighting proteins carry out multiple functions in distinct cellular compartments, their mutations can disrupt different biological processes at different stages of disease progression, exacerbating disease phenotypes. In the case of MAP1B, patient-derived mutations lead to its aberrant nuclear accumulation, where it enhances BRG1 binding, resulting in excessive NSC maintenance. Subsequently, its nuclear retention causes a loss of its cytoplasmic function in neuronal migration, further contributing to PH by preventing proper neuronal positioning. This dual dysfunction exemplifies how mutations in moonlighting proteins can amplify pathological outcomes by disrupting multiple molecular and cellular pathways at once.

4.3 Outlook

The current knowledge of moonlighting proteins solely depends on serendipity, and we are probably only touching the tip of the iceberg. Our findings add to this growing body of knowledge, demonstrating that MAP1B, traditionally recognized as a cytoskeletal protein, exhibits nuclear functions that modulate NSC fate. The compartmental localization of these proteins plays a crucial role in their function, emphasizing the importance of spatial regulation in NSC maintenance and differentiation.

Surprisingly, immunostaining of TGIF2 in human cancer cells reveals that it is also located in the centrosome besides the nucleus (*Subcellular - TGIF2 - The Human Protein Atlas*, n.d.), raising the possibility of alternative, yet unexplored, functions beyond transcriptional repression. This underscores the need to maintain an open perspective when studying proteins with well-characterized canonical roles—there is always more to uncover.

Moving forward, a more systematic approach to identifying moonlighting functions will be essential. Advances in high-throughput proteomics, subcellular fractionation, and functional genomics could reveal novel roles for proteins across different cellular compartments. Understanding how proteins like MAP1B and TGIF2 integrate diverse regulatory mechanisms, from transcriptional control to intracellular localization, will not only deepen our knowledge of

neurogenesis, but may also offer new therapeutic strategies for neurodevelopmental disorders and regenerative medicine.

Bibliography

Akoumianaki, T., Kardassis, D., Polioudaki, H., Georgatos, S. D., & Theodoropoulos, P. A. (2009). Nucleocytoplasmic shuttling of soluble tubulin in mammalian cells. *Journal of Cell Science*, *122*(8), 1111–1118. https://doi.org/10.1242/jcs.043034

Alsiö, J. M., Tarchini, B., Cayouette, M., & Livesey, F. J. (2013). Ikaros promotes early-born neuronal fates in the cerebral cortex. *Proceedings of the National Academy of Sciences*, *110*(8), E716–E725. https://doi.org/10.1073/pnas.1215707110

Amador-Arjona, A., Cimadamore, F., Huang, C.-T., Wright, R., Lewis, S., Gage, F. H., & Terskikh, A. V. (2015). SOX2 primes the epigenetic landscape in neural precursors enabling proper gene activation during hippocampal neurogenesis. *Proceedings of the National Academy of Sciences*, *112*(15), E1936–E1945. https://doi.org/10.1073/pnas.1421480112

Aragona, M., Panciera, T., Manfrin, A., Giulitti, S., Michielin, F., Elvassore, N., Dupont, S., & Piccolo, S. (2013). A Mechanical Checkpoint Controls Multicellular Growth through YAP/TAZ Regulation by Actin-Processing Factors. *Cell*, *154*(5), 1047–1059. https://doi.org/10.1016/j.cell.2013.07.042

Arendt, D., Musser, J. M., Baker, C. V. H., Bergman, A., Cepko, C., Erwin, D. H., Pavlicev, M., Schlosser, G., Widder, S., Laubichler, M. D., & Wagner, G. P. (2016). The origin and evolution of cell types. *Nature Reviews Genetics*, *17*(12), 744–757. https://doi.org/10.1038/nrg.2016.127

Asami, M., Pilz, G. A., Ninkovic, J., Godinho, L., Schroeder, T., Huttner, W. B., & Götz, M. (2011). The role of Pax6 in regulating the orientation and mode of cell division of progenitors in the mouse cerebral cortex. *Development*, *138*(23), 5067–5078. https://doi.org/10.1242/dev.074591

Barral, A., & Zaret, K. S. (2024). Pioneer factors: Roles and their regulation in development. *Trends in Genetics*, *40*(2), 134–148. https://doi.org/10.1016/j.tig.2023.10.007

Basso, M., Mahuzier, A., Ali, S. K., Marty, A., Faucourt, M., Lennon-Duménil, A.-M., Srivastava, A., Khoury Damaa, M., Bankolé, A., Meunier, A., Yamada, A., Plastino, J., Spassky, N., & Delgehyr, N. (2024). Actin-based deformations of the nucleus control mouse multiciliated ependymal cell differentiation. *Developmental Cell*. https://doi.org/10.1016/j.devcel.2024.11.008

Bel-Vialar, S., Medevielle, F., & Pituello, F. (2007). The on/off of Pax6 controls the tempo of neuronal differentiation in the developing spinal cord. *Developmental Biology*, *305*(2), 659–673.

Bettinger, B. T., Gilbert, D. M., & Amberg, D. C. (2004). Actin up in the nucleus. *Nature Reviews Molecular Cell Biology*, *5*(5), 410–415. https://doi.org/10.1038/nrm1370

Blackshaw, S., & Cayouette, M. (2025). Timing neural development and regeneration. *Current Opinion in Neurobiology*, *91*, 102976. https://doi.org/10.1016/j.conb.2025.102976

Bloom, G. S., Luca, F. C., & Vallee, R. B. (1985). Microtubule-associated protein 1B: Identification of a major component of the neuronal cytoskeleton. *Proceedings of the National Academy of Sciences*, *82*(16), 5404–5408. https://doi.org/10.1073/pnas.82.16.5404

Booeshaghi, A. S., Yao, Z., van Velthoven, C., Smith, K., Tasic, B., Zeng, H., & Pachter, L. (2021). Isoform cell-type specificity in the mouse primary motor cortex. *Nature*, *598*(7879), 195–199. https://doi.org/10.1038/s41586-021-03969-3

Boyer, L. A., Lee, T. I., Cole, M. F., Johnstone, S. E., Levine, S. S., Zucker, J. P., Guenther, M. G., Kumar, R. M., Murray, H. L., Jenner, R. G., Gifford, D. K., Melton, D. A., Jaenisch, R., & Young, R. A. (2005). Core Transcriptional Regulatory Circuitry in Human Embryonic Stem Cells. *Cell*, *122*(6), 947–956. https://doi.org/10.1016/j.cell.2005.08.020

Brancaccio, M., Pivetta, C., Granzotto, M., Filippis, C., & Mallamaci, A. (2010). Emx2 and Foxg1 Inhibit Gliogenesis and Promote Neuronogenesis. *Stem Cells*, *28*(7), 1206–1218. https://doi.org/10.1002/stem.443

Bravo González-Blas, C., De Winter, S., Hulselmans, G., Hecker, N., Matetovici, I., Christiaens, V., Poovathingal, S., Wouters, J., Aibar, S., & Aerts, S. (2023). SCENIC+: Single-cell multiomic inference of enhancers and gene regulatory networks. *Nature Methods*, *20*(9), 1355–1367. https://doi.org/10.1038/s41592-023-01938-4

Campbell, C. E., Piper, M., Plachez, C., Yeh, Y.-T., Baizer, J. S., Osinski, J. M., Litwack, E. D., Richards, L. J., & Gronostajski, R. M. (2008). The transcription factor Nfixis essential for normal brain development. *BMC Developmental Biology*, *8*(1), 52. https://doi.org/10.1186/1471-213X-8-52

Cardoso-Moreira, M., Halbert, J., Valloton, D., Velten, B., Chen, C., Shao, Y., Liechti, A., Ascenção, K., Rummel, C., Ovchinnikova, S., Mazin, P. V., Xenarios, I., Harshman, K., Mort, M., Cooper, D. N., Sandi, C., Soares, M. J., Ferreira, P. G., Afonso, S., … Kaessmann, H. (2019). Gene expression across mammalian organ development. *Nature*, *571*(7766), 505–509. https://doi.org/10.1038/s41586-019-1338-5

Castanza, A. S., Ramirez, S., Tripathi, P. P., Daza, R. A. M., Kalume, F. K., Ramirez, J.-M., & Hevner, R. F. (2021). AUTS2 Regulates RNA Metabolism and Dentate Gyrus Development in Mice. *Cerebral Cortex*, *31*(10), 4808–4824. https://doi.org/10.1093/cercor/bhab124

Castro, D. S., Martynoga, B., Parras, C., Ramesh, V., Pacary, E., Johnston, C., Drechsel, D., Lebel-Potter, M., Garcia, L. G., Hunt, C., Dolle, D., Bithell, A., Ettwiller, L., Buckley, N., & Guillemot, F. (2011). A novel function of the proneural factor Ascl1 in progenitor proliferation identified by genome-wide characterization of its targets. *Genes & Development*, *25*(9), 930–945. https://doi.org/10.1101/gad.627811

Cau, E., Gradwohl, G., Fode, C., & Guillemot, F. (1997). Mash1 activates a cascade of bHLH regulators in olfactory neuron progenitors. *Development*, *124*(8), 1611–1621. https://doi.org/10.1242/dev.124.8.1611

Chanda, S., Ang, C. E., Davila, J., Pak, C., Mall, M., Lee, Q. Y., Ahlenius, H., Jung, S. W., Südhof, T. C., & Wernig, M. (2014). Generation of Induced Neuronal Cells by the Single Reprogramming Factor ASCL1. *Stem Cell Reports*, *3*(2), 282–296. https://doi.org/10.1016/j.stemcr.2014.05.020

Chatrikhi, R., Mallory, M. J., Gazzara, M. R., Agosto, L. M., Zhu, W. S., Litterman, A. J., Ansel, K. M., & Lynch, K. W. (2019). RNA Binding Protein CELF2 Regulates Signal-Induced Alternative Polyadenylation by Competing with Enhancers of the Polyadenylation Machinery. *Cell Reports*, *28*(11), 2795-2806.e3. https://doi.org/10.1016/j.celrep.2019.08.022

Chou, S.-J., & O'Leary, D. D. M. (2013). Role for Lhx2 in corticogenesis through regulation of progenitor differentiation. *Molecular and Cellular Neurosciences*, *56*, 1–9. https://doi.org/10.1016/j.mcn.2013.02.006

Cochella, L., & Hobert, O. (2012). Embryonic priming of a miRNA locus predetermines postmitotic neuronal left/right asymmetry in C. elegans. *Cell*, *151*(6), 1229–1242. https://doi.org/10.1016/j.cell.2012.10.049

Cong, F., & Varmus, H. (2004). Nuclear-cytoplasmic shuttling of Axin regulates subcellular localization of β-catenin. *Proceedings of the National Academy of Sciences*, *101*(9), 2882–2887. https://doi.org/10.1073/pnas.0307344101

Copley, S. D. (2014). An evolutionary perspective on protein moonlighting. *Biochemical Society Transactions*, *42*(6), 1684–1691. https://doi.org/10.1042/BST20140245

Cueille, N., Blanc, C. T., Popa-Nita, S., Kasas, S., Catsicas, S., Dietler, G., & Riederer, B. M. (2007). Characterization of MAP1B heavy chain interaction with actin. *Brain Research Bulletin*, *71*(6), 610–618. https://doi.org/10.1016/j.brainresbull.2006.12.003

Dopie, J., Skarp, K.-P., Kaisa Rajakylä, E., Tanhuanpää, K., & Vartiainen, M. K. (2012). Active maintenance of nuclear actin by importin 9 supports transcription. *Proceedings of the National Academy of Sciences*, *109*(9), E544–E552. https://doi.org/10.1073/pnas.1118880109

Dou, C.-L., Li, S., & Lai, E. (1999). Dual Role of Brain Factor-1 in Regulating Growth and Patterning of the Cerebral Hemispheres. *Cerebral Cortex*, *9*(6), 543–550. https://doi.org/10.1093/cercor/9.6.543

Driscoll, T. P., Cosgrove, B. D., Heo, S.-J., Shurden, Z. E., & Mauck, R. L. (2015). Cytoskeletal to Nuclear Strain Transfer Regulates YAP Signaling in Mesenchymal Stem Cells. *Biophysical Journal*, *108*(12), 2783–2793. https://doi.org/10.1016/j.bpj.2015.05.010

Dupont, S., Morsut, L., Aragona, M., Enzo, E., Giulitti, S., Cordenonsi, M., Zanconato, F., Le Digabel, J., Forcato, M., Bicciato, S., Elvassore, N., & Piccolo, S. (2011). Role of YAP/TAZ in mechanotransduction. *Nature*, *474*(7350), 179–183. https://doi.org/10.1038/nature10137

Ehinger, S., Schubert, W.-D., Bergmann, S., Hammerschmidt, S., & Heinz, D. W. (2004). Plasmin(ogen)-binding α-Enolase from *Streptococcus pneumoniae*: Crystal Structure and Evaluation of Plasmin(ogen)-binding Sites. *Journal of Molecular Biology*, *343*(4), 997–1005. https://doi.org/10.1016/j.jmb.2004.08.088

Elosegui-Artola, A., Andreu, I., Beedle, A. E. M., Lezamiz, A., Uroz, M., Kosmalska, A. J., Oria, R., Kechagia, J. Z., Rico-Lastres, P., Roux, A.-L. L., Shanahan, C. M., Trepat, X., Navajas, D., Garcia-Manyes, S., & Roca-Cusachs, P. (2017). Force Triggers YAP Nuclear Entry by Regulating Transport across Nuclear Pores. *Cell*, *171*(6), 1397-1410.e14. https://doi.org/10.1016/j.cell.2017.10.008

Elsen, G. E., Bedogni, F., Hodge, R. D., Bammler, T. K., MacDonald, J. W., Lindtner, S., Rubenstein, J. L. R., & Hevner, R. F. (2018). The Epigenetic Factor Landscape of Developing Neocortex Is Regulated by Transcription Factors Pax6→ Tbr2→ Tbr1. *Frontiers in Neuroscience*, *12*. https://doi.org/10.3389/fnins.2018.00571

Esgleas, M., Falk, S., Forné, I., Thiry, M., Najas, S., Zhang, S., Mas-Sanchez, A., Geerlof, A., Niessing, D., Wang, Z., Imhof, A., & Götz, M. (2020). Trnp1 organizes diverse nuclear membrane-less compartments in neural stem cells. *The EMBO Journal*, *39*(16), e103373. https://doi.org/10.15252/embj.2019103373

Fagotto, F., Glück, U., & Gumbiner, B. M. (1998). Nuclear localization signal-independent and importin/karyopherin-independent nuclear import of β-catenin. *Current Biology*, *8*(4), 181–190. https://doi.org/10.1016/S0960-9822(98)70082-X

Fasano, C. A., Phoenix, T. N., Kokovay, E., Lowry, N., Elkabetz, Y., Dimos, J. T., Lemischka, I. R., Studer, L., & Temple, S. (2009). Bmi-1 cooperates with Foxg1 to maintain neural stem cell self-renewal in the forebrain. *Genes & Development*, *23*(5), 561–574. https://doi.org/10.1101/gad.1743709

Fleck, J. S., Jansen, S. M. J., Wollny, D., Zenk, F., Seimiya, M., Jain, A., Okamoto, R., Santel, M., He, Z., Camp, J. G., & Treutlein, B. (2023). Inferring and perturbing cell fate regulomes in human brain organoids. *Nature*, *621*(7978), 365–372. https://doi.org/10.1038/s41586-022-05279-8

Fode, C., Ma, Q., Casarosa, S., Ang, S.-L., Anderson, D. J., & Guillemot, F. (2000). A role for neural determination genes in specifying the dorsoventral identity of telencephalic neurons. *Genes & Development*, *14*(1), 67–80. https://doi.org/10.1101/gad.14.1.67

Franco, S. J., Gil-Sanz, C., Martinez-Garay, I., Espinosa, A., Harkins-Perry, S. R., Ramos, C., & Müller, U. (2012). Fate-Restricted Neural Progenitors in the Mammalian Cerebral Cortex. *Science*, *337*(6095), 746–749. https://doi.org/10.1126/science.1223616

Franco-Serrano, L., Huerta, M., Hernández, S., Cedano, J., Perez-Pons, J., Piñol, J., Mozo-Villarias, A., Amela, I., & Querol, E. (2018). Multifunctional Proteins: Involvement in Human Diseases and Targets of Current Drugs. *The Protein Journal*, *37*(5), 444–453. https://doi.org/10.1007/s10930-018-9790-x

Gao, Z., Lee, P., Stafford, J. M., von Schimmelmann, M., Schaefer, A., & Reinberg, D. (2014). An AUTS2–Polycomb complex activates gene expression in the CNS. *Nature*, *516*(7531), 349–354. https://doi.org/10.1038/nature13921

Gazzara, M. R., Mallory, M. J., Roytenberg, R., Lindberg, J. P., Jha, A., Lynch, K. W., & Barash, Y. (2017). Ancient antagonism between CELF and RBFOX families tunes mRNA splicing outcomes. *Genome Research*, *27*(8), 1360–1370. https://doi.org/10.1101/gr.220517.117

Ghysen, A., & Dambly-Chaudière, C. (1988). From DNA to form: The achaete-scute complex. *Genes & Development*, *2*(5), 495–501. https://doi.org/10.1101/gad.2.5.495

Götz, M., & Huttner, W. B. (2005). The cell biology of neurogenesis. *Nature Reviews Molecular Cell Biology*, *6*(10), 777–788. https://doi.org/10.1038/nrm1739

Götz, M., Sirko, S., Beckers, J., & Irmler, M. (2015). Reactive astrocytes as neural stem or progenitor cells: In vivo lineage, In vitro potential, and Genome-wide expression analysis. *Glia*, *63*(8), 1452–1468. https://doi.org/10.1002/glia.22850

Graham, V., Khudyakov, J., Ellis, P., & Pevny, L. (2003). SOX2 Functions to Maintain Neural Progenitor Identity. *Neuron*, *39*(5), 749–765. https://doi.org/10.1016/S0896-6273(03)00497-5

Hanashima, C., Li, S. C., Shen, L., Lai, E., & Fishell, G. (2004). Foxg1 Suppresses Early Cortical Cell Fate. *Science*, *303*(5654), 56–59. https://doi.org/10.1126/science.1090674

Harkins, D., Harvey, T. J., Atterton, C., Miller, I., Currey, L., Oishi, S., Kasherman, M., Davila, R. A., Harris, L., Green, K., Piper, H., Parton, R. G., Thor, S., Cooper, H. M., & Piper, M. (2022). Hydrocephalus in Nfix−/− Mice Is Underpinned by Changes in Ependymal Cell Physiology. *Cells*, *11*(15), Article 15. https://doi.org/10.3390/cells11152377

Harris, L., Genovesi, L. A., Gronostajski, R. M., Wainwright, B. J., & Piper, M. (2015). Nuclear factor one transcription factors: Divergent functions in developmental versus adult stem cell populations. *Developmental Dynamics : An Official Publication of the American Association of Anatomists*, *244*(3), 227–238. https://doi.org/10.1002/dvdy.24182

Harris, L., Zalucki, O., Gobius, I., McDonald, H., Osinki, J., Harvey, T. J., Essebier, A., Vidovic, D., Gladwyn-Ng, I., Burne, T. H., Heng, J. I., Richards, L. J., Gronostajski, R. M., & Piper, M. (2016). Transcriptional regulation of intermediate progenitor cell generation during hippocampal development. *Development*, *143*(24), 4620–4630. https://doi.org/10.1242/dev.140681

Heins, N., Malatesta, P., Cecconi, F., Nakafuku, M., Tucker, K. L., Hack, M. A., Chapouton, P., Barde, Y.-A., & Götz, M. (2002). Glial cells generate neurons: The role of the transcription factor Pax6. *Nature Neuroscience*, *5*(4), 308–315. https://doi.org/10.1038/nn828

Henderson, B. R. (2000). Nuclear-cytoplasmic shuttling of APC regulates β-catenin subcellular localization and turnover. *Nature Cell Biology*, *2*(9), 653–660. https://doi.org/10.1038/35023605

Hendriks, W., Mulders, J. W., Bibby, M. A., Slingsby, C., Bloemendal, H., & de Jong, W. W. (1988). Duck lens epsilon-crystallin and lactate dehydrogenase B4 are identical: A single-copy gene product with two distinct functions. *Proceedings of the National Academy of Sciences of the United States of America*, *85*(19), 7114–7118. https://doi.org/10.1073/pnas.85.19.7114

Heng, Y. H. E., McLeay, R. C., Harvey, T. J., Smith, A. G., Barry, G., Cato, K., Plachez, C., Little, E., Mason, S., Dixon, C., Gronostajski, R. M., Bailey, T. L., Richards, L. J., & Piper, M. (2014). NFIX Regulates Neural Progenitor Cell Differentiation During Hippocampal Morphogenesis. *Cerebral Cortex*, *24*(1), 261–279. https://doi.org/10.1093/cercor/bhs307

Hoang, T., Wang, J., Boyd, P., Wang, F., Santiago, C., Jiang, L., Yoo, S., Lahne, M., Todd, L. J., Jia, M., Saez, C., Keuthan, C., Palazzo, I., Squires, N., Campbell, W. A., Rajaii, F., Parayil, T., Trinh, V., Kim, D. W., … Blackshaw, S. (2020). Gene regulatory networks controlling vertebrate retinal regeneration. *Science*, *370*(6519), eabb8598. https://doi.org/10.1126/science.abb8598

Hobert, O. (2021). Homeobox genes and the specification of neuronal identity. *Nature Reviews Neuroscience*, *22*(10), 627–636. https://doi.org/10.1038/s41583-021-00497-x

Hofmann, W. A., Stojiljkovic, L., Fuchsova, B., Vargas, G. M., Mavrommatis, E., Philimonenko, V., Kysela, K., Goodrich, J. A., Lessard, J. L., Hope, T. J., Hozak, P., & de Lanerolle, P. (2004). Actin is part of pre-initiation complexes and is necessary for transcription by RNA polymerase II. *Nature Cell Biology*, *6*(11), 1094–1101. https://doi.org/10.1038/ncb1182

Hori, K., Nagai, T., Shan, W., Sakamoto, A., Taya, S., Hashimoto, R., Hayashi, T., Abe, M., Yamazaki, M., Nakao, K., Nishioka, T., Sakimura, K., Yamada, K., Kaibuchi, K., & Hoshino, M. (2014). Cytoskeletal Regulation by AUTS2 in Neuronal Migration and Neuritogenesis. *Cell Reports*, *9*(6), 2166–2179. https://doi.org/10.1016/j.celrep.2014.11.045

Hori, K., Shimaoka, K., & Hoshino, M. (2021). AUTS2 Gene: Keys to Understanding the Pathogenesis of Neurodevelopmental Disorders. *Cells*, *11*(1), 11. https://doi.org/10.3390/cells11010011

Huang, C., Chan, J. A., & Schuurmans, C. (2014). Proneural bHLH genes in development and disease. *Current Topics in Developmental Biology*, *110*, 75–127. https://doi.org/10.1016/B978-0-12-405943-6.00002-6

Huberts, D. H. E. W., & van der Klei, I. J. (2010). Moonlighting proteins: An intriguing mode of multitasking. *Biochimica et Biophysica Acta (BBA) - Molecular Cell Research*, *1803*(4), 520–525. https://doi.org/10.1016/j.bbamcr.2010.01.022

Hulme, A. J., Maksour, S., St-Clair Glover, M., Miellet, S., & Dottori, M. (2021). Making neurons, made easy: The use of Neurogenin-2 in neuronal differentiation. *Stem Cell Reports*, *17*(1), 14–34. https://doi.org/10.1016/j.stemcr.2021.11.015

Hülsken, J., Birchmeier, W., & Behrens, J. (1994). E-cadherin and APC compete for the interaction with beta-catenin and the cytoskeleton. *Journal of Cell Biology*, *127*(6), 2061–2069. https://doi.org/10.1083/jcb.127.6.2061

Ilik, İ. A., Malszycki, M., Lübke, A. K., Schade, C., Meierhofer, D., & Aktaş, T. (2020). SON and SRRM2 are essential for nuclear speckle formation. *eLife*, *9*, e60579. https://doi.org/10.7554/eLife.60579

Imayoshi, I., Isomura, A., Harima, Y., Kawaguchi, K., Kori, H., Miyachi, H., Fujiwara, T., Ishidate, F., & Kageyama, R. (2013). Oscillatory control of factors determining multipotency and fate in mouse neural progenitors. *Science (New York, N.Y.)*, *342*(6163), 1203–1208. https://doi.org/10.1126/science.1242366

ISH Data: Allen Brain Atlas: Developing Mouse Brain. (n.d.). Retrieved January 13, 2025, from https://developingmouse.brain-map.org/

Iwata, R., Casimir, P., Erkol, E., Boubakar, L., Planque, M., Gallego López, I. M., Ditkowska, M., Gaspariunaite, V., Beckers, S., Remans, D., Vints, K., Vandekeere, A., Poovathingal, S., Bird, M., Vlaeminck, I., Creemers, E., Wierda, K., Corthout, N., Vermeersch, P., … Vanderhaeghen, P. (2023). Mitochondria metabolism sets the species-specific tempo of neuronal development. *Science*, *379*(6632), eabn4705. https://doi.org/10.1126/science.abn4705

Jang, E. S., & Goldman, J. E. (2011). Pax6 Expression Is Sufficient to Induce a Neurogenic Fate in Glial Progenitors of the Neonatal Subventricular Zone. *PLOS ONE*, *6*(6), e20894. https://doi.org/10.1371/journal.pone.0020894

Jayaraman, D., Bae, B.-I., & Walsh, C. A. (2018). The Genetics of Primary Microcephaly. *Annual Review of Genomics and Human Genetics*, *19*(Volume 19, 2018), 177–200. https://doi.org/10.1146/annurev-genom-083117-021441

Jeffery, C. J. (2017). Protein moonlighting: What is it, and why is it important? *Philosophical Transactions of the Royal Society B: Biological Sciences*, *373*(1738), 20160523. https://doi.org/10.1098/rstb.2016.0523

Jiang, M., Yu, D., Xie, B., Huang, H., Lu, W., Qiu, M., & Dai, Z.-M. (2020). WNT signaling suppresses oligodendrogenesis via Ngn2-dependent direct inhibition of Olig2 expression. *Molecular Brain*, *13*(1), 155. https://doi.org/10.1186/s13041-020-00696-0

Kim, J., Han, K. Y., Khanna, N., Ha, T., & Belmont, A. S. (2019). Nuclear speckle fusion via long-range directional motion regulates speckle morphology after transcriptional inhibition. *Journal of Cell Science*, *132*(8), jcs226563. https://doi.org/10.1242/jcs.226563

Kjell, J., Fischer-Sternjak, J., Thompson, A. J., Friess, C., Sticco, M. J., Salinas, F., Cox, J., Martinelli, D. C., Ninkovic, J., Franze, K., Schiller, H. B., & Götz, M. (2020). Defining the Adult Neural Stem Cell Niche Proteome Identifies Key Regulators of Adult Neurogenesis. *Cell Stem Cell*, *26*(2), 277-293.e8. https://doi.org/10.1016/j.stem.2020.01.002

Kohwi, M., & Doe, C. Q. (2013). Temporal fate specification and neural progenitor competence during development. *Nature Reviews. Neuroscience*, *14*(12), 823–838. https://doi.org/10.1038/nrn3618

Krieghoff, E., Behrens, J., & Mayr, B. (2006). Nucleo-cytoplasmic distribution of β-catenin is regulated by retention. *Journal of Cell Science*, *119*(7), 1453–1463. https://doi.org/10.1242/jcs.02864

Kumeta, Yoshimura, Horigome, & Takeyasu. (2013). *Kumeta: Antibody-based analysis reveals "filamentous... - Google Scholar*. https://scholar.google.com/scholar_lookup?doi=10.1016%2Fj.yexcr.2013.07.021&pmid=23911988

Kuwabara, T., Hsieh, J., Muotri, A., Yeo, G., Warashina, M., Lie, D. C., Moore, L., Nakashima, K., Asashima, M., & Gage, F. H. (2009). Wnt-mediated activation of NeuroD1 and retro-elements during adult neurogenesis. *Nature Neuroscience*, *12*(9), 1097–1105. https://doi.org/10.1038/nn.2360

Lacomme, M., Liaubet, L., Pituello, F., & Bel-Vialar, S. (2012). NEUROG2 Drives Cell Cycle Exit of Neuronal Precursors by Specifically Repressing a Subset of Cyclins Acting at the G1 and S Phases of the Cell Cycle. *Molecular and Cellular Biology*, *32*(13), 2596–2607. https://doi.org/10.1128/MCB.06745-11

Lahti, L., Volakakis, N., Gillberg, L., Salmani, B. Y., Tiklová, K., Kee, N., Lundén-Miguel, H., Piper, M., Gronostajski, R., & Perlmann, T. (2024). *Sox9 and Nfi transcription factors regulate the timing of neurogenesis and ependymal maturation in dopamine progenitors* (p. 2024.11.12.623209). bioRxiv. https://doi.org/10.1101/2024.11.12.623209

Lei, J., Deng, Y., & Ma, S. (2022). Downregulation of TGIF2 is possibly correlated with neuronal apoptosis and autism-like symptoms in mice. *Brain and Behavior*, *12*(6), e2610. https://doi.org/10.1002/brb3.2610

Li, Z., Tyler, W. A., Zeldich, E., Baró, G. S., Okamoto, M., Gao, T., Li, M., Sestan, N., & Haydar, T. F. (2020). Transcriptional priming as a conserved mechanism of lineage diversification in the developing mouse and human neocortex. *Science Advances*. https://doi.org/10.1126/sciadv.abd2068

Liu, J., Xiao, Q., Xiao, J., Niu, C., Li, Y., Zhang, X., Zhou, Z., Shu, G., & Yin, G. (2022). Wnt/β-catenin signalling: Function, biological mechanisms, and therapeutic opportunities. *Signal Transduction and Targeted Therapy*, *7*(1), 1–23. https://doi.org/10.1038/s41392-021-00762-6

Liu, N., Dai, Q., Zheng, G., He, C., Parisien, M., & Pan, T. (2015). N6-methyladenosine-dependent RNA structural switches regulate RNA–protein interactions. *Nature*, *518*(7540), 560–564. https://doi.org/10.1038/nature14234

Lledo, P.-M., Merkle, F. T., & Alvarez-Buylla, A. (2008). Origin and function of olfactory bulb interneuron diversity. *Trends in Neurosciences*, *31*(8), 392–400. https://doi.org/10.1016/j.tins.2008.05.006

Lodato, M. A., Ng, C. W., Wamstad, J. A., Cheng, A. W., Thai, K. K., Fraenkel, E., Jaenisch, R., & Boyer, L. A. (2013). SOX2 Co-Occupies Distal Enhancer Elements with Distinct POU Factors in ESCs and NPCs to Specify Cell State. *PLOS Genetics*, *9*(2), e1003288. https://doi.org/10.1371/journal.pgen.1003288

Madrigal, P., Deng, S., Feng, Y., Militi, S., Goh, K. J., Nibhani, R., Grandy, R., Osnato, A., Ortmann, D., Brown, S., & Pauklin, S. (2023). Epigenetic and transcriptional regulations

prime cell fate before division during human pluripotent stem cell differentiation. *Nature Communications*, *14*(1), 405. https://doi.org/10.1038/s41467-023-36116-9

Magnusson, J. P., Göritz, C., Tatarishvili, J., Dias, D. O., Smith, E. M. K., Lindvall, O., Kokaia, Z., & Frisén, J. (2014). A latent neurogenic program in astrocytes regulated by Notch signaling in the mouse. *Science (New York, N.Y.)*, *346*(6206), 237–241. https://doi.org/10.1126/science.346.6206.237

Magrinelli, E., Baumann, N., Wagener, R. J., Glangetas, C., Bellone, C., Jabaudon, D., & Klingler, E. (2022). Heterogeneous fates of simultaneously-born neurons in the cortical ventricular zone. *Scientific Reports*, *12*, 6022. https://doi.org/10.1038/s41598-022-09740-6

Mahmood, S. R., Xie, X., Hosny El Said, N., Venit, T., Gunsalus, K. C., & Percipalle, P. (2021). β-actin dependent chromatin remodeling mediates compartment level changes in 3D genome architecture. *Nature Communications*, *12*(1), 5240. https://doi.org/10.1038/s41467-021-25596-2

Mani, M., Chen, C., Amblee, V., Liu, H., Mathur, T., Zwicke, G., Zabad, S., Patel, B., Thakkar, J., & Jeffery, C. J. (2015). MoonProt: A database for proteins that are known to moonlight. *Nucleic Acids Research*, *43*(D1), D277–D282. https://doi.org/10.1093/nar/gku954

Manuel, M., Tan, K. B., Kozic, Z., Molinek, M., Marcos, T. S., Razak, M. F. A., Dobolyi, D., Dobie, R., Henderson, B. E. P., Henderson, N. C., Chan, W. K., Daw, M. I., Mason, J. O., & Price, D. J. (2022). Pax6 limits the competence of developing cerebral cortical cells to respond to inductive intercellular signals. *PLoS Biology*, *20*(9), e3001563. https://doi.org/10.1371/journal.pbio.3001563

Masserdotti, G., Gillotin, S., Sutor, B., Drechsel, D., Irmler, M., Jørgensen, H. F., Sass, S., Theis, F. J., Beckers, J., Berninger, B., Guillemot, F., & Götz, M. (2015). Transcriptional Mechanisms of Proneural Factors and REST in Regulating Neuronal Reprogramming of Astrocytes. *Cell Stem Cell*, *17*(1), 74–88. https://doi.org/10.1016/j.stem.2015.05.014

Mayer, C., Hafemeister, C., Bandler, R. C., Machold, R., Batista Brito, R., Jaglin, X., Allaway, K., Butler, A., Fishell, G., & Satija, R. (2018). Developmental diversification of cortical inhibitory interneurons. *Nature*, *555*(7697), 457–462. https://doi.org/10.1038/nature25999

McCrea, P. D., Turck, C. W., & Gumbiner, B. (1991). A Homolog of the armadillo Protein in Drosophila (Plakoglobin) Associated with E-Cadherin. *Science*, *254*(5036), 1359–1361. https://doi.org/10.1126/science.1962194

Meng, Y., & Nerlov, C. (2024). Epigenetic regulation of hematopoietic stem cell fate. *Trends in Cell Biology*, *0*(0). https://doi.org/10.1016/j.tcb.2024.08.005

Mi, D., Li, Z., Lim, L., Li, M., Moissidis, M., Yang, Y., Gao, T., Hu, T. X., Pratt, T., Price, D. J., Sestan, N., & Marín, O. (2018). Early emergence of cortical interneuron diversity in the mouse embryo. *Science*, *360*(6384), 81–85. https://doi.org/10.1126/science.aar6821

Miller, J., & Moon, R. (1996). *Miller: Signal transduction through -catenin and... - Google Scholar*. https://scholar.google.com/scholar_lookup?doi=10.1101%2Fgad.10.20.2527&pmid=8895655

Murphy, D. B., Wiese, S., Burfeind, P., Schmundt, D., Mattei, M.-G., Schulz-Schaeffer, W., & Thies, U. (1994). Human Brain Factor 1, a New Member of the *Fork Head* Gene Family. *Genomics*, *21*(3), 551–557. https://doi.org/10.1006/geno.1994.1313

Ninkovic, J., Steiner-Mezzadri, A., Jawerka, M., Akinci, U., Masserdotti, G., Petricca, S., Fischer, J., von Holst, A., Beckers, J., Lie, C. D., Petrik, D., Miller, E., Tang, J., Wu, J., Lefebvre, V., Demmers, J., Eisch, A., Metzger, D., Crabtree, G., … Götz, M. (2013). The BAF Complex Interacts with Pax6 in Adult Neural Progenitors to Establish a Neurogenic Cross-Regulatory Transcriptional Network. *Cell Stem Cell*, *13*(4), 403–418. https://doi.org/10.1016/j.stem.2013.07.002

Nishimoto, N., Watanabe, M., Watanabe, S., Sugimoto, N., Yugawa, T., Ikura, T., Koiwai, O., Kiyono, T., & Fujita, M. (2012). Heterocomplex formation by Arp4 and β-actin is involved in the integrity of the Brg1 chromatin remodeling complex. *Journal of Cell Science*, *125*(16), 3870–3882. https://doi.org/10.1242/jcs.104349

Nowakowski, T. J., Bhaduri, A., Pollen, A. A., Alvarado, B., Mostajo-Radji, M. A., Di Lullo, E., Haeussler, M., Sandoval-Espinosa, C., Liu, S. J., Velmeshev, D., Ounadjela, J. R., Shuga, J., Wang, X., Lim, D. A., West, J. A., Leyrat, A. A., Kent, W. J., & Kriegstein, A. R. (2017). Spatiotemporal gene expression trajectories reveal developmental hierarchies of the human cortex. *Science*, *358*(6368), 1318–1323. https://doi.org/10.1126/science.aap8809

Oberst, P., Fièvre, S., Baumann, N., Concetti, C., Bartolini, G., & Jabaudon, D. (2019). Temporal plasticity of apical progenitors in the developing mouse neocortex. *Nature*, *573*(7774), 370–374. https://doi.org/10.1038/s41586-019-1515-6

Oksenberg, N., Haliburton, G. D. E., Eckalbar, W. L., Oren, I., Nishizaki, S., Murphy, K., Pollard, K. S., Birnbaum, R. Y., & Ahituv, N. (2014). Genome-wide distribution of Auts2 binding localizes with active neurodevelopmental genes. *Translational Psychiatry*, *4*(9), e431–e431. https://doi.org/10.1038/tp.2014.78

Olave, I. A., Reck-Peterson, S. L., & Crabtree, G. R. (2002). Nuclear Actin and Actin-Related Proteins in Chromatin Remodeling. *Annual Review of Biochemistry*, *71*(Volume 71, 2002), 755–781. https://doi.org/10.1146/annurev.biochem.71.110601.135507

Osumi, N., Shinohara, H., Numayama-Tsuruta, K., & Maekawa, M. (2008). Concise review: Pax6 transcription factor contributes to both embryonic and adult neurogenesis as a multifunctional regulator. *Stem Cells (Dayton, Ohio)*, *26*(7), 1663–1672. https://doi.org/10.1634/stemcells.2007-0884

Park, J., Lee, K., Kim, K., & Yi, S.-J. (2022). The role of histone modifications: From neurodevelopment to neurodiseases. *Signal Transduction and Targeted Therapy*, *7*(1), 1–23. https://doi.org/10.1038/s41392-022-01078-9

Petrik, D., Myoga, M. H., Grade, S., Gerkau, N. J., Pusch, M., Rose, C. R., Grothe, B., & Götz, M. (2018). Epithelial Sodium Channel Regulates Adult Neural Stem Cell Proliferation in a Flow-Dependent Manner. *Cell Stem Cell*, *22*(6), 865-878.e8. https://doi.org/10.1016/j.stem.2018.04.016

Piper, M., Barry, G., Hawkins, J., Mason, S., Lindwall, C., Little, E., Sarkar, A., Smith, A. G., Moldrich, R. X., Boyle, G. M., Tole, S., Gronostajski, R. M., Bailey, T. L., & Richards, L. J. (2010). NFIA Controls Telencephalic Progenitor Cell Differentiation through Repression of the Notch Effector Hes1. *Journal of Neuroscience*, *30*(27), 9127–9139. https://doi.org/10.1523/JNEUROSCI.6167-09.2010

Plachez, C., Lindwall, C., Sunn, N., Piper, M., Moldrich, R. X., Campbell, C. E., Osinski, J. M., Gronostajski, R. M., & Richards, L. J. (2008). Nuclear factor I gene expression in the

developing forebrain. *The Journal of Comparative Neurology*, *508*(3), 385–401. https://doi.org/10.1002/cne.21645

Regan-Fendt, K. E., & Izumi, K. (2024). Nuclear speckleopathies: Developmental disorders caused by variants in genes encoding nuclear speckle proteins. *Human Genetics*, *143*(4), 529–544. https://doi.org/10.1007/s00439-023-02540-6

Ren, G., Ku, W. L., Ge, G., Hoffman, J. A., Kang, J. Y., Tang, Q., Cui, K., He, Y., Guan, Y., Gao, B., Liu, C., Archer, T. K., & Zhao, K. (2024). Acute depletion of BRG1 reveals its primary function as an activator of transcription. *Nature Communications*, *15*(1), 4561. https://doi.org/10.1038/s41467-024-48911-z

Reynolds, N., Salmon-Divon, M., Dvinge, H., Hynes-Allen, A., Balasooriya, G., Leaford, D., Behrens, A., Bertone, P., & Hendrich, B. (2012). NuRD-mediated deacetylation of H3K27 facilitates recruitment of Polycomb Repressive Complex 2 to direct gene repression. *The EMBO Journal*, *31*(3), 593–605. https://doi.org/10.1038/emboj.2011.431

Ribeiro, D. M., Briere, G., Bely, B., Spinelli, L., & Brun, C. (2019). MoonDB 2.0: An updated database of extreme multifunctional and moonlighting proteins. *Nucleic Acids Research*, *47*(D1), D398–D402. https://doi.org/10.1093/nar/gky1039

Ringeling, F. R., Chakraborty, S., Vissers, C., Reiman, D., Patel, A. M., Lee, K.-H., Hong, A., Park, C.-W., Reska, T., Gagneur, J., Chang, H., Spletter, M. L., Yoon, K.-J., Ming, G., Song, H., & Canzar, S. (2022). Partitioning RNAs by length improves transcriptome reconstruction from short-read RNA-seq data. *Nature Biotechnology*, *40*(5), 741–750. https://doi.org/10.1038/s41587-021-01136-7

Rosenbloom, A. B., Tarczyński, M., Lam, N., Kane, R. S., Bugaj, L. J., & Schaffer, D. V. (2020). β-Catenin signaling dynamics regulate cell fate in differentiating neural stem cells. *Proceedings of the National Academy of Sciences*, *117*(46), 28828–28837. https://doi.org/10.1073/pnas.2008509117

Sansom, S. N., Griffiths, D. S., Faedo, A., Kleinjan, D.-J., Ruan, Y., Smith, J., Heyningen, V. van, Rubenstein, J. L., & Livesey, F. J. (2009). The Level of the Transcription Factor Pax6 Is Essential for Controlling the Balance between Neural Stem Cell Self-Renewal and Neurogenesis. *PLOS Genetics*, *5*(6), e1000511. https://doi.org/10.1371/journal.pgen.1000511

Sarkar, A., & Hochedlinger, K. (2013). The Sox Family of Transcription Factors: Versatile Regulators of Stem and Progenitor Cell Fate. *Cell Stem Cell*, *12*(1), 15–30. https://doi.org/10.1016/j.stem.2012.12.007

Scardigli, R., Bäumer, N., Gruss, P., Guillemot, F., & Le Roux, I. (2003). Direct and concentration-dependent regulation of the proneural gene Neurogenin2 by Pax6. *Development*, *130*(14), 3269–3281. https://doi.org/10.1242/dev.00539

Schuurmans, C., Armant, O., Nieto, M., Stenman, J. M., Britz, O., Klenin, N., Brown, C., Langevin, L., Seibt, J., Tang, H., Cunningham, J. M., Dyck, R., Walsh, C., Campbell, K., Polleux, F., & Guillemot, F. (2004). Sequential phases of cortical specification involve Neurogenin-dependent and -independent pathways. *The EMBO Journal*, *23*(14), 2892–2902. https://doi.org/10.1038/sj.emboj.7600278

Schwarzerová, K., Bellinvia, E., Martinek, J., Sikorová, L., Dostál, V., Libusová, L., Bokvaj, P., Fischer, L., Schmit, A. C., & Nick, P. (2019). Tubulin is actively exported from the nucleus through the Exportin1/CRM1 pathway. *Scientific Reports*, *9*(1), 5725. https://doi.org/10.1038/s41598-019-42056-6

Sen, B., Xie, Z., Thomas, M. D., Pattenden, S. G., Howard, S., McGrath, C., Styner, M., Uzer, G., Furey, T. S., & Rubin, J. (2024). Nuclear actin structure regulates chromatin accessibility. *Nature Communications*, *15*(1), 4095. https://doi.org/10.1038/s41467-024-48580-y

Sessa, A., Ciabatti, E., Drechsel, D., Massimino, L., Colasante, G., Giannelli, S., Satoh, T., Akira, S., Guillemot, F., & Broccoli, V. (2017). The Tbr2 Molecular Network Controls Cortical Neuronal Differentiation Through Complementary Genetic and Epigenetic Pathways. *Cerebral Cortex*, *27*(6), 3378–3396. https://doi.org/10.1093/cercor/bhw270

Shen, Q., Wang, Y., Dimos, J. T., Fasano, C. A., Phoenix, T. N., Lemischka, I. R., Ivanova, N. B., Stifani, S., Morrisey, E. E., & Temple, S. (2006). The timing of cortical neurogenesis is encoded within lineages of individual progenitor cells. *Nature Neuroscience*, *9*(6), 743–751. https://doi.org/10.1038/nn1694

Shimojo, H., Masaki, T., & Kageyama, R. (2024). The Neurog2-Tbr2 axis forms a continuous transition to the neurogenic gene expression state in neural stem cells. *Developmental Cell*, *59*(15), 1913-1923.e6. https://doi.org/10.1016/j.devcel.2024.04.019

Siegenthaler, J. A., Tremper-Wells, B. A., & Miller, M. W. (2008). Foxg1 Haploinsufficiency Reduces the Population of Cortical Intermediate Progenitor Cells: Effect of Increased p21 Expression. *Cerebral Cortex*, *18*(8), 1865–1875. https://doi.org/10.1093/cercor/bhm209

Singh, N., & Bhalla, N. (2020). Moonlighting Proteins. *Annual Review of Genetics*, *54*(Volume 54, 2020), 265–285. https://doi.org/10.1146/annurev-genet-030620-102906

Stahl, R., Walcher, T., De Juan Romero, C., Pilz, G. A., Cappello, S., Irmler, M., Sanz-Aquela, J. M., Beckers, J., Blum, R., Borrell, V., & Götz, M. (2013). Trnp1 Regulates Expansion and Folding of the Mammalian Cerebral Cortex by Control of Radial Glial Fate. *Cell*, *153*(3), 535–549. https://doi.org/10.1016/j.cell.2013.03.027

Stepien, B., Naumann, R., Holtz, A., Helppi, J., Huttner, W., & Vaid, S. (2020). Lengthening Neurogenic Period during Neocortical Development Causes a Hallmark of Neocortex Expansion. *Current Biology : CB*, *30*. https://doi.org/10.1016/j.cub.2020.08.046

Stüven, T., Hartmann, E., & Görlich, D. (2003). Exportin 6: A novel nuclear export receptor that is specific for profilin·actin complexes. *The EMBO Journal*, *22*(21), 5928–5940. https://doi.org/10.1093/emboj/cdg565

Subcellular—TGIF2—The Human Protein Atlas. (n.d.). Retrieved February 27, 2025, from https://www.proteinatlas.org/ENSG00000118707-TGIF2/subcellular

Sultan, K. T., Liu, W. A., Li, Z.-L., Shen, Z., Li, Z., Zhang, X.-J., Dean, O., Ma, J., & Shi, S.-H. (2018). Progressive divisions of multipotent neural progenitors generate late-born chandelier cells in the neocortex. *Nature Communications*, *9*, 4595. https://doi.org/10.1038/s41467-018-07055-7

Sun, S., Zhu, X.-J., Huang, H., Guo, W., Tang, T., Xie, B., Xu, X., Zhang, Z., Shen, Y., Dai, Z.-M., & Qiu, M. (2019). WNT signaling represses astrogliogenesis via Ngn2-dependent direct suppression of astrocyte gene expression. *Glia*, *67*(7), 1333–1343. https://doi.org/10.1002/glia.23608

Sun, T., & Hevner, R. F. (2014). Growth and folding of the mammalian cerebral cortex: From molecules to malformations. *Nature Reviews Neuroscience*, *15*(4), 217–232. https://doi.org/10.1038/nrn3707

Takebayashi, K., Sasai, Y., Sakai, Y., Watanabe, T., Nakanishi, S., & Kageyama, R. (1994). Structure, chromosomal locus, and promoter analysis of the gene encoding the mouse

helix-loop-helix factor HES-1. Negative autoregulation through the multiple N box elements. *Journal of Biological Chemistry*, *269*(7), 5150–5156. https://doi.org/10.1016/S0021-9258(17)37668-8

Telley, L., Agirman, G., Prados, J., Amberg, N., Fièvre, S., Oberst, P., Bartolini, G., Vitali, I., Cadilhac, C., Hippenmeyer, S., Nguyen, L., Dayer, A., & Jabaudon, D. (2019). Temporal patterning of apical progenitors and their daughter neurons in the developing neocortex. *Science*, *364*(6440), eaav2522. https://doi.org/10.1126/science.aav2522

Thakurela, S., Tiwari, N., Schick, S., Garding, A., Ivanek, R., Berninger, B., & Tiwari, V. K. (2016). Mapping gene regulatory circuitry of Pax6 during neurogenesis. *Cell Discovery*, *2*(1), 1–22. https://doi.org/10.1038/celldisc.2015.45

Toma, K., Kumamoto, T., & Hanashima, C. (2014). The Timing of Upper-Layer Neurogenesis Is Conferred by Sequential Derepression and Negative Feedback from Deep-Layer Neurons. *Journal of Neuroscience*, *34*(39), 13259–13276. https://doi.org/10.1523/JNEUROSCI.2334-14.2014

Urbán, N., & Guillemot, F. (2014). Neurogenesis in the embryonic and adult brain: Same regulators, different roles. *Frontiers in Cellular Neuroscience*, *8*, 396. https://doi.org/10.3389/fncel.2014.00396

Valcanis, H., & Tan, S.-S. (2003). Layer Specification of Transplanted Interneurons in Developing Mouse Neocortex. *The Journal of Neuroscience*, *23*(12), 5113–5122. https://doi.org/10.1523/JNEUROSCI.23-12-05113.2003

Viita, T., Kyheröinen, S., Prajapati, B., Virtanen, J., Frilander, M. J., Varjosalo, M., & Vartiainen, M. K. (2019). Nuclear actin interactome analysis links actin to KAT14 histone acetyl transferase and mRNA splicing. *Journal of Cell Science*, *132*(8), jcs226852. https://doi.org/10.1242/jcs.226852

Vitali, I., Fièvre, S., Telley, L., Oberst, P., Bariselli, S., Frangeul, L., Baumann, N., McMahon, J. J., Klingler, E., Bocchi, R., Kiss, J. Z., Bellone, C., Silver, D. L., & Jabaudon, D. (2018). Progenitor hyperpolarization regulates the sequential generation of neuronal subtypes in the developing neocortex. *Cell*, *174*(5), 1264-1276.e15. https://doi.org/10.1016/j.cell.2018.06.036

Walcher, T., Xie, Q., Sun, J., Irmler, M., Beckers, J., Öztürk, T., Niessing, D., Stoykova, A., Cvekl, A., Ninkovic, J., & Götz, M. (2013). Functional dissection of the paired domain of Pax6 reveals molecular mechanisms of coordinating neurogenesis and proliferation. *Development (Cambridge, England)*, *140*(5), 1123–1136. https://doi.org/10.1242/dev.082875

Wang, M., Wei, P.-C., Lim, C. K., Gallina, I. S., Marshall, S., Marchetto, M. C., Alt, F. W., & Gage, F. H. (2020). Increased Neural Progenitor Proliferation in a hiPSC Model of Autism Induces Replication Stress-Associated Genome Instability. *Cell Stem Cell*, *26*(2), 221-233.e6. https://doi.org/10.1016/j.stem.2019.12.013

Wang, Y., Li, Y., Yue, M., Wang, J., Kumar, S., Wechsler-Reya, R. J., Zhang, Z., Ogawa, Y., Kellis, M., Duester, G., & Zhao, J. C. (2018). N6-methyladenosine RNA modification regulates embryonic neural stem cell self-renewal through histone modifications. *Nature Neuroscience*, *21*(2), 195–206. https://doi.org/10.1038/s41593-017-0057-1

Wu, R., Ye, Y., Dong, D., Zhang, Z., Wang, S., Li, Y., Wright, N., Redding-Ochoa, J., Chang, K., Xu, S., Tu, X., Zhu, C., Ostrow, L. W., Roca, X., Troncoso, J. C., Wu, B., & Sun, S. (2024).

Disruption of nuclear speckle integrity dysregulates RNA splicing in C9ORF72-FTD/ALS. *Neuron*, *112*(20), 3434-3451.e11. https://doi.org/10.1016/j.neuron.2024.07.025

Wu, X., Tu, X., Joeng, K. S., Hilton, M. J., Williams, D. A., & Long, F. (2008). Rac1 Activation Controls Nuclear Localization of β-catenin during Canonical Wnt Signaling. *Cell*, *133*(2), 340–353. https://doi.org/10.1016/j.cell.2008.01.052

Xie, X., Almuzzaini, B., Drou, N., Kremb, S., Yousif, A., Farrants, A.-K. Ö., Gunsalus, K., & Percipalle, P. (2018). β-Actin-dependent global chromatin organization and gene expression programs control cellular identity. *The FASEB Journal*, *32*(3), 1296–1314. https://doi.org/10.1096/fj.201700753R

Xie, X., Jankauskas, R., Mazari, A. M. A., Drou, N., & Percipalle, P. (2018). β-actin regulates a heterochromatin landscape essential for optimal induction of neuronal programs during direct reprograming. *PLOS Genetics*, *14*(12), e1007846. https://doi.org/10.1371/journal.pgen.1007846

Xuan, S., Carlos, S., Gabriela, B., Wufan, T., Vera, S., & Eseng, L. (1995). *Xuan: Winged helix transcription factor BF-1 is essential... - Google Scholar*. https://scholar.google.com/scholar_lookup?doi=10.1016%2F0896-6273%2895%2990262-7&pmid=7605629

Yokoya, F., Imamoto, N., Tachibana, T., & Yoneda, Y. (1999). β-Catenin Can Be Transported into the Nucleus in a Ran-unassisted Manner. *Molecular Biology of the Cell*, *10*(4), 1119–1131. https://doi.org/10.1091/mbc.10.4.1119

Yoo, S., Kim, J., Lyu, P., Hoang, T. V., Ma, A., Trinh, V., Dai, W., Jiang, L., Leavey, P., Duncan, L., Won, J.-K., Park, S.-H., Qian, J., Brown, S. P., & Blackshaw, S. (2021). Control of neurogenic competence in mammalian hypothalamic tanycytes. *Science Advances*, *7*(22), eabg3777. https://doi.org/10.1126/sciadv.abg3777

Yoon, K.-J., Ringeling, F. R., Vissers, C., Jacob, F., Pokrass, M., Jimenez-Cyrus, D., Su, Y., Kim, N.-S., Zhu, Y., Zheng, L., Kim, S., Wang, X., Doré, L. C., Jin, P., Regot, S., Zhuang, X., Canzar, S., He, C., Ming, G., & Song, H. (2017). Temporal Control of Mammalian Cortical Neurogenesis by m6A Methylation. *Cell*, *171*(4), 877-889.e17. https://doi.org/10.1016/j.cell.2017.09.003

Zahr, S. K., Yang, G., Kazan, H., Borrett, M. J., Yuzwa, S. A., Voronova, A., Kaplan, D. R., & Miller, F. D. (2018). A Translational Repression Complex in Developing Mammalian Neural Stem Cells that Regulates Neuronal Specification. *Neuron*, *97*(3), 520-537.e6. https://doi.org/10.1016/j.neuron.2017.12.045

Zamboni, M., Llorens-Bobadilla, E., Magnusson, J. P., & Frisén, J. (2020). A Widespread Neurogenic Potential of Neocortical Astrocytes Is Induced by Injury. *Cell Stem Cell*, *27*(4), 605-617.e5. https://doi.org/10.1016/j.stem.2020.07.006

Zhang, S., Bell, E., Zhi, H., Brown, S., Imran, S. A. M., Azuara, V., & Cui, W. (2019). OCT4 and PAX6 determine the dual function of SOX2 in human ESCs as a key pluripotent or neural factor. *Stem Cell Research & Therapy*, *10*(1), 122. https://doi.org/10.1186/s13287-019-1228-7

Zhang, Y.-H., Xu, M., Shi, X., Sun, X.-L., Mu, W., Wu, H., Wang, J., Li, S., Su, P., Gong, L., He, M., Yao, M., & Wu, Q.-F. (2021). Cascade diversification directs generation of neuronal diversity in the hypothalamus. *Cell Stem Cell*, *28*(8), 1483-1499.e8. https://doi.org/10.1016/j.stem.2021.03.020

Zimmer, C., Tiveron, M.-C., Bodmer, R., & Cremer, H. (2004). Dynamics of Cux2 Expression Suggests that an Early Pool of SVZ Precursors is Fated to Become Upper Cortical Layer Neurons. *Cerebral Cortex*, *14*(12), 1408–1420. https://doi.org/10.1093/cercor/bhh102

Abbreviations

APA	alternative polyadenylation
ASCL1	Achaete-scute Complex Homolog 1
ASD	autism spectrum disorder
AUTS2	autism susceptibility candidate 2
bHLH	basic-helix–loop–helix
CELF2	CUG-BP Elav-like family 2
ChR	chromatin regulator
CK2	casein kinase 2
co-IP-MS	mass spectrometry after co-immunoprecipitation
Co-REST	corepressor for element-1-silencing transcription factor
CP	cortical plate
CRE	cis-regulatory element
CTX	cortex
DAR	differentially accessible region
DE	differentially expressed
DG	dentate gyrus
DL	deep layer
dpt	days post-transfection
E	embryonic day
EC	ependymal cell
ECM	extracellular matrix
EMT	epithelial-mesenchymal transition
ESC	embryonic stem cell
FACS	fluorescence-activated cell sorting
FDR	false discovery rate
FOXG1	forkhead Box G1
GE	ganglionic eminence
GEF	guanine nucleotide-exchange factor
GFAP	glial fibrillary acidic protein
GLUT	glutamatergic
GMC	ganglion mother cell
GO	gene ontology
GRN	gene regulatory network

GSK3	glycogen synthase kinase 3
H3K27	histone H3 lysine 27
HDAC	histone deacetylase
HSC	hematopoietic stem cells
IDR	intrinsically disordered region
IN	interneuron
IPC	intermediate progenitor cell
iPSC	induced pluripotent stem cell
IRES	internal ribosome entry site
IUE	in utero electroporation
IZ	intermediate zone
JNK2	c-Jun N-terminal kinase 2
KD	knockdown
KI	knock-in
KO	knockout
LGE	lateral ganglionic eminence
LINC	linker of nucleoskeleton and cytoskeleton
LLPS	liquid–liquid phase separation
LUAD	lung adenocarcinoma
m6A	N6-methyladenosine
MAP	microtubule-associated protein
MAP1B	microtubule-associated protein 1B
MGE	medial ganglionic eminence
MLO	membrane-less organelle
NEC	neuroepithelial cell
Neurod1	neurogenic differentiation 1
NFI	nuclear factor one
NGN2	Neurogenin 2
NLS	nuclear localization signal
NPC	neural progenitor cell
NSC	neural stem cell
NuRD	nucleosome-remodeling and deacetylase
OCT4	octamer-binding transcription factor 4
OE	overexpression
OPC	oligodendrocyte progenitor cell

PAX6	paired box protein 6
PCA	principal component analysis
PH	periventricular heterotopia
pH3	phospho-histone 3
PRC2	polycomb repressive complex 2
RAX	neural fold homeobox
scRNA-seq	single-cell RNA-sequencing
SEZ	subependymal zone
SID	SIN3A-interacting domain
SIN3	switch-independent 3
SNP	single nucleotide polymorphism
SOX2	sex determining region Y-box 2
SVZ	subventricular zone
TF	transcription factor
TFBS	transcription-factor-binding site
TGIF2	TGFbeta-induced factor 2
TKO	triple knock out
TRNP1	TMF1-regulated nuclear protein 1
UL	upper layer
VZ	ventricular zone
YAP	yes-associated protein

Acknowledgements

This thesis is completed with help from many people; without them, I could not have come to this day with so much joy, gratefulness, and curiosity to learn more and beyond.

First and foremost, I would like to thank Magdalena for her patience and mentorship to me throughout my PhD years. She has been a role model in enthusiasm, critical thinking, and sharp insights in science, all of which I have been constantly drawing inspiration from. This has been a special journey with her and all the priceless lessons I learned from her will stay me for years to come.

I am also very thankful to all the people from the Götz lab and our neighboring labs—the Stricker, Ninkovic, Cappello, and Bonev labs. Their doors are always open whenever I have questions or need help in their expertise. Particularly, I want to thank Fernanda, Florencia, Daniela, Anthi, Giulia, Giorgia, Ana, Maroussia, Yvette, Fabio, Matteo, Luisa, Apara, and Maritta. It is them who make the life inside lab such a fun and nourishing environment. They are among the most friendly, helpful, and intelligent people I have met. I would like to specially thank Fernanda, my music companion, Mensa dinner buddy, and brilliant friend. Our friendship has encouraged me and inspired me in many ways, both inside and outside of lab. Additionally, I want to thank all the technicians, Tatiana, Paulina, Martina, Ines, and Manja. I learned so many skills from them and their timely assistance in daily experiments was tremendously helpful.

I want to thank my TAC members, Hongjun and Jovica. They are always positive, encouraging, and offering their unique perspectives during each TAC meeting. Especially Hongjun, who always sharply points out the directions that benefit my PhD project the most. In this regard, I would like to thank GSN for their organization and help in various steps during my PhD.

I am very grateful to my previous supervisor of master thesis, Martina, who helped me prepare for this PhD journey. I need to thank another important person for my science journey—my friend, Jing. She ignited my interests for biology and pursuing PhD when I was a bachelor student in psychology. Until today, she is always offering support and guidance in various aspects of both science and life.

Finally, I would like to thank my family, who always support every decision I make, guide me whenever I needed advice, and fill my life with so much positive energy and love. I also want to thank my precious friend, Wendy. Even when she is living on another continent, I always feel we are the same soul. Last but not least, I want to thank Kang, a special person I met in Munich. He has shared with me both joyful and difficult times throughout last years and taught me to be more open-minded and humble.

List of publications

2025 **Li, Y.**, et al. *TGIF2 is a major regulator of neural stem cell fate and neurogenic priming*. Manuscript in preparation.

2025 Merino, F., Miranda, L., **Li, Y.**, et al. *Nuclear function of the microtubule-associated protein MAP1B in neural stem cells drives periventricular heterotopia*. Manuscript in preparation.